THE SEPARATION AND REMOVAL OF INORGANIC IONS AND ORGANICS FROM AQUEOUS SOLUTIONS

EDITED BY: Shenxu Bao, Hong Peng, Feng Rao and Wencai Zhang
PUBLISHED IN: Frontiers in Chemistry

frontiers Research Topics

ISSN 1664-8714
ISBN 978-2-88971-736-1
DOI 10.3389/978-2-88971-736-1

About Frontiers

Frontiers is more than just an open-access publisher of scholarly articles: it is a pioneering approach to the world of academia, radically improving the way scholarly research is managed. The grand vision of Frontiers is a world where all people have an equal opportunity to seek, share and generate knowledge. Frontiers provides immediate and permanent online open access to all its publications, but this alone is not enough to realize our grand goals.

Frontiers Journal Series

The Frontiers Journal Series is a multi-tier and interdisciplinary set of open-access, online journals, promising a paradigm shift from the current review, selection and dissemination processes in academic publishing. All Frontiers journals are driven by researchers for researchers; therefore, they constitute a service to the scholarly community. At the same time, the Frontiers Journal Series operates on a revolutionary invention, the tiered publishing system, initially addressing specific communities of scholars, and gradually climbing up to broader public understanding, thus serving the interests of the lay society, too.

Dedication to Quality

Each Frontiers article is a landmark of the highest quality, thanks to genuinely collaborative interactions between authors and review editors, who include some of the world's best academicians. Research must be certified by peers before entering a stream of knowledge that may eventually reach the public - and shape society; therefore, Frontiers only applies the most rigorous and unbiased reviews.
Frontiers revolutionizes research publishing by freely delivering the most outstanding research, evaluated with no bias from both the academic and social point of view. By applying the most advanced information technologies, Frontiers is catapulting scholarly publishing into a new generation.

What are Frontiers Research Topics?

Frontiers Research Topics are very popular trademarks of the Frontiers Journals Series: they are collections of at least ten articles, all centered on a particular subject. With their unique mix of varied contributions from Original Research to Review Articles, Frontiers Research Topics unify the most influential researchers, the latest key findings and historical advances in a hot research area! Find out more on how to host your own Frontiers Research Topic or contribute to one as an author by contacting the Frontiers Editorial Office: frontiersin.org/about/contact

THE SEPARATION AND REMOVAL OF INORGANIC IONS AND ORGANICS FROM AQUEOUS SOLUTIONS

Topic Editors:
Shenxu Bao, Wuhan University of Technology, China
Hong Peng, The University of Queensland, Australia
Feng Rao, Michoacana University of San Nicolás de Hidalgo, Mexico
Wencai Zhang, Virginia Tech, United States

Citation: Bao, S., Peng, H., Rao, F., Zhang, W., eds. (2021). The Separation and Removal of Inorganic Ions and Organics From Aqueous Solutions. Lausanne: Frontiers Media SA. doi: 10.3389/978-2-88971-736-1

Table of Contents

frontiers in Chemistry

EDITORIAL
published: 01 November 2021
doi: 10.3389/fchem.2021.757447

Editorial: The Separation and Removal of Inorganic Ions and Organics From Aqueous Solutions

Shenxu Bao[1]*, *Hong Peng*[2], *Feng Rao*[3] and *Wencai Zhang*[4]

[1]School of Resources and Environmental Engineering, Wuhan University of Technology, Wuhan, China, [2]School of Chemical Engineering, The University of Queensland, Brisbane, QLD, Australia, [3]Institute Investigation Metallurgy and Materials, Universidad Michoacana de San Nicolas de Hidalgo, Morelia, Mexico, [4]Department of Mining and Minerals Engineering, Virginia Polytechnic Institute and State University, Blacksburg, VA, United States

Keywords: editorial, separation and recovery, extraction, removal, capacitive deionization, hydrometallurgy

Editorial on the Research Topic

The Separation and Removal of Inorganic Ions and Organics From Aqueous Solutions

Dear Colleagues,

This issue of *The Separation and Removal of Inorganic Ions and Organics from Aqueous Solutions* contains nine papers from the regular submissions to the Frontiers in Chemistry journal.

The separation and removal of inorganic ions and organics from aqueous solutions is an essential question in many fields. With the development of modern science and engineering, there are various techniques that have been developed and applied in the separation and removal of ions and organic pollutants from aqueous solutions. These techniques aim at solving separation problems encountered in the emerging technologies including fields such as any separation and/or purification of liquids, green technology, and resource recovery and recycling. Of particular interest is that the separation and removal of wanted metals from leaching solutions, which is an indispensable procedure for most hydrometallurgy processes. Ion exchange and solvent extraction, the well-established methods for resource extraction from aqueous solutions, have become effective and versatile techniques to recover wanted metals from low-grade ore or secondary resources.

In this Research Topic, Laxman et al. used the activated carbon cloth (ACC) electrode-based capacitive deionization (CDI) device to remove ionic contaminants in water, and they studied the effect of ion concentrations on the electrosorption and disinfection functions of the CDI device. This technology has a minimal impact on the environment and can be recommended as a green alternative for water treatment for deionization and microbial disinfection. The electrochemical treatment of wastewater is widely used for cleaning due to its efficiency. A comparative study on the electrochemical treatment of cyanide wastewater by two-dimensional (2D) and three-dimensional (3D) electrochemical systems was carried out (Lei and Song). The 3D electrode electrochemical system treatment technique has a bright prospect for the removal of organic material and heavy metal ions from industrial wastewater of chemical, metallurgical, and material industries. Li et al. synthesized 1-(2-hydroxyphenyl) dec-2-en-1-one oxime (HPDO) using 2-hydroxy acetophenone and octanal. The research results indicated that HPDO is a special collector for malachite flotation, whose collecting ability was improved as desired. In addition, they reported in 2021 that tert-octylsalicylaldoxime with its new structure exhibited excellent extraction ability and selectivity for Cu(II), and can be successfully used to recover copper from copper-nickel alloy electroplating wastewater. This product has the potential to be used as a powerful copper extractant in future. To overcome the problems of arsenic separation and enrichment from an alkaline leaching solution in

Edited and reviewed by:
Valeria Conte,
University of Rome Tor Vergata, Italy

***Correspondence:**
Shenxu Bao
sxbao@whut.edu.cn

Specialty section:
This article was submitted to Green and Sustainable Chemistry, a section of the journal Frontiers in Chemistry

Received: *12 August 2021*
Accepted: *26 August 2021*
Published: *01 November 2021*

Citation:
Bao S, Peng H, Rao F and Zhang W (2021) Editorial: The Separation and Removal of Inorganic Ions and Organics From Aqueous Solutions. Front. Chem. 9:757447. doi: 10.3389/fchem.2021.757447

arsenic-containing dust, a CO32--type tri-n-octylmethyl-ammonium chloride (TOMAC) was proposed to extract thioarsenite. This study provides an alternative for the removal of arsenic via alkaline leaching from high arsenic flue dust produced by heavy metal smelting (Yan et al.). The separation of Cr^{3+}/Fe^{3+} from the acid leaching solution of electroplating sludge by the selective complex precipitation has been successfully achieved and the developed procedure will help to promote further research in this area (Jinhui et al.). The selective leaching of tellurium from telluride-type gold concentrate by the Na_2S + NaOH cooperative leaching process provides new ideas for the separation and extraction of tellurium, a rare element, from telluride-type gold concentrate (Yang et al.). Zhuo et al. reported the leaching process of weathered crust elution-deposited rare Earth ore with formate salts. Formate salts are a green and sustainable rare Earth leaching agent, which can strengthen the rare Earth leaching process and weaken the hydration of clay minerals for preventing landslides. The ion-exchange mechanism in the leaching process of weathered crust elution-deposited rare Earth ores with different leaching agents was studied, which can improve the rare Earth leaching efficiency and mine safety (Zhang et al.).

With this Research Topic, we have collated new insights about the separation and removal of inorganic ions and organics from aqueous solutions. Studies addressed the application of CDI technology and electrochemicals in water treatment, the leaching process of telluride-type gold concentrate and weathered crust elution-deposited rare Earth ore, and the extraction of Cu(II) and thioarsenite with new extractants, etc. The aim of this Research Topic is to provide an interdisciplinary platform for researchers to exchange and share their experiences and latest achievements in various aspects of the separation and purification field and, in this way, promote the progress in theory and technology. The published papers present new ideas, research, and technologies, which can lead to not only economic but more environmentally friendly processes.

AUTHOR CONTRIBUTIONS

SB, as the chief guess editor of the Research Topic: *The Separation and Removal of Inorganic Ions and Organics from Aqueous Solutions* in Frontiers in Chemistry, proposed this research topic and cooperated with Dr. Hong Peng from The University of Queensland, Australia, Dr. Feng Rao from Universidad Michoacana de San Nicolas de Hidalgo, Mexico, and Dr. Wencai Zhang from Virginia Polytechnic Institute and State University, United States to contact potential authors, pre-review the submitted manuscript, seek peer reviewers and deal with the publication process.

Conflict of Interest: The author declares that the research was conducted in the absence of any commercial or financial relationships that could be construed as a potential conflict of interest.

Publisher's Note: All claims expressed in this article are solely those of the authors and do not necessarily represent those of their affiliated organizations, or those of the publisher, the editors and the reviewers. Any product that may be evaluated in this article, or claim that may be made by its manufacturer, is not guaranteed or endorsed by the publisher.

frontiers in Chemistry

ORIGINAL RESEARCH
published: 31 August 2020
doi: 10.3389/fchem.2020.00774

Disinfection of Bacteria in Water by Capacitive Deionization

*Karthik Laxman[1], Priyanka Sathe[2,3], Mohammed Al Abri[2,4], Sergey Dobretsov[3,5] and Joydeep Dutta[1]**

[1] Functional Materials Group, Department of Applied Physics, School of Engineering Sciences (SCI), KTH Royal Institute of Technology, Stockholm, Sweden, [2] Nanotechnology Research Centre, Sultan Qaboos University, Muscat, Oman, [3] Department of Marine Science and Fisheries, College of Agricultural and Marine Sciences, Sultan Qaboos University, Muscat, Oman, [4] Department of Petroleum and Chemical Engineering, College of Engineering, Sultan Qaboos University, Muscat, Oman, [5] Center of Excellence in Marine Biotechnology, Sultan Qaboos University, Muscat, Oman

Clean water is one of the primary UN sustainable development goals for 2,030 and sustainable water deionization and disinfection is the backbone of that goal. Capacitive deionization (CDI) is an upcoming technique for water deionization and has shown substantial promise for large scale commercialization. In this study, activated carbon cloth (ACC) electrode based CDI devices are used to study the removal of ionic contaminants in water and the effect of ion concentrations on the electrosorption and disinfection functions of the CDI device for mixed microbial communities in groundwater and a model bacterial strain *Escherichia coli*. Up to 75 % of microbial cells could be removed in a single pass through the CDI unit for both synthetic and groundwater, while maintaining the salt removal activity. Mortality of the microbial cells were also observed during the CDI cell regeneration and correlated with the chloride ion concentrations. The power consumption and salt removal capacity in the presence and absence of salt were mapped and shown to be as low as 0.1 kWh m^{-3} and 9.5 mg g^{-1}, respectively. The results indicate that CDI could be a viable option for single step deionization and microbial disinfection of brackish water.

Keywords: capacitive deionization, water treatment, desalination, antibacterial, disinfection

OPEN ACCESS

Edited by:
Feng Rao,
Michoacana University of San Nicolás de Hidalgo, Mexico

Reviewed by:
Gerardo Rosas,
Michoacana University of San Nicolás de Hidalgo, Mexico
Ilaria Braschi,
University of Bologna, Italy

***Correspondence:**
Joydeep Dutta
joydeep@kth.se

Specialty section:
This article was submitted to Green and Sustainable Chemistry, a section of the journal Frontiers in Chemistry

Received: *19 May 2020*
Accepted: *24 July 2020*
Published: *31 August 2020*

Citation:
Laxman K, Sathe P, Al Abri M, Dobretsov S and Dutta J (2020) Disinfection of Bacteria in Water by Capacitive Deionization. Front. Chem. 8:774. doi: 10.3389/fchem.2020.00774

INTRODUCTION

Desalination and disinfection are the two most important aspects related to the production of clean water in several regions of the world. Desalination refers to the reduction of salt content in water, while disinfection relates to neutralization of microbial species in water (World Health Organization, 2011). While desalination is primarily known for production of potable water from seawater, the declining fresh-water quality globally has increased its utilization in a wide array of applications, including that of municipal and groundwater desalination for producing drinking water. Membrane based processes like reverse osmosis (RO), nanofiltration, and ultrafiltration are widely accepted in the drinking water market and it is not uncommon for these systems to de-couple the desalination and disinfection functions (Wang Y. H. et al., 2019). Typically, RO membranes are used to reduce the ionic content of water and work in conjunction with other techniques which reduce the organics and microbial content (disinfection) of the water prior to it being passed through the RO membrane. Managing the biological matter is a pre-requisite to reduce the membrane biofouling propensity of the water and subsequent propagation of water-based infections (Al-Abri et al., 2019; Wang Y. H. et al., 2019).

Technologies for water disinfection have constantly evolved with time, from simple sedimentation processes to chemical treatments and advanced oxidation techniques including chlorination and ozonation (von Gunten, 2003; Richardson and Postigo, 2012; Ding et al., 2019). Among them, chlorination is the most widely used technique providing both primary and residual disinfection, albeit with certain disadvantages (Kimbrough and Suffet, 2002; Hua and Reckhow, 2007; Richardson and Postigo, 2012; Al-Abri et al., 2019; Stefán et al., 2019; Zhong et al., 2019). However it is fast being replaced with new technologies like photocatalysis, UV light treatment, ultrasonication, magnetic enhanced disinfection, and electrochemical methods (Baruah et al., 2012; Bora et al., 2017; Cheema et al., 2018; Cho et al., 2019; Jiang et al., 2019; Wang C. et al., 2019; You et al., 2019). Please note that most of the new methods are good primary disinfectants which kill/disable the microbes instantly upon contact, but not for residual disinfection, which demands persistence of the disinfection process over time.

It is evident that a single step process and its associated technology which can provide both desalination and disinfection would be a step forward in the water purification sector. This is where Capacitive Deionization (CDI) becomes interesting, as it has been demonstrated to desalinate and disinfect water (Laxman et al., 2015a). CDI is an offshoot of the better known electrochemical oxidation, wherein an electric potential is used to produce short lived Reactive Oxygen Species (ROS, namely ·OH, ClO^- etc.) in water, which increases the microbial mortality, providing both primary, and residual disinfection mechanisms (Gusmão et al., 2009; Gil et al., 2019). However, unlike the electrochemical technique, it has been argued that since CDI uses a lower DC voltage, limited number of ROS species would be produced (Kim et al., 2019). CDI typically comprises of two high surface area and electrically conductive electrodes, usually different forms of porous activated carbons, like powders, fabric, aerogels etc. separated by a non-conductive spacer (Suss et al., 2015; Ahmed and Tewari, 2018; Oladunni et al., 2018; Choi et al., 2019; Teow and Mohammad, 2019). When a low DC potential (typically <2.0 V_{DC}) is applied across the electrodes, non-Faradaic processes occur, leading to the electrosorption of charged species in water (cations and anions) onto the electrode surfaces, resulting in deionization of the input water (Nordstrand et al., 2019; Tang et al., 2019). Following similar principles, the negative charge on the Gram-positive and Gram-negative bacterial cell wall mediates their adsorption onto the positively charged electrode surface through electrosorption processes, thus removing the microbes from the treated water (Laxman et al., 2015a; Wang et al., 2018; Yasin et al., 2018). The inter-electrode electric field magnitude and the total surface area of the electrodes available for electrosorption are important in determining the charged species removal efficacy of CDI devices (Laxman et al., 2015b, 2019). While CDI systems have been well-studied for removing a variety of ionic contaminants from water, the dynamics of microbial removal, especially in the presence of ionic species has not been reported.

In this study, we investigated the potential of an activated carbon cloth (ACC) based capacitive deionization (CDI) cell for the removal of high concentrations (10^7 CFU mL^{-1}) of a Gram-negative coliform bacterium *Escherichia coli* from synthetically prepared water with various salt (NaCl) concentrations. The adsorption dynamics for *E. coli* and the effect of competing ionic species on the bacterial removal and disinfection capacity were investigated by using *E. coli* spiked water. Additionally, removal of Gram-positive and Gram-negative bacteria from inland brackish water collected from a well in Oman was tested. The relative ion adsorption capacities, power consumption and anti-microbial activity of the CDI device were evaluated to assess the viability of using CDI for groundwater deionization and disinfection.

MATERIALS AND METHODS

Chemicals and Materials

Groundwater with pH 8.0 (at 28°C) and a total dissolved solids (TDS) level of 2,500 mg L^{-1} was obtained from Al Musanaah wilayat (North Western Oman, 23.7474°N, 57.6326°E). Analytical grade nitric acid 65% and sodium chloride were purchased from MERCK (Germany) and used as obtained. Double woven activated carbon cloth (ACC) with a thickness of 1.0 mm (Brasquet and Le Cloirec, 1999; Shim et al., 2001) was obtained from Chemviron (Zorflex FM-100). Prior to its use as electrodes in the CDI device, it was cleaned overnight with 2 M nitric acid (heated to 115°C), after which it was thoroughly rinsed with copious amounts of deionized water and dried in a vacuum oven at 150°C.

Capacitive Deionization (CDI) Cell

The CDI cell comprised of two 25 cm^2 ACC electrodes separated by a cellulosic spacer. A 50 ml reservoir made up of poly-methyl methacrylate (PMMA) (Dow Corning SYLGARD® 184 Silicone elastomer kit), two graphite rod current collectors and an acrylic plate for support comprised the rest of the CDI cell. Uniformity in potential distribution was maintained by inserting flat graphite sheets between the electrical contacts (acting as current collectors) and the ACC electrodes. The water flow was maintained in a mixed mode (flow-through and flow between), while the applied potential and current data were extracted from the current collectors.

Deionization Experiments

Experiments With *E. coli*

The adsorption/desorption experiments were conducted with the Gram-negative bacterium *Escherichia coli* (ATCC 25922) and synthetic (distilled, DI) water with different salt concentrations 0, 1 and 10 g L^{-1} NaCl. Bacteria were cultured in Luria Bertani (LB) broth (Difco, USA) at 37°C for 12 h. Then, the bacterial cells were centrifuged at 5,000 rpm at 25°C for 10 min and re-suspended in feed solution of DI water with different salt concentrations or without salt. The final concentration of bacteria in feed solution was 2.5×10^7 CFU mL^{-1}. The experiments were conducted with continuous water flow, where bacterial cells mixed with feed solutions were passed through the cell at a flow rate of 5 mL min^{-1} in order to carry out the disinfection processes under operating conditions found optimal for standard deionization processes. A peristaltic pump (Heidolph pump drive 5201) was

used to maintain a constant flow rate of the feed water into the CDI cell. During the deionization/adsorption cycle, a DC potential of 1.6 V_{DC} was applied across the CDI electrodes and water coming out from CDI unit was sampled at various stages of the deionization cycle. Samples were used for counting of live bacteria (**Figure 1**). The charging current dynamics and potential voltage across the cell were monitored using Gwinstek GDM-396 online multimeters. Change in conductivity was recorded using eDAQ ET 908 online conductivity probe with a cell volume of 93 μL.

Groundwater Experiments

For groundwater deionization and disinfection, brackish water [TDS 2.5 g L^{-1} (Cond. = 1.6 g L^{-1}); pH 8.0] with a microbial content of 3×10^4 CFU mL^{-1} was collected from a well in Oman's Al Musanaah Wilayat (north western Oman, GPS coordinates 23.48.21 N, 57.34.10 E). Besides, *E. coli*, this water was found to contain other Gram-negative and positive bacteria, such as *Bacillus* spp., *Shigella* spp., *Vibrio* spp., *Klugiella* spp., *Coccus* spp., and *Polynucleobacter* spp. For groundwater, the deionization cycle was continued until the point of minimum conductivity was reached, after which the electrode was regenerated. The cation adsorption efficiencies were observed by collecting water samples (10 mL) at the point of minimum conductivity and measured using an ICP-OES after a 10-fold dilution. Bacterial electrosorption efficiencies were studied by collecting 10 mL of samples during deionization. The number of live bacteria in the sample were determined by the number of colony forming units (CFU, see below) in the desalinated water samples. Electrode regeneration was carried out by electrically shorting the electrodes while continuing to flow the feed water through the CDI cell. The regeneration cycle was continued until original feed water conductivity was reached.

Determination of the Number of Live Bacterial Cells

The number of live bacteria in samples were determined by counting the number of colony forming units (CFU) and live and dead staining (Al-Hinai et al., 2017; Sathe et al., 2017). To determine CFU, serial 10-fold dilutions of collected groundwater or synthetic water samples were made with sterile distilled water. 0.1 mL of the sample from each serial dilution was plated onto each Petri dish containing sterile nutrient agar (Difco, USA). The plates were incubated at 37°C for up to 48 h to permit microbial growth. Colonies were counted manually after 48 h. The concentration of live bacterial cells in CFU mL^{-1} was calculated using the following formula.

$$\text{CFU } mL^{-1} = \frac{\textit{Number of colonies x Dilution factor}}{\textit{Plated volume in mL}}$$

The number of live and dead cells in collected synthetic water samples with different salinity and groundwater samples were additionally counted by an epifluorescent microscope (Zeiss, Germany) at 1,000 × magnification (Al-Hinai et al., 2017). One hundred microliters of collected samples were immediately stained with the LIVE/DEAD BacLight^{TM} kit (Molecular Probes, USA), which is a mixture of SYTO 9 and propidium iodide dyes in DMSO. SYTO 9 preferentially stains cells in green color with intact membranes while PI stains cells in red color with damaged membranes, enabling the quantification of live, and dead cells in the water samples. The stained samples were applied on a microscope slide and representative pictures of randomly selected fields of view (area = 0.001 mm^2) were made by a camera (Muthukrishnan et al., 2017).

Characterization of CDI Electrodes and Ionic Composition of Water

Active surface area of ACC was calculated by a nuclear magnetic resonance (NMR) relaxation technique in Xigo Nanotools, using water as the solvent. The changes in the T2 relaxation time was measured and analyzed by Acorn area software (Xigo Nanotools, NJ, USA) to calculate the active surface area of the electrode (using the specific surface relaxivity on activated carbon). Zeta potential measurements of the flat electrodes were carried out in SurPass Electrokinetic analyzer (Anton Paar, Austria). The electrolyte concentration was maintained at 0.001 M KCl. Electrode size was kept constant with an L × W of 20 mm × 10 mm and the gap between the two electrodes was maintained at ∼100 μm for all measurements. The electrolyte flow was ramped from 0 to 400 mbar with a ramping duration of 20 s, while the rinsing period was maintained at 5 min for all measurements. Each zeta potential was determined by averaging four measurements. Electrode surface was studied by imaging in JEOL JSM-7200 field emission scanning electron microscope (FESEM, JEOL, Japan) working at 20 kV. Specific salt adsorption capacity was calculated using the following formula:

$$\Gamma = \frac{(C_o - C)\,V}{M}$$

Where, 'Γ' is the electrosorption capacity in mg g^{-1}, "C_o" is the initial salt concentration in mg L^{-1}, "C" is the minimum concentration in mg L^{-1}, "V" is the volume of NaCl solution passing through the cell during deionization in "L," and "M" is the total mass of the electrodes in grams.

Cation concentrations were determined by Varian 710-ES inductively coupled plasma optical emission spectrometer (ICP-OES, Varian, CA, USA). The power consumed was calculated by integrating the charging current to obtain the total charge. The charge was then multiplied by the applied potential (1.6 V_{DC}) to obtain the work done in joules, which was subsequently converted to kilo-watt hour (kWh) units per 1,000 liters (1 m^{-3}) of water treated.

RESULTS

ACC Electrode Characterization

NMR surface area measurements indicated that the activated carbon cloth (ACC) electrode used for the experiments has an active surface area of 980 m^2 g^{-1}. Based on reports available from Zorflex, the FM-100 ACC is predominantly microporous with a mean pore diameter of ∼0.7 nm. The total pore volume for ACC is 1.417 cm^3 g^{-1}, with micropores accounting for 0.56 cm^3 g^{-1}, macropores for 0.85 cm^3 g^{-1} and mesopores for <0.001 cm^3 g^{-1}.

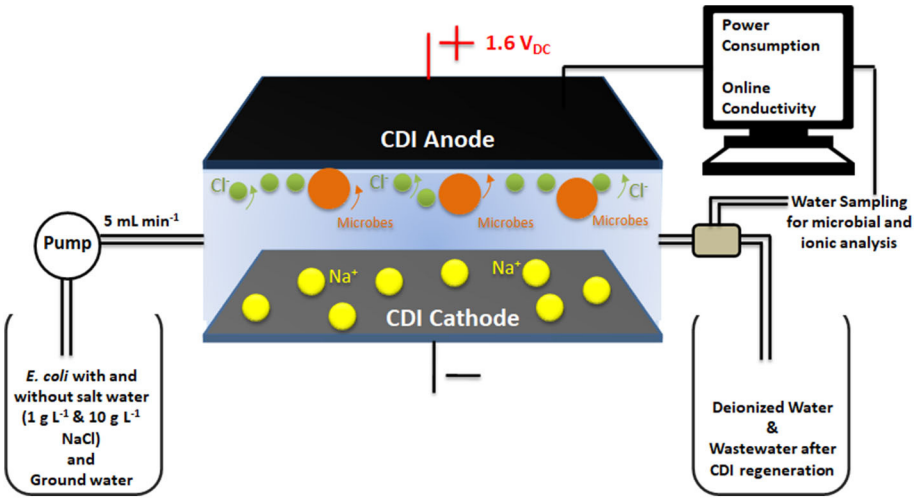

FIGURE 1 | Representation of the experimental set-up comprising of the CDI cell in continuous flow mode and water sampling to measure the microbial and ionic content in water outflow.

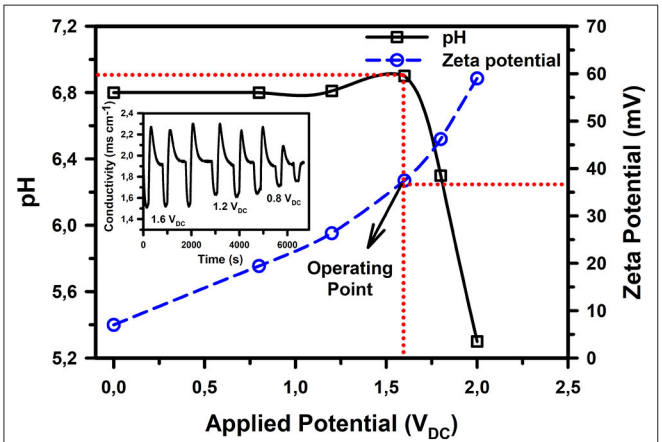

FIGURE 2 | Change in ACC surface zeta potential and pH of the exit solution with applied potential at 25°C. Inset shows the continuously varying conductivity curve of a 1 g L^{-1} NaCl solution at potentials of 1.6, 1.2, and 0.8 V_{DC}.

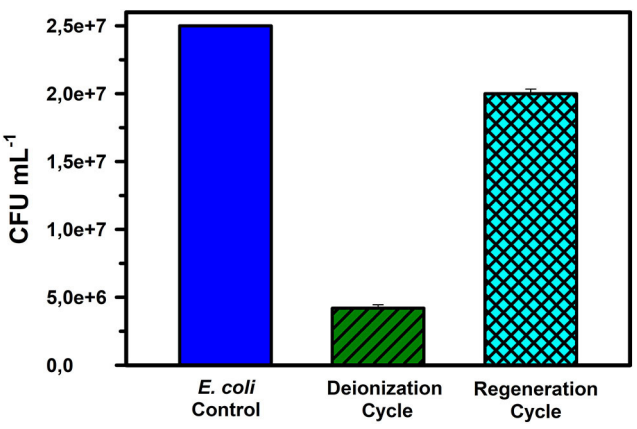

FIGURE 3 | The number of live *E. coli* cells expressed as CFU mL^{-1} counts for samples in the reservoir (control), during deionization, and during regeneration cycles in DI water. The data are the means of 3 replicates + standard errors.

While this porosity is well-suited for ionic adsorption, its efficacy for bacterial cell removal within a mixed water matrix which comprises of multiple ionic and organic/microbial species needs to be evaluated. Secondly, the overpotential of ACC for water electrolysis and gas evolution (which typically takes place at 1.23 V vs. SHE) needs to be determined to ensure that the applied DC potential is limited to values at which ACC surface oxidation is not enhanced.

As can be observed from **Figure 2**, the overpotential for ACC, which is a function of the device construction (cell interfaces and power transfer efficiency) and material properties extends the noticeable electrolysis potential for water to ~1.6 V_{DC} (at a peak current density of 1.25 mA cm^{-2}), above which faradaic reactions become significant enough to bring about a noticeable change in the water pH. Nonetheless, the surface zeta potential and ion adsorption capacity of ACC were observed to be directly proportional to the applied DC voltage (**Figure 2** and insert). This provides a plausible justification to operate the CDI unit at the upper potential limit of 1.6 V_{DC}, wherein we have previously observed good ion removal capacity (Laxman et al., 2015a, 2019).

E. coli Removal From Deionized Water

At the applied potential of 1.6 V_{DC}, the *E. coli* removal capacity was observed to be ~85 % from an initial concentration of 2.5×10^7 CFU mL^{-1} in DI water (**Figure 3**). Staining images (as discussed later) indicate that both the absolute density of bacterial cells and the viable cells were reduced in the desalinated water stream, while simultaneously, the number of dead bacterial cells increased in the regenerated water samples.

TABLE 1 | Ionic and microbial removal efficiencies of CDI during deionization and regeneration for well-water and synthetic water with 1 g L^{-1} and 10 g L^{-1} NaCl concentrations.

Parameter	DI Water + *E. coli* culture	1 g L^{-1} NaCl + *E. coli* culture	10 g L^{-1} NaCl + *E. coli* culture	Groundwater
Na^+ removal (0.36 g L^{-1})	–	–	–	11%
Ca^{2+} removal (0.13 g L^{-1})	–	–	–	63%
K^+ removal (0.009 g L^{-1})	–	–	–	46%
Al^{3+} removal (0.012 g L^{-1})	–	–	–	84%
Reduction in CFU mL^{-1} (Deionization)	85%	64%	62%	67%
Reduction in CFU mL^{-1} (Regeneration)	20%	60%	75%	33%
Spec. salt ads. Capacity	–	6.1 mg g^{-1}	9.5 mg g^{-1}	5.9 mg g^{-1}
Power consumption	0.1 kWh m^{-3}	0.4 kWh m^{-3}	0.73 kWh m^{-3}	0.48 kWh m^{-3}

The numbers in brackets in column 1 represent the initial concentration of the well water ions in g L^{-1}.

During electrode regeneration conducted under short-circuit conditions, the concentration of live bacteria was close to 80% of the control (inlet microbial concentration) value. Since this was a continuous flow mode experiment with *E. coli* culture, the results indicate that only 15% of the microbes escaped the treatment during deionization and even during regeneration, the CFU mL^{-1} of water exiting the CDI device was 20% lower than the CFU mL^{-1} of incoming water (control) (**Table 1**).

Effect of Salt on *E. coli* Removal

E. coli removal capacity of CDI in the presence of two different concentrations of NaCl (1 g L^{-1} and 10 g L^{-1}) was also characterized. In general, the conductivity curve for both the NaCl concentrations showed an initial fast decay indicating a high rate of charged species electrosorption/neutralization. However, the slope of the conductivity curve keeps decreasing with time until a quasi-steady state is reached which indicates the rate of electrosorption and release of charged species is identical. After this period, the conductivity curve starts rising again as a result of the reduced kinetics of electrosorption as the electrode is moving toward saturation. For these experiments, the CDI devices were switched to regeneration mode once quasi-steady state was reached. During regeneration, the desorption of ions from electrodes leads to a rise in the electrical conductivity of water as observed in **Figure 4A**. The water samples collected during three different deionization periods (**Figure 4A**) were analyzed and it was observed that the number of live bacteria was lowest in period 1 (**Figure 4B**), compared to periods 2 and 3.

The addition of salt reduced the microbial neutralization capacity of the electrodes to ∼64% at 1 g L^{-1} salinity and 62% at 10 g L^{-1} salinity (**Figure 5** and **Table 1**). This is also supported by **Figure 6**, where it is clear that the presence of salt in the *E. coli* water samples increases the number of live bacteria during the deionization. Thus, the electrosorption and chemical neutralization capacity of the deionization cycle on *E. coli* are affected depending on the absence and presence of salt. However, it can be observed that the absolute amount of salt or the ionic strength of the solution seemed to have little effect on the electrosorption and neutralization process (Lytle et al., 1999).

However, during CDI cell regeneration, there were differences observed in the survival and mortality of *E. coli* cells in water with different salinity levels (**Figures 5**, **6**). While 20% of incoming bacterial cells were neutralized during regeneration phase of CDI electrodes for *E. coli* in DI water, the relative percentages of neutralized cells increased to 60% with 1 g L^{-1} of NaCl in DI water and 75% for 10 g L^{-1} NaCl in DI water, respectively (**Table 1** and **Figures 5**, **6**). Some mortality of *E. coli* was also observed in the control treatment with 1 g L^{-1} and 10 g L^{-1} NaCl, due to the fact that it is a non-halophilic bacterium (Kunin et al., 1992).

Groundwater Decontamination

Analysis of the groundwater samples indicated that it mainly contained a mixture of monovalent, divalent and trivalent ions along with microbial cells (**Table 1**). The ions were electrosorbed at the electrodes to different extents during the deionization period. Ions with a higher oxidation number were adsorbed more effectively as they present a more energetically favorable option for screening the electrode surface charge (Hou and Huang, 2013; Li et al., 2016). However, when the charge on the ions was similar, the absolute concentrations took precedence, wherein ions with higher concentration like Na^+ are electrosorbed to a larger extent as compared to ions with lower concentrations like K^+ (**Table 1**) (Nordstrand and Dutta, 2020). In addition to *E. coli*, the groundwater contains other bacterial species, such as *Bacillus* spp., *Shigella* spp., *Vibrio* spp., *Klugiella* spp., *Coccus* spp., and *Polynucleobacter* spp. Among these, *E. coli, Shigella* spp., and *Salmonella* spp. are the main pathogens that are known to cause serious diseases outbreaks (Pandey et al., 2014). During deionization, the number of viable microbial cells in groundwater was reduced by ∼67% from 3×10^4 CFU mL^{-1} to 1×10^4 CFU mL^{-1}. During electrode regeneration, the number of viable microbes was found to increase 2-fold (to 2×10^4 CFU mL^{-1}), which is essentially a 33% reduction in the CFU counts (**Table 1**). The SSA of ACC is found to be 5.9 mg g^{-1} with a power consumption of 0.48 kWh m^{-3} of water treated (**Table 1**). It is noteworthy to observe that the power consumption and SSA of groundwater and low salinity synthetic water (1 g L^{-1}

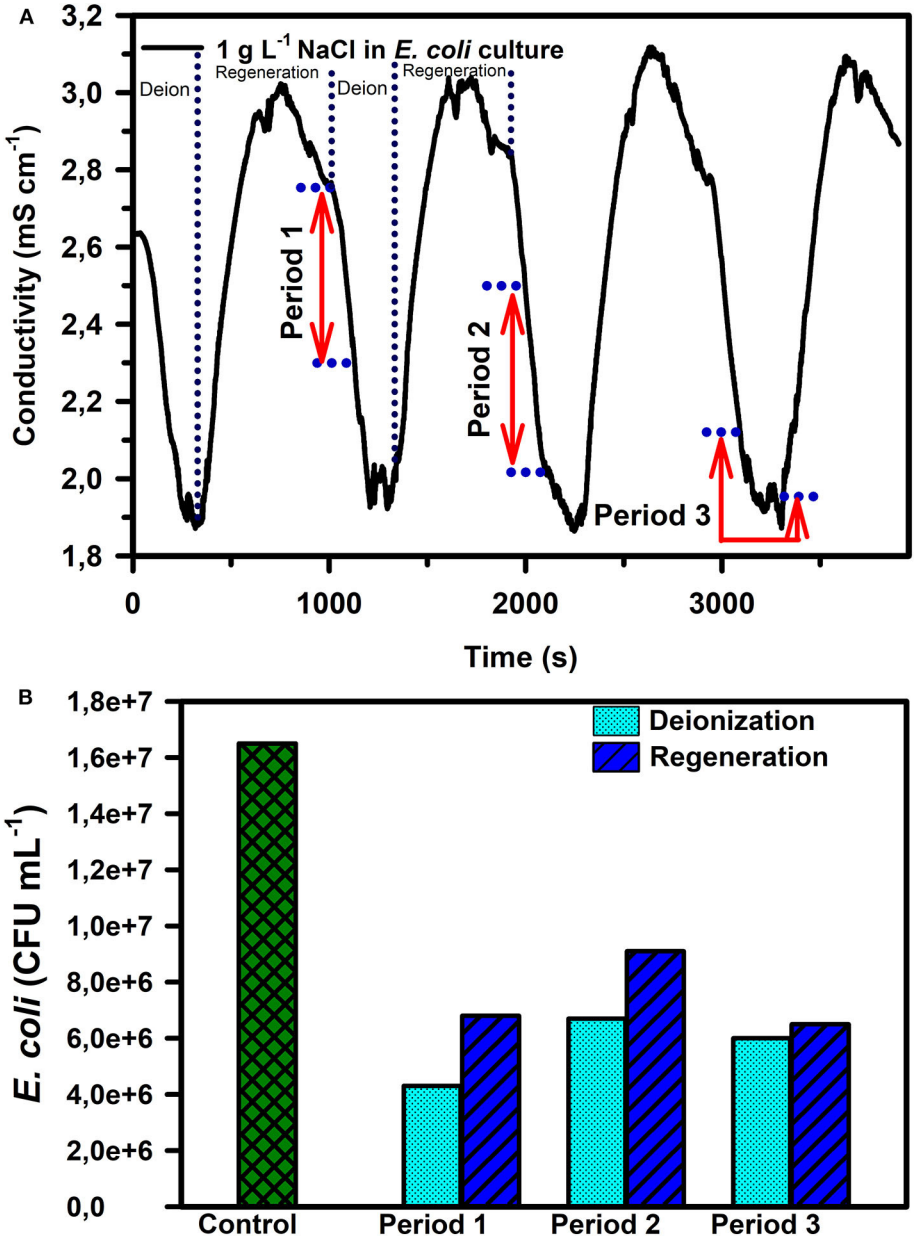

FIGURE 4 | (A) Conductivity curve during deionization and regeneration cycles for a 1 g L^{-1} NaCl in *E. coli* culture and **(B)** *E. coli* CFU mL^{-1} for different sample collection periods marked in **(A)**. The reported measurements in **(B)** are an average of 3 repetitions with the following standard error percentages from the mean (± 5.5, ± 2.0, & ± 4.0% for deionization periods 1, 2, and 3 respectively and ± 1.9, ± 5.0, & ± 7.0% during regeneration for periods 1, 2, and 3, respectively).

NaCl) contaminated with *E. coli* were comparable (**Table 1**). As expected, the SSA and power consumption for the high salinity synthetic water sample (10 g L^{-1} NaCl) was much larger at 9.5 mg g^{-1} and 0.73 kWh m^{-3}, respectively (**Table 1**).

DISCUSSION

Based on results obtained in **Figure 3**, we hypothesize that the strong electric field and acidic water pH in the vicinity of the positive electrode (where microbes are adsorbed) may be responsible for the bacterial cell mortality during deionization and regeneration. Previously it has been shown that electrical field causes irreversible permeabilization of bacterial cells (Feng et al., 2004; del Pozo et al., 2009). Additionally, even though no change in water pH was observed during the experiment, faradaic reactions are known to occur at the electrodes, which could lead to the formation of hydrogen peroxide (H_2O_2) and hydronium ions (H_3O^+) at the CDI cathode and anode, respectively (He et al., 2016). These chemical oxidants deactivate *E. coli* cells during the deionization phase and are released

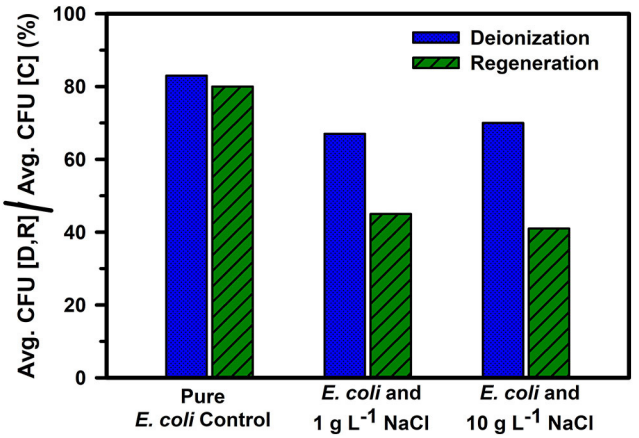

FIGURE 5 | Comparison of ratio of viable *E. coli* cells after the deionization and regeneration for *E. coli* in DI water (control) and with 1 g L^{-1} and 10 g L^{-1} NaCl concentrations with the control sample. "D," "R," and "C" stand for deionization, regeneration, and control, respectively. Averages were calculated over 4 deionization and regeneration cycles.

into the water stream during regeneration of the electrodes. Removal of bacterial cells by electrically generated reagent species have been reported earlier (Durán Moreno et al., 2004; Wang et al., 2014). The mechanisms stated above are a function of the operating conditions like applied potential (1.6 V_{DC}) and fluid flow rate (at 5 ml min^{-1} or specific flow rate of 0.13 mL min^{-1} cm^{-2} of electrode surface area). Together, they resulted in 85% mortality of the *E. coli* cells. The mortality % is of course subject to change depending on modifications in the above-mentioned parameters.

However, most natural water samples, including groundwater, comprise of a mixed matrix of ionic, organic, and microbial contaminants (Chilton, 1996). The results in the manuscript clearly indicate that the presence of ionic matter can alter the bacterial electrosorption and neutralization processes in a CDI device. Primarily, this is due to the better electrosorption kinetics of the smaller and more mobile ionic species, which can compete with the microbial cells for binding sites on the electrode surface. As a result, the electric field strength is lowered quickly, essentially reducing its effect on the microbes. However, simultaneously, the higher concentration of ionic species at the electrode surfaces may very well create an environment for dehydration of the microbials cells present at the electrode surfaces (Li et al., 2002). Thus, ionic species can have both a positive and negative effect on microbial neutralization. **Figure 4A** shows that the initial fast conductivity transition period (period 1) has the highest mass transfer rate of ions toward the electrode surface (Demirer et al., 2013), which reduces with time as the electrode approaches saturation (Nordstrand and Dutta, 2019, 2020). The lower quantity of live bacterial cells in period 1 (**Figure 4B**) is plausible as the electric field strength between the CDI device electrodes is the strongest during period 1. This period 1 action on *E. coli* cells also indicates that irrespective of the size and charge type (electronic vs. chemical), the action on the ions and microbial cells, be it electrosorption or neutralization through electro-chemical action, is proportional to the electric field strength and possibly to the surface charge. It should be noted that while *E. coli* cells are larger and have a slower mass transfer rate compared to the ions, the outer layer of lipopolysaccharides on the Gram-negative cell imparts a strong negative zeta potential ranging from −23 mV to −50 mV at pH ∼7 (Lytle et al., 1999; Martins et al., 2013), which can significantly assist in their migration toward the positive electrode surface. Nonetheless, the net electrosorption/neutralization capacity of CDI is reduced in the presence of salt, which we attribute to the preferential electrosorption of the ions at the electrode surface due to their smaller size. The same result is also reflected visually through fluorescence microscopy images as observed in **Figure 6**.

Despite lower net *E. coli* neutralization in the presence of salt, there could be multiple mechanisms effecting this observed mortality. The first being electrosorption, wherein the negatively charged bacterial cells will be in the same vicinity of the electrosorbed chloride ions (Cl^-) (Marugán et al., 2010) and the higher concentrations of Cl^- ions may lead to oxidative stress on the cell walls resulting in cell death. Secondly, the electric field may affect electrosorbed bacterial cells (Feng et al., 2004; del Pozo et al., 2009). Thirdly, since the reduction potential for chloride is 1.36 V (vs. SHE), it is possible that some of the Cl^- ions get reduced to $Cl_2(g)$, in turn leading to the generation of hypochlorous acid (HClO), which increases the mortality of bacterial cells in the vicinity of the anode (Zhang et al., 2018). Typically, the formation of HClO has been observed to be proportional to the amount of electrosorbed Cl^- ions (Wouters et al., 2013). It should be noted that when the CDI device is switched from deionization to regeneration (at the quasi steady state point), the absolute quantity of electrosorbed Cl^- ions for the 1 g L^{-1} and 10 g L^{-1} NaCl samples are comparable. Hence the potential HClO concentrations at the electrode surface are also comparable, which partially justifies the similarity in microbial cell neutralization capacity for the two salinities (**Figures 5**, **6**). In addition, and as mentioned previously, some oxygen based oxidative species (like H_2O_2 and H_3O^+) may also contribute to be microbial mortality. Based on similar reasoning, the higher mortality of *E. coli* during CDI regeneration in saline water (compared to DI water in **Table 1**) can be attributed to the release of the chloride and chloride based radical species into the water stream (Zhang et al., 2018), which effectively doubles the chloride concentration in the water stream creating an environment where bacterial cells can be effectively neutralized during regeneration. Hence in summary, a reduction in *E. coli* cell mortality during the deionization phase was only observed between deionized water and 1 g L^{-1} NaCl water (**Figures 4**, **5**). A further 10-fold increase in salt concentration (10 g L^{-1}) resulted in mere 15% increase in bacterial cell mortality. On a similar note but contrarily, a significant increase in *E. coli* cell mortality during the regeneration phase was only observed between deionized water and 1 g L^{-1} NaCl water; while a further increase in salinity did not contribute much to the enhancement in mortality percentages.

For real groundwater samples, the co-occurrence of multiple ions and microbial species, along with the organic contaminants

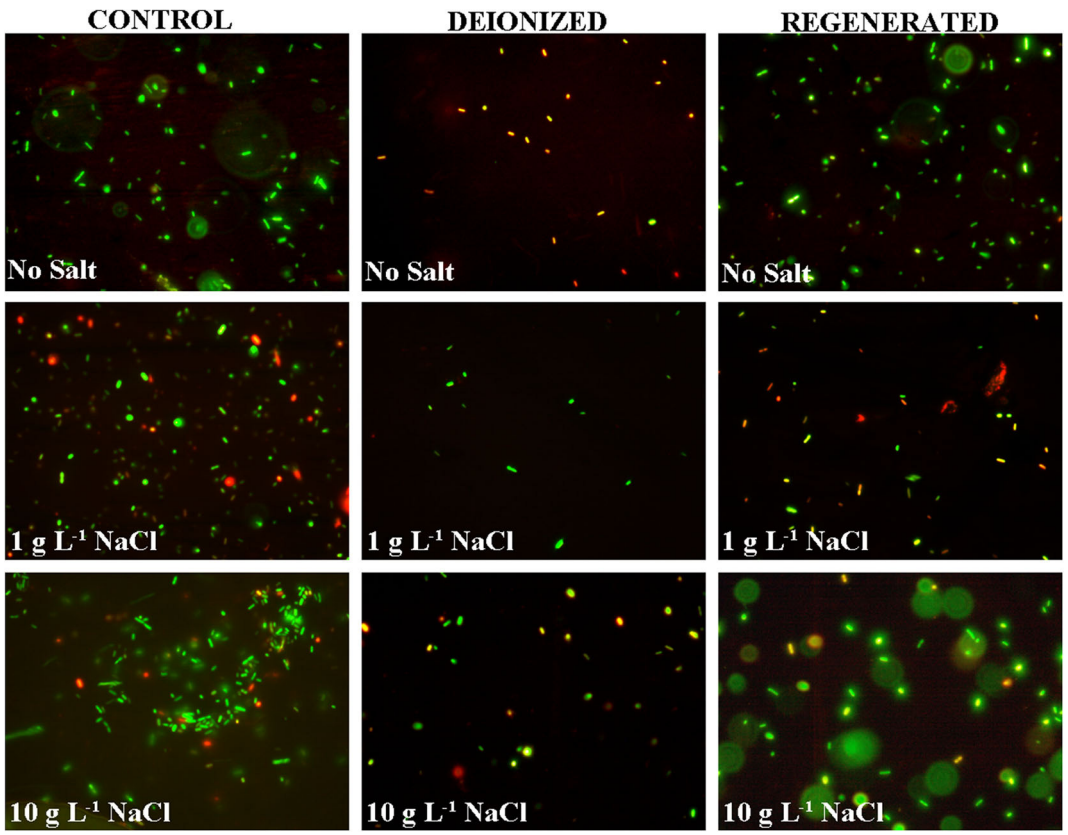

FIGURE 6 | Live and dead stained *E. coli* cells in the control, deionized (after CDI), and regenerated water samples for DI water, and DI water with 1 g L^{-1} and 10 g L^{-1} NaCl.

pose different conditions and outcomes for a CDI cell operation (Laxman et al., 2015a). Live and dead staining indicated that the proportion of microbes neutralized during deionization (**Figure 7**) was similar to the saline water samples prepared in the laboratory (**Figure 6**), which is feasible, since the salinity percentages were similar. However, during regeneration of groundwater the microbial cell mortality is reduced compared to that of the synthetic samples, which although not certain, could be attributed to the multiple bacterial species in the groundwater which can respond differently to the CDI effect. In addition, the organic load in the water can also modulate the radical formation capacity and in turn hinder the cell neutralization during regeneration. Nonetheless, the results clearly indicate that a CDI device effectively eliminates multiple species of Gram-positive and negative bacteria from the groundwater. However, the extent to which microbes can be removed show dependence on the surface charge, size and sensitivity of the microbial surface charge to electrolyte concentration and pH (Lytle et al., 1999). This would be interesting to study in further details in the future.

In addition, while not much discussion has been given on the electrode performance in the various experiments, it should be noted that the specific salt adsorption capacity (SSA) and power consumption of the CDI device did not vary significantly for the groundwater and *E. coli* spiked NaCl water samples of similar TDS levels (**Table 1**). SSA and power requirements primarily increases with high salt concentration which allows the electric field to be better neutralized, leading to thinner but denser electrical double layers as compared to the lower salt containing water samples (Suss et al., 2015). Overall there were no surprising results in the electrode performance criteria with the *E. coli* spiked DI water samples showing the lowest power requirements (0.1 kWh m^{-3}), followed by 1 g L^{-1} and 10 g L^{-1} *E. coli* spiked NaCl samples.

CONCLUSIONS

In conclusion, activated carbon cloth (ACC) was used as an electrode material in capacitive deionization (CDI) process and the technique was found to be effective for the simultaneous deionization and elimination of microbes from water. This process can be applied in a multi-ion water matrix and is feasible for both pathogenic and biofouling bacteria. The bacterial neutralization during the deionization and regeneration processes was observed to be a function of the presence or absence of salt, but not so much on the absolute salt concentrations. During deionization, bacterial neutralization is proposed to occur through multiple mechanisms due to electric field, osmotic effects and chemical action, while during

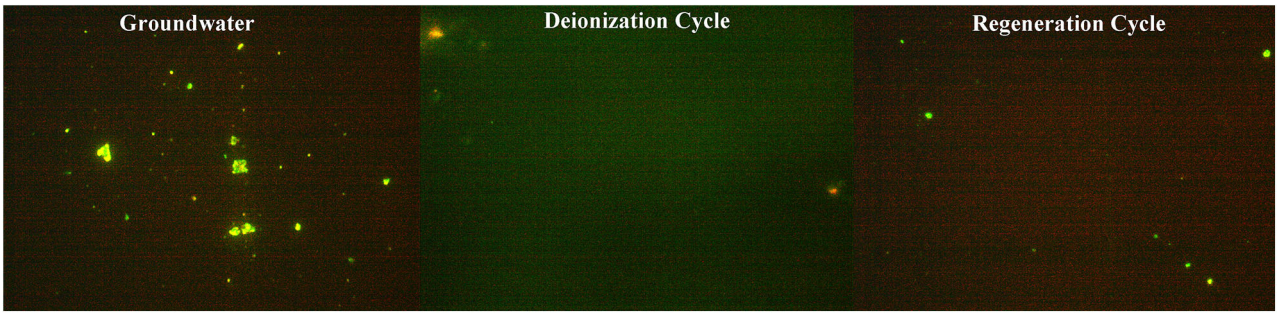

FIGURE 7 | Microbial cells stained with life and dead BacLight™ stain in original, deionized, and regeneration groundwater samples. Salinity of groundwater was ~1.5 g L^{-1} and comprises of multiple ions (**Table 1**).

regeneration, we hypothesize that the close proximity of the bacterial cells to the chloride ions and formation of oxidative oxygen and chloride species in water dominated the neutralization process. Thus, CDI using ACC electrodes is found to be potentially viable for the purification and disinfection of groundwater with reasonably high microbial concentrations. Since CDI does not use synthetic biocides but eliminates bacteria from the water primarily through electrosorption and other naturally occurring radical species in water, this method has a minimal impact on the environment and can be recommended as a green alternative for water treatment for deionization and microbial disinfection.

DATA AVAILABILITY STATEMENT

All datasets presented in this study are included in the article/supplementary material.

AUTHOR CONTRIBUTIONS

KL and PS conducted the experiments and wrote the manuscript. MA, SD, and JD planned the experiments and edited the manuscript. All authors contributed to the article and approved the submitted version.

FUNDING

KL and JD would like to thank MISTRA Terraclean (Diary No. 2015/31) and the Swedish Research Council (Diary No. 2018-05387) for financial support. KL, PS, SD, and MA would like to thank the Chair in Nanotechnology program of The Research Council of Oman (TRC) and Sultan Qaboos University for financial support. SD acknowledges a South Africa-Oman collaborative Grant No. CL/SQU-SA/18/01, OMSA170413227101.

REFERENCES

Ahmed, M. A., and Tewari, S. (2018). Capacitive deionization: processes, materials and state of the technology. *J. Electroanal. Chem.* 813, 178–192. doi: 10.1016/j.jelechem.2018.02.024

Al-Abri, M., Al-Ghafri, B., Bora, T., Dobretsov, S., Dutta, J., Castelletto, S., et al. (2019). Chlorination disadvantages and alternative routes for biofouling control in reverse osmosis desalination. *NPJ Clean Water* 2:2. doi: 10.1038/s41545-019-0033-2

Al-Hinai, M. H., Sathe, P., Al-Abri, M. Z., Dobretsov, S., Al-Hinai, A. T., and Dutta, J. (2017). Antimicrobial activity enhancement of poly(ether sulfone) membranes by in situ growth of ZnO nanorods. *ACS Omega* 2, 3157–3167. doi: 10.1021/acsomega.7b00314

Baruah, S., Jaisai, M., and Dutta, J. (2012). Development of a visible light active photocatalytic portable water purification unit using ZnO nanorods. *Catal. Sci. Technol.* 2, 918–921. doi: 10.1039/c2cy20033c

Bora, T., Sathe, P., Laxman, K., Dobretsov, S., and Dutta, J. (2017). Defect engineered visible light active ZnO nanorods for photocatalytic treatment of water. *Catal. Today* 284, 11–18. doi: 10.1016/j.cattod.2016.09.014

Brasquet, C., and Le Cloirec, P. (1999). Effects of activated carbon cloth surface on organic adsorption in aqueous solutions. Use of statistical methods to describe mechanisms. *Langmuir* 15, 5906–5912. doi: 10.1021/la9811160

Cheema, W. A., Andersen, H. R., and Kaarsholm, K. M. S. (2018). Improved DBP elimination from swimming pool water by continuous combined UV and ozone treatment. *Water Res.* 147, 214–222. doi: 10.1016/j.watres.2018.09.030

Chilton, J. (1996). "Groundwater," *in Water Quality Assessments: A Guide to the Use of Biota, Sediments and Water in Environmental Monitoring,* eds D. V. Chapman and O. World Health (London: UNESCO, P. United Nations Environment, E & FN Spon).

Cho, K., Lee, S., Kim, H., Kim, H. E., Son, A., Kim, E. J., et al. (2019). Effects of reactive oxidants generation and capacitance on photoelectrochemical water disinfection with self-doped titanium dioxide nanotube arrays. *Appl. Catal. B-Environ.* 257:117910. doi: 10.1016/j.apcatb.2019.117910

Choi, J., Dorji, P., Shon, H. K., and Hong, S. (2019). Applications of capacitive deionization: Desalination, softening, selective removal, and energy efficiency. *Desalination* 449, 118–130. doi: 10.1016/j.desal.2018.10.013

del Pozo, J. L., Rouse, M. S., Mandrekar, J. N., Steckelberg, J. M., and Patel, R. (2009). The electricidal effect: reduction of *Staphylococcus* and pseudomonas biofilms by prolonged exposure to low-intensity electrical current. *Antimicrob. Agents Chemother.* 53, 41–45. doi: 10.1128/AAC.00680-08

Demirer, O. N., Naylor, R. N., Rios Perez, C. A., Wilkes, E., and Hidrovo, C. (2013). Energetic performance optimization of a capacitive deionization system operating with transient cycles and brackish water. *Desalination* 314, 130–138. doi: 10.1016/j.desal.2013.01.014

Ding, W., Jin, W., Cao, S., Zhou, X., Wang, C., Jiang, Q., et al. (2019). Ozone disinfection of chlorine-resistant bacteria in drinking water. *Water Res.* 160, 339–349. doi: 10.1016/j.watres.2019.05.014

Durán Moreno, A., Frontana-Uribe, B. A., and Ramírez Zamora, R. M. (2004). Electro-Fenton as a feasible advanced treatment process to produce

reclaimed water. *Water Sci. Technol.* 50, 83–90. doi: 10.2166/wst.2004.0095

Feng, C., Suzuki, K., Zhao, S., Sugiura, N., Shimada, S., and Maekawa, T. (2004). Water disinfection by electrochemical treatment. *Bioresour. Technol.* 94, 21–25. doi: 10.1016/j.biortech.2003.11.021

Gil, M. I., López-Gálvez, F., Andújar, S., Moreno, M., and Allende, A. (2019). Disinfection by-products generated by sodium hypochlorite and electrochemical disinfection in different process wash water and fresh-cut products and their reduction by activated carbon. *Food Control* 100, 46–52. doi: 10.1016/j.foodcont.2018.12.050

Gusmão, I. C. P., Moraes, P. B., and Bidoia, E. D. (2009). A thin layer electrochemical cell for disinfection of water contaminated with *Staphylococcus aureus*. *Braz. J. Microbiol.* 40, 649–654. doi: 10.1590/S1517-83822009000300029

He, D., Wong, C. E., Tang, W., Kovalsky, P., and Waite, T. D. (2016). Faradaic reactions in water desalination by batch-mode capacitive deionization. *Environ. Sci. Technol. Lett.* 3, 222–226. doi: 10.1021/acs.estlett.6b00124

Hou, C. H., and Huang, C. Y. (2013). A comparative study of electrosorption selectivity of ions by activated carbon electrodes in capacitive deionization. *Desalination* 314, 124–129. doi: 10.1016/j.desal.2012.12.029

Hua, G., and Reckhow, D. A. (2007). Comparison of disinfection byproduct formation from chlorine and alternative disinfectants. *Water Res.* 4, 1667–1678. doi: 10.1016/j.watres.2007.01.032

Jiang, Z., Wang, B., Li, Y., Chan, H. S., Sun, H., Wang, T., et al. (2019). Solar-light-driven rapid water disinfection by ultrathin magnesium titanate/carbon nitride hybrid photocatalyst: band structure analysis and role of reactive oxygen species. *Appl. Catal. B Environ.* 257:117898. doi: 10.1016/j.apcatb.2019.117898

Kim, Y. H., Tang, K., Chang, J., Sharma, K., Yiacoumi, S., Mayes, R. T., et al. (2019). Potential limits of capacitive deionization and membrane capacitive deionization for water electrolysis. *Sep. Sci. Technol.* 54, 2112–2125. doi: 10.1080/01496395.2019.1608243

Kimbrough, D. E., and Suffet, I. H. (2002). Electrochemical removal of bromide and reduction of THM formation potential in drinking water. *Water Res.* 36, 4902–4906. doi: 10.1016/S0043-1354(02)00210-5

Kunin, C. M., Hua, T. H., Van Arsdale White, L., and Villarejo, M. (1992). Growth of *Escherichia coli* in human urine: role of salt tolerance and accumulation of glycine betaine. *J. Infect. Dis.* 166, 1311–1315. doi: 10.1093/infdis/166.6.1311

Laxman, K., Husain, A., Nasser, A., Al Abri, M., and Dutta, J. (2019). Tailoring the pressure drop and fluid distribution of a capacitive deionization device. *Desalination* 449, 111–117. doi: 10.1016/j.desal.2018.10.021

Laxman, K., Myint, M. T. Z., Al Abri, M., Sathe, P., Dobretsov, S., and Dutta, J. (2015a). Desalination and disinfection of inland brackish ground water in a capacitive deionization cell using nanoporous activated carbon cloth electrodes. *Desalination* 362, 126–132. doi: 10.1016/j.desal.2015.02.010

Laxman, K., Myint, M. T. Z., Khan, R., Pervez, T., and Dutta, J. (2015b). Effect of a semiconductor dielectric coating on the salt adsorption capacity of a porous electrode in a capacitive deionization cell. *Electrochim. Acta* 166, 329–337. doi: 10.1016/j.electacta.2015.03.049

Li, X. Y., Ding, F., Lo, P. S. Y., and Sin, S. H. P. (2002). Electrochemical disinfection of saline wastewater effluent. *J. Environ. Eng.* 128, 697–704. doi: 10.1061/(ASCE)0733-9372(2002)128:8(697)

Li, Y., Zhang, C., Jiang, Y., Wang, T. J., and Wang, H. (2016). Effects of the hydration ratio on the electrosorption selectivity of ions during capacitive deionization. *Desalination* 399, 171–177. doi: 10.1016/j.desal.2016.09.011

Lytle, D. A., Rice, E. W., Johnson, C. H., and Fox, K. R. (1999). Electrophoretic mobilities of *Escherichia coli* O157:H7 and wild-type *Escherichia coli* strains. *Appl. Environ. Microbiol.* 65, 3222–3225. doi: 10.1128/AEM.65.7.3222-3225.1999

Martins, J. M. F., Majdalani, S., Vitorge, E., Desaunay, A., Navel, A., Guiné, V., et al. (2013). Role of macropore flow in the transport of Escherichia coli cells in undisturbed cores of a brown leached soil. *Environ. Sci.* 15, 347–356. doi: 10.1039/C2EM30586K

Marugán, J., van Grieken, R., and Pablos, C. (2010). Kinetics and influence of water composition on photocatalytic disinfection and photocatalytic oxidation of pollutants. *Environ. Technol.* 31, 1435–1440. doi: 10.1080/09593331003646653

Muthukrishnan, T., Govender, A., Dobretsov, S., and Abed, R. (2017). Evaluating the reliability of counting bacteria using epifluorescence microscopy. *J. Mar. Sci. Eng.* 5:4. doi: 10.3390/jmse5010004

Nordstrand, J., and Dutta, J. (2019). Dynamic langmuir model: a simpler approach to modeling capacitive deionization. *J. Phys. Chem. C* 123, 16479–16485. doi: 10.1021/acs.jpcc.9b04198

Nordstrand, J., and Dutta, J. (2020). Simplified prediction of ion removal in capacitive deionization of multi-ion solutions. *Langmuir* 36, 1338–1344. doi: 10.1021/acs.langmuir.9b03571

Nordstrand, J., Laxman, K., Myint, M. T. Z., and Dutta, J. (2019). An easy-to-use tool for modeling the dynamics of capacitive deionization. *J. Phys. Chem. A* 123, 6628–6634. doi: 10.1021/acs.jpca.9b05503

Oladunni, J., Zain, J. H., Hai, A., Banat, F., Bharath, G., and Alhseinat, E. (2018). A comprehensive review on recently developed carbon based nanocomposites for capacitive deionization: from theory to practice. *Sep. Purif. Technol.* 207, 291–320. doi: 10.1016/j.seppur.2018.06.046

Pandey, P. K., Kass, P. H., Soupir, M. L., Biswas, S., and Singh, V. P. (2014). Contamination of water resources by pathogenic bacteria. *AMB Express* 4:51. doi: 10.1186/s13568-014-0051-x

Richardson, S. D., and Postigo, C. (2012). "Drinking water disinfection by-products," in: *Emerging Organic Contaminants and Human Health*, eds D. Barceló (Berlin: Springer), 93–137. doi: 10.1007/698_2011_125

Sathe, P., Laxman, K., Myint, M. T. Z., Dobretsov, S., Richter, J., and Dutta, J. (2017). Bioinspired nanocoatings for biofouling prevention by photocatalytic redox reactions. *Sci. Rep.* 7:3624. doi: 10.1038/s41598-017-03636-6

Shim, J. W., Park, S.-J., and Ryu, S.-K. (2001). Effect of modification with HNO3 and NaOH on metal adsorption by pitch-based activated carbon fibers. *Carbon N. Y.* 39, 1635–1642. doi: 10.1016/S0008-6223(00)00290-6

Stefán, H., Erdélyi, N., Izsák, B., Záray, G., and Vargha, M. (2019). Formation of chlorination by-products in drinking water treatment plants using breakpoint chlorination. *Microchem. J.* 149:104008. doi: 10.1016/j.microc.2019.104008

Suss, M. E., Porada, S., Sun, X., Biesheuvel, P. M., Yoon, J., and Presser, V. (2015). Water desalination via capacitive deionization: what is it and what can we expect from it? *Energy. Environ. Sci.* 8, 2296–2319. doi: 10.1039/C5EE00519A

Tang, W., Liang, J., He, D., Gong, J., Tang, L., Liu, Z., et al. (2019). Various cell architectures of capacitive deionization: Recent advances and future trends. *Water Res.* 150, 225–251. doi: 10.1016/j.watres.2018.11.064

Teow, Y. H., and Mohammad, A. W. (2019). New generation nanomaterials for water desalination: a review. *Desalination* 451, 2–17. doi: 10.1016/j.desal.2017.11.041

von Gunten, U. (2003). Ozonation of drinking water: part II. Disinfection and by-product formation in presence of bromide, iodide or chlorine. *Water Res.* 37, 1469–1487. doi: 10.1016/S0043-1354(02)00458-X

Wang, C., Moore, N., Bircher, K., Andrews, S., and Hofmann, R. (2019). Full-scale comparison of UV/H2O2 and UV/Cl2 advanced oxidation: the degradation of micropollutant surrogates and the formation of disinfection byproducts. *Water Res.* 161, 448–458. doi: 10.1016/j.watres.2019.06.033

Wang, J., Wang, G., Wu, T., Wang, D., Yuan, Y., Wang, J., et al. (2018). Quaternary ammonium compound functionalized activated carbon electrode for capacitive deionization disinfection. *ACS Sustain. Chem. Eng.* 6, 17204–17210. doi: 10.1021/acssuschemeng.8b04573

Wang, X. Q., Liu, C. P., Yuan, Y., and Li, F. B. (2014). Arsenite oxidation and removal driven by a bio-electro-fenton process under neutral pH conditions. *J. Hazard. Mater.* 275, 200–209. doi: 10.1016/j.jhazmat.2014.05.003

Wang, Y. H., Wu, Y. H., Tong, X., Yu, T., Peng, L., Bai, Y., et al. (2019). Chlorine disinfection significantly aggravated the biofouling of reverse osmosis membrane used for municipal wastewater reclamation. *Water Res.* 154, 246–257. doi: 10.1016/j.watres.2019.02.008

World Health Organization. (2011). *Safe Drinking-Water From Desalination*. Geneva: World Health Organization (2011).

Wouters, J. J., Lado, J. J., Tejedor-Tejedor, M. I., Perez-Roa, R., and Anderson, M. A. (2013). Carbon fiber sheets coated with thin-films of SiO2 and γ-Al2O3 as electrodes in capacitive deionization: relationship between properties of the oxide films and electrode performance. *Electrochim. Acta* 112, 763–773. doi: 10.1016/j.electacta.2013.08.170

Yasin, A. S., Mohamed, I. M. A., Mousa, H. M., Park, C. H., and Kim, C. S. (2018). Facile synthesis of TiO2/ZrO2 nanofibers/nitrogen co-doped activated carbon to enhance the desalination and bacterial inactivation via capacitive deionization. *Sci. Rep.* 8:541. doi: 10.1038/s41598-017-19027-w

You, J., Guo, Y., Guo, R., and Liu, X. (2019). A review of visible light-active photocatalysts for water disinfection: features and prospects. *Chem. Eng. J.* 373, 624–641. doi: 10.1016/j.cej.2019.05.071

Zhang, C., He, D., Ma, J., Tang, W., and Waite, T. D. (2018). Faradaic reactions in capacitive deionization (CDI) - problems and possibilities: a review. *Water Res.* 128, 314–330. doi: 10.1016/j.watres.2017.10.024

Zhong, Y., Gan, W., Du, Y., Huang, H., Wu, Q., Xiang, Y., et al. (2019). Disinfection byproducts and their toxicity in wastewater effluents treated by the mixing oxidant of ClO2/Cl2. *Water Res.* 162, 471–481. doi: 10.1016/j.watres.2019.07.012

Conflict of Interest: The authors declare that the research was conducted in the absence of any commercial or financial relationships that could be construed as a potential conflict of interest.

frontiers in Chemistry

ORIGINAL RESEARCH
published: 26 November 2020
doi: 10.3389/fchem.2020.592771

Synthesis of 1-(2-Hydroxyphenyl) Dec-2-en-1-One Oxime and Its Flotation and Adsorption Behavior for Malachite

Liqing Li[1]*, *Lin Yang*[1] and *Fangxu Li*[2]*

[1] Faculty of Materials Metallurgy and Chemistry, Jiangxi University of Science and Technology, Ganzhou, China, [2] Institute of Resources Comprehensive Utilization, Guangdong Academy of Science, Guangzhou, China

A novel collector of 1-(2-hydroxyphenyl) dec-2-en-1-one oxime (HPDO) was synthesized from 2-hydroxy acetophenone and octanal, and its flotation and adsorption behavior for malachite were studied by flotation tests and x-ray photoelectron spectroscopy (XPS) analysis. The flotation results of a single mineral show HPDO is a special collector for malachite. Compared with benzohydroxamic acid (BHA), isobutyl xanthate (SIBX), and dodecylamine (DA), HPDO exhibits excellent flotation performance for malachite and satisfied selectivity against quartz and calcite over a wide pH range. The HPDO with a concentration of 200 mg/L can float 94% malachite at pH 8, while only recovering 7.8% quartz and 28% calcite. XPS data give clear evidence for the formation of a Cu-oxime complex on malachite surfaces after HPDO adsorption.

Keywords: collector, flotation, adsorption, malachite, 1-(2-hydroxyphenyl) dec-2-en-1-one oxime

OPEN ACCESS

Edited by:
Shenxu Bao,
Wuhan University of Technology, China

Reviewed by:
Priyanka Sharma,
Stony Brook University, United States
Zuohua Liu,
Chongqing University, China

***Correspondence:**
Liqing Li
liliqing79@126.com
Fangxu Li
lifangxu28@163.com

Specialty section:
This article was submitted to Green and Sustainable Chemistry, a section of the journal Frontiers in Chemistry

Received: *08 August 2020*
Accepted: *13 October 2020*
Published: *26 November 2020*

Citation:
Li L, Yang L and Li F (2020) Synthesis of 1-(2-Hydroxyphenyl) Dec-2-en-1-One Oxime and Its Flotation and Adsorption Behavior for Malachite. Front. Chem. 8:592771. doi: 10.3389/fchem.2020.592771

INTRODUCTION

Copper was one of the first metals utilized by humans and had a profound impact on the progress of early human civilization. Copper is still an important material today and is widely used in the electrical and electronic markets, transportation, industrial machinery and equipment, organic chemistry, and medicine (Rao et al., 2015; Hussain et al., 2018; Snoussi et al., 2018; Aslam et al., 2019). Copper demand is expected to reach 26.4 million tons by 2020 (Elshkaki et al., 2016). The amount of copper in the earth's crust is about 0.01%, and native copper is rare in nature, found mostly in the form of copper ore. More than 170 copper-containing minerals have already been found. However, only 10–15 of these minerals have been successfully developed commercially. Because the mineral process often brings environmental pollution problems, it is very important to apply copper resources reasonably and efficiently (Chan et al., 2014; Li et al., 2019b). The most common copper sulfide includes chalcopyrite, bornite, and beryllium copper ore. With the further exploitation of known copper sulfide ores, copper oxide ore can serve as a new source of copper to meet the huge market demand (Huang et al., 2018; Wang et al., 2020).

Malachite is one of the most common copper oxide ores. Leaching-SX (solvent extraction)-EW (electrowinning) is a commercial method used for processing copper oxide ores (Li et al., 2015). While this process has shortcomings, such as its lengthy processing steps, high agent consumption, and high extractant cost (Liu et al., 2016) its flotation of malachite can overcome the above disadvantages and gradually become a hotspot for flotation scientists and engineers (Marion et al., 2017). Recently, two methods of sulfide flotation and direct flotation

were used in the flotation of malachite. As for sulfide flotation, traditional copper sulfide flotation collectors do not perform well with hydrophilic malachite, unless it is activated by Na_2S, NaHS, $(NH_4)_2S$, NH_4HS, 8-hydroxyquinoline or diethylamine phosphate (Shengo et al., 2014; Cui et al., 2015; Park et al., 2016; Feng et al., 2018a,b; Qin et al., 2018). In addition, sulphidisation for copper oxide ore was hard to control because of the complex ore properties (Corin et al., 2017). As for direct flotation, fatty acids, fatty amines, sulfonates, and phosphonates reveal poor selectivity in separating malachite from calcite (Li et al., 2015, 2018). Hydroxamic acids, such as BA and Octyl hydroxamic acid, show a satisfying flotation performance for malachite (Hope et al., 2012; Mao et al., 2014). However, oxime collectors have not received enough attention over the past two decades.

Oxime, which is in the C=NH-OH group, is similar to hydroxamic surfactants and has proven to be an impressive collector for malachite in minerals engineering. Salicylaldoxime has a strong affinity to Cu(II), and is widely studied in copper oxide ore. Li found the recovery of malachite reached 97% by using salicylaldoxime as a collector with the help of 10^{-2} mol/L Na_2CO_3 (Li et al., 2019). Han used a combination collector of salicylaldoxime and xanthate to deal with complex copper oxide ores from the Yulong copper mine in China. However, the synergy mechanism of salicylaldoxime and xanthate has not yet received the attention of researchers (Han et al., 2017; Wang et al., 2019). Li found that Tert-butyl salicylaldoxime is a powerful collector for malachite (Li et al., 2019a). 2-hydroxy-5-nonylphenyl (phenyl) methanone oxime has proven to be proficient at the beneficiation of copper oxide ore (Yang et al., 2011). The other oximes, such as 2-ethyl-2-hexenaloxime (Xu et al., 2014), are effective collectors for malachite or chalcopyrite. However, 1-(2-hydroxyphenyl) dec-2-en-1-one oxime (HPDO) for the recovery of copper oxide ore has been hardly studied.

The aim of this paper is to provide a reference for the flotation performance adjustment through efficient molecular structure modification. A novel ketoxime collector was synthesized through aldol condensation and ammoximation reaction. The chemical structure of HPDO is characterized by FTIR and LC-MS. The flotation performance of HPDO to malachite was studied by micro and batch flotation tests. And the

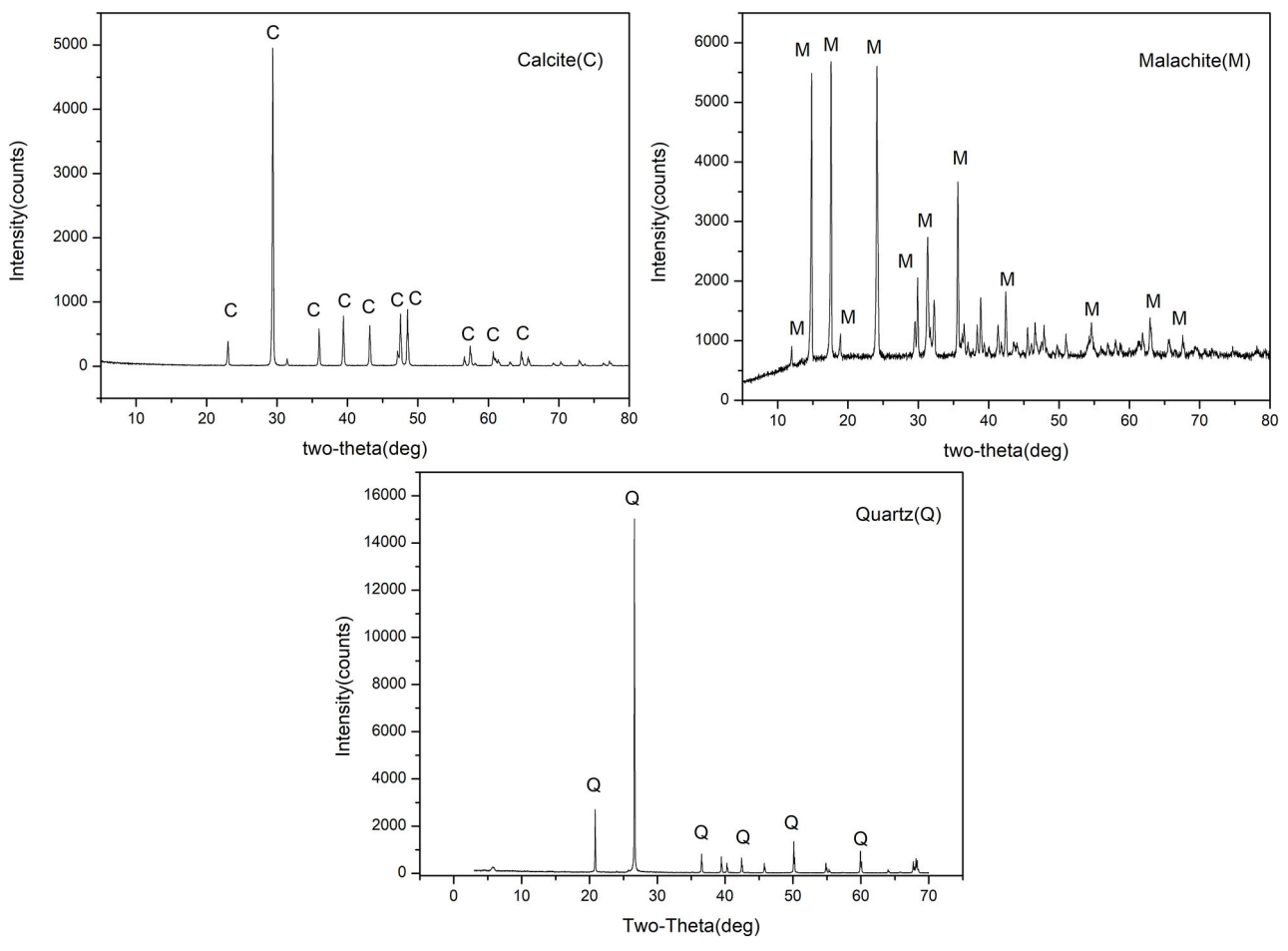

FIGURE 1 | XRD of malachite, quartz, and calcite.

adsorption mechanism of HPDO on malachite was discussed by XPS analysis.

EXPERIMENTAL

Materials

The XRD of malachite, quartz, and calcite were shown in **Figure 1**. The element analysis of malachite, quartz, and calcite were listed in **Table 1**. $-75 + 38\,\mu m$ fractions of single minerals were utilized in micro-flotation experiments, and $-5\,\mu m$ fractions were prepared for XPS measurement. Copper oxide ore from Jiangxi province in China was used in batch flotation. The most abundant copper oxide mineral was malachite (1.24%). The major gangue minerals in the ore were quartz (70.68%) and calcite (24.31%). BHA and SIBX were obtained from Zhuzhou Flotation Reagents & Chemicals Co., Ltd in China. DA was purchased in Aladdin Reagent Company. HPDO was synthesized in our laboratory. Before flotation, collectors were dispersed by NaOH or HCl aqueous solution through ultrasound.

Flotation

A micro-flotation experiment was implemented on a flotation machine (Jilin Province Prospecting Machinery Factory) with an effective cell volume of 40 mL. First, a single mineral was dispersed in water for 2 min. Secondly, Na_2CO_3 (1%) or HCl (1%) were introduced to adjust the pH of the pulp. Next, a collector was added for 2 min. Fourthly, the frother was conditioned for 1 min. Finally, the conditioned slurry was floated for 5 min. The flotation results of the single mineral were calculated from the dry weights of the concentrates and tails. The flowstep of the micro-flotation experiment is shown in **Figure 2**.

A batch-flotation test was conducted by operating a flotation machine (Jilin Province Prospecting Machinery Factory) with an effective cell volume of 750 mL. First, the copper oxide ore was ground to $-74\mu m$ (>80 wt%) in an XMB-70 rod mill. After that, the pH of the copper oxide ore for batch flotation was adjusted at around 8.0. Then, the collector was added for 3 min. The conditioned slurry was floated for 6 min. Finally, the concentrates and tailings were dried and weighed, and the amount of Cu was detected through chemical analyses. The flowstep of the batch-flotation experiment is shown in **Figure 3**.

XPS Analysis

XPS analyses were operated on a Thermo Scientific ESCALAB 250 Xi instrument using an Al Kα X-ray source; the condition was 200 W with pass energy of 20 eV. All samples were tested under vacuum pressure. In order to reveal the adsorption mechanism, the data of malachite before and after HPDO treatment were carefully collected and treated by using Thermo Scientific Advantage 4.52 software.

RESULTS AND DISCUSSION

Preparation and Characterization of HPDO

HPDO was prepared by using 2-hydroxy acetophenone, octanal, and $NH_2OH{\cdot}HCl$ as the starting materials. First, 2-hydroxy acetophenone and octanal were added to methanol (50 mL) using 10% NaOH (5 mL) as a catalyst and stirred at 60°C for 6 h. Next, $NH_2OH{\cdot}HCl$ (7.65 g, 0.11 mol) in H_2O (50 mL) were added to a mixture of 1-(2-hydroxyphenyl) dec-2-en-1-one. After this, NaOH solution (5%) was added to adjust the pH range of the solution to 7–8 and reacted for 4 h at 50°C. Finally, the brown crude mixture was obtained after removing the solvent. Product characterization: 1-(2-hydroxyphenyl) dec-2-en-1-one oxime (HPDO), yield of 56.35%. IR (film, cm^{-1}): 3,328 (-OH), 3,056 (aromatic C-H), 2,925 and 2,854 (CH_3- and -CH_2-), 1,628 (C=N), 1,607, 1,587, 1,501, and 1,466 (aromatic C-H), 1,254 (H-C=C), 750 (-CH_2-). ESI-MS (ESI^+): calculated for $C_{16}H_{23}NO_2$ 261.17; found 262.18 [M + H] (See **Figure 4**).

TABLE 1 | The compositions of malachite, calcite, and quartz samples analyzed by element analysis.

Composition (wt%)	CuO	CaO	SiO_2	CO_2	Others
Malachite	70.53	–	0.19	19.58	9.7
Quartz	–	–	98.12	–	1.88
Calcite	–	53.90	–	42.14	3.96

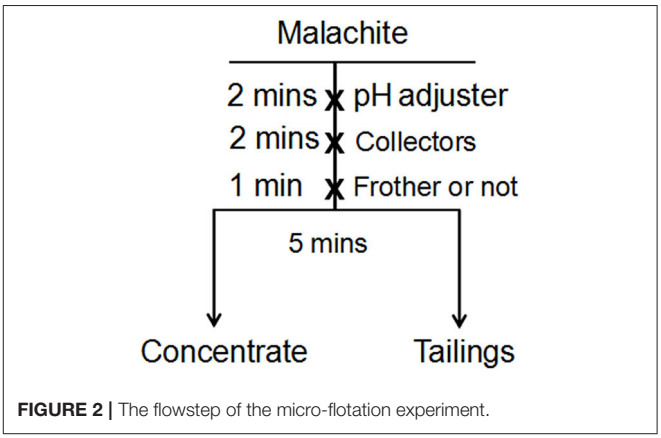

FIGURE 2 | The flowstep of the micro-flotation experiment.

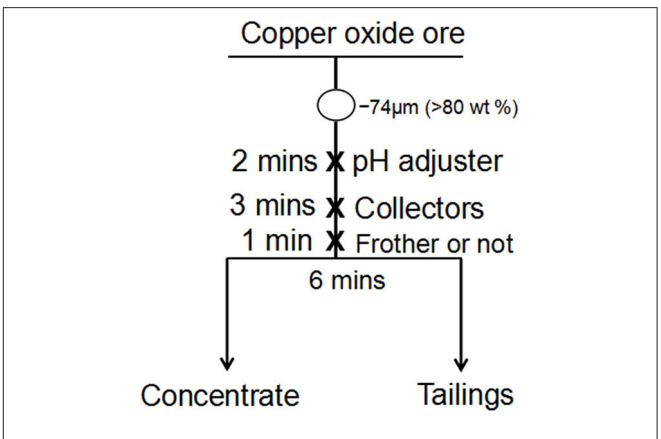

FIGURE 3 | The flowstep of the batch-flotation experiment.

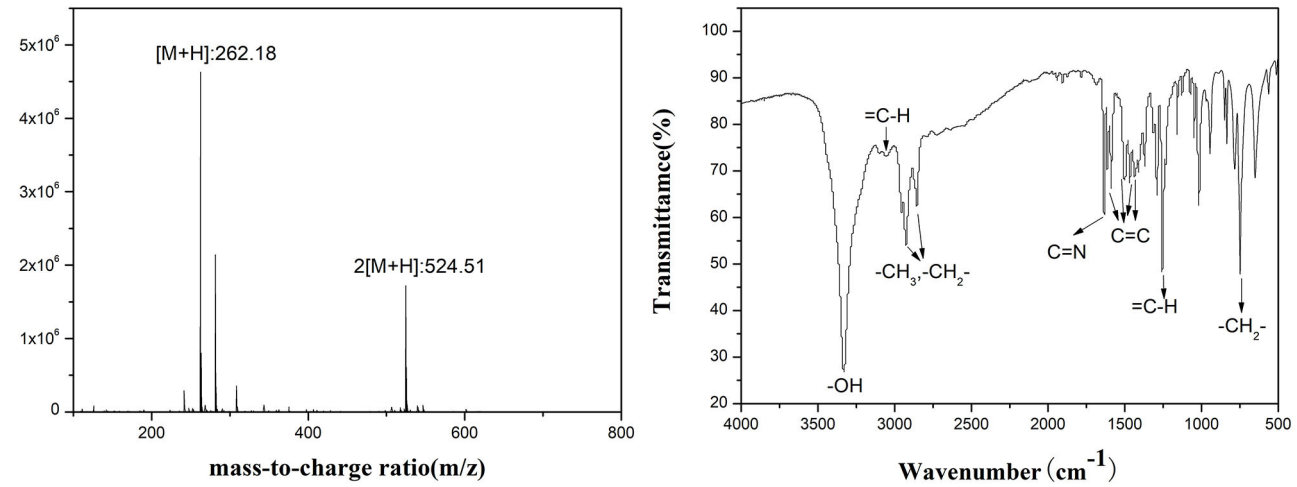

FIGURE 4 | FTIR and ESI-MS of HPDO.

Flotation Tests

The flotation results of malachite, quartz, and calcite by four collectors are shown in **Figure 5**. The effect of pH on the flotation recovery of malachite is given in **Figure 5A**. It shows that the best flotation results for HPDO, BHA, SIBX, and DA are obtained at a pH of 8, 8, 8, and 6, respectively. The maximum recovery of malachite with HPDO, SIBX, and DA are close to 95%, but the maximum recovery of malachite with BHA is just 48.0%. When the pH is <8, the recovery of malachite gradually increased by using HPDO, BHA, and SIBX as collectors. When the pH is more than 8, the recovery of malachite decreased swiftly, except with HPDO. These results indicate that HPDO has wider flotation pH values for malachite than BHA, SIBX, or DA. The effect of the collector dosage on the flotation recovery of malachite is shown in **Figure 5B**. The result of HPDO shows that the flotation recovery increases rapidly at an initial dosage ranging from 40 to 200 mg/L and almost reaches maximum (94%), and when the dosage of HPDO is more than 200 mg/L, the recovery slowly increases. SIBX shows a similar flotation performance to HPDO. As for DA, the recovery increases swiftly at low dosage, and DA can recover 94.6% malachite at a dosage of 70 mg/L. When the dosage of BHA is 200 mg/L, its recovery of malachite is just 48%. Even if the dosage of BHA is up to 1,000 mg/L, its recovery is just up to 65%. The effects of pH values on the flotation recoveries of quartz and calcite are listed in **Figures 5C,D**. It is clear from **Figures 5C,D** that HPDO, BHA, and SIBX show good selectivity to quartz or calcite, and those recoveries are <40%. While for DA, the recovery of calcite and quartz are more than 70% at a wide pH; it indicates that DA is not a good choice for a Cu-Ca-Si flotation system.

Micro-flotation tests showed that HPDO is a powerful collector for malachite, and achieves a satisfactory selectivity against quartz. While DA lacks selectivity to calcite and quart; SIBX needs additional Na_2S and foaming agent added; BHA has a weak collecting power. Compared with BHA, SIBX, and DA, HPDO exhibited an excellent collecting power for malachite without an additional reagent. This seems to indicate that our method of introducing a long carbon chain into a precursor with chelating ability is effective.

The batch flotation results of malachite with collectors are shown in **Table 2**. When the dosage of HPDO is 300 g/t through single roughing flow, the copper concentrate grade and recovery are 4.38% and 66.64%, respectively. With BHA (300 g/t), SIBX (300 g/t), or DA (100 g/t), the copper concentrate grade and recovery are not satisfied (detailed in **Table 2**). BHA and SIBX show poor recovery, and <35% copper is obtained. DA shows bad selectivity to Jiangxi copper oxide. It seems that HPDO has the potential to be used in flotation of copper oxide ores.

XPS Analyses of Malachite Before and After HPDO Adsorption

XPS was used to check the changes of surface compositions and atoms of malachite with or without HPDO treatment. The survey XPS spectra of malachite before and after HPDO modification are shown in **Figure 6A**. The relative changes in the elements on the malachite surface can prove whether the mineral surface is covered by collectors. It is obvious that the relative intensity of C1s and N1s increase after HPDO adsorption, while the relative intensity of O1s decreases. It indicates that the malachite surface had been coated by numerous HPDOs with a high concentration of O element. The nitrogen signal observed in **Figure 6A** is consistent with the flotation result of malachite in the HPDO solution.

In order to get more data for HPDO adsorption on a malachite surface, it is important to verify that high-resolution XPS spectra of N1s, O1s, and Cu2p before and after HPDO modification (Yumitori, 2000). Compared with malachite without any treatment, the binding energy of Cu2p3/2 and Cu2p1/2 of malachite-HPHO products both decreased by

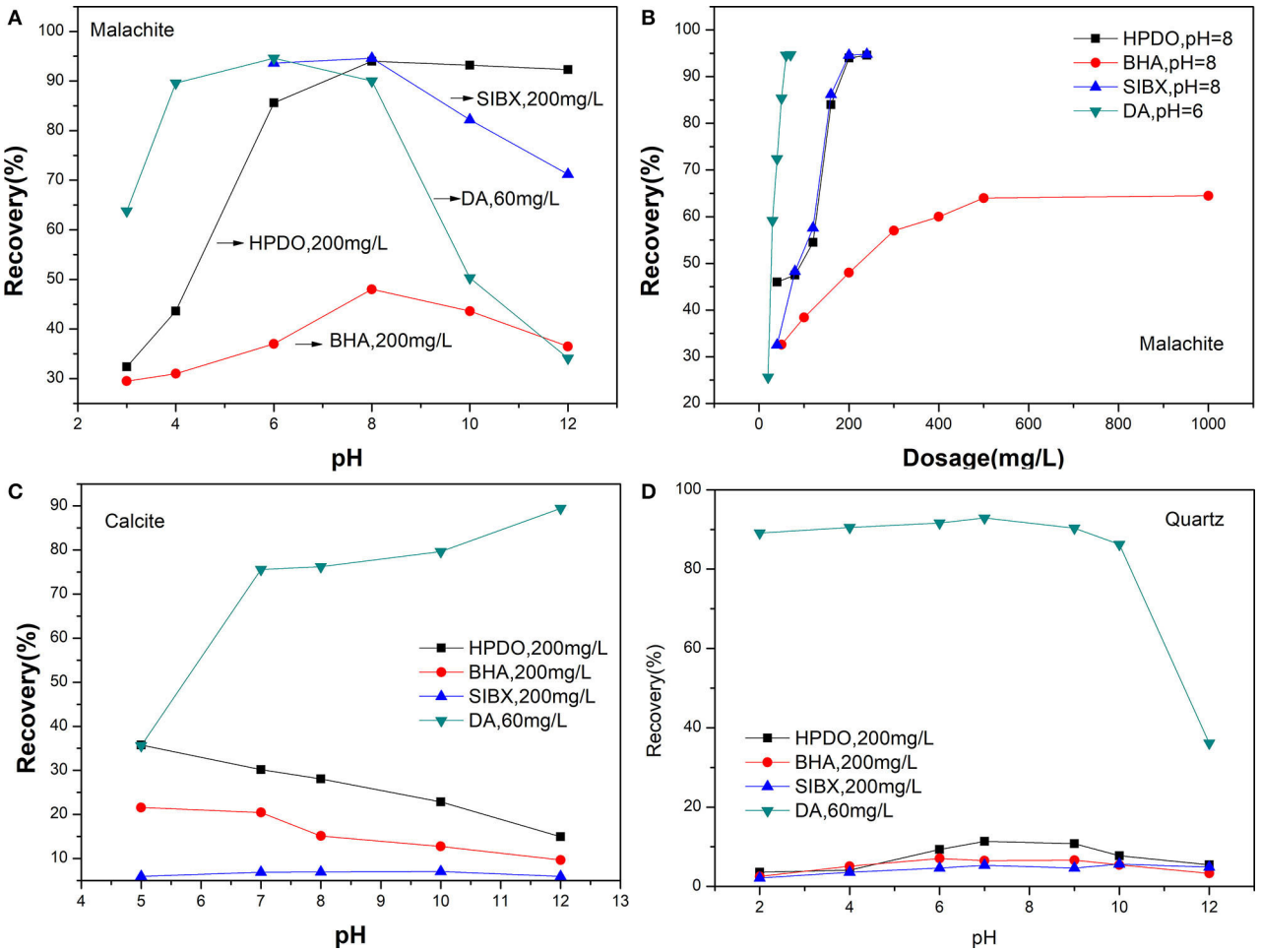

FIGURE 5 | (A) Flotation recovery of malachite with different collectors. **(B)** The effect of the collector dosage on the flotation recovery of malachite. **(C)** The effects of pH values on the flotation recoveries of quartz. **(D)** The effects of pH values on the flotation recoveries of calcite.

TABLE 2 | Flotation results of copper oxide with different collectors.

Collectors	Dosage (g/t)	MIBC (g/t)	Na2S (g/t)	Na2SiO3 (g/t)	Recovery (%)	Grade Cu (%)
HPDO	300	–	–	800	66.64	4.38
BHA	300	40	–	800	15.90	2.44
SIBX	300	40	200	800	34.26	3.25
DA	100	–	–	800	71.12	0.98

1.2 eV (See **Figure 6B**). It hinted that copper atoms received electron form electronegative HPDO. As can be seen in **Figure 6C**), the binding energy of N1s stands around 400.3 eV after HPDO adsorption on the malachite surface. The N1s signal offered clear evidence that HPDO reacted with Cu species on malachite. The inspection of the O1s XPS is very important to examine the chemical changes on malachite after HPDO modification (See **Figure 6D**). The decrease of the relative peak ratio of -OH with respect to CO_3^{2-} after HPDO treatment indicated the OH groups on malachite were replaced and coupled by HPDO, which was consistent with the analysis of Cu2p.

CONCLUSION

(1) HPDO was synthesized through aldol condensation and ammoximation reaction.
(2) The flotation results indicated that HPHO was a special collector for malachite flotation, whose collecting ability is improved as we desired. This indicates that HPDO has the potential to deal with low-grade copper ores in minerals engineering.
(3) XPS results offer clear evidence that OH groups on malachite surfaces were replaced and coupled by HPHO, and Cu(II) species was bound with HPDO.

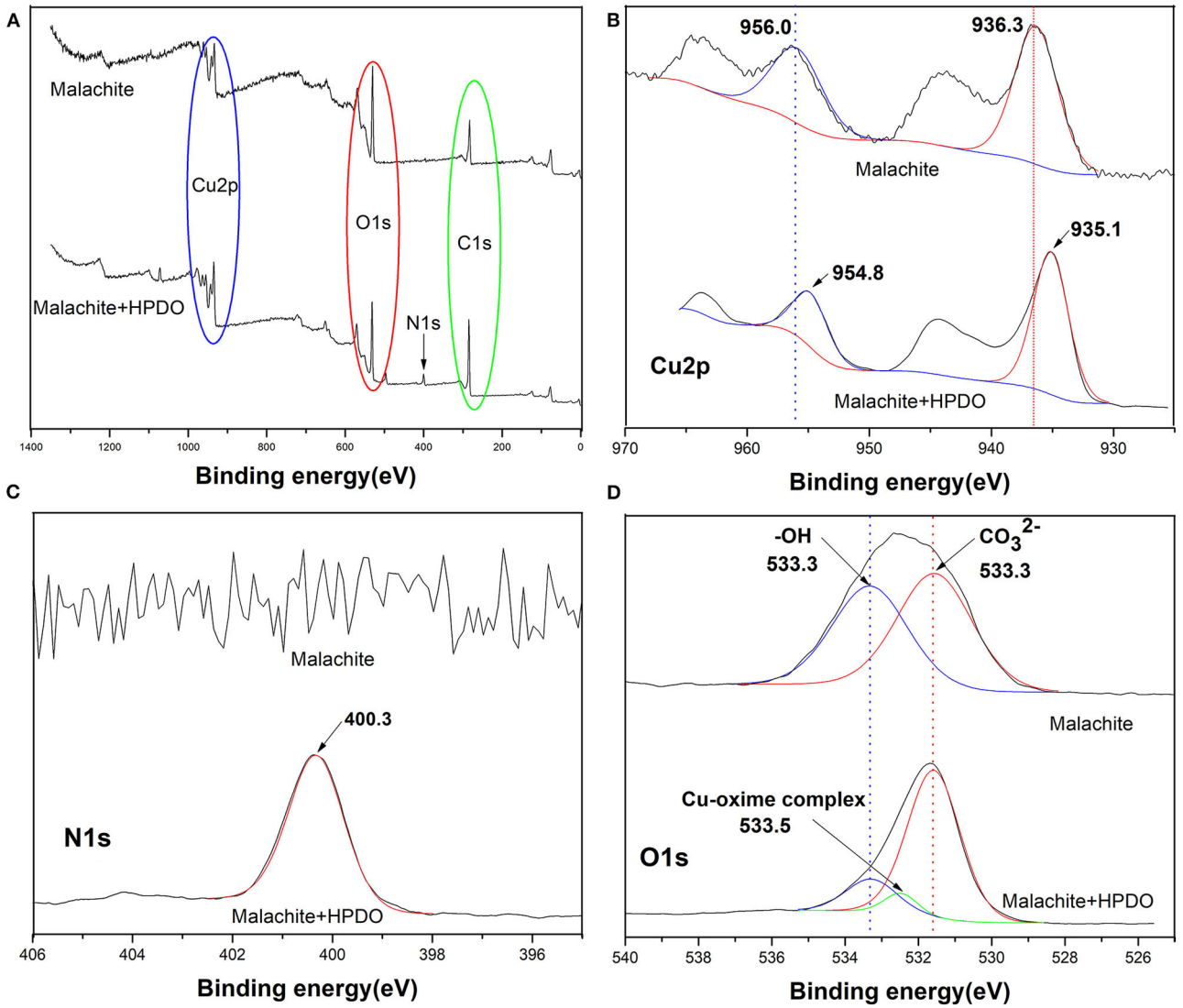

FIGURE 6 | (A) XPS spectra of malachite before and after HPDO adsorption. **(B)** XPS spectra of Cu 2p. **(C)** XPS spectra of N1s. **(D)** XPS spectra of O1s.

(4) In the future, the solution chemistry of HPDO and the changes in hydrophilicity and hydrophobicity of malachite before and after HPDO, and adsorption thermodynamics, will be more thoroughly studied.

DATA AVAILABILITY STATEMENT

All datasets presented in this study are included in the article/supplementary material.

AUTHOR CONTRIBUTIONS

LL performed the experiments, analyzed all the data, drafted all the figures, and prepared the manuscript. LY performed the experiments. FL revised the manuscript. All authors contributed to the article and approved the submitted version.

FUNDING

This research was supported by the National Natural Science Foundation of China (Nos. 21406097), the National Science Foundation for Post-doctoral Scientists of China (Nos. 2016M592118), the Jiangxi Province Post-doctoral Sustentation Fund of China (Nos. 2015KY11 and 2015RC17), the Jiangxi Province Funds for Distinguished Young Scientists (Nos. 20192BCB23016), and GDAS' Project of Science and Technology Development (2020GDASYL-20200302004).

ACKNOWLEDGMENTS

The authors thank Hong Zhong from Central South University in China for this research.

REFERENCES

Aslam, M., Kalyar, A., and Raza, A. (2019). Effect of separate zinc, copper and graphene oxides nanofillers on electrical properties of pva based composite strips. *J. Electron. Mater.* 48, 1116–1121. doi: 10.1007/s11664-018-6793-5

Chan, A., Salsali, H., and Mcbean, E. (2014). Heavy metal removal (copper and zinc) in secondary effluent from wastewater treatment plants by microalgae. *ACS Sustain. Chem. Eng.* 2, 130–137. doi: 10.1021/sc400289z

Corin, K., Kalichini, M., Connor, C., and Simukanga, S. (2017). The recovery of oxide copper minerals from a complex copper ore by sulphidisation. *Miner. Eng.*102, 15–17. doi: 10.1016/j.mineng.2016.11.011

Cui, C., Xian, J., Wen, S., and Wang, Y. (2015). Investigation on copper flotation from a complex copper ore, Yunnan Province. *Adv. Mat. Res.* 1094, 389–392. doi: 10.4028/www.scientific.net/AMR.1094.389

Elshkaki, A., Graedel, T., Ciacci, L., and Reck, B. (2016). Copper demand, supply, and associated energy use to 2050. *Glob. Environ. Change Hum. Policy Dimens.* 39, 305–315. doi: 10.1016/j.gloenvcha.2016.06.006

Feng, Q., Zhao, W., and Wen, S. (2018a). Ammonia modification for enhancing adsorption of sulfide species onto malachite surfaces and implications for flotation. *J. Alloys Compd.* 744, 301–309. doi: 10.1016/j.jallcom.2018.02.056

Feng, Q., Zhao, W., and Wen, S. (2018b). Surface modification of malachite with ethanediamine and its effect on sulfidization flotation. *Appl. Surf. Sci.* 436, 823–831. doi: 10.1016/j.apsusc.2017.12.113

Han, J., Xiao, J., Qin, W., and Chen, D., Liu, W. (2017). Copper recovery from yulong complex copper oxide ore by flotation and magnetic separation. *JOM* 69, 1563–1569. doi: 10.1007/s11837-017-2383-x

Hope, G., Buckley, A., Parker, G., Numprasanthai, A., Woods, R., and Mclean, J. (2012). The interaction of n -octanohydroxamate with chrysocolla and oxide copper surfaces. *Miner. Eng.* 36, 2–11. doi: 10.1016/j.mineng.2012.01.013

Huang, Y., Liu, G., Liu, J., Yang, X., and Zhang, Z. (2018). Thiadiazole-thione surfactants: preparation, flotation performance and adsorption mechanism to malachite. *J. Ind. Eng. Chem.* 67, 99–108. doi: 10.1016/j.jiec.2018.06.020

Hussain, M., Feng, Y., Hu, L., Deng, Q., Zhang, X., and Xiong, Y. (2018). Copper-catalyzed oxidative difunctionalization of terminal unactivated alkenes. *J. Org. Chem.* 83, 7852–7859. doi: 10.1021/acs.joc.8b00729

Li, F., Zhong, H., Xu, H., Jia, H., and Liu, G. (2015). Flotation behavior and adsorption mechanism of α-hydroxyoctylphosphinic acid to malachite. *Miner. Eng.* 71, 188–193. doi: 10.1016/j.mineng.2014.11.013

Li, L., Zhao, J., Sun, Y., Yu, F., and Ma, J. (2019a). Ionically cross-linked sodium alginate/?-carrageenan double-network gel beads with low-swelling, enhanced mechanical properties, and excellent adsorption performance. *Chem. Eng. J.* 372, 1091–1103. doi: 10.1016/j.cej.2019.05.007

Li, L., Zhao, J., Xiao, Y., Huang, Z., and Guo, Z., Li, F., et al. (2019b). Flotation performance and adsorption mechanism of malachite with tert-butylsalicylaldoxime. *Sep. Purif. Technol.* 210, 843–849. doi: 10.1016/j.seppur.2018.08.073

Li, Z., Rao, F., García, R., Li, H., and Song, S. (2018). Partial replacement of sodium oleate using alcohols with different chain structures in malachite flotation. *Miner. Eng.*127, 185–190. doi: 10.1016/j.mineng.2018.08.022

Li, Z., Rao, F., Song, S., Uribe-Salas, A., and López-Valdivieso, A. (2019). Effects of common ions on adsorption and flotation of malachite with salicylaldoximes. *Colloid Surf. A Physicochem. Eng. Asp.* 577, 421–428. doi: 10.1016/j.colsurfa.2019.06.004

Liu, G., Huang, Y., Qu, X., Xiao, J., Yang, X., and Xu, Z. (2016). Understanding the hydrophobic mechanism of 3-hexyl-4-amino-1, 2, 4-triazole-5-thione to malachite by ToF-SIMS, XPS, FTIR, contact angle, zeta potential and micro-flotation. *Colloid Surf. A Physicochem. Eng. Asp.* 503, 34–42. doi: 10.1016/j.colsurfa.2016.05.028

Mao, Y., Wen, S., and Fang, J. (2014). Studying on oxide copper ore flotation with different collectors. *Adv. Mat. Res.* 1010–1012, 1626–1629. doi: 10.4028/www.scientific.net/AMR.1010-1012.1626

Marion, C., Jordens, A., Li, R., Rudolph, M., and Waters, K. (2017). An evaluation of hydroxamate collectors for malachite flotation. *Sep. Purif. Technol.* 183, 258–269. doi: 10.1016/j.seppur.2017.02.056

Park, K., Park, S., Choi, J., Kim, G., Tong, M., and Kim, H. (2016). Influence of excess sulfide ions on the malachite-bubble interaction in the presence of thiol-collector. *Sep. Purif. Technol.* 168, 1–7. doi: 10.1016/j.seppur.2016.04.053

Qin, J., Liu, G., Fan, H., and Tan, W. (2018). The hydrophobic mechanism of di(2-ethylhexyl) phosphoric acid to hemimorphite flotation. *Colloid Surf. A Physicochem. Eng. Asp.* 545, 68–77. doi: 10.1016/j.colsurfa.2018.02.058

Rao, J., Raizada, A., Ganguly, D., Mankad, M., Satayanarayana, S., and Madhu, G. (2015). Investigation of structural and electrical properties of novel CuO-PVA nanocomposite films. *J. Mater. Sci.*50, 7064–7074. doi: 10.1007/s10853-015-9261-0

Shengo, L., Gaydardzhiev, S., and Kalenga, N. (2014). Assessment of water quality effects on flotation of copper–cobalt oxide ore. *Miner. Eng.* 65, 145–148. doi: 10.1016/j.mineng.2014.06.005

Snoussi, L., Ouerfelli, N., Sharma, K., Narcisa, V., Chamkha, A., and Guizani, A. (2018). Numerical simulation of nanofluids for improved cooling efficiency in a 3D copper microchannel heat sink (MCHS). *Phys. Chem. Liq.* 56, 311–331. doi: 10.1080/00319104.2017.1336237

Wang, Y., Li, J., Gao, Y., Yang, Y., Gao, Y., and Xu, Z. (2020). Removal of aluminum from rare-earth leaching solutions via a complexation-precipitation process. *Hydrometallurgy*. 191:105220. doi: 10.1016/j.hydromet.2019.105220

Wang, Y., Wang, R., Qiu, G., Zhou, H., Xie, W., and Liu, J. (2019). Ortho-amide-directed 2,4-dibromohydration of conjugated enynes. *Org. Chem. Front.* 6, 2471–2479. doi: 10.1039/C9QO00540D

Xu, H., Zhong, H., Wang, S., Niu, Y., and Liu, G. (2014). Synthesis of 2-ethyl-2-hexenal oxime and its flotation performance for copper ore. *Miner. Eng.* 66, 173–180. doi: 10.1016/j.mineng.2014.06.011

Yang, S., Pelton, R., Raegen, A., Montgomery, M., and Dalnoki-Veress, K. (2011). Nanoparticle flotation collectors: mechanisms behind a new technology. *Langmuir* 27, 10438–10446. doi: 10.1021/la2016534

Yumitori, S. (2000). Correlation of C1s chemical state intensities with the O1s intensity in the XPS analysis of anodically oxidized glass-like carbon samples. *J. Mater. Sci.* 35, 139–146. doi: 10.1023/A:1004761103919

Conflict of Interest: The authors declare that the research was conducted in the absence of any commercial or financial relationships that could be construed as a potential conflict of interest.

frontiers in Chemistry

ORIGINAL RESEARCH
published: 03 December 2020
doi: 10.3389/fchem.2020.598752

Leaching Process of Weathered Crust Elution-Deposited Rare Earth Ore With Formate Salts

Zhuo Chen[1], *Zhenyue Zhang*[1,2]* *and Ruan Chi*[1,2]

[1] School of XingFa Mining Engineering, Wuhan Institute of Technology, Wuhan, China, [2] Key Laboratory for Green Chemical Process of Ministry of Education, Wuhan Institute of Technology, Wuhan, China

To strengthen the rare earth leaching process and weaken the hydration of clay minerals for preventing landslides, it is of great importance to adopt a green and sustainable leaching agent in the industry. In this work, the leaching process of weathered crust elution-deposited rare earth ores with formate salts (ammonium formate, potassium formate, and sodium formate) was investigated. The effects of formate salts on the linear swelling ratio and zeta potential of the clay minerals were studied. The experimental results showed that ammonium formate could effectively recover the rare earth elements from weathered crust elution-deposited rare earth as well as inhibit the leaching of impurity aluminum. At room temperature, when the ammonium formate concentration was 1% wt, the leaching efficiencies of rare earth and aluminum were 87 and 37%, respectively. Compared with traditional inorganic ammonium salts, the inhibition effect of impurity aluminum was obvious. In addition, the results of the linear swelling ratio in the clay minerals showed that the inhibit ability of formate salts on the hydration of clay minerals enhanced with the increase of the formate concentration, and the order of the inhabitation on the clay minerals followed: 1% ammonium formate > 1.5% potassium formate > 2.5% sodium formate > distilled water. Based on the double layer theory, ammonium formate and potassium formate could effectively compress clay mineral particles to avoid water intake, which could increase the interaction between clay mineral particles and greatly reduce the electronegative property of the clay minerals, so as to effectively reduce the surface hydration of clay minerals to decrease the swelling of rare earth ore. The results of this experiment have important and practical significance in guiding the prevention of landslides, promoting the *in-situ* leaching technology, and effectively protecting the ecological environment in mining areas.

Keywords: weathered crust elution-deposited rare earth ore, formate salts, leaching process, rare earth, aluminum, swelling

OPEN ACCESS

Edited by:
Shenxu Bao,
Wuhan University of Technology, China

Reviewed by:
Hongbo Zhao,
Central South University, China
Haisheng Han,
Central South University, China

***Correspondence:**
Zhenyue Zhang
zhenyuezhangemail@uni.edu;
zyzxmu@126.com

Specialty section:
This article was submitted to Green and Sustainable Chemistry, a section of the journal Frontiers in Chemistry

Received: *25 August 2020*
Accepted: *05 October 2020*
Published: *03 December 2020*

Citation:
Chen Z, Zhang Z and Chi R (2020) Leaching Process of Weathered Crust Elution-Deposited Rare Earth Ore With Formate Salts. Front. Chem. 8:598752. doi: 10.3389/fchem.2020.598752

INTRODUCTION

Medium and heavy rare earth elements are widely adopted in the material field of the high-tech and national defense industry which has led to the supplement growth of this strategic resource (Kynicky et al., 2012; Simandl, 2014). Weathered crust elution-deposited rare earth ores are rich in medium and heavy rare earth elements, which makes up for the shortage of medium and heavy rare earth elements in mineral-type rare earth minerals (Zhang et al., 2016).

FIGURE 1 | The landslide scene in the weathered crust elution-deposited rare earth ore.

These weathered crust elution-deposited rare earth ores are distributed in the southern part of China. The rare earth elements mainly exist as hydrated ions or hydroxyl hydrated ions which are adsorbed on the surface of the clay mineral in this kind of rare earth ore (He et al., 2016a). Based on the special characteristics of the weathered crust elution-deposited rare earth ore, conventional beneficiation technology cannot separate and enrich rare earth elements. Therefore, the rare earth elements are recovered under the ion exchange law with electrolytes. The leaching chemical reaction with mono valence salts is written as (Chi and Tian, 2006; Li, 2014; He et al., 2016b):

$$[Al_4(Si_4O_{10})(OH)_8]_m \cdot nRE^{3+}_{(S)} + 3nA^{+}_{(aq)} \rightleftharpoons [Al_4(Si_4O_{10})(OH)_8]_m \cdot (A^{+}_{(aq)})_{3n(s)} + nRE^{3+}_{(aq)} \quad (1)$$

where s represents the solid phase, and a represents the liquid phase.

After decades of development, ammonium chloride, and ammonium sulfate are mainly used as leaching agents to recover rare earth elements from the ore by the *in-situ* leaching technology in the industry at present.

However, there is normally high impurity content in lixivium which raises the cost of following industrial procedures. Besides, due to the improper injection of leaching agents, it would lead to the swelling of clay minerals under the physical and chemical function in the weathered crust elution-deposited rare earth ore body, which cause landslides and other geological disasters. An example landslide is shown in **Figure 1**. These problems would affect the mine safety and reduce the rare earth recovery efficiency.

To better improve the rare earth leaching efficiency and decrease the risks in the mining area, many experts have undertaken a great deal of research on the selection of new types of leaching agents which can effectively recover rare earth elements and reduce the swelling of clay minerals. Zhang et al. carried out research on the field of the swelling properties in clay minerals within the various layers of weathered crust elution-deposited ore bodies and found that the clay minerals in the humus layer were the most prone to expansion (Zhang et al., 2018a,b). Chen et al. found that magnesium salts can recover rare earth elements and inhibit the swelling of clay minerals effectively in the leaching process (Chen et al., 2018a,b, 2020). Norrish et al. found that with the decrease of electrolyte concentration in the solution, the intergranular spacing of the clay minerals would increase, which led to the swelling phenomenon (Norrish, 1954). Jiang et al. studied the inhibiting effect of sodium methyl silicate on shale expansion, and found that methyl silicate ions could adsorb on the edges and angles of clay mineral particles, making the hydrophilic surface of the clay mineral particles hydrophobic, thus preventing the water molecules from entering the interlayer of the clay mineral particles (Jiang et al., 2014). Ammonium acetate can readily exchange with exchangeable cations on the surface of clay minerals, and the molecular weight of acetic acid ions is small and electronegative, which can be absorbed between the clay mineral particles through electrostatic attraction and hydrogen bonds, thus reducing the tendency of clay minerals to absorb water (Erwan et al., 2011).

Although some achievements have been made in the development and research of new leaching agents to recover the rare earth elements effectively and environmentally, there are still some problems to be solved. Fomate salts can effectively improve the leaching rate of rare earth to a greater extent, while the inhibition on aluminum leaching by formate salts has been discovered. Meanwhile, the formate can promote the permeability of the leaching solution in the rare earth ore body. The purpose of this paper is to explore the leaching kinetic process of rare earth and aluminum from weathered crust elution-deposited rare earth ores with three formate salts (ammonium formate, potassium formate, and sodium formate), and to study the swelling properties of clay minerals during the leaching process. It could provide a new method to extract rare earth from ores with high efficiency, low consumption, and environmental protection, providing a theoretical basis for the industrial application of new leaching agents.

EXPERIMENTS

Experimental Samples

The rare earth ore samples used in the experiments were collected from weathered crust elution-deposited rare earth ore in the Jiangxi Province, China. The main chemical composition of the rare earth ore was determined by x-ray fluorescence (Axios advanced, Panalytical B.V.), and the results of the rare earth ore sample is listed in **Table 1**.

It can be seen from **Table 1** that the main components are SiO_2 and Al_2O_3, accounting for 66.48 and 15.23% in the rare earth ore. The content of rare earth in the ore sample is 0.14%. Aluminum is the main impurity in the leaching lixivium. The existence of impurities will increase the difficulty of rare earth recovery and reduce the purity of rare earth productions.

TABLE 1 | Main chemical composition of the rare earth ores (wt.%).

Component	REO	Al_2O_3	MnO_2	ZnO	CaO	MgO	K_2O	SiO_2
Content	0.14	15.23	0.01	0.01	0.02	0.62	3.54	66.48
Component	**SO_3**	**TiO_2**	**Fe_2O_3**	**Rb_2O**	**SrO**	**ZrO_2**	**BaO**	**Loss**
Content	0.04	1.40	4.07	0.01	0.01	0.02	0.04	8.36

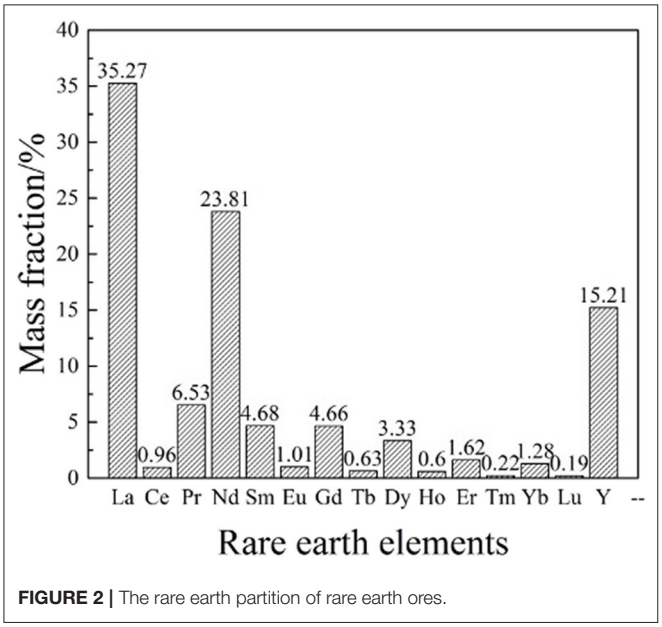

FIGURE 2 | The rare earth partition of rare earth ores.

Besides, the distribution of weathered crust elution-deposited rare earth ore is one of the important indexes to measure its industrial value. The rare earth partition of exchangeable phase state in the ore sample was measured by inductively coupled plasma mass spectrometry (ICP-MS, Agilent 7700x, Agilent Technologies Inc.) and the result is shown in **Figure 2**.

It can be seen from **Figure 2** that the total content of La_2O_3 and Nd_2O_3 account for 88.71% of the total amount of light rare earth and rare earth oxides, while the content of Y_2O_3 accounts for 45.63% of the medium heavy rare earth, indicating that the rare earth ore sample is mainly rich in heavy rare earth elements and has great commercial value.

Ammonium formate, potassium formate, sodium formate, and other chemical reagents used in the experiments were of analytical (AR) grade and were purchased from the Shanghai Chemical Reagent Company (Shanghai, China).

Experimental Device and Method

The Leaching Experiments of Weathered Crust Elution-Deposited Rare Earth Ore

In this experiment, the rare earth ore samples were fully mixed evenly and the quartering method was adopted for sampling. Each group of 250 g ore samples were weighed into the leaching column and the surface was lined with filter paper to make the leaching agent seepage even. The formate salts solutions with different concentrations were added into the glass column slowly according to the liquid-solid ratio of 2:1 through the controlled leaching device. By recording the time, the centrifuge tubes were used to receive the mother liquid of rare earth at certain intervals. The rare earth and aluminum contents were analyzed by ICP-MS and the rare earth and aluminum leaching efficiencies were calculated. The leaching device is shown in **Figure 3**. The rare earth leaching or aluminum efficiency was calculated according to the follow formula:

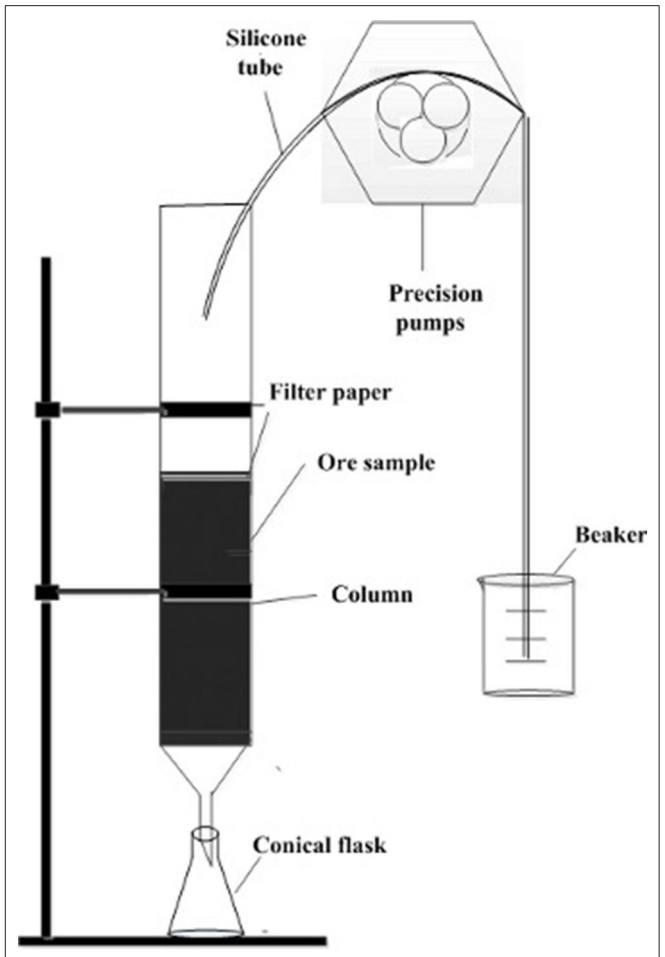

FIGURE 3 | The leaching device of the weathered crust elution-deposited rare earth ore.

$$L(\%) = \frac{(C \times V)}{W \times C_S} \times 100\%$$

where L is the rare earth or aluminum leaching efficiency/%, C is the concentration of rare earth or aluminum in leaching lixivium/g/L^{-1}, V is the volume of leaching lixivium/L, W is the weight of rare earth ore sample/g, and Cs is the content of rare earth or aluminum in the ionic phase of the ore samples/%.

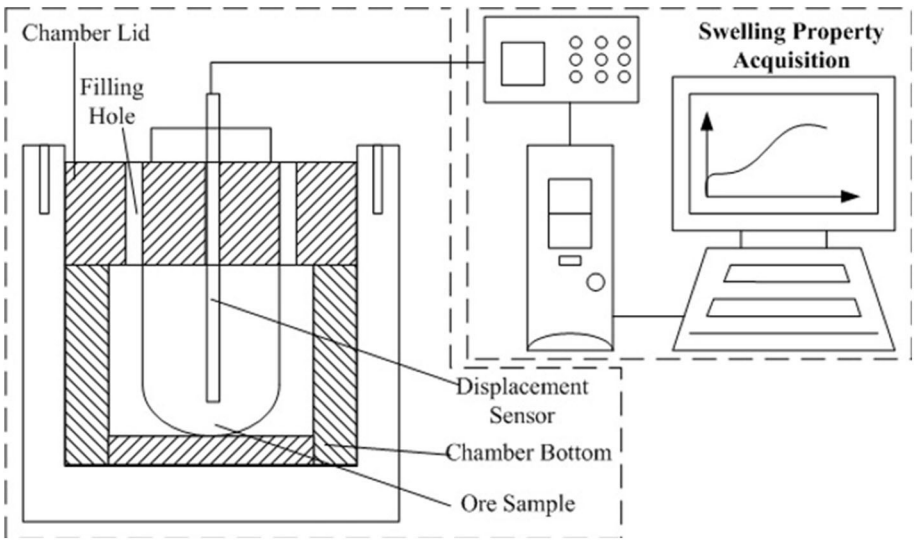

FIGURE 4 | Schematic diagram of PCY intelligent dilatometer.

The Swelling Experiments of Weathered Crust Elution-Deposited Rare Earth Ore

The swelling of the clay minerals was conducted using a PCY intelligent dilatometer, with the schematic diagram shown in **Figure 4**.

The swelling ratio of the ore sample was measured by the following equation:

$$\delta = \frac{\Delta H}{H_0} \times 100 \quad (2)$$

where ΔH is the change in height, and H_0 is the initial height of the ore sample.

RESULTS AND DISCUSSIONS

Effects of Formate Salts on the Rare Earth Leaching of Weathered Crust Elution-Deposited Rare Earth Ore

To investigate the effects of formate salts on the leaching kinetics process of rare earth, various concentrations of ammonium formate, potassium formate, and sodium formate were used as leaching agents, respectively, to undertake leaching experiments under the condition of 2:1 for liquid/solid (mL/g) and pH 5.5–6.0 at room temperature. The results are presented in **Figure 5**.

It can be seen from **Figure 5**, with the increase of the concentration in the formate salts, the rare earth leaching rate accelerated. The leaching efficiencies of rare earth increased with the time passed, and the equilibrium was maintained until the maximum leaching efficiencies were reached. As the formate salts solution concentration continued to increase, the leaching rate of rare earth slowed down significantly. With the increase of the concentration of formate salts solution, the leaching rate of rare earth was faster and the time to reach the leaching equilibrium was shorter. The main reason is that the cation (NH_4^+, Na^+, and K^+) concentration difference between the flow center of the leaching solution (formate salts) and the surface of the clay mineral particle grows larger as the cation concentration in the leaching agent increases. The diffusion ability of the formate salts solution would increase, and the enhancement of the cation concentration will increase the strength of the ion exchange reaction between NH_4^+, K^+, Na^+, and RE^{3+}, thus speeding up the leaching process (Li et al., 2009; Qiu et al., 2014). In addition, the higher the formate salts solution concentration, the greater its viscosity, and the slower the penetration rate of formate salts into the ore body. The effects of different formate salt concentrations on the leaching efficiencies of rare earth are shown in **Figure 6**.

According to **Figure 6**, when ammonium formate, potassium formate, and sodium formate were used as leaching agents, respectively, the rare earth leaching efficiencies gradually increased with the increase of cation (NH_4^+, Na^+, and K^+) concentration in the leaching agent. When the concentration of ammonium ion, potassium ion, and sodium ion reached 1% wt, 1.5% and 2.5% wt, respectively, the rare earth leaching efficiencies reached a relatively large value, which was 87, 80, and 79%, respectively. It is obvious that the order of the rare earth leaching efficiencies followed $NH_4^+ > Na^+ > K^+$ under the same mass concentrations in the leaching experiments. The cation concentration of formate salts continued to increase, and then maintained a relatively stable trend, and the rare earth leaching efficiencies did not increase significantly. This is mainly due to the fact that formic acid ions can cooperate with rare earth ions well and form complexes with rare earth ions, which can be easily separated and have good water-solubility, which can encourage rare earth ions to leave the clay minerals surface and enter into the leaching solution.

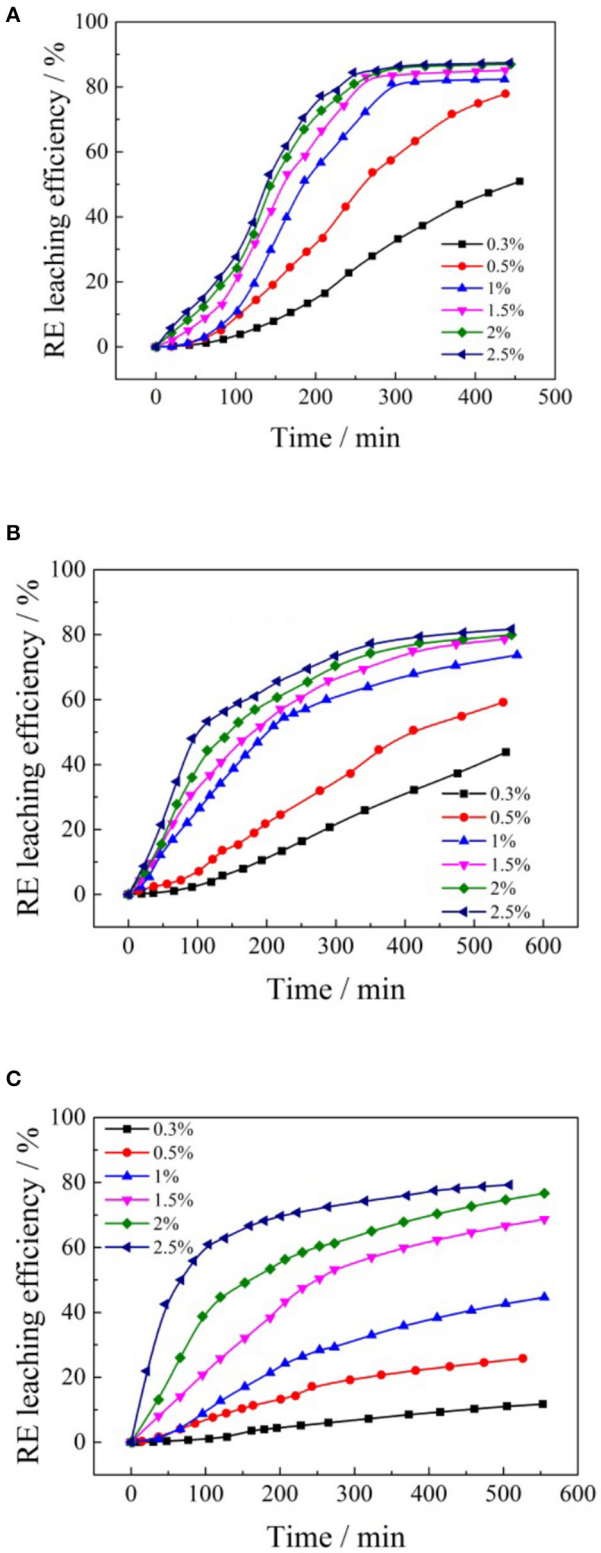

FIGURE 5 | Leaching kinetic curves of different concentrations formate salts for rare earth: **(A)** ammonium formate; **(B)** potassium formate; **(C)** sodium formate.

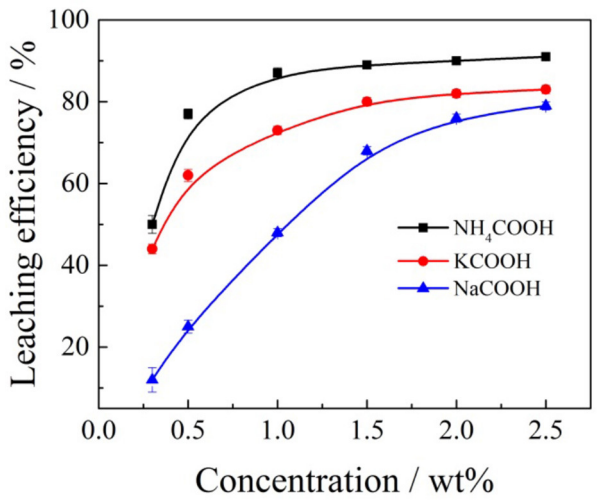

FIGURE 6 | Effects of formate salts concentration on the rare earth leaching efficiency.

Effects of Formate Salts on the Aluminum Leaching of Weathered Crust Elution-Deposited Rare Earth Ore

To investigate the effects of formate salts on the leaching kinetics process of aluminum, various concentrations of ammonium formate, potassium formate, and sodium formate were used as leaching agents to undertake leaching experiments under the condition of 2:1 for liquid/solid (mL/g) and pH 5.5–6.0 of the leaching agent at room temperature. The results are presented in **Figure 7**.

It can be seen from **Figure 7** that the whole leaching process of aluminum can be divided into two stages. In the initial stage of the ion exchange reaction, the leaching rate of aluminum increases rapidly with time. As the cation concentrations of formate salt increased, the leaching rate of aluminum increased obviously, and the time required to reach the leaching equilibrium decreased. In the same leaching period, more ammonium ions participated in the reaction, and the leaching efficiency of aluminum was improved. The effects of cation concentrations of the formate salts on the leaching efficiencies of aluminum are shown in **Figure 8**.

According to **Figure 8**, when ammonium formate, potassium formate, and sodium formate were used as leaching agents, respectively, the aluminum leaching efficiencies gradually increased with the increase of cation (NH_4^+, Na^+, and K^+) concentration in the formate salts leaching agent. When the concentration of ammonium, potassium, and sodium ions reached 1, 1.5, and 2.5% wt, respectively, the aluminum leaching efficiencies reached a relatively large value, which was 37, 39, and 55%, respectively. The cation concentration of formate salts continued to increase, and then maintained a relatively stable trend. This is the main reason the formate ions in the leaching solutions have stronger polarity to transform ion-exchangeable

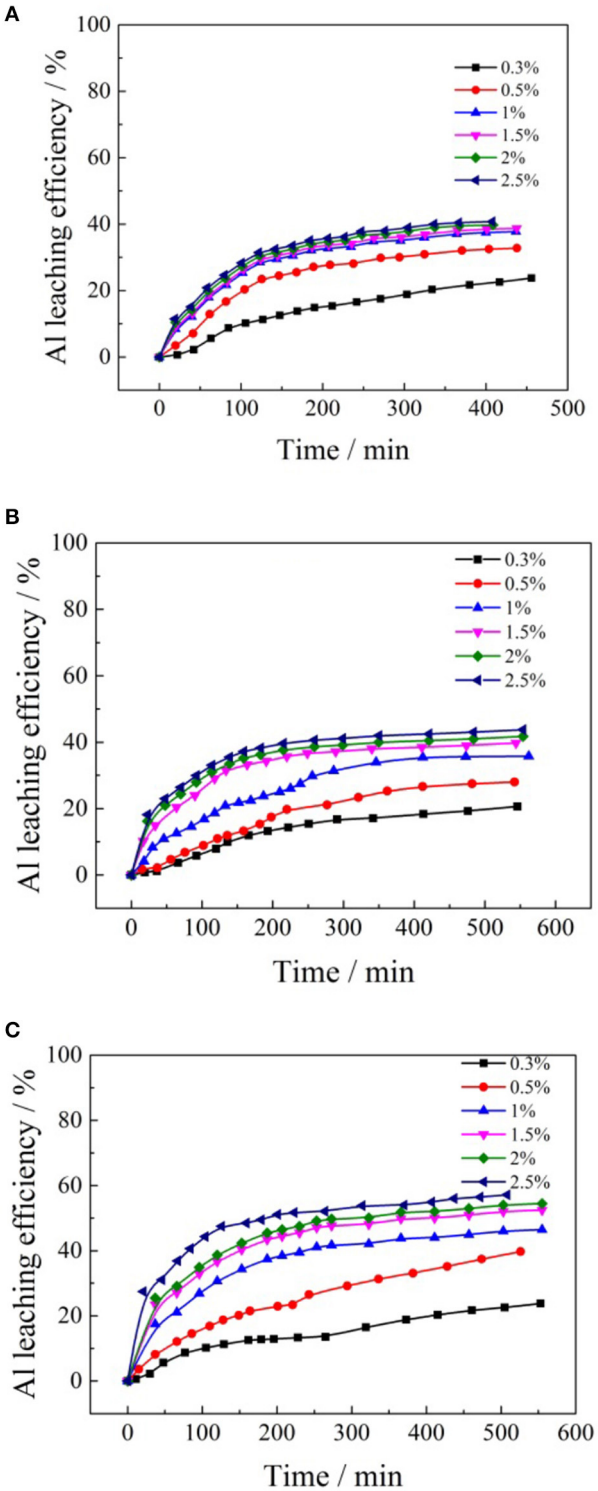

FIGURE 7 | Leaching kinetics of different concentrations formate salts for aluminum: **(A)** ammonium formate; **(B)** potassium formate; **(C)** sodium formate.

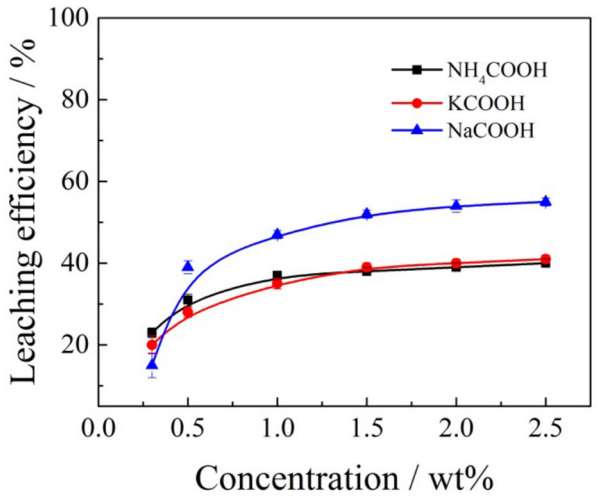

FIGURE 8 | Effects of formate salts concentration on the aluminum leaching efficiency.

aluminum into inorganic hydroxyl aluminum and other forms to be retained in the tailing ore samples (Li et al., 2013). Besides, because ammonium formate can ionize more formate ions in the leaching solution, the content of ionic phase aluminum in the lixivium is relatively lower. Therefore, the ammonium formate shows a better inhibiting effect on the aluminum. The impurity aluminum in the lixivium is thus reduced conspicuously, which will be beneficial in improving the efficiency and reducing the cost of the following purification of impurities and the purity of the final production.

Effects of Formate Salts on the Swelling of Clay Minerals in the Weathered Crust Elution-Deposited Rare Earth Ores

To understand the effects of the formate salt concentrations on the swelling of the clay minerals, the ore samples were subjected to various concentrations of ammonium formate, potassium formate, and sodium formate. Swelling kinetic curves were constructed using the experimental data, and the results are displayed in **Figure 9**.

As shown in **Figure 9**, the clay minerals of the ore sample expanded rapidly after it made contact with the formate solutions of different concentrations. And the swelling ratio of the clay minerals reached a stable equilibrium state within 50 min. After that, the linear expansion rate of the clay minerals remained almost unchanged in the following stage. The effects of cation concentrations of the formate salts on the final swelling ratio of clay minerals in the weathered crust elution-deposited rare earth ore are shown in **Figure 10**.

According to **Figure 10**, when ammonium formate, potassium formate, and sodium formate were used to immerse the ore samples to investigate the swelling properties, it was obvious that the swelling ratio decreased gradually with the enhancement of the formate salt concentration. Under the same cation concentrations of the formate salts, the order of the inhibiting swelling ability followed: formate ammonium > formate potassium > formate sodium. The ability of the formate salts to inhibit the hydration of clay minerals in the weathered

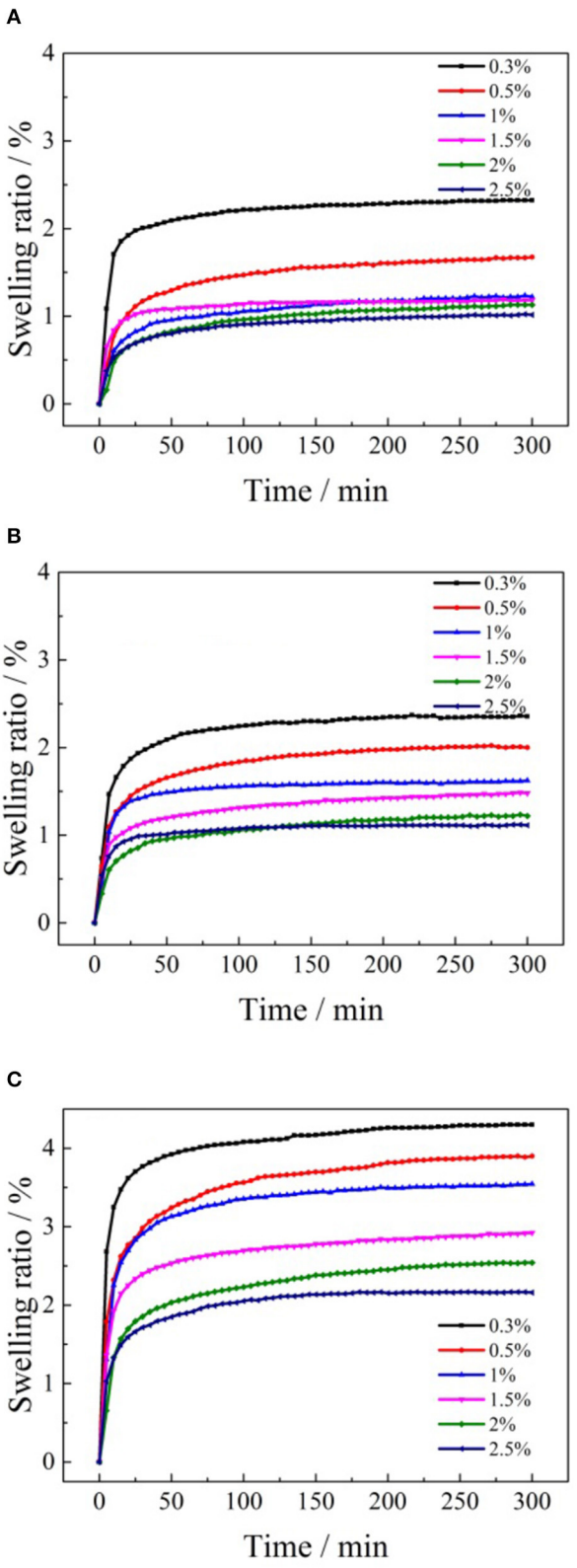

FIGURE 9 | Swelling kinetic curves of ore samples in various formate salt concentrations: **(A)** ammonium formate; **(B)** potassium formate; **(C)** sodium formate.

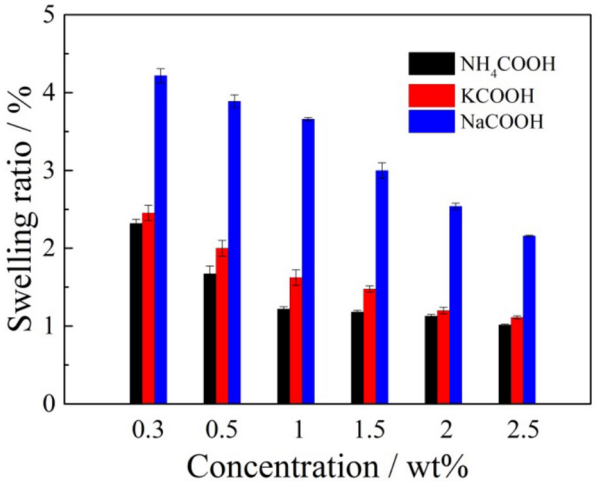

FIGURE 10 | Effects of formate salts on the swelling ratio of clay minerals.

TABLE 2 | Cation radius and hydration cation radius.

Cations (M^+)	NH_4^+	K^+	Na^+
Cation radius (nm)	0.143	0.133	0.098
Hydration cation radius (nm)	0.532	0.537	0.790
Ion exchange ability	1	2	3

crust elution-deposited rare earth ore is often related to the cation radius and hydration cation radius in the electrolyte solution (Berrin et al., 2006). The cation radius and hydration cation radius are listed in **Table 2**.

According to **Table 2**, comparing the cation radius and hydration cation radius of NH_4^+, K^+, and Na^+, the larger the cation radius is, the weaker the hydration ability is, and the smaller the hydration radius is, the stronger the adsorption ability is, and the easier it is to enter the layer of the clay mineral to decrease the swelling effects.

Swelling Kinetics of Clay Minerals in the Weathered Crust Elution-Deposited Rare Earth Ores With Formate Salts

The swelling ratios of the clay mineral samples with formate salts are closely related and changed with time. For example, the swelling kinetic curves of the formate salts under the optimal leaching conditions and distilled water are shown in **Figure 11**.

According to **Figure 11**, the swelling process of clay minerals in the weathered crust elution-deposited rare earth ore with formate salts can be divided into two stages: rapid expansion stage and steady state stage (Al-Rawas et al., 1998; Tan and Kong, 2004). In the initial stage, the expansion of the clay mineral sample occurs at the critical surface in contact with the formate salt solution. The clay mineral particles absorb water rapidly, expand at a fast rate, and the expansion rate

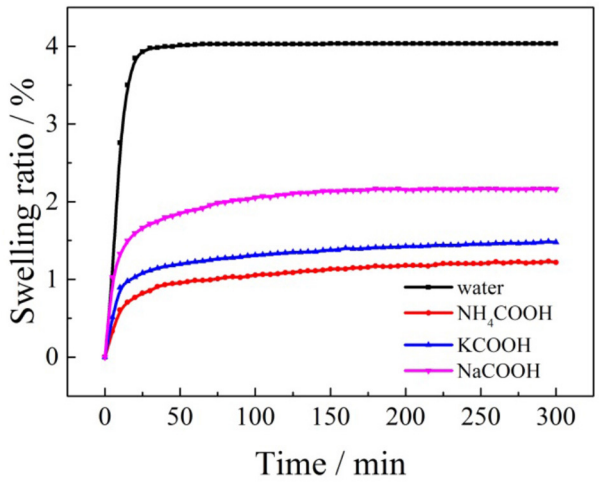

FIGURE 11 | The swelling curves of the formate salts under optimal conditions.

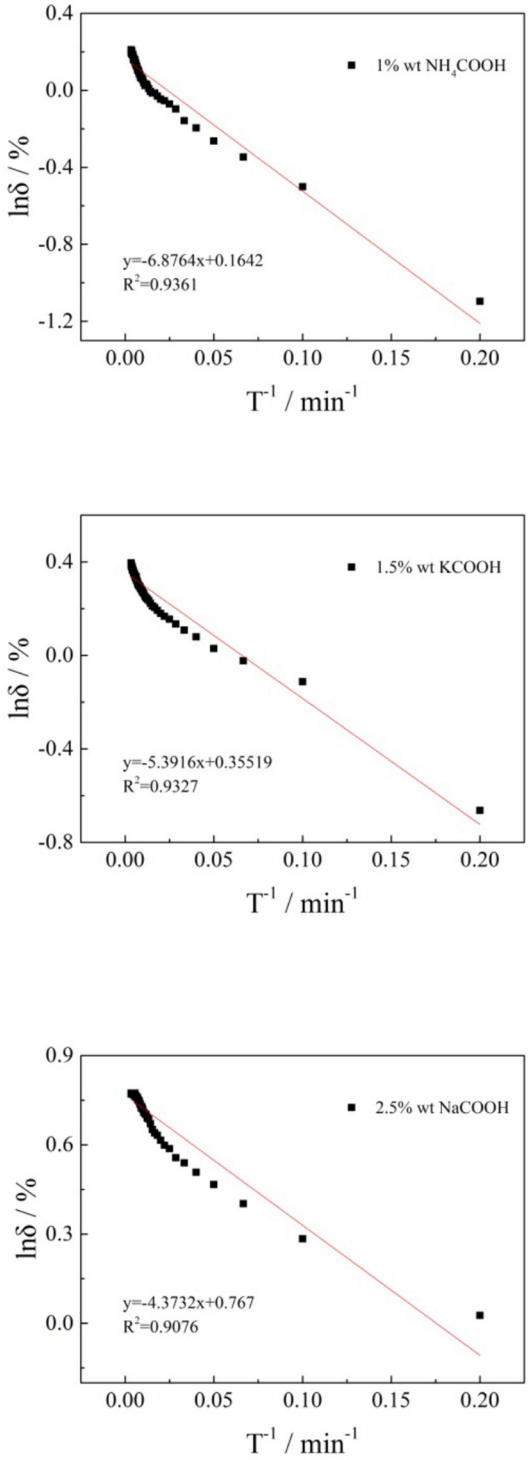

FIGURE 12 | The relation between the natural logarithm of the swelling ratio and the reciprocal of time.

increases significantly. As the formate salt solution penetrates deeply into the clay mineral and immerses the clay mineral particles totally, the interface between the clay mineral particles and the formate salt solution increases and the ore sample begins to swell completely. Later, after some time, when the clay minerals are completely soaked in the formate salt solution, the water absorption decreases gradually, and the ore sample slowly expands. At this time, the expansion state of the clay mineral enters the second stage, and the expansion rate is greatly reduced and tends to be stable.

Now take 1 wt% ammonium formate, 1.5 wt% potassium formate, and 2.5 wt% sodium formate as examples to fit their expansion kinetic curves. **Figure 12** is shown as the reciprocal of the natural logarithm of the expansion rate to time.

According to **Figure 12**, there is a certain relationship between the natural logarithm of the clay mineral swelling ratio and the reciprocal of time in the semilog coordinate. In the first part of the expansion, experimental data were concentrated, which reflects the steady stage of the swelling process. In the second half of the expansion, experimental data were relatively separate. By analyzing and calculating the results, the equation of the relationship between the swelling of the clay mineral with 1 wt% ammonium formate, 1.5 wt% potassium formate, and 2.5 wt% sodium formate were presented, respectively: $\delta = 1.1784 \bullet e^{-6.8764/t}$, $R^2 = 0.9361$, $\delta = 1.4265 \bullet e^{-5.3916/t}$, $R^2 = 0.9327$, and $\delta = 2.1532 \bullet e^{-4.3732/t}$, $R^2 = 0.9076$, fitting coefficients >0.9. It shows that the fitting relation was ideal and meets the requirements.

It can be seen from the above results, when formate salts were used as leaching agents to recover the rare earth from the weathered crust elution-deposited rare earth ore, lnδ and t^{-1} showed a good linear relationship which can obtain the relationship between swelling ratio and time: $\delta = A \cdot e^{-B/t}$, type A and B are all in the fitting analysis of regression coefficients (Erguler and Ulusay, 2003; Tan and Kong, 2004; Huang et al., 2016).

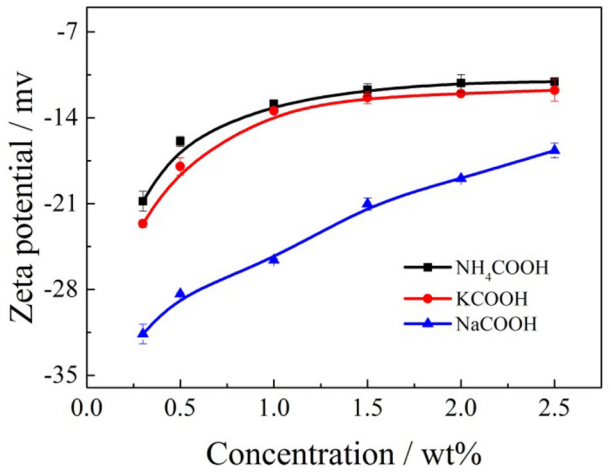

FIGURE 13 | Zeta potential of clay minerals with formate salts.

Inhibiting Swelling Mechanism of Formate Salts on the Clay Minerals of Weathered Crust Elution-Deposited Rare Earth Ore

During the leaching process of weathered crust elution-deposited rare earth ore with formate salts, the utilization of formate salts can effectively inhibit the swelling of clay minerals for preventing landslides and other disasters. The inhibition mechanism of the formate salts on the clay minerals is mainly reflected in the following three aspects (Chen and Wang, 2003; Li et al., 2006; Huang et al., 2013):

(1) Charge neutralization. The hydration of the clay minerals is normally relative to the surface potential of the clay minerals when it makes contact with the formate salts solution. The results of the zeta potential of clay minerals with formate salts are presented in **Figure 13**.

According to **Figure 13**, with the enhancement of the formate salts concentration, it was evident that the zeta potential between clay mineral particles and formate salts solution increase. The lower the zeta potential, and the higher the effective negative charges of the clay mineral particles, the stronger the ability was of the clay mineral particles to adsorb cations. The layers became thicker, and the flocculation tendency of the clay mineral particles was smaller after they have been soaked in the formate salts, indicating that the clay minerals swell more easily in the low concentration leaching solution. However, with the enhancement of the formate salts concentration, more cations entered the layer, leading to the electronegativity of clay minerals decreasing to some extent, which means the high concentration of formate salt solution can effectively compress the double electric layer. And it finally weakened the hydration of clay minerals to inhibit swelling.

(2) Low activity. Due to the high ion concentration of the formate salts solution, there is less free water and the activity of water is relatively low. According to the activity balance theory, osmotic pressure can reverse the flow of water in rare earth ores. Such reverse osmosis reduces the net flow of water from the formate salts solution to the clay minerals, resulting in the decrease of hydration of the clay minerals and an increase in the strength and actual stress of the capillary pressure, which is beneficial to rare earth ore stability.

(3) The viscosities of formate salts solution are high, making it difficult for leaching solutions to enter the formation. With relatively high salinity and low surface tension, the positive charge on the end surface of clay mineral particles and HCOO– attracts each other, forming a barrier between HCOO– and water to prevent the hydration of clay minerals and stabilize the rare earth ore. Meanwhile, HCOO– and water molecules can form hydrogen bonds and have a strong binding ability to free water, making the filtrate viscosity of formate salts solution high and making it difficult to enter the interlayer of the clay minerals.

CONCLUSION

Rare earth is a significant resource all over the world. To recover the rare earth with high efficiency safety, formate salts were used as leaching agents for recovering the rare earth elements. Meanwhile, the swelling proprieties of clay minerals with formate salts were investigated and the anti-swelling mechanism was analyzed. The following conclusions have been drawn:

The rare earth leaching efficiency can reach 87% when 1 wt% ammonium formate was used to leach the rare earth ore, while the leaching efficiency of aluminum was 37%. Besides, at the optimal concentration of 1.5 and 2.5 wt% of potassium formate and sodium formate, the leaching efficiencies of rare earth were 80 and 79%, respectively. Considering the cation radius and hydration cation radius of NH_4^+, K^+, and Na^+, the effects of inhibiting the swelling of clay minerals follow the order: ammonium formate > potassium formate > sodium formate. The swelling process of clay minerals has a strong dependence on time. The relationship between the swelling ratio of clay minerals and time is represented by the swelling kinetic equations: formate ammonium $\delta = 1.1784 \cdot e^{-6.8764/t}$, $R^2 = 0.9361$, the formate potassium $\delta = 1.4265 \cdot e^{-5.3916/t}$, $R^2 = 0.9327$, and the formate sodium $\delta = 2.1532 \cdot e^{-4.3732/t}$, $R^2 = 0.9076$. The fitting coefficients are all >0.9, indicating that the relationship between the swelling ratio of clay minerals and time is in agreement with the equation $\delta = A \cdot e^{B/t}$ in the leaching process with formate salts.

The result of this research could provide a theoretic guide to the application of formate salts in the industry.

DATA AVAILABILITY STATEMENT

The raw data supporting the conclusions of this article will be made available by the authors, without undue reservation.

AUTHOR CONTRIBUTIONS

ZZ and RC designed the project. ZC performed the experiments. ZZ and ZC analyzed the data. ZC, ZZ, and RC wrote the manuscript. All authors contributed to the article and approved the submitted version.

FUNDING

This study was supported by the National Nature Science Foundation of China (U1802252; 21808176), the Key Research & Development Plan of the Ministry of Science and Technology (2018YFC1801800), the Education Department Scientific Research Project of Hubei Provincial (Q20191503), and the Youths Science Foundation of Wuhan Institute of Technology (18QD57).

REFERENCES

Al-Rawas, A. A., and Guba, I., Mcgown, A. (1998). Geological and engineering characteristics of expansive soils and rocks in northern Oman. *Eng. Geol.* 50, 267–281. doi: 10.1016/S0013-7952(98)00023-4

Berrin, T., John, S., and Tony, R. (2006). Significance of hydrated radius and hydration shells on ionic permeability during nanofiltration in dead end and cross flow modes. *Sep. Purif. Technol.* 51:40. doi: 10.1016/j.seppur.2005.12.020

Chen, L. L., and Wang, G. J. (2003). An overview of formate base drilling and completion fluids system. *Drill Fluid Complet Fluid.* 20, 31–36. doi: 10.3969/j.issn.1001-5620.2003.01.012

Chen, Z., Zhang, Z., Sun, N., Zhang, H., Liu, Z., and Chi, R. (2018a). Leaching kinetics of weathered crust elution-deposited rare earth ore with magnesium salt. *Metal Mine*. 8, 84–91.

Chen, Z., Zhang, Z. Y., He, Z. Y., and Chi, R. A. (2018b). Mass transfer process of leaching weathered crust elution-deposited rare earth ore with magnesium salts. *Physicochem. Prob. Min. Process.* 54, 1004–1013. doi: 10.5277/ppmp18102

Chen, Z., Zhang, Z. Y., He, Z. Y., and Chi, R. A. (2020). Swelling of clay minerals during the leaching process of weathered crust elution-deposited rare earth ores by magnesium salts. *Powder Technol.* 367, 889–900. doi: 10.1016/j.powtec.2020.04.008

Chi, R. A., and Tian, J. (2006). *Hydrometallurgy of the Weathered Crust Elution-Deposited Rare Earth Ores*. New York, NY: Science Press.

Erguler, Z. A., and Ulusay, R. (2003). A simple test and predictive models for assessing swell potential of Ankara (Turkey) Clay [J]. *Eng. Geol.* 67, 331–352. doi: 10.1016/S0013-7952(02)00205-3

Erwan, P., Isabelle, B., Christophe, B., and Adrian-Marie, P. (2011). Aqueous suspensions of natural swelling clay minerals. *Struc. Electrostat. Interact. Langmuir.* 27:5562. doi: 10.1021/la2001255

He, Z. Y., Zhang, Z. Y., Yu, J. X., and Chi, R. A. (2016a). Process optimization of rare earth and aluminum leaching from weathered crust elution-deposited rare earth ore with compound ammonium salts. *Rare Earth* 34, 413–419. doi: 10.1016/S1002-0721(16)60042-X

He, Z. Y., Zhang, Z. Y., Yu, J. X., Zhou, F., Xu, Y. L., Xu, Z. G., et al. (2016b). Kinetics of column leaching of rare earth and aluminum from weathered crust elution-deposited rare earth ore with ammonium salt solutions. *Hydrometallurgy* 163, 33–39. doi: 10.1016/j.hydromet.2016.02.016

Huang, Q. W., Xu, J. W., Wang, X. H., Hu, G. W., and Chen, C. F. (2013). Application of inhibiting clay hydration and expansion by organic salt. *Oilfield Chem.* 30, 496–499. doi: 10.19346/j.cnki.1000-4092.2013.04.005

Huang, Z. Q., and Zhang, X., Wu, C., Zhang, Z. *H.* (2016). Experimental study on the variational regularity of dynamic characteristics of expansive soil. *J. North China Univ. Water Resour. Electric Power* 37, 78–82. doi: 10.3969/j.issn.1002-5634.2016.02.014

Jiang, G. C., Wang, J. S., and Xuan, Y. (2014). Performance and functional mechanism of potassium methyl siliconate as shale inhibitor. *Sci. Technol. Eng.* 14, 6–10. doi: 10.3969/j.issn.1671-1815.2014.08.002

Kynicky, J., Smith, M. P., and Xu, C. (2012). Diversity of rare earth deposits: the key example of China. *Elements* 8, 361–367. doi: 10.2113/gselements.8.5.361

Li, M., Zhang, X., Liu, Z., Hu, Y., Wang, M., Liu, J., et al. (2013). Kinetics of leaching fluoride from mixed rare earth concentrate with hydrochloric acid and aluminum chloride. *Hydrometallurgy* 140, 71–76. doi: 10.1016/j.hydromet.2013.09.004

Li, Y., Tu, A., Zhang, Y., Zhang, M., and Chi, R. (2009). Kinetics of leaching rare earth from a weathered crust elution-deposited rare earth ore in south China with mixed ammonium salt. *Indust. Miner. Process.* 38, 19–24. doi: 10.3969/j.issn.1008-7524.2009.02.006

Li, Y. X. (2014). *Ion Adsorption Rare Earths and Their Green Extraction*. New York, NY: Chemical Industry Press.

Li, Z. Y., Yan, J. N., Wang, J. H., and Wang, X. L. (2006). A novel formate/positive-charged polyglycol drilling fluid. *Petrol. Drill. Techniq.* 34, 34–38. doi: 10.3969/j.issn.1001-0890.2006.05.010

Norrish, K. (1954). The swelling of montmorillonite. *Discuss. Faraday Soc.* 18, 120–134. doi: 10.1039/df9541800120

Qiu, T., Zhu, D., Fang, X., Zeng, Q., Gao, G., Zhu, H., et al. (2014). Leaching kinetics of ionic rare-earth in ammonia-nitrogen wastewater system added with impurity inhibitors. *J. Rare Earths* 32, 1175–1183. doi: 10.1016/S1002-0721(14)60200-3

Simandl, G. J. (2014). Geology and market-dependent significance of rare earth element resources. *Miner. Deposit.* 49, 889–904. doi: 10.1007/s00126-014-0546-z

Tan, L. R., and Kong, L. W. (2004). Study on variation regularity of swelling behavior of expansive soil [J]. *Rock and Soil Mechanic*. 25(10):1555–1559. doi: 10.16285/j.rsm.2004.10.009

Zhang, Z. Y., He, Z. Y., Yu, J. X., Xu, Z. G., and Chi, R. A. (2016). Novel solution injection technology for *in-situ* leaching of weathered crust elution-deposited rare earth ores. *Hydrometallurgy* 164, 248–256. doi: 10.1016/j.hydromet.2016.06.015

Zhang, Z. Y., He, Z. Y., Zhou, F., and Chi, R. A. (2018a). Swelling of clay minerals in ammonium leaching of weathered crust elution-deposited rare earth ores. *Rare Metals.* 37, 72–78. doi: 10.1007/s12598-017-0977-7

Zhang, Z. Y., Sun, N., He, Z. Y., and Chi, R. A. (2018b). Local concentration of middle and heavy rare earth elements in the col on the weathered crust elution-deposited rare earth ores. *Rare Earths* 36, 552–558. doi: 10.1016/j.jre.2017.12.004

Conflict of Interest: The authors declare that the research was conducted in the absence of any commercial or financial relationships that could be construed as a potential conflict of interest.

frontiers in Chemistry

ORIGINAL RESEARCH
published: 15 December 2020
doi: 10.3389/fchem.2020.605968

Effects of Ion Characteristics on the Leaching of Weathered Crust Elution-Deposited Rare Earth Ore

Zhenyue Zhang[1,2], *Ru'an Chi*[1,2], *Zhuo Chen*[1] *and Wendou Chen*[1]*

[1] School of Xingfa Mining Engineering, Wuhan Institute of Technology, Wuhan, China, [2] Key Laboratory for Green Chemical Process of Ministry of Education, Wuhan Institute of Technology, Wuhan, China

To reveal the ion-exchange mechanism in the leaching process of weathered crust elution-deposited rare earth ores with different leaching agents, the effects of a variety of cations and anions at different concentrations on the leaching process were investigated, including Al^{3+}, Fe^{3+}, Ca^{2+}, Mg^{2+}, Na^{+}, K^{+}, NH_4^+ and Cl^-, NO_3^-, and SO_4^{2-}. Meanwhile, the relationships between different concentrations of cations and anions and leaching efficiency were investigated, as was the relationship between different concentrations of cations and anions and zeta potential. The effect of different ions on the swelling of clay minerals during leaching process was also investigated. The results shown that NH_4^+ was the most affected electrolyte cation in terms of rare earth leaching efficiency during the leaching process of weathered crust elution-deposited rare earth ore among three different cationic valence states, and the leaching efficiency was 86.93% at the optimal leaching concentration. The influence of the three anions on the leaching efficiency of rare earth was $NO_3^- > Cl^- > SO_4^{2-}$, and the leaching efficiency of rare earth were 83.21, 81.52, and 80.12% at the optimal leaching concentration, respectively. The NH_4^+ had the greatest effect on the zeta potential of weathered crust elution-deposited rare earth ore, and the zeta potential was −18.1 mV at the optimal leaching concentration. Additionally, the order of the effect of three anions on zeta potential was $SO_4^{2-} > NO_3^- > Cl^-$. Combined with the effect on the rare earth leaching process, anions and cations were considered separately, and NH_4^+ and Cl^- were selected; the relationship between the rare earth leaching efficiency and zeta potential conforms to the follow equations: NH_4^+:$Y = -0.48X^2 - 13.51X - 1.58$, $R^2 = 0.98133$ and Cl^-:$Y = -1.22X^2 - 17.64X + 23.29$, $R^2 = 0.99010$. It was also found in the swelling experiment of the weathered crust elution-deposited rare earth ore that the swelling ratio of clay minerals was the lowest when the cation and anion were NH_4^+ and Cl^- and the swelling ratios were 1.874 and 2.015%, respectively.

Keywords: weathered crust elution-deposited rare earth ores, cation, anion, leaching efficiency, zeta potential, swelling ratio

OPEN ACCESS

Edited by:
Shenxu Bao, Wuhan University of Technology, China

Reviewed by:
Yunliang Zhao, Wuhan University of Technology, China
Haisheng Han, Central South University, China

***Correspondence:**
Wendou Chen
witcwd@163.com

Specialty section:
This article was submitted to Green and Sustainable Chemistry, a section of the journal Frontiers in Chemistry

Received: *14 September 2020*
Accepted: *17 November 2020*
Published: *15 December 2020*

Citation:
Zhang Z, Chi R, Chen Z and Chen W (2020) Effects of Ion Characteristics on the Leaching of Weathered Crust Elution-Deposited Rare Earth Ore. Front. Chem. 8:605968. doi: 10.3389/fchem.2020.605968

INTRODUCTION

Weathered crust elution-deposited rare earth ore is of extremely high economic and strategic value, it is a special rare earth resource in the world (Simandl, 2014; Zhang B. et al., 2018; Zou et al., 2020). As a unique resource, it contains almost rare earth elements, including the light rare earth and middle and heavy rare earth, being especially rich in middle and heavy rare earth (Xiao et al., 2015a;

Chi and Liu, 2019). The rare earth elements mainly existed in the ionic or hydrated ionic state on the surface of the clay minerals (Huang et al., 2005). Due to this special property, the essential process during leaching is an ion exchange reaction between the surface of clay minerals of absorbed rare earth ions and cations in lixiviant. Rare earth ions were obtained by way of an ion exchange reaction, and this method has been applied in industry. In addition, the *in-situ* leaching process, with ammonium sulfate as the main leaching agent, was gradually formed (Chi and Wang, 1993; Chi et al., 2012). However, the leaching process causes the swelling of clay minerals, which has a certain influence on the safety of mine production and the low efficiency of the leaching agents, resulting in high consumption of electrolyte solution in actual industrial production.

In order to improve the efficiency of the leaching process and mine safety, a large number of studies have been conducted on the rare earth leaching process of weathered crust elution-deposited rare earth ores under various leaching systems (Xiao et al., 2015b). Zhang et al. (2013) and He et al. (2016) found that the order of the leaching efficiency of rare earth by inorganic ammonium salt was $(NH_4)_2\,SO_4 < NH_4Cl < NH_4NO_3$, which was related to the complexation capacity between rare earth ions and anions. Chen et al. (2018a) and Chen Z. et al. (2020) found that the order of mass transfer efficiency of rare earth under three magnesium salts was $Mg(NO_3)_2 > Mg(Cl)_2 > MgSO_4$ in the study of mass transfer process of weathered crust elution-deposited rare earth ores by magnesium salts. The inhibiting swelling effect was highest with magnesium nitrate as the leaching agent, and the mass transfer efficiency of rare earth was related to the type of anion. Li et al. (2019) proposed that the cationic activity of the leaching agent was an important factor affecting the leaching quality of rare earth, and the molar concentration of the leaching agent affected the leaching efficiency to a certain extent. The effects of different electrolyte solutions on leaching were considered. Zhang Z. Y. et al. (2018) studied ammonium salt leaching weathered crust elution-deposited rare earth ores and found in the study that the zeta potential of rare earth ore decreased with the increase of leaching solution pH, and the zeta potential increased with the increase of ammonium concentration. Besides, zeta potentials of rare earth ores with $AlCl_3$, NH_4Cl, KCl, and $MgCl_2$ solution were negative. Wang et al. (2018) studied the effect of ion interaction on rare earth leaching, and they mentioned that the leaching capacity of leaching agent on rare earth at low concentration was consistent with the adsorption capacity of cation; SO_4^{2-} showed stronger coordination and leaching aid than Cl^- with rare earth ions. On the other hand, when the leaching agent concentration increased, the electrostatic interaction between ions will inhibit the leachate of rare earth, especially for the higher cations. Therefore, it is necessary to consider the anionic and cationic properties in the leaching process.

There were many studies on the weathered crust elution-deposited rare earth ore with single cation under different experimental conditions. However, the leaching process of weathered crust elution-deposited rare earth ores with different anions and cations was rarely studied systematically. Seven common cations and three anions were therefore selected to study the effects of ion property on the leaching efficiency of rare earth and zeta potential of rare earth ore in this paper, including Al^{3+}, Fe^{3+}, Ca^{2+}, Mg^{2+}, Na^+, K^+, and NH_4^+ as well as Cl^-, NO_3^-, and SO_4^{2-}. Meanwhile, the effect of ion property on swelling ratio of rare ore was also investigated. The effects of different cation and anion concentration on leaching process of weathered crust elution-deposited rare earth ores and zeta potential were studied. The relationship between the zeta potential of clay mineral and rare earth leaching efficiency were discussed. The effects of various ions on the swelling properties of clay minerals were also discussed. It would also enrich the study of the leaching process of weathered crust elution-deposited rare earth ores with electrolyte solution and provide theoretical guidance for efficient recovery of rare earth.

MATERIALS AND METHODS

Materials

Chemical Composition

The weathered crust elution-deposited rare earth ore samples were collected from Fujian Province, China. The main chemical composition of the rare earth ore was analyzed by X-ray fluorescence (Axios advanced, Panalytical B.V.), and the results are shown in **Table 1**.

It can be seen from **Table 1** that SiO_2 and Al_2O_3 were the main chemical components of the sample, accounting for 51.236 and 37.649% of the total mass, respectively, and the REO content was 0.129% in the ore samples.

Rare Earth Partitioning

Rare earth partitioning is an important index to evaluate the industrial value of the rare earth ore (Zhang et al., 2016a,b). The rare earth elements partitioning of the rare earth ore was analyzed by ICP-MS (Inductively Coupled Plasma Mass Spectrometry), as shown in **Figure 1**.

As can be seen from **Figure 1**, the content of light rare earths was 46.88% in the total rare earth content. The remaining medium and heavy rare earths accounted for 53.12%, which indicated that this rare earth mine has a great industrial utilization value.

Apparatus and Experimental Procedure

Leaching Mechanism of Rare Earth Ore

The ion exchange reaction occurs between the rare earth ions and different valence cations can be represented by the following equations (Chi et al., 2012):

TABLE 1 | Main chemical composition of the RE ores (mass fraction, %).

Component	REO	SiO_2	Al_2O_3	Fe_2O_3	K_2O	Na_2O	MgO	CaO
Content	0.129	51.236	37.649	4.033	2.318	0.062	0.536	0.382
Component	TiO_2	MnO	ZrO_2	Rb_2O	ZnO	CuO	SrO	Loss
Content	0.398	0.052	0.011	0.013	0.005	0.006	0.01	3.207

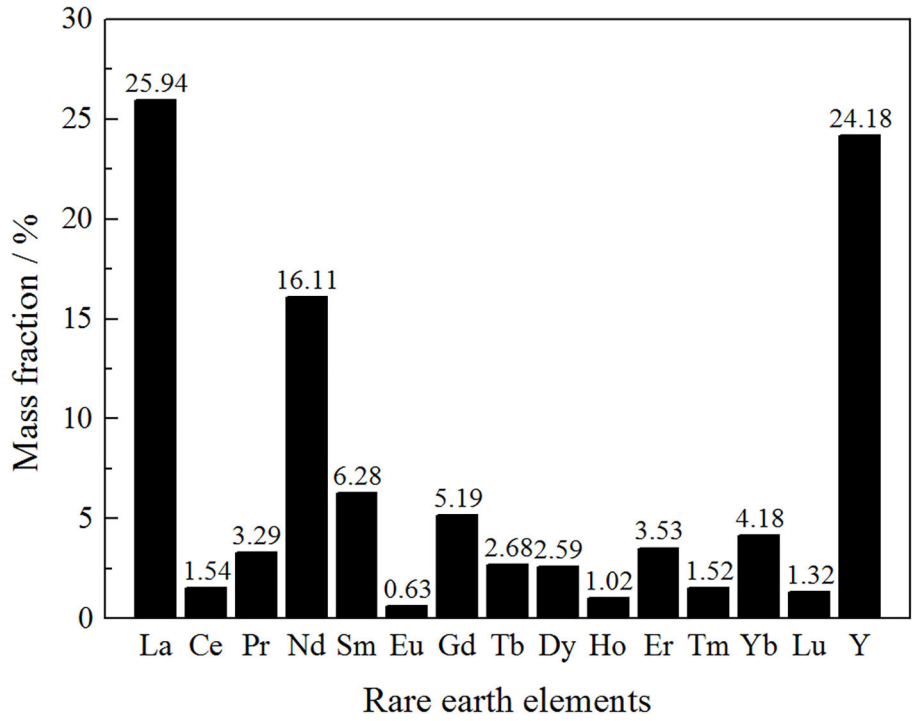

FIGURE 1 | Rare earth elements of the ore sample.

$$[Al_2(Si_2O_5)(OH)_4]_m nRE^{3+}(s) + 3nA^{+}(a) = [Al_2(Si_2O_5)(OH)_4]_m 3nA^{+}(s) + nRE^{3+}(a) \quad (1)$$

$$[Al_2(Si_2O_5)(OH)_4]_m 2nRE^{3+}(s) + 3nB^{2+}(a) = [Al_2(Si_2O_5)(OH)_4]_m 3nB^{2+}(s) + 2nRE^{3+}(a) \quad (2)$$

$$[Al_2(Si_2O_5)(OH)_4]_m nRE^{3+}(s) + nC^{3+}(a) = [Al_2(Si_2O_5)(OH)_4]_m nC^{3+}(s) + nRE^{3+}(a) \quad (3)$$

where s represents the solid phase and a represents the liquid phase.

As shown in the equation, minerals $[Al_2(Si_2O_5)(OH)_4]_m$ can be described as resin, which adsorbed RE^{3+}. When leaching agent flow through the resin, different valence cations migrate to the mineral surface and then take ion-exchange reaction with RE^{3+}.

Experimental Procedure

The column leaching method was adopted to simulate the *in-situ* leaching technology in the paper. The dried ore sample was weighed to 250 g by the quartering method and packed into the column tightly. The leaching agent was added at the ratio of 2:1 for liquid/solid. The leaching agent was added into the glass column under the control of precision pump at a speed of 0.5 mL/min (Chen et al., 2018b). The self-made leaching device was shown in **Figure 2**. The lixivium was collected into centrifuge tube from the bottom of the glass column, the rare earth content was analyzed by ICP-MS, and the rare earth leaching efficiency was calculated according to the follow formula (Yang et al., 2018):

$$L(\%) = \frac{(C \times V)}{W \times C_S} \times 100 \quad (4)$$

where L is the rare earth leaching efficiency/ %, C is the concentration of rare earth in leaching lixivium/ g/L^{-1}, V is the volume of leaching lixivium/ L, W is the weight of rare earth ore sample/ g, and Cs is the content of rare earth in ionic phase of the ore samples/ %

The swelling of clay mineral was conducted by PCY intelligent dilatometer. A total of 2 g of ore sample was weighed and pressed for 5 min with a tablet press under a pressure of 8 MPa. The initial length of the sample was recorded, and it was loaded it into a PCY intelligent clay dilatometer to determine its swelling ratio. The PCY intelligent dilatometer is shown in **Figure 3**. The swelling ratio of the ore sample was measured by the following formula (Zhang et al., 2013; Chen W. D. et al., 2020):

$$\delta = \frac{\Delta H}{H_0} \times 100 \quad (5)$$

where H is the variation of height/ mm, and H_0 is the initial height of the ore sample/ mm

The zeta potential was detected by Zetasizer Nano (Malvern Instruments Corporate, UK).

All chemicals used in the experiments were of analytical grade. All the solutions were prepared with deionized water.

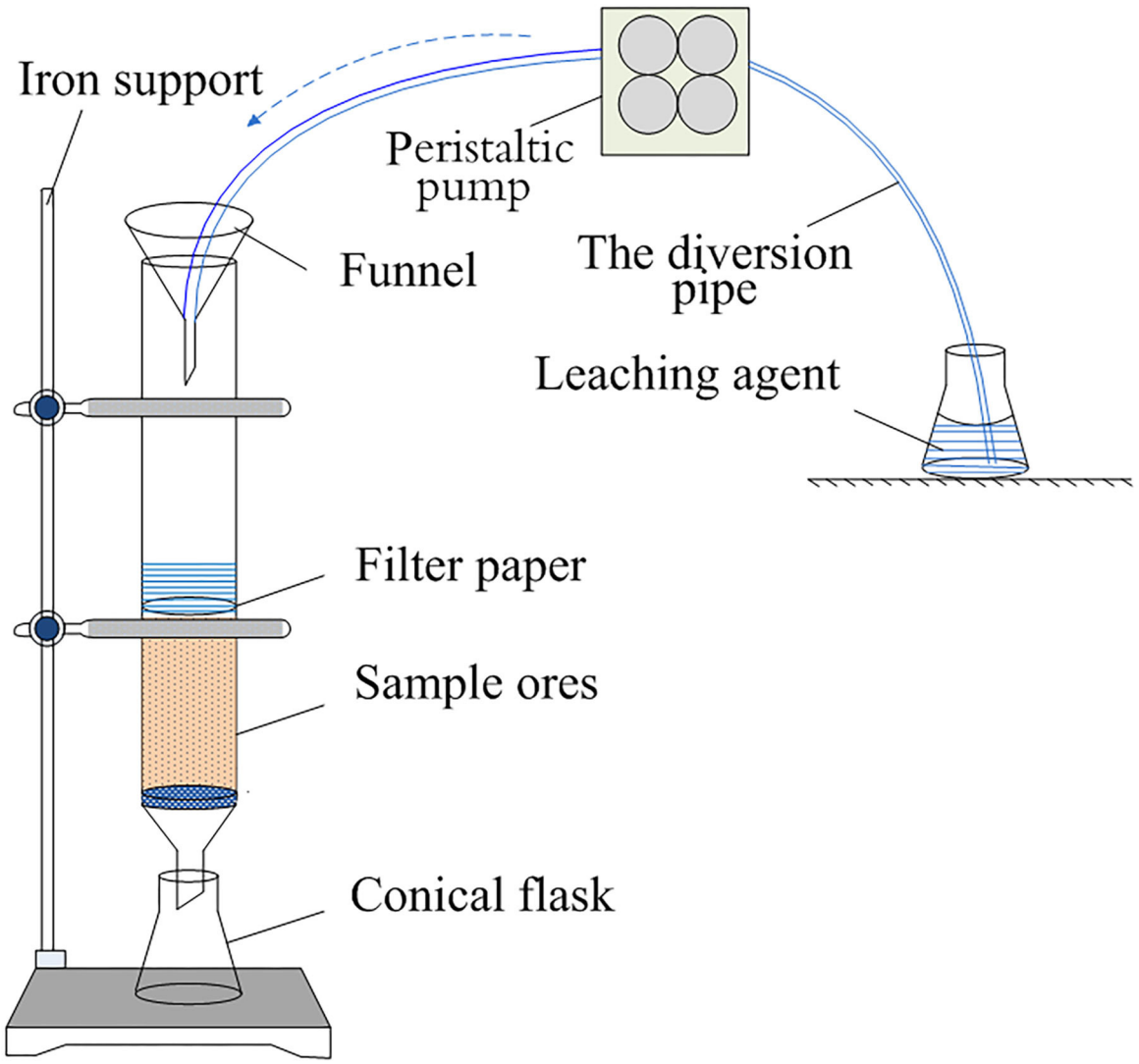

FIGURE 2 | Self-made leaching device.

RESULTS

Relationship Between Rare Earth Leaching Efficiency and Zeta Potential of Rare Earth Ore

In order to analyze the relationship between the rare earth leaching efficiencies and zeta potentials of clay minerals with leaching agent, the effects of NH_4Cl concentrations on the rare earth leaching were investigated. The result is shown in the **Figure 4**.

It can be seen from the **Figure 4** that the rare earth leaching efficiencies and zeta potentials of rare earth both increased with the increase of leaching agent concentration, and the rate of increase was both fast and then slow when the ammonium concentration exceeded 0.2 mol/L and finally tended to keep balance to some extent. The rare earth leaching efficiency was basically balanced when the solvent concentration was 0.2 mol/L and the leaching efficiency was 86.93%. At that time, the zeta potential on the clay mineral surface was −18.1 mV, which was also close to the equilibrium value. It was obvious that the rare earth leaching efficiencies and zeta potentials displayed similar trends in the leaching process. To better understand this phenomenon, the electronic double-layer theory was used to analyze the results.

The ion exchange process of ammonium ions in the electrolyte solution and rare earth ions, which are adsorbed on the surface of the clay minerals, is illustrated in **Figure 5**.

When rare earth ions are adsorbed on the surface of clay minerals in contact with the ammonium chloride solution, the ammonium hydrate ions were mainly distributed within the diffusion layer of the double electric layer. In fact, the ion exchange process of ammonium ions with rare earth ions

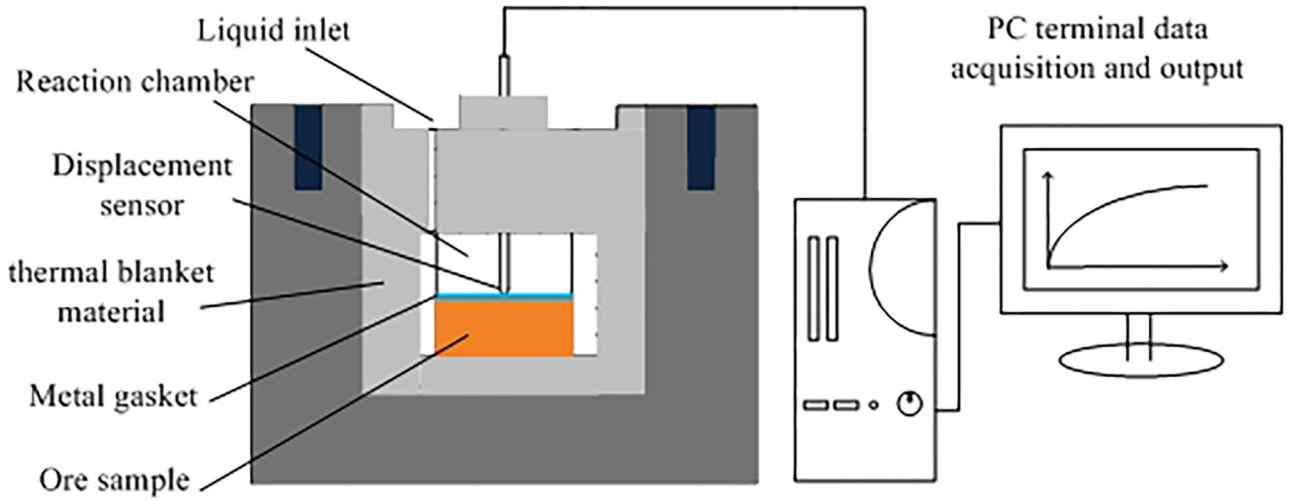

FIGURE 3 | PCY intelligent dilatometer.

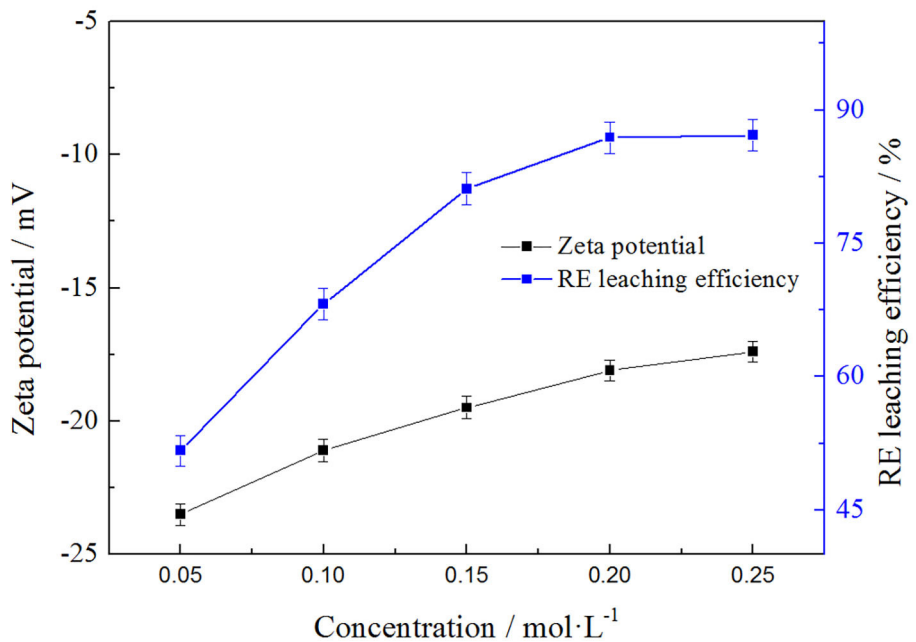

FIGURE 4 | Relationship between zeta potential and rare earth efficiency.

was a thermodynamic non-spontaneous process. Increasing the concentration of ammonium chloride, high concentrations of ammonium hydrate ions have the chemical potential to make it from the diffusion layer, migrating to the stern layer, and further cross through the fixed layer to then, according to the concentration of advantage, gather near the surface of the clay minerals in the weathered crust elution-deposited rare earth ore. The large amount of ammonium ions formed a multilayer adsorption, competing for the original adsorption sites that are occupied by the hydration of rare earth ions to promote the rare earth ions desorption; the excluded rare earth ion of monolayer adsorption gradually migrated out of the fixed layer and diffusion layer and spread to the leaching agent solution. In a high concentration electrolyte solution, the zeta potentials of the clay mineral particles were not very positive because there were more hydrated ions in the tight layer. By separating the bulk solution containing rare earth ions, the leaching process of rare earth can be realized, and clay minerals loaded with ammonium ions can be obtained.

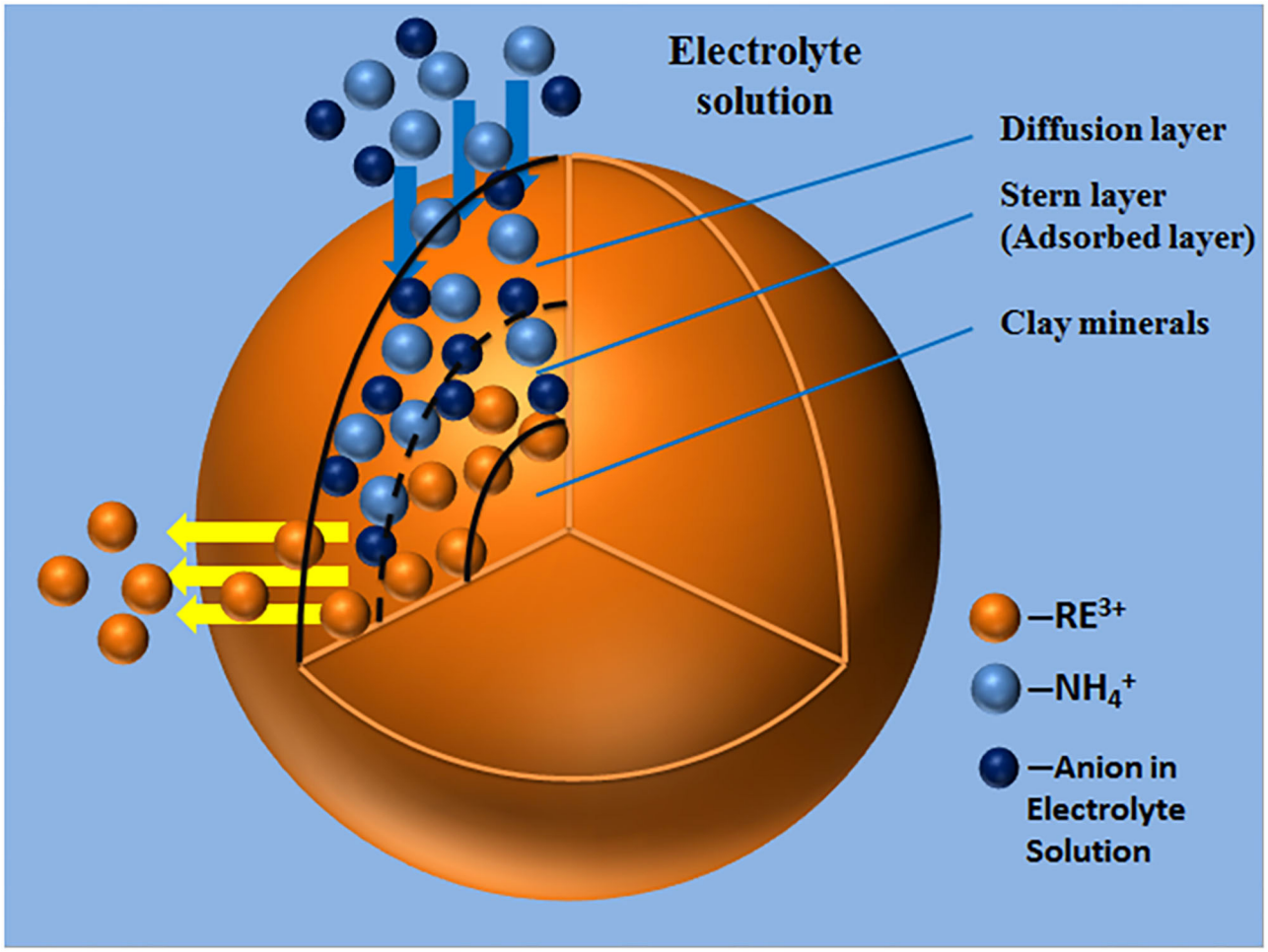

FIGURE 5 | Ion exchange process.

Effects of Cation on Rare Earth Leaching in Weathered Crust Elution-Deposited Rare Earth Ore

Effects of Cation on Rare Earth Leaching Efficiency

In order to explore the influence of different cations on rare earth leaching efficiency, Al^{3+}, Fe^{3+}, Ca^{2+}, Mg^{2+}, Na^{+}, K^{+}, and NH_4^{+} 7 cations were selected to recover the rare earth from the rare earth ore samples under the same anion of Cl^{-}. The effects of cations at different concentrations on rare earth leaching efficiencies were investigated, as shown in **Figures 6A–C**. At a cation concentration of 0.2 mol/L, the rare earth leaching efficiencies in all electrolyte solutions were compared, as shown in **Figure 6D**.

As can be seen from **Figure 6**, the rare earth leaching efficiency gradually increased with the increase of cation concentration. When the cation concentration exceeded 0.2 mol/L, the rare earth leaching efficiencies gradually stabilized. This is because when the electrolyte concentration reached a certain value, most of the adsorption sites on the clay mineral surface were occupied by the cation of the leaching agent. The promotion effect of rising electrolyte concentration on rare earth leaching was limited (Wang et al., 2018). Besides, it can be seen from **Figures 6A–C** that the electrolyte cations with the highest rare earth leaching efficiency among the three valence cations was NH_4^{+}. It can be seen from **Figure 6D** that, under the same electrolyte concentration, NH_4^{+} showed a stronger leaching effect of rare earth than Mg^{2+} and Al^{3+}, and the leaching efficiencies of rare earth were 86.93, 81.21, and 53.16%, respectively, indicating that NH_4^{+} had the best leaching effect on rare earth under the same anion.

Effects of Cations on Zeta Potential of Clay Minerals

In order to understand the effect of cations on zeta potential of clay mineral surface, Al^{3+}, Fe^{3+}, Ca^{2+}, Mg^{2+}, Na^{+}, K^{+}, and NH_4^{+} 7 cations were selected under the same anion of Cl^{-}. The effects of cations on zeta potential on clay mineral surface at different cation concentrations were investigated, as shown in **Figures 7A–C**. When the cation concentrations

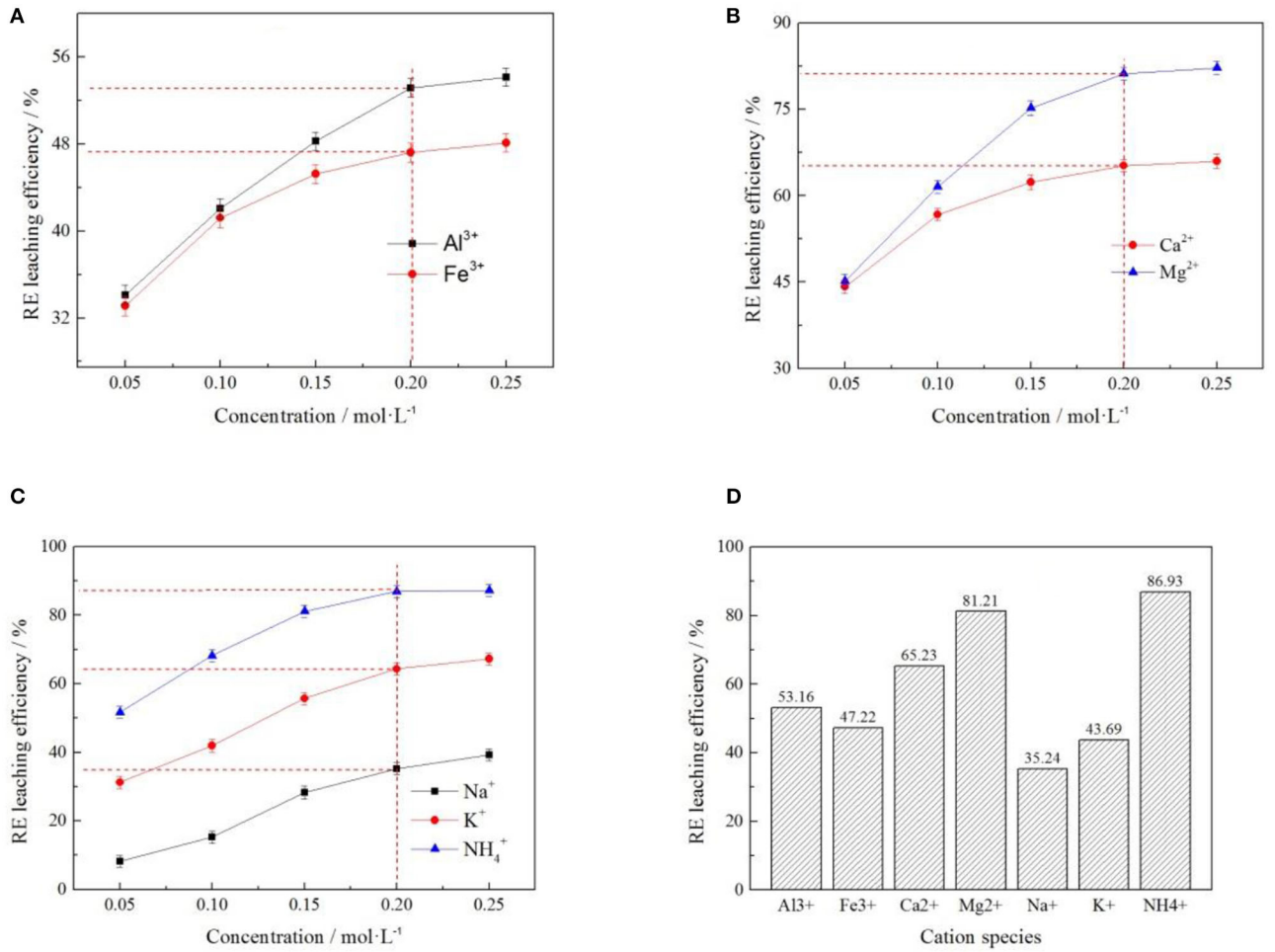

FIGURE 6 | Effect of cation concentration on rare earth leaching efficiency [where **(A?C)** represent +3, +2, and +1 valence cations respectively, **(D)** represents the rare earth leaching efficiency when the concentration of various cations was 0.2 mol/L].

were 0.2 mol/L, the zeta potentials of clay minerals under different electrolyte solutions were compared, as shown in **Figure 7D**.

As can be seen from **Figure 7**, the zeta potential on the clay mineral surface decreased with the increase of electrolyte concentration in +3-valent cationic electrolyte solution. In +2 and +1 valence cationic electrolyte solutions, zeta potential on the clay mineral surface increased with the increase of electrolyte solution concentration. Different cations have a greater impact on zeta potential, and cations in the same valence state have different zeta potentials, which was mainly due to the difference in the ion radius leading to different zeta potentials (Zhang Z. Y. et al., 2018). According to **Figure 7D**, by comparing the zeta potential of clay minerals at the same concentration of each electrolyte cation, the NH_4^+ absolute value of zeta potential was the largest, and the zeta potential value was negative. It was therefore easier to exchange the rare earth ions from weathered crust elution-deposited rare earth ore, verifying the ion-exchange effect of NH_4^+ with rare earth ions was better than other cations.

Correlation Between Rare Earth Leaching Efficiency and Zeta Potential Under Different Cation

In order to explore the relationship between the zeta potential on the clay mineral surface and the rare earth leaching efficiency, seven cations with different valence states were selected under the same anion of Cl^-. The zeta potential and rare earth leaching efficiency under each electrolyte were presented through electronic double-layer model, as shown in **Figure 8**. The fitting equations of zeta potential with leaching efficiency was shown in **Table 2**.

When the cation concentrations were 0.05, 0.10, 0.15, 0.20, and 0.25 mol/L, respectively, various rare earth leaching efficiencies and zeta potentials under different leaching conditions were shown in the above **Figure 8**. It can be seen from **Figure 8** that the zeta potential of clay minerals had

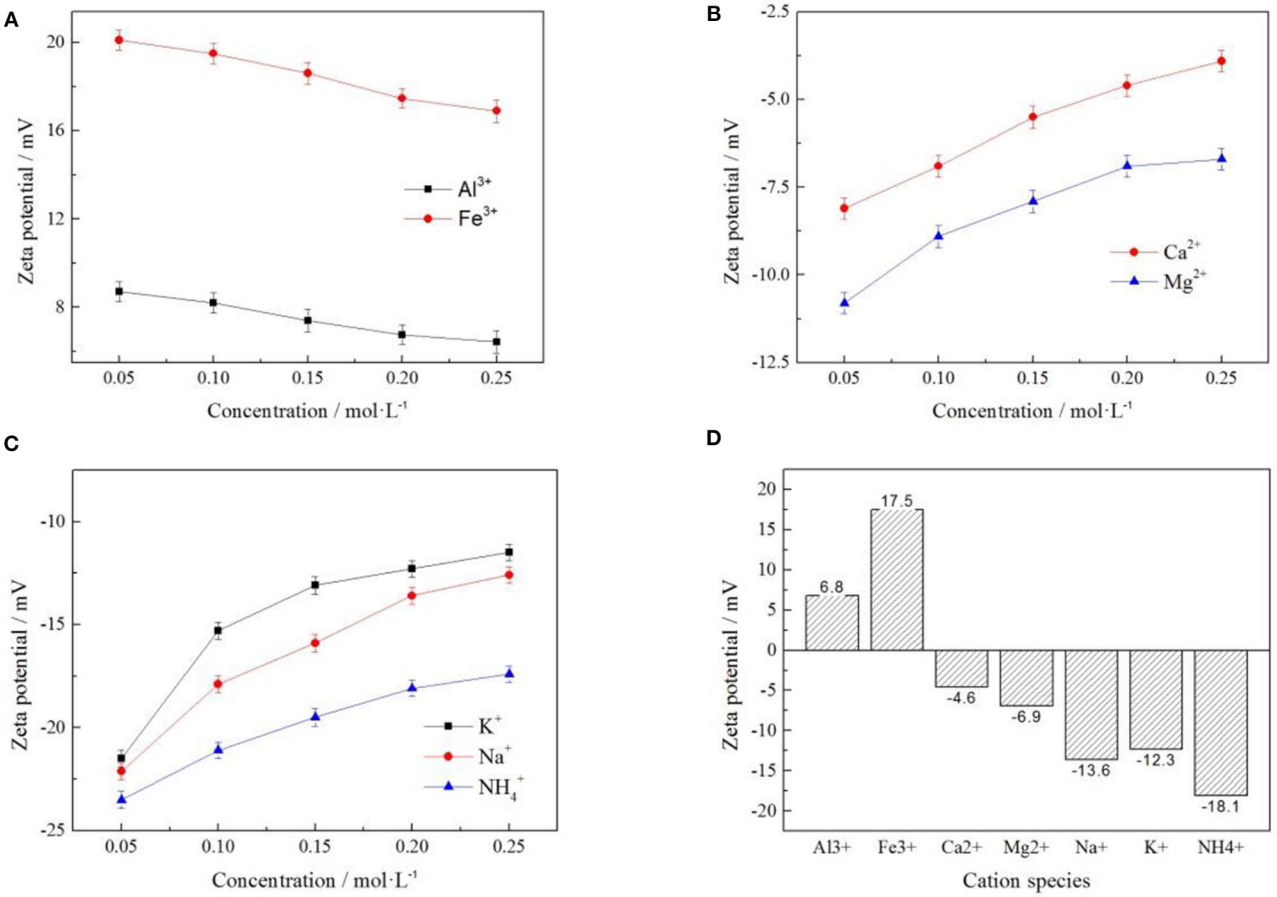

FIGURE 7 | Effect of cation concentration on zeta potential of clay minerals [where **(A?C)** represent +3, +2, and +1 valence cations respectively, **(D)** represents the zeta potential of clay minerals when the concentration of various cations was 0.2 mol/L].

a curve relationship with the rare earth leaching efficiency, which conforms to the Quadratic function fitting of the curve $Y = a + bX + cX^2$ (Yang et al., 2018; Qiu et al., 2019); this was related to the characteristic adsorption between ions. Under the conditions of trivalent cations Al^{3+} and Fe^{3+} electrolyte solution, the leaching efficiency of rare earth decreased with the increase of zeta potential of clay mineral in the leaching process. Under +1 and +2 valence cationic electrolyte solutions, the rare earth leaching efficiency increased with the zeta potential of the clay mineral. The leaching efficiency of rare earth increased with the decrease of the absolute value of zeta potential of clay minerals in electrolyte solution. Different cation exchange capacities of rare earth were different, and this exchangeable capacity was manifested in different cation valence states: $Al^{3+} > Fe^{3+}$, $Mg^{2+} > Ca^{2+}$, $NH_4^+ > K^+ > Na^+$. By comparing the three curves corresponding to Al^{3+}, Mg^{2+}, and NH_4^+, the rare earth leaching efficiency of NH_4^+ was the highest, and the corresponding zeta potential was negative with the largest absolute value. NH_4^+ was therefore selected to have the best effect on the rare earth leaching process.

Effects of Anion on Rare Earth Leaching in Weathered Crust Elution-Deposited Rare Earth Ore

Effect of Anion on Rare Earth Leaching Efficiency

In order to explore the influence of anion concentration on rare earth leaching efficiency, Cl^- NO_3^-, and SO_4^{2-}, three anions were selected under the same cation of NH_4^+ to investigate the effect of their different concentrations on rare earth leaching efficiency. The result was shown in **Figure 9**.

It can be seen from **Figure 9** that the rare earth leaching efficiency increased with the increase of anionic concentration. When the anion concentrations were in the range of 0.05–0.2 mol/L, the rare earth leaching efficiencies increased rapidly. When the anionic concentration was >0.2 mol/L, the growth rate of rare earth leaching efficiencies was gradually stable. Therefore, 0.2 mol/L was the optimal leaching concentration. The order of influence of three kinds of anions on rare earth leaching efficiencies as follows: $NO_3^- > Cl^- > SO_4^{2-}$. The rare earth leaching efficiency were 83.21, 81.52, and 80.12%, respectively. NO_3^- therefore had the best effect on the rare earth leaching process. In actual production, nitrate product belongs to

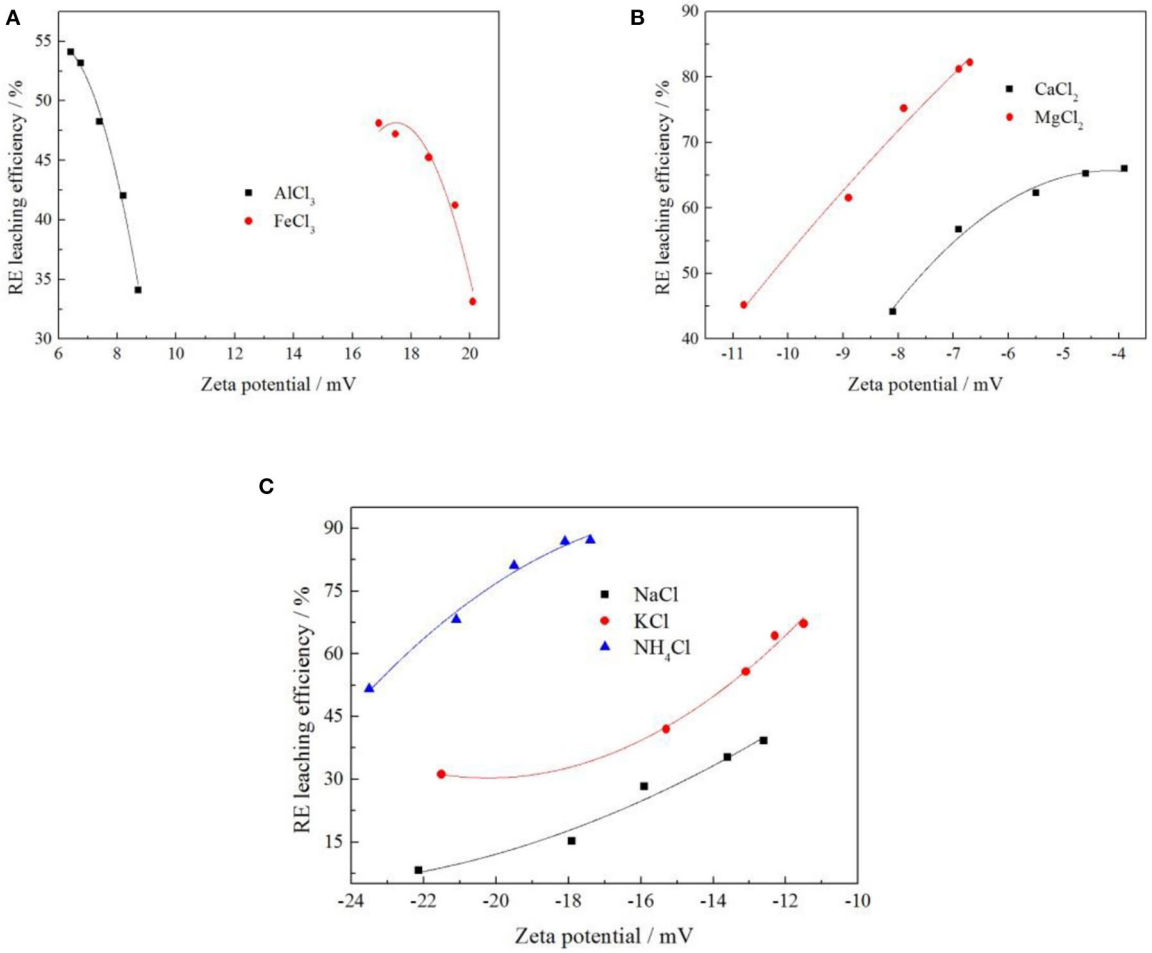

FIGURE 8 | Fitting of zeta potential and leaching efficiency under different cation [where **(A–C)** represent +3, +2, and +1 valence cations, respectively].

TABLE 2 | The fitting equation of cationic zeta potential—leaching efficiency.

Cation	Fitting equation	R^2
Al^{3+}	$Y = -2.52X^2 + 29.60X - 31.96$	0.98903
Fe^{3+}	$Y = -2.08X^2 + 72.77X - 588.15$	0.94190
Ca^{2+}	$Y = -1.36X^2 - 11.35X + 42.03$	0.98323
Mg^{2+}	$Y = -0.27X^2 + 4.50X + 125.45$	0.97740
Na^{+}	$Y = 0.18X^2 + 9.62X + 132.78$	0.94684
K^{+}	$Y = 0.51X^2 + 20.45X + 237.01$	0.98285
NH_4^+	$Y = -0.48X^2 - 13.51X - 1.58$	0.98133

restricted product, so Cl^-, which had little difference in leaching efficiency of rare earth, was normally chosen in the industry.

Effects of Anions on Zeta Potential of Clay Minerals

In order to explore the effects of anion concentration on the zeta potential of clay minerals, Cl^-, NO_3^-, and SO_4^{2-}, three anions were selected under the same cation of NH_4^+ to investigate the effects of these three anions on zeta potential of clay minerals at different concentrations. The result is shown in **Figure 10**.

As can be seen from **Figure 10**, the zeta potential of the clay mineral decreased with the increase of anion concentration, while the absolute value of zeta potential of the clay mineral gradually increased. The zeta potential order of the three kinds of anions on the clay mineral was $SO_4^{2-} > NO_3^- > Cl^-$, and this was because SO_4^{2-} itself contains more negative charges, which resulted in a higher zeta potential value, Cl^- and NO_3^- with the same negative charges having a similar effect on zeta potential, effects of binding anions on rare earth leaching efficiency, and NO_3^- having the best effect on rare earth leaching process. But in the actual production, the nitrate product mostly belongs to the controlled product, and we therefore chose Cl^-, which made little difference to the leaching efficiency.

Correlation Between RE Leaching Efficiency and Zeta Potential Under Different Anion

In order to explore the relationship between zeta potential of clay mineral and rare earth leaching efficiency under different anion.

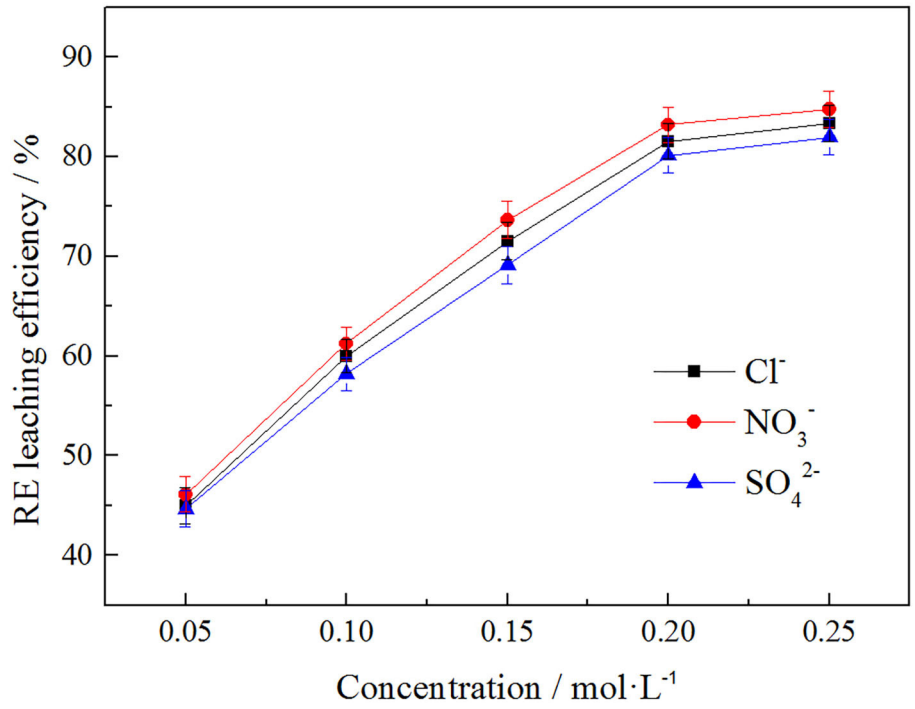

FIGURE 9 | Effect of anion concentration on rare earth leaching efficiency.

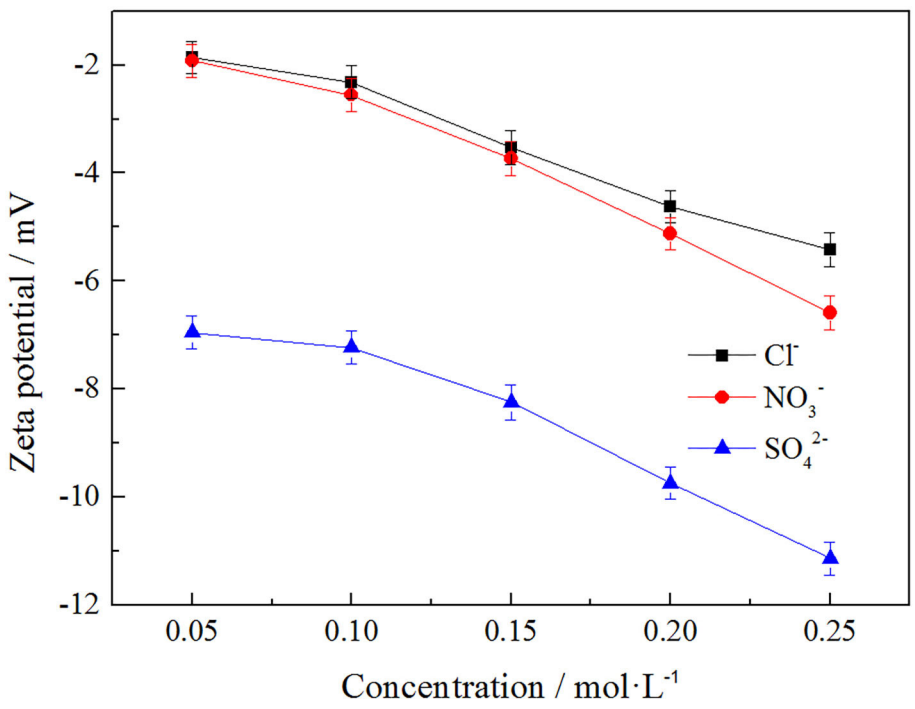

FIGURE 10 | Effect of anion concentration on surface potential of clay minerals.

The relationship between rare earth leaching efficiency and zeta potential was fitted when the electrolyte solution anions were Cl^{-}, NO_3^{-}, and SO_4^{2-}. The fitting results are shown in **Figure 11**, and the fitting equations are shown in **Table 3**.

It can be seen from **Figure 11** that under each electrolyte solution, the zeta potential of clay minerals had a curve relationship with the rare earth leaching efficiency, which conformed to the quadratic function fitting of the curve Y =

$aX^2 + bX + c$, and the fitting equations are shown in **Table 3**. **Figure 11** shows that the rare earth leaching efficiency decreased with the increase of zeta potential of clay minerals. The greater the absolute value of zeta potential of the clay mineral with the higher the rare earth leaching efficiencies. Because there were more exchangeable ions on the surface of the clay minerals, more rare earth ions were exchanged by the electrolyte solution. In **Figure 11B**, there was no significant difference between Cl^- and NO_3^- on zeta potential and rare earth leaching efficiency of clay minerals. In the actual production process, the nitrate product belongs to controlled products. When there were only negative monovalent anions, Cl^- was selected as the electrolyte anion to achieve better leaching effect of rare earth. When the SO_4^{2-} acted as an anion in the electrolyte solution, the zeta potential of clay minerals was relatively high due to its large negative charge. However, from the perspective of the influence of anions on the leaching efficiency of rare earth, the rare earth leaching efficiency of Cl^- as an electrolyte anion was higher than SO_4^{2-}; when Cl^- was available as an electrolyte anion, Cl^- can thus be preferred.

Effect of Different Ions on Swelling of Weathered Crust Elution-Deposited Rare Earth Ores

Effect of Different Cation on Swelling Ratio of Clay Minerals

To understand the effects of the different cation and cation concentration on the swelling ratio of the clay minerals, the samples were subjected to various cation and cation concentrations with the same anion. Swelling ratios were constructed using the experimental data, and the results are shown in **Figure 12**.

It can be seen from **Figure 12** when the cation of electrolyte solution for Al^{3+}, Fe^{3+}, and Ca^{2+} clay minerals swelling ratio increased as the concentration of electrolyte solution increased, as when the cation concentration increases, more cations were exchanged into the layered structure of clay mineral content. Due to ionic radius of Al^{3+}, Fe^{3+}, and Ca^{2+} were bigger, leading to the rise in swelling ratio of the clay minerals. When the cation of the electrolyte solution for Mg^{2+}, Na^+, K^+, and NH_4^+ clay mineral swelling ratio decreased as the concentration of electrolyte solution increased, the ion displayed a certain inhibition in terms of the swelling of clay minerals. Under the optimal electrolyte concentration of 0.2 mol/L, the swelling ratio of NH_4^+ and K^+ to clay minerals were 1.874 and 1.714%, respectively. In the actual production, NH_4^+ was easy to obtain and had low cost, so NH_4^+ was selected as the electrolyte cation with better technological value.

Effect of Different Anions on Swelling Ratio of Clay Minerals

To understand the effects of the different anion and anion concentration on the swelling ratio of the clay minerals, the samples were subjected to various anion and anion concentration with the same cation. Swelling ratios were constructed using the experimental data, and the results are shown in **Figure 13**.

It can be seen from **Figure 13** that the swelling ratio of clay minerals decreases with the increase of electrolyte solution anion concentration. The order of swelling ratio of the three types of anions to clay minerals was as follows: $SO_4^{2-} > NO_3^- > Cl^-$. When the electrolyte solution concentration was 0.2 mol/L, the swelling ratios of clay minerals were 2.297, 2.174, and 2.015%, respectively; when the anion was Cl^-, the swelling ratio of clay minerals was 2.015% at the minimum, and the rare earth leaching efficiency was 81.52% in this case. This indicates that in actual

TABLE 3 | The fitting equation of anionic potential—leaching efficiency.

Anion	Fitting equation	R^2
Cl^-	$Y = -1.22\,X^2 - 17.64X + 23.29$	0.99010
NO_3^-	$Y = -1.31\,X^2 - 18.33X + 20.99$	0.99675
SO_4^{2-}	$Y = -1.99\,X^2 - 44.23X - 163.93$	0.96463

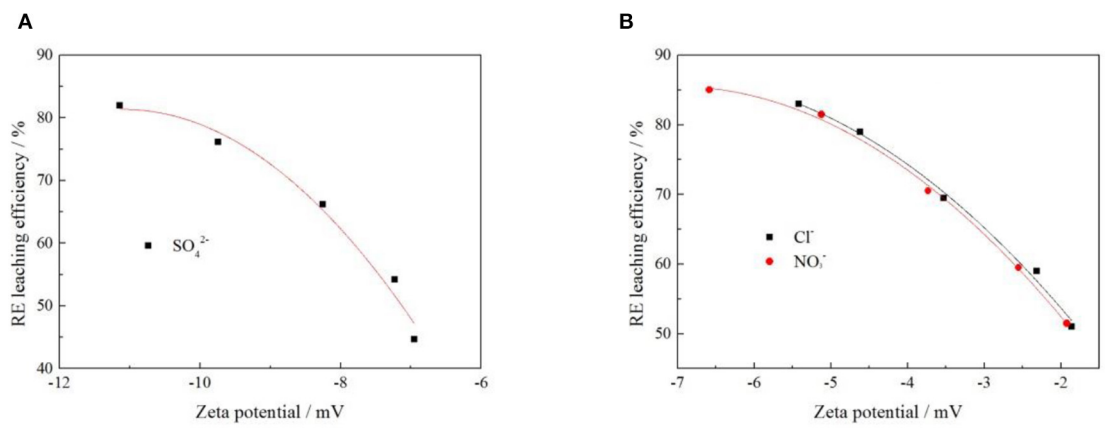

FIGURE 11 | Fitting of zeta potential and leaching efficiency under different anion [where **(A,B)** represent −2 and −1 valence anions, respectively].

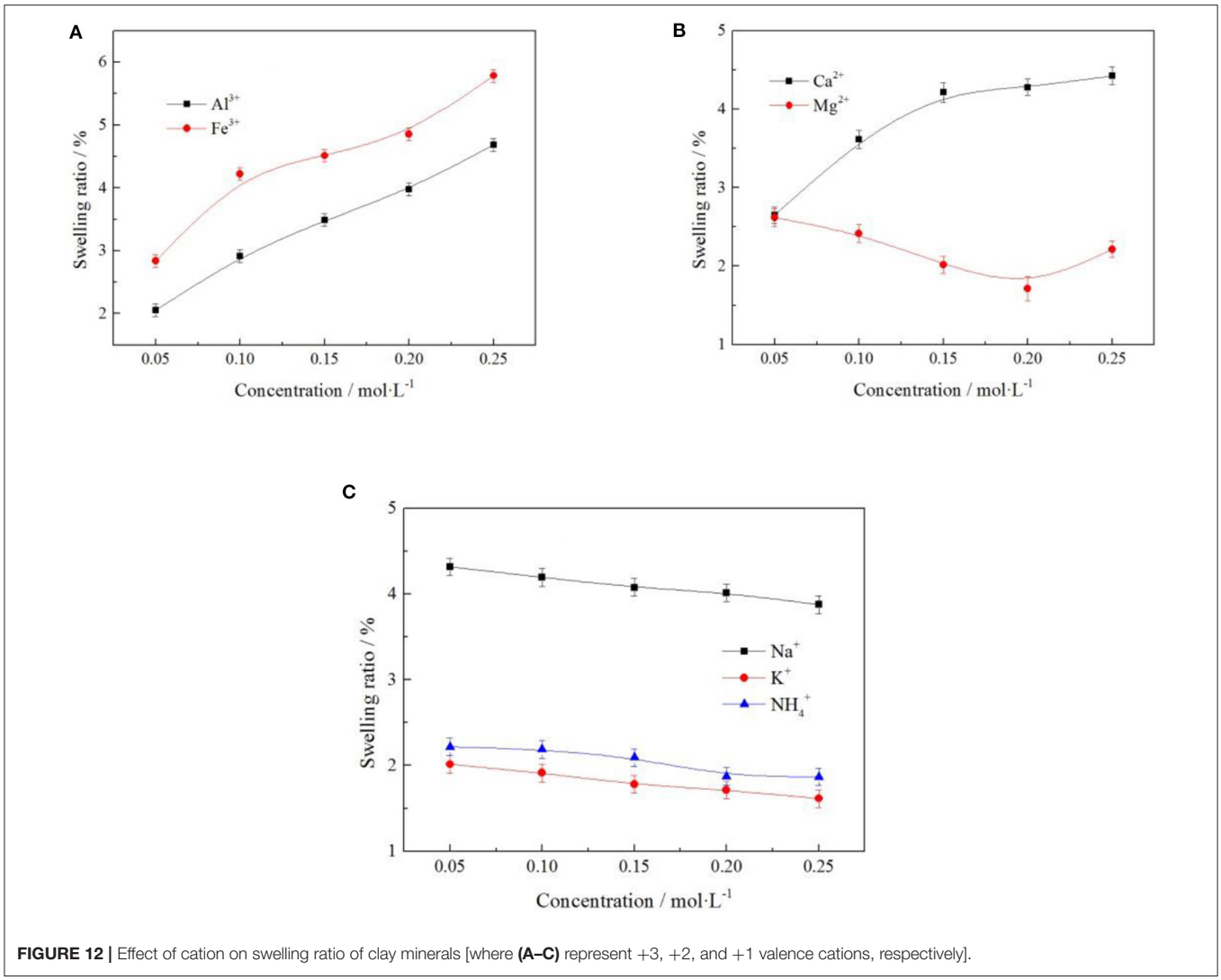

FIGURE 12 | Effect of cation on swelling ratio of clay minerals [where **(A–C)** represent +3, +2, and +1 valence cations, respectively].

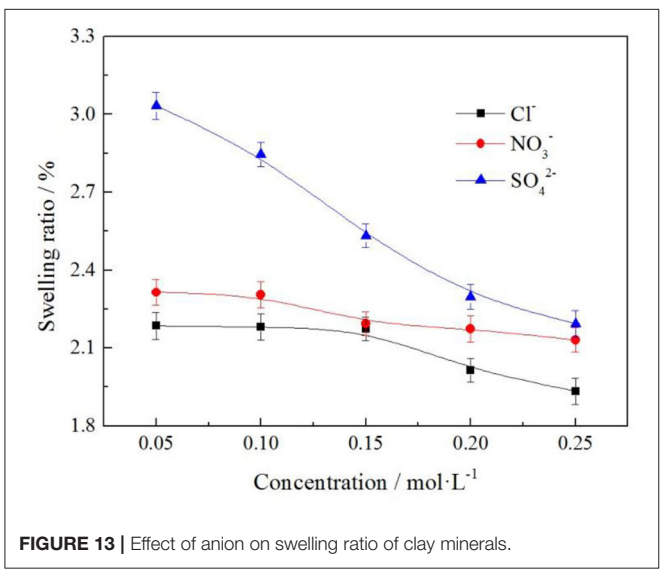

FIGURE 13 | Effect of anion on swelling ratio of clay minerals.

production, the anion selection Cl^- of electrolyte solution had the least influence on mine swelling but had a high rare earth leaching efficiency.

CONCLUSIONS

In the study of the influence of anion and cation on weathered crust elution-deposited rare earth ore, it was found that the order of the rare earth leaching ability in three valence cations of $NH_4^+ > K^+ > Na^+$, $Mg^{2+} > Ca^{2+}$, $Al^{3+} > Fe^{3+}$ and the NH_4^+ were the most affected electrolyte cations on rare earth leaching efficiency; rare earth leaching efficiency was 86.93% at the optimal leaching concentration. The influence of the three anions on the leaching efficiency of rare earth was as follows: $NO_3^- > Cl^- > SO_4^{2-}$. The leaching efficiencies of rare earth were 83.21, 81.52, and 80.12% at the optimal leaching concentration. Meanwhile, in the study of zeta potential on clay mineral surface, it was found that NH_4^+ had the greatest effect

on zeta potential in the influence of different cations on zeta potential of weathered crust elution-deposited rare earth ore, and the zeta potential was −18.1 mV at the optimal leaching concentration. The order of the effect of three anions on zeta potential was $SO_4^{2-} > NO_3^- > Cl^-$ in terms of the influence of anions on zeta potential of a weathered crust elution-deposited rare earth ore. Considering the relation between rare earth leaching efficiency and zeta potential, NH_4^+ was selected as the electrolyte cation to have the best effect on rare earth leaching process, while the anion was selected as NO_3^- to have the best effect. But in the actual production, the nitric acid product mostly belongs to the controlled product and therefore chose the Cl^-, which made little difference to the leaching efficiency. To sum up, when considering which electrolyte solution to use for cation and anion alone, the cation chooses NH_4^+, the anion chooses Cl^-, and the relationship between the rare earth leaching efficiency and zeta potential conforms to the following equations: NH_4^+:Y $= -0.48X^2 - 13.51X - 1.58$, $R^2 = 0.98133$; Cl^-:Y$= -1.22\ X^2 - 17.64X + 23.29$, and $R^2 = 0.99010$. In the experiment of the effect of various ions on the swelling of weathered crust elution-deposited rare earth ore, it is found that NH_4^+ and Cl^- have the least influence on the swelling of clay minerals, and the swelling ratios of NH_4^+ and Cl^- under the optimal rare earth leaching concentration were 1.874 and 2.015%, respectively.

DATA AVAILABILITY STATEMENT

The original contributions presented in the study are included in the article/supplementary materials, further inquiries can be directed to the corresponding author.

AUTHOR CONTRIBUTIONS

ZZ and RC designed the project. WC performed the experiments. ZZ and WC analyzed the data. WC, ZZ, and ZC wrote the manuscript. All authors contributed to the article and agreed to the published version of the manuscript.

FUNDING

All sources of funding of the study were supported by National Nature Science Foundation of China (52074195, 91962211, 21808176, and U1802252), Science and Technology Planing Projects of Guangdong Province, China (2020B1212060055), and Key Research & Development Plan of the Ministry of Science and Technology (2018YFC1801800).

REFERENCES

Chen, Z., Zhang, Z. Y., He, Z. Y., and Chi, R. A. (2018a). Mass transfer process of leaching weathered crust elution-deposited rare earth ore with magnesium salts. *Physicochem. Prob. Miner. Process.* 54, 1004–1013. doi: 10.5277/ppmp18102

Chen, Z., Zhang, Z. Y., Liu, D. F., Chi, X. W., Chen, W. D., and Chi, R. A. (2020). Swelling of clay minerals during the leaching process of weathered crust elution-deposited rare earth ores by magnesium salts. *Powder Technol.* 367, 889–900. doi: 10.1016/j.powtec.2020.04.008

Chen, W. D., Zhang, Z. Y., and Chi, R. A. (2020). Assisted leaching process of weathered crust elution-deposited rare earth ore by ammonium carboxylate. *Metal Mine* 5, 191–196.doi: 10.19614/j.cnki.jsks.202005028

Chen, Z., Zhang, Z. Y., Sun, N. J., Zhang, H., Liu, Z., and Chi, R. A. (2018b). Leaching kinetics of weathered crust elution-deposited rare earth ore with magnesium salt. *Metal Mine* 8, 84–91. doi: 10.19614/j.cnki.jsks.201808016

Chi, R. A., Wang, D. Z. (1993). REE distribution and application of LZX rare earth ore. *Chin. J. Rare Metals* 2, 16–21.

Chi, R. A., and Liu, X. M. (2019). Prospect and development of weathered crust elution-deposited rare earth ore. *J. Chin. Soc. Rare Earths* 37, 129–140. doi: 10.11785/S1000-4343.20190201

Chi, R. A., Tian, J., Luo, X. P., Xu, Z. G., and He, Z. Y. (2012). Basic research on weathered crust elution-deposited rare earth ores. *Jiangxi Nonferrous Metals* 4, 1–13. doi: 10.13264/j.cnki.ysjskx.2012.04.010

He, Z. Y., Zhang, Z. Y., Yu, J. X., Xu, Z. G., Xu, Y. L., Zhou, F., et al. (2016). Column leaching process of rare earth and aluminum from weathered crust elution-deposited rare earth ore with ammonium salts. *Trans. Nonfer. Metals Soc. China* 26, 3024–3033. doi: 10.1016/S1003-6326(16)64433-3

Huang, X. W., Long, Z. Q., Li, H. W., Ying, W. J., Zhang, G. C., and Xue, X. X. (2005). Development of rare earth hydrometallurgy technology in China. *J. Rare Earths* 23, 1–4. doi: 10.1166/jnn.2005.029

Li, S. C., Wang, X. J., Zou, Y. G., Huang, G. L., and Nie, Y. L. (2019). Study on the relationship between cationic activity of leaching agent and leaching characteristics of rare earth. *Min. Res. Dev.* 39, 104–108. doi: 10.13827/j.cnki.kyyk.2019.03.023

Qiu, H. X., Yuan, Y. S., Li, F. Y., Cui, C. L., Xue, Z. Z., Wei, F. C., et al. (2019). Leaching mechanism of ion-adsorption rare earth by mono valence cation electrolytes and the corresponding environmental impact. *J. Clean. Prod.* 211, 566–573. doi: 10.1016/j.jclepro.2018.11.112

Simandl, G. J. (2014). Geology and market-dependent significance of rare earth element resources. *Miner Deposit.* 49, 889–904. doi: 10.1007/s00126-014-0546-z

Wang, L., Wang, C., Liao, C. F., and Yang, Y. M. (2018). Effect of ionic interaction on leaching behavior of ion-adsorption type rare earth ore. *Chin. J. Rare Metals* 42, 1002–1008. doi: 10.13373/j.cnki.cjrm.XY17080018

Xiao, Y. F., Chen, Y. Y., Feng, Z. Y., Huang, X. W., Huang, L., Long, Z. Q., et al. (2015a). Leaching characteristics of ion-adsorption type rare earths ore with magnesium sulfate. *Trans. Nonfer. Metals Soc. China* 25, 3784–3790. doi: 10.1016/S1003-6326(15)64022-5

Xiao, Y. F., Liu, X. S., Feng, Z. Y., Huang, X. W., Huang, L., Chen, Y. Y., et al. (2015b). Role of minerals properties on leaching process of weathered crust elution-deposited rare earth ore. *J. Rare Earths* 33, 545–552. doi: 10.1016/S1002-0721(14)60454-3

Yang, L. F., Wang, D. S., Li, C. C., Sun, Y. Y., Zhou, X. Z., and Li, Y. X. (2018). Searching for a high efficiency and environmental benign reagent to leach ion-adsorption rare earths based on the zeta potential of clay particles. *Green Chem.* 20, 4528–4536. doi: 10.1039/C8GC01569D

Zhang, B., Ning, Y. K., Cao, F., and Yang, H. P. (2018). Current situation of worldwide rare earth resources. *Multipurpose Utilization Mineral Resourc.* 4, 7–12. doi: 10.3969/j.issn.1000-6532.2018.04.002

Zhang, Z. Y., He, Z. Y., Xu, Z. G., Yu, J. X., Zhang, Y. F., and Chi, R. A. (2016a). Rare earth partitioning characteristics of china rare earth ore. *Chin. Rare Earths* 37, 121–127. doi: 10.16533/J.CNKI.15-1099/TF.201601020

Zhang, Z. Y., He, Z. Y., Yu, J. X., Xu, Z. G., and Chi, R. A. (2016b). Novel solution injection technology for in-situ leaching of weathered crust elution-deposited rare earth ores. *Hydrometallurgy* 164, 248–256. doi: 10.1016/j.hydromet.2016.06.015

Zhang, Z. Y., He, Z. Y., Zhou, F., Zhong, C. B., Sun, N. J., and Chi, R. A. (2018). Swelling of clay minerals in ammonium leaching of weathered crust elution-deposited rare earth ores. *Rare Metals* 37, 72–78. doi: 10.1007/s12598-017-0977-7

Zhang, Z. Y., Xu, Z. G., Wu, M., Zhang, T. T., Li, Q., and Chi, R. A. (2013). Study on leaching of rare earth ore with complex ammonium agents. *Nonfer. Metals* 4, 32–35. doi: 10.3969/j.issn.1007-7545.2013.04.009

Zou, H. L., Zhang, Z. Y., Chen, Z., Liu, D. F., Chai, X. W., Zhang, H., et al. (2020). Seepage process on weathered crust elution-deposited rare earth ores with ammonium carboxylate solution. *Physicochem. Problems Miner. Process.* 56:89–101. doi: 10.5277/ppmp19084

Conflict of Interest: The authors declare that the research was conducted in the absence of any commercial or financial relationships that could be construed as a potential conflict of interest.

frontiers in Chemistry

ORIGINAL RESEARCH
published: 20 January 2021
doi: 10.3389/fchem.2020.592837

Study on Extraction Separation of Thioarsenite Acid in Alkaline Solution by CO_3^{2-}-Type Tri-n-Octylmethyl-Ammonium Chloride

Kang Yan[1], *Liping Liu*[1], *Hongxing Zhao*[1], *Lei Tian*[1,2], *Zhifeng Xu*[3]* *and Ruixiang Wang*[1]*

[1] School of Metallurgical Engineering, Jiangxi University of Science and Technology, Ganzhou, China, [2] Henan Yuguang Gold and Lead Group Co., Ltd., Jiyuan, China, [3] President Office, Jiangxi College of Applied Technology, Ganzhou, China

To overcome the problem of arsenic separation and enrichment from an alkaline leaching solution in arsenic-containing dust, a CO_3^{2-}-type tri-n-octylmethyl-ammonium chloride (TOMAC) method for extracting thioarsenite is proposed in this paper. Considering an alkaline leaching solution as the research object, after vulcanization pretreatment, TOMAC transformation and organic phase saturated extraction capacity were measured, and the extraction mechanism was preliminarily studied. First, Cl^--type quaternary ammonium salt was effectively transformed to HCO_3^--type by treating organic phase with saturated $NaHCO_{3five}$ times. TOMAC was effectively transformed from HCO_3^- to CO_3^{2-} type by alkaline washing with 1.0 mol/l NaOH solution; this washing was repeated thrice. Thereafter, the effects of organic phase composition, phase ratio, extraction time, and temperature on the extraction and separation of arsenic were investigated. The results show that under the conditions of 30% CO_3^{2-}-type TOMAC + 15% sec-octanol + 55% sulfonated kerosene, V_O/V_A = 1/1, and 5 min extraction at room temperature, the single-stage extraction rate of As^{III} is 85.2%. The As^{III} concentration in raffinate can be reduced to less than 1.33×10^{-3} mol/l by four-stage countercurrent extraction, and the extraction rate of As^{III} can exceed 98.4%.

Keywords: extraction separation, thioarsenite acid, alkaline solution, CO_3^{2-}-type, tri-n-octylmethyl-ammonium chloride

OPEN ACCESS

Edited by:
Wencai Zhang,
Virginia Tech, United States

Reviewed by:
Jotheeswari Kothandaraman,
Pacific Northwest National Laboratory (DOE), United States
Junwei Han,
Central South University, China

***Correspondence:**
Zhifeng Xu
xzf_1@163.com
Ruixiang Wang
wrx9022@163.com

Specialty section:
This article was submitted to Green and Sustainable Chemistry, a section of the journal Frontiers in Chemistry

Received: *08 August 2020*
Accepted: *08 December 2020*
Published: *20 January 2021*

Citation:
Yan K, Liu L, Zhao H, Tian L, Xu Z and Wang R (2021) Study on Extraction Separation of Thioarsenite Acid in Alkaline Solution by CO_3^{2-}-Type Tri-n-Octylmethyl-Ammonium Chloride. Front. Chem. 8:592837. doi: 10.3389/fchem.2020.592837

INTRODUCTION

Arsenic and its compounds are volatile. Arsenic is mainly concentrated in smelting dust, owing to the high-temperature volatilization, airflow movement, and mechanical inclusion during the smelting process of heavy non-ferrous metals, such as copper, lead, and zinc (Christof Lanzerstorfer, 2016). Arsenite or subarsenite is formed by the collision and adsorption of arsenic with lead, antimony, zinc, and other elements in high-temperature gas. The content of arsenic has a wide range from 10 to 40% (Jarošíková et al., 2018). Besides arsenic, high arsenic dust also contains a large amount of valuable metals, such as copper, lead, zinc, tin, and indium, which have high economic value (Asanov et al., 2016). High arsenic dust has the environmental characteristics of large production and high toxicity.

The arsenic content in smelting dust is volatile, which has the characteristics of large production and high toxicity. Therefore, it is necessary to efficiently separate arsenic from smelting dust for further recycling (Ermolin et al., 2019). There have been many studies on arsenic removal from smelting dust, including roasting, leaching, and combined pyro-hydrometallurgical processes. Arsenic removal by calcination serves mainly to volatilize arsenic in the form of arsenic trioxide in materials containing arsenic at high temperature, separate it from other valuable metals, and then obtain crude arsenic trioxide products through condensation and dust collection (Montenegro et al., 2013).

Arsenic is extracted from copper dust by leaching process; leaching can be classified as hot water leaching, acid leaching, and alkaline leaching according to the properties of leaching solution (Guo et al., 2016). The following methods for separating and enriching arsenic from leaching liquid include evaporation concentration crystallization, lime precipitation, ferric salt precipitation, sodium sulfide precipitation, adsorption, and solvent extraction (Hoffmann, 1993; Sanchez de la Campa et al., 2008; Morales et al., 2010). Sahu et al. investigated the acid leaching of copper from the soot of electrostatic precipitator (ESP) liner used in a copper smelter plant. Results showed that the acid concentration of 1.5 M and pulp density of 20% was found to be optimum, and the leaching efficiency of copper was 97% at 97°C (Sahu et al., 2012).

To achieve the resource utilization of flue dust, most copper smelters send flue dust and copper concentrate directly back to the smelting system, which greatly increases the content of impurities (especially arsenic) in the flash-smelting furnace. The Kosaka smelter in Japan has been operated with the open-process hydrometallurgical treatment for flue dust since 1975. This process involves recovering copper and zinc from the flue dust leaching solution and lead from the leaching slag. Similarly, most studies in this area have adopted the combined process of "hydro and pyro metallurgy" to treat the flue dust, i.e., to leach copper and zinc using water or dilute sulfuric acid and recover lead from the leaching slag through reduction smelting.

Karimov et al. studied the sulfuric acid leaching of dust left over from the reduction smelting at the Middle Ural Copper Smelter. The results showed that the optimum parameters for leaching dust were a temperature of 60°C and an initial acid concentration of 25 g/dm^3. Performing the leaching operation with these parameters maximizes the yields of arsenic, copper, and zinc (98% As, 39% Cu, and 82% Zn) (Karimov and Naboichenko, 2016). Yang et al. reported the recovery of metals from copper smelting dust via H_2SO_4 and H_2O_2 leaching. Under optimum conditions, the leaching efficiencies achieved for Cu, As, Fe, Cd, and Zn were 93.4, 94.2, 39.7, 98.1, and 90.7%, respectively (Yang et al., 2017). Liu et al. investigated the metal extraction from copper smelting dust using oxidation leaching and the control of potential technology. The results showed that under the conditions of an H_2O_2 dosage of 0.8 ml/g (redox potential is 429 mV), H_2O_2 feeding speed of 1.0 ml/min, initial H_2SO_4 concentration of 1.0 mol/l, initial HCl concentration of 1.0 mol/l, leaching temperature of 80°C, initial liquid-to-solid ratio of 5:1 ml/g, and leaching time of 1.5 h, copper and arsenic can be effectively leached from copper smelting dust, leaving residue as a suitable lead resource. The average leaching efficiencies of copper, arsenic, and iron were 95.27, 96.82, and 46.65%, respectively (Liu et al., 2018). Xu et al. studied pressure-leaching technology in the treatment of high-copper and high-arsenic dust. At a liquid-to-solid ratio (ml/g) of 5:1, a leaching temperature of 453 K, a retention time of 2 h, an initial sulfuric acid concentration of 0.74 mol/l, an oxygen partial pressure of 0.7 MPa, and an agitation speed of 500 r/min, 95% of copper, 99% of zinc, and only 6% of iron in the dust were leached, whereas ∼20% of arsenic was also leached. The leaching technique was optimized further to restrain the leaching of arsenic through the addition of a small amount of ferrous iron into the leaching system [$c(\mathrm{Fe}(2+)) = 0.036$ mol/l] (Xu et al., 2010).

While extracting arsenic from flue dust using dilute acid, significant dispersibility can be observed; ∼50% of arsenic enters the solution, whereas the other half enters the slag. The chemical precipitation of arsenic in the leaching solution can result in a loss of valuable metals, whereas the landfilling and stockpiling of the arsenic slag can result in potential secondary pollution. Consequently, the separation and enrichment of arsenic using the traditional extraction process is low; therefore, it is not suitable for the resource utilization and harmless disposal of high arsenic flue dust.

In contrast, arsenic oxides and arsenates are easily soluble in alkaline medium, based on which some studies have proposed the use of alkaline leaching to achieve arsenic concentration in the water phase. Reynolds et al. carried out NaOH leaching on the pressure-leaching slag of copper smelting dust (arsenic and iron slag), reaching an arsenic leaching rate of 88.3% (Reynolds, 1981). Furthermore, the NaOH-Na_2S alkaline leaching process for the oxidation leaching of high arsenic flue dust led to an arsenic leaching rate of greater than 90% (Liu et al., 2009). Rappas et al. adopted a two-stage alkaline leaching process to effectively separate arsenic from lead and bismuth (Rappas et al., 1990). In fact, for high arsenic materials (e.g., arsenic sulfide slag), alkaline leaching is equally effective in arsenic removal (Zheng et al., 2008).

Although the effective separation of arsenic and the treatment of valuable metals can be achieved by alkaline leaching, how to recycle the alkali liquor and enrich arsenic efficiently to facilitate a final harmless disposal are the key difficulties. Therefore, a new process has been proposed; this process involves closed alkaline leaching, double-sulfuration synergistic solvent extraction, de-arsenic–lime cascade precipitation, and arsenic–carbon thermal reduction for high arsenic copper smelting ash (as shown in **Figure 1**).

Based on previous experimental studies (Xu et al., 2016), the sulfurized products of arsenous acid under alkaline conditions are mainly $HAsO_2S^{2-}$ and $HAsOS_2^{2-}$; however, there are currently still some limitations on the extraction and stripping of thioarsenite in alkaline solutions. In alkaline media, arsenic exists in the form of thioarsenite anions, and quaternary ammonium salt is a strong base salt, which contains R_4N^+ groups to extract complex anion (Guan and Zhang, 2011). Therefore, herein, experiments on the extraction and stripping of thioarsenite in NaOH solutions were conducted

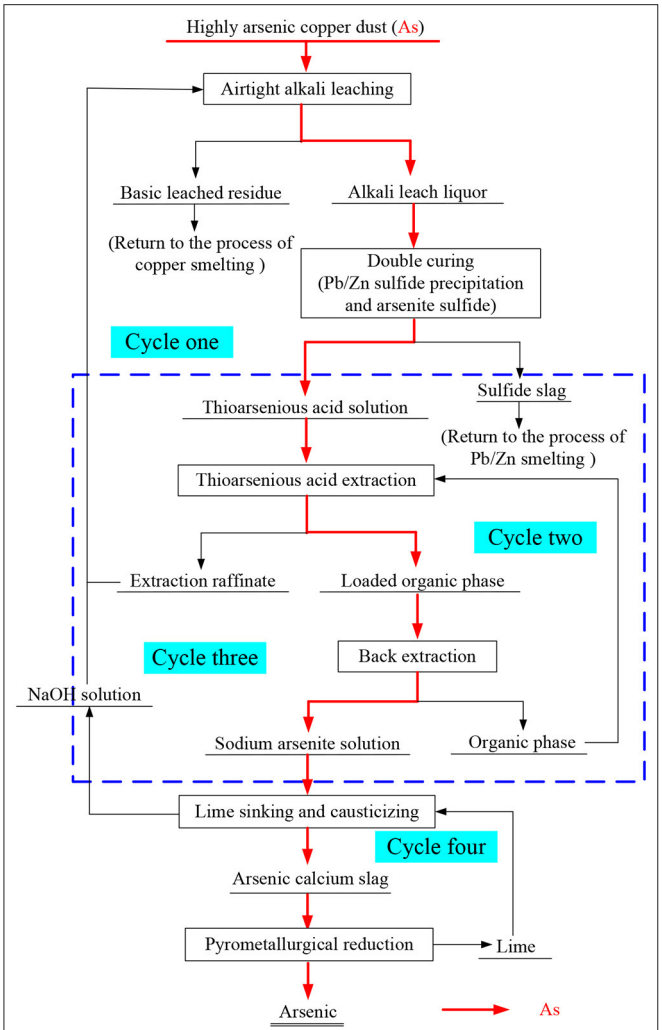

FIGURE 1 | Process flow chart of "closed" alkali leaching double sulfurization coordination solvent extraction arsenic removal lime cascade arsenic deposition carbothermal reduction".

using tri-n-octylmethyl-ammonium chloride (TOMAC) as the extractant and CO_3^{2-} for anion conversion. This study provided solutions for the extraction and separation of arsenic in an alkaline medium and laid the theoretical foundation for the realization of a highly efficient process of arsenic separation, improvement in arsenic resource utilization, and establishment of a comprehensive recovery system of valuable metals.

EXPERIMENTAL

Materials

TOMAC was kindly supplied by Shanghai Titan Technology Co., Ltd. All the extractants were used without further purification and dissolved in sulfonated kerosene provided by Nanjing Runchuan Petrochemical Co. Ltd., China at the required concentrations. The thioarsenious acid solutions were prepared by dissolving $NaAsO_2$ and $Na_2S{\cdot}9H_2O$ (Aladdin, Shanghai) in lye

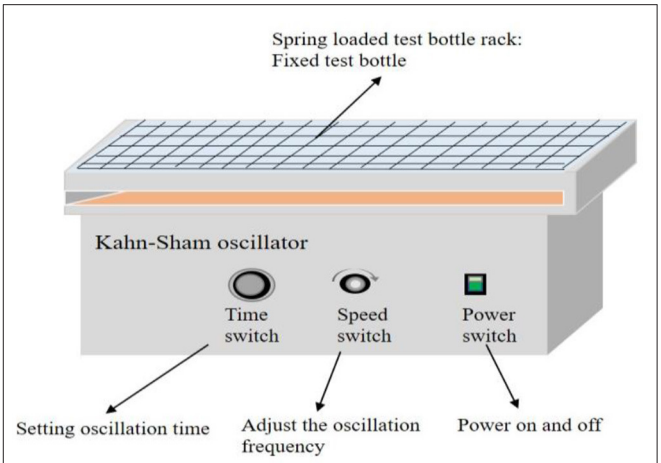

FIGURE 2 | Construction of Kahn-Sham oscillator.

(NaOH) to the required concentration under different conditions of temperature and time. All the other reagents and chemicals used were of analytical reagent grade.

Leaching Experiment

TOMAC Transformation From Cl^- to CO_3^{2-} -Type Experiment

After the addition of a certain amount of TOMAC into a pear-shaped funnel, $NaHCO_3$ saturated solution was added, $V_O/V_A = 1/1$, and the conditions of water phase are as follows: the concentration of NaOH is 0.5 mol/l and the concentration of As^{III} is 9.69×10^{-2} mol/l. The first extractant transformation was completed after 10 min of mixing in a Kohn–Sham (KS) oscillator, and the construction is shown in **Figure 2**. Then, the organic phase and water phase were separated, and the concentration of Cl^- in the solution after transformation was analyzed to obtain the anion conversion rate of TOMAC from Cl^- to HCO_3^- type. The second mixed organic phase transformation was conducted using NaOH solution at a certain concentration by the same experimental procedure as the first. After the second extractant transformation, the concentrations of CO_3^{2-} and OH^- in the solution were analyzed again to obtain the anion conversion rate of TOMAC from HCO_3^- to CO_3^{2-} type.

Extraction of Thioarsenious Acid With CO_3^{2-}-Type TOMAC

CO_3^{2-}-type TOMAC and thioarsenious acid solutions were mixed in a pear-shaped separating funnel according to a certain ratio of O/A for a certain period of time in an air bath constant temperature oscillator at a set temperature and then settled for phase separation; then, the concentration of As^{III} in the liquid after exchange was analyzed. In this manner, the As^{III} extraction rate of CO_3^{2-}-type TOMAC was obtained.

Loaded Organic Reverse Extraction Experiment

After a stripping agent was prepared according to a certain concentration, it was placed into a pear-shaped funnel with loaded organic phase at a certain O/A ratio. Then, the phase was

separated at room temperature after mixing in the KS oscillator for a certain period of time. Then, the As^{III} concentration in the solution after conversion was analyzed to obtain its stripping rate in the loaded organic phase.

Analysis Method and Data Processing

Detection of As Content in Solution

The concentration of As is mainly determined using potassium bromate titration in GB/T3884-20128. Using KBr as the catalyst, arsenic (V) is reduced to a lower valence state in HCl; thereafter, arsenic is separated with As_2Cl_3. After the absorption of water by As_2Cl_3, sodium p-dimethylaminoazobenzene sulfonate is used as an indicator. Finally, As is titrated with a prepared $KBrO_3$ standard solution. The final concentration of As is expressed by Equation (1),

$$\beta = V_2 \times c_1 \times M_1 / V_1 \times 10^3, \tag{1}$$

where β is the concentration of As (mg/l), V_1 is the volume of the aqueous phase (ml), V_2 is the volume of $KBrO_3$ consumed during the titration (ml), c is the concentration of the $KBrO_3$ standard solution (mol/l), and M_1 is the molar mass of 1/2 As (37.46 g/mol).

Determination of Cl^- Concentration in Solution

The concentration of Cl^- is determined by the molar method, and the analytical procedure is mainly referred to GB/T 15453-2008, with a determination range of 10–120 mg/l. For the pH value of 5.0–9.5, using K_2CrO_4 as the indicator, $AgNO_3$ solution with a known accurate concentration was used to titrate the sample to be determined. $AgNO_3$ reacts with chloride to produce AgCl, and excessive $AgNO_3$ reacts with K_2CrO_4 to produce Ag_2CrO_4. When a precipitate is produced, the indicator stops dropping. The final concentration of Cl^- is expressed by Equation (2),

$$\rho = V_4 \times c_2 \times M_2 / V_3 \times 10^3, \tag{2}$$

where ρ is the concentration of Cl^- (mg/l), V_3 is the volume of the aqueous phase (ml), V_4 is the volume of $AgNO_3$ consumed during the titration (ml), c is the concentration of the $AgNO_3$ standard solution (mol/l), and M_2 is the molar mass of Cl^- (35.50 g/mol).

Determination of CO_3^{2-} and OH^- Concentrations in Solution

The concentrations of CO_3^{2-} and OH^- were determined using titration. The analysis steps were mainly referred to as DZ/T0064.49-93; the detection range for CO_3^{2-} and OH^- concentration was no less than 10 and 4 mg/l, respectively. The titrant solution of HCl with a precise known concentration was used; the indicators were phenolphthalein and sodium dimethylaminoazobenzene sulfonic acid solution.

After the addition of an appropriate volume (V) of the feed solution into a conical flask, a few drops of phenolphthalein were added. If the solution turned red, HCl solution with a precise known concentration was added until the red color in the feed solution faded, and its added amount (V_5) was recorded. Subsequently, three drops of sodium dimethylaminoazobenzene sulfonic acid solution was also added into the conical flask. The continuous addition of HCl solution with a precise known concentration was performed until the feed solution turned orange, and the amount of HCl (V_6) added was recorded.

The contents of CO_3^{2-} and OH^- are expressed by Equations (3) and (4), respectively:

$$C_1 = (V_5 - V_6) \times c_3 \times M_3 / V_7 \times 10^3, \tag{3}$$

$$C_2 = 2V_6 \times c_3 \times M_4 / V_7 \times 10^3, \tag{4}$$

where C_1 and C_2 are the concentrations of OH^- and CO_3^{2-} (mg/l), respectively, V_5 and V_6 are the volumes of HCl consumed by the first and second titrations (ml), respectively, V_7 is the volume of the aqueous phase (ml), c is the concentration of the HCl standard solution (mol/l), and M_3 and M_4 are the molar mass of OH^- (17.01 g/mol) and 1/2 CO_3^{2-} (30.01 g/mol), respectively.

Extraction Rate and Back Extraction Rate of As

After solvent extraction, the extraction rate of As is calculated using Equation (5),

$$\eta = (C_3 \times V_8 - C_4 \times V_9) / (C_3 \times V_8) \times 100\%. \tag{5}$$

The arsenic-supported organic phase is back-extracted, whereas the back extraction rate of arsenic is calculated by Equation (6):

$$\sigma = (C_5 \times V_{10}) / (C_3 \times V_8 - C_4 \times V_9) \times 100\%, \tag{6}$$

where η is the extraction ratio of As (%), σ is the stripping ratio of As (%), C_3 is the concentration of As in the feed solution (g/l), V_8 is the volume of feed solution (ml), C_4 is the concentration of As in the raffinate (g/l), V_9 is the volume of raffinate (ml), C_5 is the concentration of As in the strip liquor (g/l), and V_{10} is the volume of strip liquor (ml).

RESULTS AND DISCUSSION

The Transformation of TOMAC

CO_3^{2-} Transformation Mechanism of TOMAC

According to the literature (Wu et al., 2017; Buev et al., 2018), the more lipophilic anions are more likely to react with the quaternary ammonium cations and enter the organic phase. The order of association of quaternary ammonium cations with each anion is roughly as follows:

$$ClO_4^- > I^- >> ClO_3^- > Cl^- > HSO_4^- > HCO_3^- > SO_4^{2-} > OH^- > CO_3^{2-} > S^{2-} > AsO_4^{3-} > SiO_3^{2-}$$

From the above, the association ability of Cl^- to quaternary ammonium salt cation is evidently relatively strong, whereas that

of arsenic anion is relatively weak, which is the main reason for the inhibition of arsenic extraction. A larger anion radius corresponds to a smaller charge, and a lower degree of hydration of the aqueous solution corresponds to a greater advantage in extraction (Suflet et al., 2015; Chauhan and Kaur, 2017). It can be inferred that the association ability of $HAsOS_2^{2-}$ is between CO_3^{2-} and AsO_4^{3-}, and the extraction ability of arsenic may be improved if the Cl^- quaternary ammonium salt is transformed into the CO_3^{2-} type. However, the direct transformation process may not be easy to perform, because the strong association anion is easy to exchange with the weak association anion; otherwise, it is very difficult.

The experimental results of direct transformation of TOMAC by 8% Na_2CO_3 showed that under the conditions of 30% TOMAC + 15% sec-octyl alcohol + 55% sulfonated kerosene, $V_O/V_A = 1/1$, the compositions of water phase are 0.5 mol/l NaOH, the concentration of As^{III} is 9.69×10^{-2} mol/l, and as the transformation times range from 1 to 5, the extraction rate of As^{III} is from 47.3 to 63.7%. The extraction rate hardly increased with the transformation time increase. In view of the difficulty of the direct conversion from Cl^--type TOMAC to CO_3^{2-}-type TOMAC, this study also considered a step-by-step conversion method. Because the associative ability of HCO_3^- is clearly stronger than that of CO_3^{2-} and weaker than that of Cl^-, based on the principle of concentration gradient equilibrium, the Cl^--type quaternary ammonium salt is first converted into HCO_3^--type by a high-concentration HCO_3^- solution. Then, the final conversion of CO_3^{2-} is achieved by alkaline washing.

The conversion process of Cl^-- to HCO_3^--type TOMAC can be expressed by the following Equation (7):

$$R_4NCl + HCO_3^- \rightarrow R_4NHCO_3 + Cl^-. \quad (7)$$

The intermediate product HCO_3^--type TOMAC is subjected to alkaline washing, and the reaction expressed in Equation (8) is

$$2R_4NHCO_3 + 2OH^- \rightarrow (R_4N)_2CO_3 + CO_3^{2-} + 2H_2O. \quad (8)$$

CO_3^{2-} Transformation Process of TOMAC

The experiment was conducted using a saturated $NaHCO_3$ aqueous solution as a transition agent, and the effect of the number of treatments with saturated $NaHCO_3$ solution on the conversion of TOMAC from Cl^-- to HCO_3^--type was investigated. The experimental results are shown in **Figure 3**.

As shown in **Figure 3**, the extraction rate of As^{III} from TOMAC significantly increases after the saturated $NaHCO_3$ treatment, from 16.3 to 32.8% after one saturated $NaHCO_3$ treatment. This shows that improving the extraction capacity of As^{III} is feasible through the transformation of TOMAC. Further, **Figure 3** shows that with increasing number of times of contact between organic phase and saturated $NaHCO_3$ solution, the concentration of Cl^- in the solution after conversion successively decreases, indicating that the transformation efficiency is constantly improving. Moreover, as the concentration of Cl^- in the solution after conversion decreases and gradually reaches

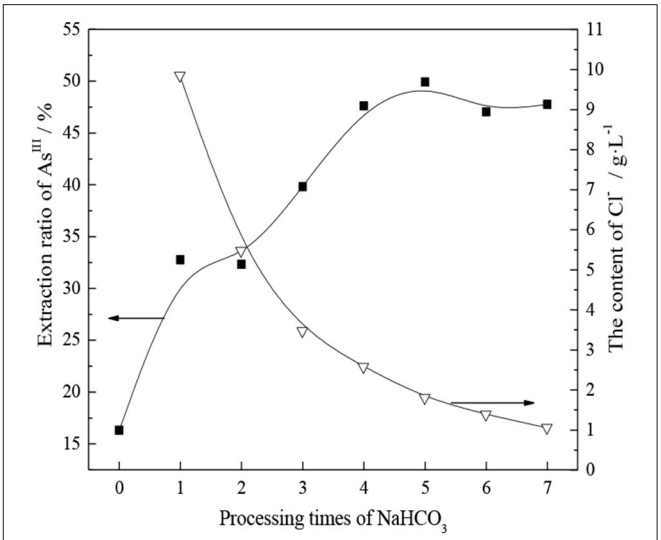

FIGURE 3 | Relationship between the extraction rate of As^{III} and the number of treatments with saturated $NaHCO_3$.

equilibrium, the extraction rate of As^{III} after the extractant transformation continues to increase to 47.5%, until a significant change is no longer observed. In summary, after treating the organic phase with saturated $NaHCO_3$ five times, the Cl^--type quaternary ammonium salt can be effectively converted into HCO_3^--type quaternary ammonium salt.

From section CO_3^{2-} Transformation Mechanism of TOMAC, TOMAC of HCO_3^- type can be further transformed into CO_3^{2-} type by alkali washing. However, in the process of alkali washing, if the concentration of NaOH is too high, TOMAC may be transformed into R_4NOH, with poor stability. If the concentration of NaOH is too low, the number of alkali washings may need to increase, which affects the transformation efficiency (Weisshaar et al., 2012). Therefore, the effects of NaOH concentration and the number of alkali washings on the further conversion of HCO_3^--type quaternary ammonium salt and the extraction rate of As^{III} were investigated, respectively, and the experimental results are shown in **Figure 4**.

As shown in **Figure 4**, with the NaOH concentration range of 0.5–1.0 mol/l in the wash solution, the treatment has little effect on the As^{III} extraction rate; however, the As^{III} extraction rate increases more significantly with an increase in the number of treatments. For an NaOH concentration of 1.5 mol/l, the extraction rate of As^{III} increases with an increase in the number of treatments. The extraction efficiency of As^{III} increases with the number of alkali washings owing to the transformation of TOMAC from HCO_3^- to CO_3^{2-} type.

The effects of NaOH concentration and number of alkaline washings on the As^{III} extraction rate were comprehensively analyzed, and results are shown in **Figure 5**. Under different alkali concentration conditions, with an increase in the number of alkali washings, the pattern of successive increases of As^{III} extraction rate remains basically the same. With an increase in

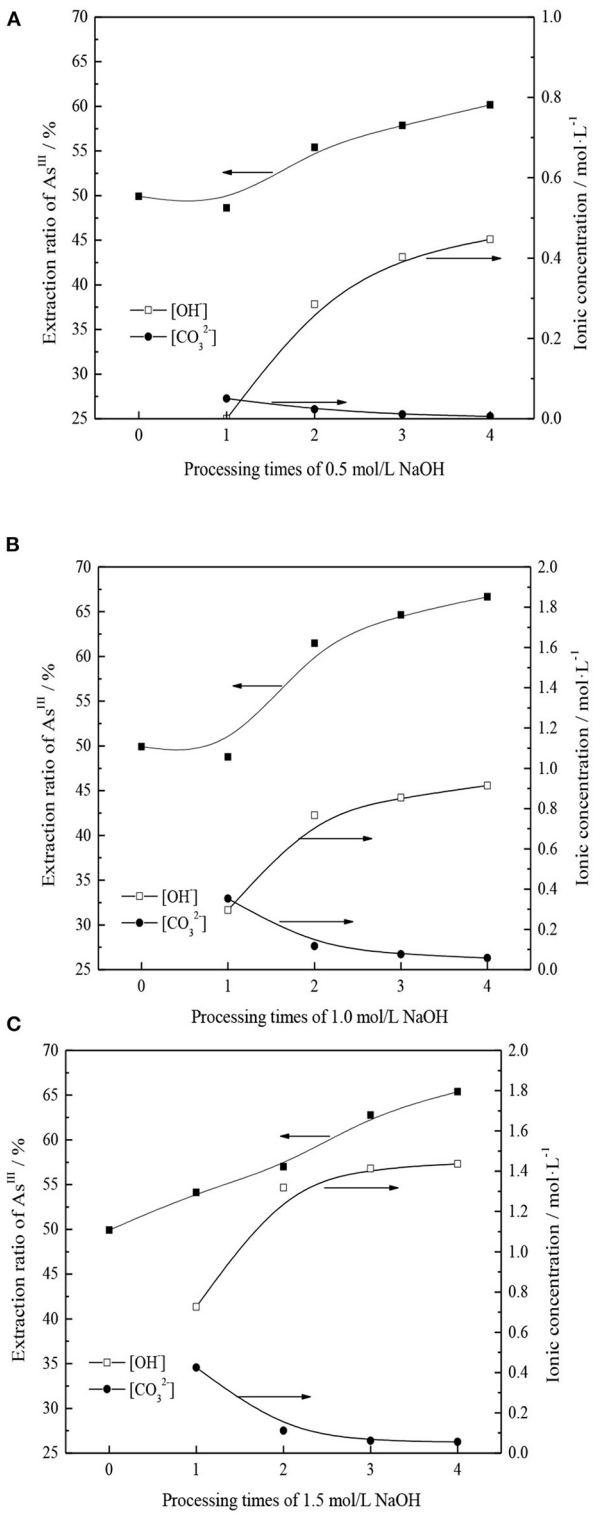

FIGURE 4 | (A) NaOH concentration is 0.5 mol/L and treatment times on As^{III} extraction rate and concentration of ions in alkaline washing solution. **(B)** NaOH concentration is 1.0 mol/L and treatment times on As^{III} extraction rate and concentration of ions in alkaline washing solution. **(C)** NaOH concentration is 1.5 mol/L and treatment times on As^{III} extraction rate and concentration of ions in alkaline washing solution.

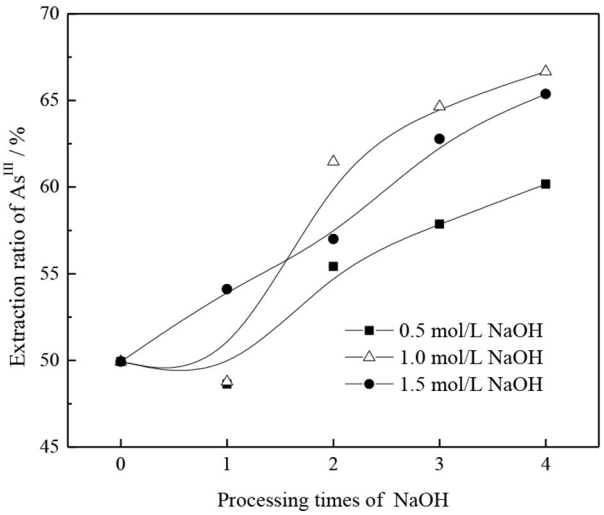

FIGURE 5 | Effect of alkaline washing times on As^{III} extraction rate under different NaOH concentrations.

the NaOH concentration from 0.5 to 1.0 mol/l, the promotion effect of alkaline washing on As^{III} extraction can be clearly demonstrated only when the number of alkaline washings is more than two. When the NaOH concentration is further increased to 1.5 mol/l and the number of alkaline washings is more than two, the extraction rate of As^{III} is significantly better than that obtained at 0.5 mol/l NaOH but lower than that obtained at 1.0 mol/l NaOH. This may be due to the fact that with an increase in alkalinity, in addition to the neutralization reaction of HCO_3^- group in organic phase, excessive OH^- replaces the generated CO_3^{2-} groups. Owing to the relatively stronger OH^- association ability, the As^{III} extraction capacity is reduced.

Based on the above, the extraction rate of As^{III}, the amount of NaOH, and the conversion efficiency are comprehensively considered to convert TOMAC from HCO_3^- to CO_3^{2-} type effectively; 1.0 mol/l NaOH solution was selected for washing three times.

It can be known from the above experimental results and analysis that CO_3^{2-}-type TOMAC has a significant effect on the extraction rate of As^{III} in alkaline solution. The transformation process of TOMAC is accomplished in two steps, Cl^- to HCO_3^- type and HCO_3^- to CO_3^{2-} type; how to improve the transformation rate of these two processes is the critical process.

Infrared Spectrum Analysis Before and After CO_3^{2-} Transformation of TOMAC

TOMAC before and after transformation (CO_3^{2-} type) is detected and analyzed, respectively, by Fourier transform infrared spectroscopy, and the obtained infrared spectrum is shown in **Figure 6**.

Figure 6 represents the FTIR spectra of TOMAC before and after the transformation. The peaks at ∼2,963, ∼2,926, and ∼2,856 cm^{-1} can be assigned to the -CH_2- stretching.

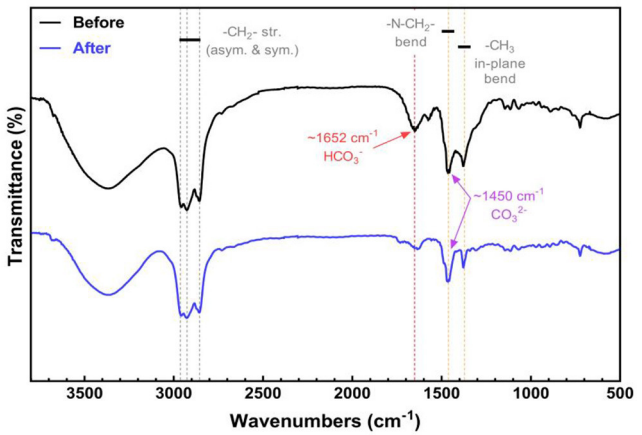

FIGURE 6 | Infrared spectra of TOMAC before and after transformation.

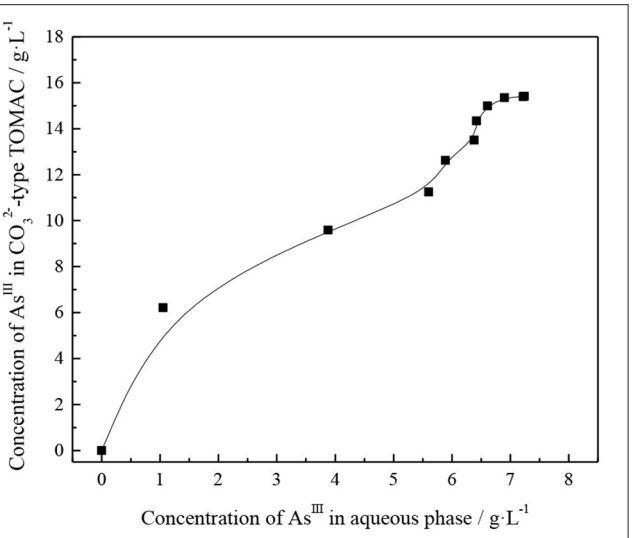

FIGURE 7 | Isotherm of thioarsenite extraction.

The characteristic vibration bands at ~1,462 and ~1,372 cm^{-1} represent the N-CH_2- bending and in-plane bending of -CH_3, respectively. The characteristic IR band of HCO_3^- at ~1,652 cm^{-1} can be found in the spectrum of TOMAC before the transformation. However, the characteristic peak of HCO_3^- disappears after the NaOH treatment, revealing the transformation from HCO_3^- to CO_3^{2-}. It should be noted that the characteristic peak of CO_3^{2-} locates at ~1,450 cm^{-1}, which overlaps with the vibration band region of N-CH_2- bending (Larkin, 2011). Thus, it is difficult to distinguish the two vibration bands from the FTIR spectra.

Extraction of Thioarsenious Acid by CO_3^{2-}-Type TOMAC

Extraction Mechanism of CO_3^{2-}-Type TOMAC

The extraction capacity of thioarsenious acid in the CO_3^{2-}-type TOMAC organic phase was determined by the continuous saturation method (Zhu, 2005).

First, the organic phase of 30% TOMAC + 15% sec-octyl alcohol + 55% sulfonated kerosene was transformed into CO_3^{2-}, and the aqueous solution containing arsenic was presulfurized. After the transformation, the organic phase was repeatedly contacted with fresh water phase under the condition of phase ratio O/A = 1/1 and vibrated and mixed for 10 min each time. The concentration of As^{III} in the raffinate was analyzed after each extraction reached equilibrium; then, the content of As^{III} in the organic phase was calculated by subtraction method and accumulated step by step. The concentration of As^{III} in the raffinate is basically the same as that in the aqueous solution before extraction, until no significant change is observed in the As^{III} concentration in the loaded organic phase. The extraction isotherms were plotted based on the concentration relationship between As^{III} in the loaded organic phase and that in the equilibrium aqueous phase, as shown in **Figure 7**.

In **Figure 7**, the As^{III} content enriched in the CO_3^{2-}-type TOMAC increases with increasing number of times of contact between the CO_3^{2-}-type TOMAC and the feed liquid. The content of As^{III} in raffinate was almost the same as that in the feed after CO_3^{2-}-type TOMAC was contacted with the feed nine times; thus, the organic phase can be considered to have been saturated, and the saturation capacity of CO_3^{2-}-type TOMAC for extracting thioarsenious acid was 15.41 G/l (0.21 mol/l). When CO_3^{2-}-type TOMAC is used to extract thioarsenious acid, the following reactions occur:

$$(R_4N)_2CO_3 + HAsOS_2^{2-} \rightarrow (R_4N)_2HAsOS_2 + CO_3^{2-}. \quad (9)$$

$$(R_4N)_2CO_3 + HAsO_2S^{2-} \rightarrow (R_4N)_2HAsO_2S + CO_3^{2-}. \quad (10)$$

Effect of Volume Fraction of CO_3^{2-}-Type TOMAC on As^{III} Extraction

Under the conditions of 15% secondary octanol concentration, V_O/V_A = 1/1, and normal temperature, oil, and water were mixed and shaken for 10 min. Then, the effects of the volume fraction of CO_3^{2-}-type TOMAC on the single-stage extraction rate of As^{III} and oil–water phase separation were investigated, and the experimental results are shown in **Figure 8**.

As seen from **Figure 8**, for a TOMAC concentration within 30%, the As^{III} extraction rate has a significant increase trend with an increase in the volume fraction of CO_3^{2-}-type TOMAC. As the volume fraction of CO_3^{2-}-type TOMAC increases from 10 to 30%, the extraction yield of As^{III} increases from 68.3 to 85.5% and further increases to 50% with the volume fraction of the CO_3^{2-}-type TOMAC. The extraction rate of As^{III} slightly increases to 86.3%, and the volume fraction has no significant effect on the extraction rate. As is further apparent from **Figure 8**, the oil–water phase time increases with the extractant concentration. When the volume fraction of CO_3^{2-}-type TOMAC reached 50%, the time of the oil–water phase was prolonged to nearly 9 min, which was unfavorable to the extraction operation.

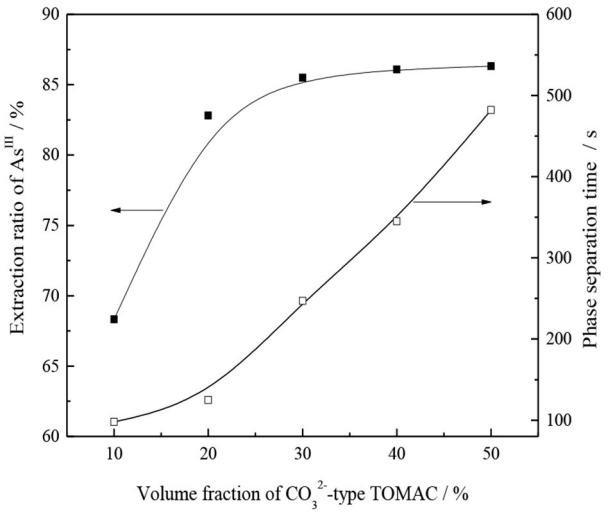

FIGURE 8 | Effect of volume fraction of CO_3^{2-}-type TOMAC on As^{III} extraction and phase separation.

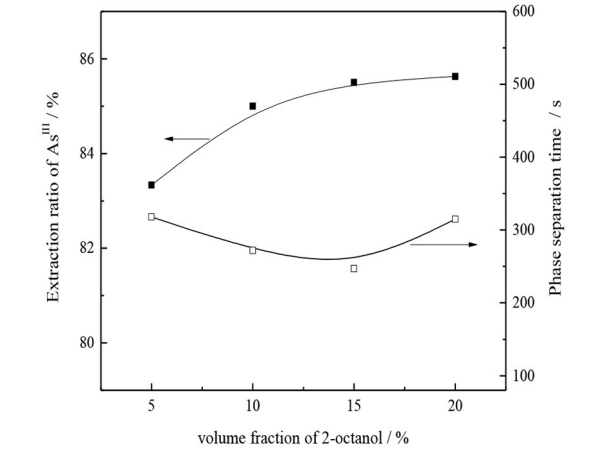

FIGURE 9 | Effect of volume fraction of 2-octanol on As^{III} extraction and phase separation.

The volume fraction of CO_3^{2-}-type TOMAC was 30%, the extraction yield of As^{III} was 85.5%, and the time of the phase separation was ∼4 min.

Effect of Volume Fraction of 2-octanol

The use of DL-2-octanol as the polarity improver is conducive to the depolymerization of CO_3^{2-}-type TOMAC (Uslu, 2008), thereby increasing the effective ion concentration of the extractant and improving the extraction effect. Under the conditions of 30% CO_3^{2-}-type TOMAC (volume fraction), $V_O/V_A = 1/1$, and room temperature, the effect of DL-2-octanol concentration on the As^{III} single-stage extraction rate and oil–water phase separation was investigated by oscillating the oil–water mixture for 10 min, and results are shown in **Figure 9**.

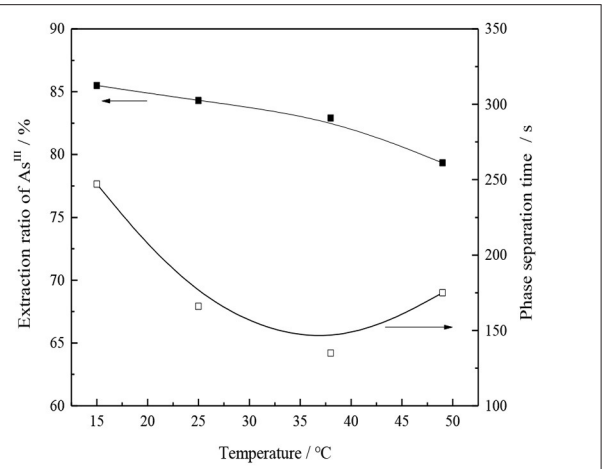

FIGURE 10 | Effect of temperature on As^{III} extraction and phase separation.

As seen from **Figure 9**, as the secondary octanol concentration increases from 5 to 15%, the As^{III} extraction yield slightly increases from 83.3 to 85.5%. With the further increase in the amount of 2-octanol, the extraction of As^{III} shows no significant improvement; however, the loss of organic phase in water may increase. Therefore, a suitable concentration of 2-octanol is 15%, for an oil–water phase time of ∼4 min, in which the phase separation is relatively fast and clear.

Effect of Extraction Temperature

The transfer rate between the oil and water phases can be affected by the change in temperature, which may also affect the equilibrium of extraction reaction. Under the condition of 30% CO_3^{2-}-type TOMAC + 15% secondary octanol + 55% sulfonated kerosene and $V_O/V_A = 1/1$, the oil and water were mixed and oscillated for 10 min, and the effect of temperature change on the single-stage extraction rate of As^{III} was investigated while the oil and water phases were carried out at room temperature. The experimental results are shown in **Figure 10**.

With the increase in the temperature, the viscosity of the organic phase normally decreases, which facilitates the extraction process; however, for the TOMAC extraction of As^{III}, the As^{III} extraction rate does not increase but rather decreases with an increase in the extraction temperature (see **Figure 10**).

According to van't Hoff equation of the chemical reaction (Richards, 1926; Deiters, 2012),

$$\frac{\mathrm{d}\ln K}{dT} = \frac{\Delta H}{RT^2}, \tag{11}$$

where K is the equilibrium constant, T is the absolute temperature (°C), ΔH is the enthalpy change (kJ/mol), and R is the universal gas constant (8.314 J·mol^{-1}·K^{-1}).

As ΔH does not vary significantly with temperature and the temperature range discussed in this experiment is narrow, ΔH can be assumed to have a certain value, independent of

TABLE 1 | Parameters such as extraction rate and partition ratio at different temperatures.

Temperature (°C)	Extraction rate (%)	Distribute ratio *D*	ln*D*	1/*T* (K^{-1})
15	85.5	5.91	1.78	0.00347
25	84.30	5.37	1.68	0.00336
38	82.09	4.58	1.52	0.00322
49	79.34	3.84	1.35	0.00311

temperature. Integrating Equation (11), we get

$$\ln K = -\frac{\Delta H}{RT} + C\,(Cisconstant). \tag{12}$$

Equation (11) shows that the equilibrium constant of the reaction is linear with $1/T$.

As most of the thioarsenious acid in the system exists in the form of $HAsOS_2^{2-}$, to simplify the calculation, only the reaction in Equation (9) is considered, from which the equilibrium constant K_{ex} is derived,

$$K_{ex} = \frac{[(R_4N)_2HAsOS_2][CO_3^{2-}]}{[(R_4N)_2CO_3][HAsOS_2^{2-}]}. \tag{13}$$

According to the distribution ratio formula,

$D = \frac{[(R_4N)_2HAsOS_2]}{[HAsOS_2{}^{2-}]}$. (13)

From Equations (12) and (13), the relationship between the reaction equilibrium constant and distribution ratio can be obtained

$$K_{ex} = \frac{D[CO_3{}^{2-}]}{[(R_4N)_2CO_3{}^{2-}]}. \tag{14}$$

Taking the logarithm of both sides at the same time yields

$$\ln K_{ex} = \ln D + ln[CO_3^{2-}] - ln[(R_4N)_2CO_3]^2. \tag{15}$$

As the concentration of the extractant TOMAC is constant at 30% and the concentration of the CO_3^{2-} ion changes slightly, the last two terms in Equation (15) can be assumed to be constants for the sake of simplification. Consequently,

$$\ln D = -\frac{\Delta H}{RT} + C' \quad (C'isconstant). \tag{16}$$

Based on the experimental data, the extraction rate, distribution ratio, and other parameters obtained under different temperature conditions are calculated, and the results are shown in **Table 1**.

Plot and fit $1/T$ and ln*D* in **Table 1**, and the result is shown in **Figure 11**.

As can be seen from **Figure 11**, $1/T$ and ln*D* have a linear relationship, and the fitted equation is

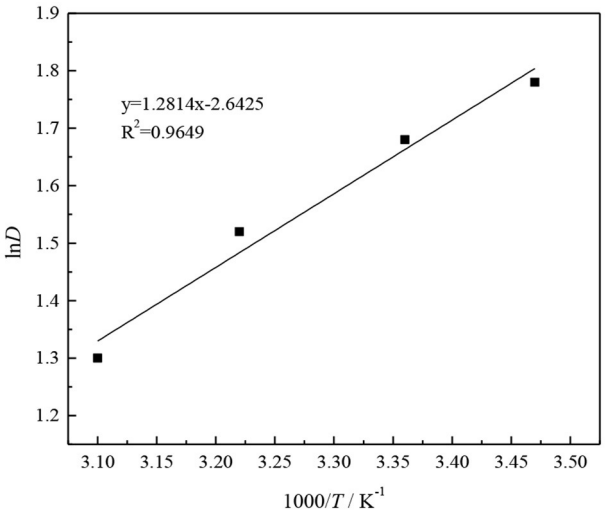

FIGURE 11 | Relationship between $1/T$ and ln*D* and fitting results.

$$y = 1.2814x - 2.6425(R^2 = 0.9649). \tag{17}$$

From Equation (17), we can see that the slope of the fitted straight line is 1.2814.

$$\Delta H = -R\times 1.2814 = -10.6536kJ/mol. \tag{18}$$

From the calculation, it is evident that the process of extracting thioarsenious acid with CO_3^{2-}-type TOMAC is an exothermic reaction, and when the extraction temperature increases, the equilibrium of the extraction reaction proceeds in the reverse direction, which is not conducive to the extraction of As^{III}.

As seen from **Figure 10**, as the extraction temperature increases from 15 to 50°C, the extraction ratio of As^{III} decreases from 85.5 to 79.33%, which indicates that the extraction of thioarsenious acid by CO_3^{2-}-type TOMAC is an exothermic reaction. Although the temperature increase speeds up the phase separation, it is still not conducive to the extraction of As^{III}; thus, with comprehensive consideration, the extraction process should be conducted at room temperature.

Effect of Extraction Time

Under the conditions of organic phase composition 30% CO_3^{2-}-type TOMAC + 15% secondary octanol + 55% sulfonated kerosene, $V_O/V_A = 1/1$, and normal temperature, the effects of the oil–water mixed extraction time on the single-stage extraction rate of As^{III} and oil–water phase separation are investigated, and the experimental results are shown in **Figure 12**.

As shown in **Figure 12**, the extraction of As^{III} can reach equilibrium in ∼3 min, extraction rate of As^{III} reaches 85.2%, and extraction rate of As^{III} does not change significantly with the further extension of the extraction time, which indicates that the extraction process is relatively fast and the phase separation

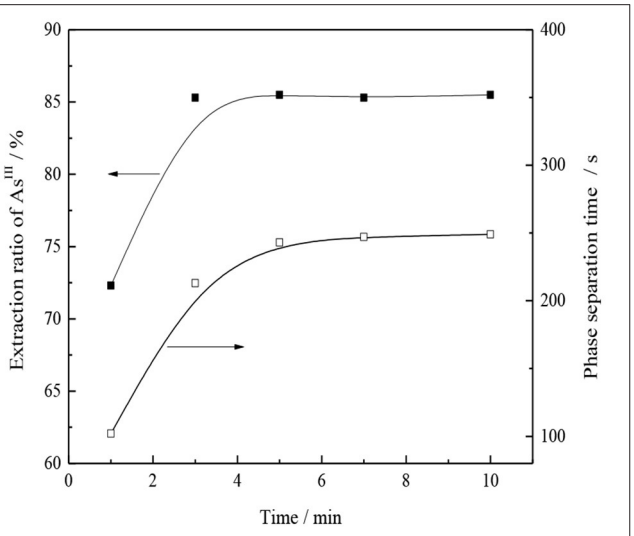

FIGURE 12 | Effect of extraction time on As^{III} extraction and phase separation.

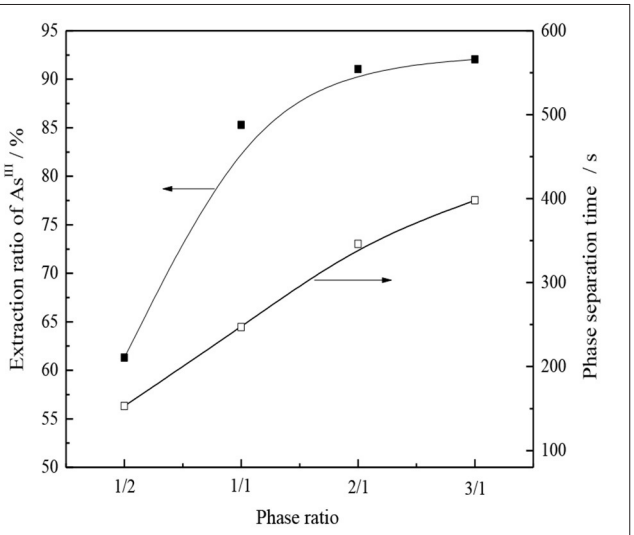

FIGURE 13 | Effect of phase ratio on As^{III} extraction and phase separation.

is also fast, i.e., ∼4 min. To ensure the full mixing of oil and water, an extraction time of 5 min was selected under the experimental conditions.

Effect of Phase Ratio

Under the condition of organic phase composition 30% CO_3^{2-}-type TOMAC + 15% secondary octanol + 55% sulfonated kerosene and extraction for 5 min at room temperature, the effect of the oil–water contact ratio on the single-stage extraction rate and phase separation of As^{III} was investigated, and the experimental results are shown in **Figure 13**.

As seen from **Figure 13**, the extraction rate of As^{III} and the phase separation time increase with an increase in the phase ratio. When the V_O/V_A ratio increased from 1/1 to 2/1, the extraction yield of As^{III} increased from 85.2 to 91.0%, and the time of the phase separation was prolonged from 4 to nearly 6 min. When the ratio of V_O/V_A increased further to 3/1, the increase in the extraction yield of As^{III} was not significant; however, the time of the phase separation was prolonged to nearly 7 min, which was disadvantageous to the extraction process. Therefore, relatively speaking, $V_O/V_A = 1/1$ was a better choice.

Countercurrent Extraction Experiment

Based on the single-stage extraction experiment, the simulated countercurrent cascade extraction experiment was conducted. Based on the Kremser–Brown–Souders equation (Szitkai et al., 2002; Ushenoy and Fraser, 2003), as shown in Equation (19), the theoretical extraction stage is calculated and determined by means of the distribution ratio, phase ratio, extraction ratio, and set value of the arsenic content in the raffinate.

$$\varphi_M = \begin{cases} \frac{E_M - 1}{E_M^{N+1} - 1} \\ \frac{1}{N+1}, E = 1 \end{cases} ,E \neq 1, \tag{19}$$

where ϕ_M is the fraction extracted from M components, E_M is the extraction ratio of M components (°C), and N is the theoretical series.

When the ratio O/A is 1/1, the distribution ratio D_{As} of the As^{III} extraction is calculated from Equation (13) as follows:

$$D_{As} = \frac{6.19}{1.07} = 5.79. \tag{20}$$

Thus, the extraction ratio E_{As} is

$$E_{As} = D_{As} \times ratio = 5.79. \tag{21}$$

After the cascade countercurrent extraction, the extraction rate of As^{III} is more than 99%, and the content of As^{III} in the raffinate is as low as 0.05 g/l. Thus, the raffinate fraction ϕ_{As} is

$$\varphi_{As} = \frac{As^{III}\text{content of the raffinate liquid}}{As^{III}\text{content of liquid}} = \frac{0.05}{7.26} = 6.89 \times 10^{-3} \tag{22}$$

In conjunction with Equations (19)–(22), the theoretical stage N of the extraction can be calculated:

$$N = \frac{\lg\left(\frac{E_{As}-1}{\phi_{As}} + 1\right)}{\lg E_{As}} - 1 = 2.73 \approx 3. \tag{23}$$

Therefore, the four-stage countercurrent cascade extraction can be used with the consideration of stage efficiency and other factors.

Under the condition of 30% CO_3^{2-}-type TOMAC + 15% sec-octyl alcohol + 55% sulfonated kerosene in the organic phase, $V_O/V_A = 1/1$, and 5 min extraction at room temperature, the feed solution with $[As^{III}] = 9.69 \times 10^{-2}$ mol/l and [NaOH] =

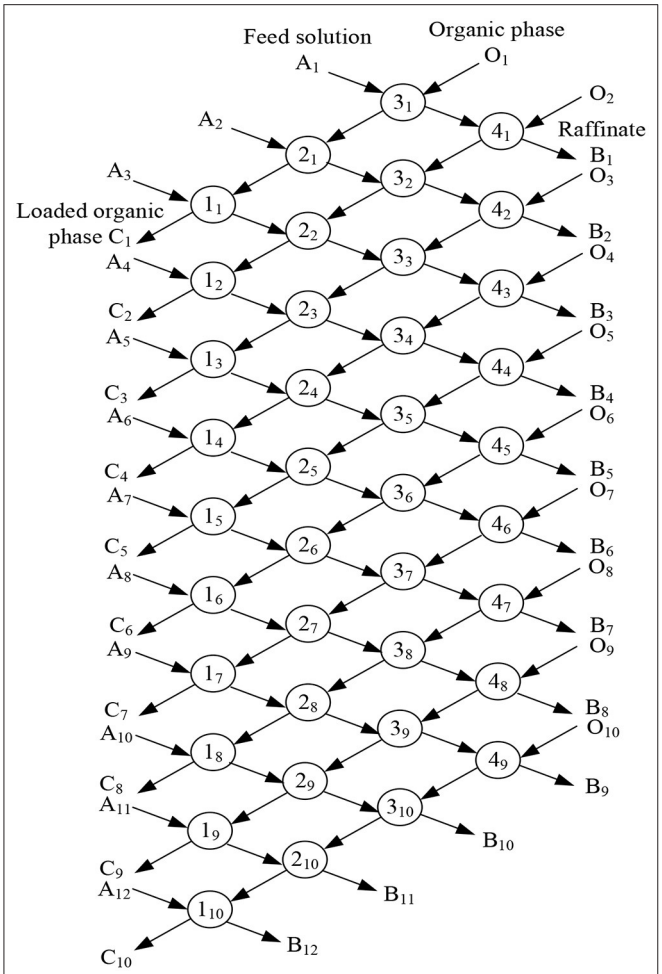

FIGURE 14 | Flow chart of four-stage countercurrent extraction.

0.5 mol/l was extracted by four-stage countercurrent extraction. The four-stage countercurrent extraction process is shown in **Figure 14**.

According to the cascade countercurrent extraction theory, the solvent extraction process can be considered to be stable only when the concentration of the extracted components tends to be stable and does not change, through the analysis of the numerous extractions in the extraction process. However, it is obviously difficult to achieve this under laboratory conditions (Ma, 2009). Practical experience shows that in the cascade countercurrent extraction experiment, when the number of rows is $\sim 3N - 2$ times of the number of stages, the extraction process will be close to equilibrium and reach a stable concentration value (Ruiz et al., 1986). Therefore, under the laboratory conditions, a total of 10 rows were carried out in the cascade extraction simulation experiment, and the raffinate of the 8, 9, and 10th rows was analyzed for As^{III} content, with the results shown in **Table 2**.

As can be seen from **Table 2**, the results of the As^{III} concentration of the raffinate in rows 8, 9, and 10 are 1.34×10^{-3}, 1.01×10^{-3}, and 1.32×10^{-3} mol/l, respectively,

TABLE 2 | Experimental results of four-stage countercurrent extraction.

Number of rows	Residual liquid concentration of As^{III} ($mol \cdot l^{-1}$)	Four-stage countercurrent extraction rate (%)
8	1.33×10^{-3}	98.62
9	1.01×10^{-3}	98.95
10	1.31×10^{-3}	98.64

exponential homogeneity, and it can be considered that the cascade extraction process reaches a steady state. Under the experimental conditions, the concentration of As^{III} in raffinate was reduced to less than 1.33×10^{-3} mol/l after the four-stage countercurrent extraction, and the extraction rate of As^{III} was more than 98.4%. The aim of removing arsenic from alkaline medium was achieved. Therefore, the extraction of thioarsenious acid with CO_3^{2-}-type TOMAC is an alternative method for arsenic removal from the alkaline leaching solution of metallurgical dust.

CONCLUSIONS

In order to improve the extraction capacity for arsenic from a high-alkali solution, TOMAC is used as an extractant. The paper proposed a CO_3^{2-}-type tri-n-octylmethyl-ammonium chloride (TOMAC) method for extracting thioarsenite. TOMAC transformation and organic phase saturated extraction capacity were measured, and the extraction mechanism was preliminarily studied. The relationship between the extraction rate of As^{III} and the number of treatments with saturated $NaHCO_3$ was investigated. The CO_3^{2-} transformation process of TOMAC and infrared spectrum analysis before and after CO_3^{2-} transformation of TOMAC were also studied. The results show that after treating the organic phase with saturated $NaHCO_3$ solution five times, the effective transformation of the Cl^-- to HCO_3^--type quaternary ammonium salt can be realized, and the effective transformation of TOMAC from HCO_3^- to CO_3^{2-} type can be achieved by alkaline washing with 1.0 mol/l NaOH solution thrice. The extraction of thioarsenite by CO_3^{2-}-type TOMAC is conducted at an association molar ratio of 2:1, with the As^{III} saturated capacity in the loaded organic phase up to 0.21 mol/l.

The study investigated the influences of extraction of thioarsenious acid by CO_3^{2-}-type TOMAC, based on the volume fraction of CO_3^{2-}-type TOMAC, volume fraction of 2-octanol, temperature, time, and phase ratio. With the organic phase composition of "30% CO_3^{2-}-type TOMAC + 15% DL-2-Octanol + 55% sulfonated kerosene," the single-stage As^{III} extraction rate reaches 85.2% with $V_O/V_A = 1/1$ at room temperature for 5 min. After the four-stage countercurrent extraction, the concentration of As^{III} in the raffinate can be reduced to less than 1.33×10^{-3} mol/l, and the extraction rate of As^{III} can reach greater than 98.4%. Hence, the extraction of thioarsenite by CO_3^{2-}-type TOMAC can serve as an alternative for the removal of arsenic via alkaline leaching from high arsenic flue dust produced by heavy metal smelting.

DATA AVAILABILITY STATEMENT

The original contributions presented in the study are included in the article/supplementary materials, further inquiries can be directed to the corresponding author/s.

AUTHOR CONTRIBUTIONS

KY: conceptualization, methodology, validation, formal analysis, investigation, writing - original draft, data curation, resources, writing – review, and editing. LL: methodology, validation, formal analysis, investigation, writing - original draft, data curation, writing – review, and editing. HZ: formal analysis. LT: writing - original draft, data curation, writing – review, and editing. ZX: supervision, project administration, resources, funding acquisition, writing – review, and editing. RW: supervision, writing – review, and editing. All authors contributed to the article and approved the submitted version.

FUNDING

Financial support was provided by the National Nature Science Foundation of China (nos. 52074136, 51904124, 51804136, and 51764016), the Distinguished Professor Program of Jinggang Scholars, China Institutions of Higher learning Jiangxi Province, China, the Jiangxi Province Nature Science Foundation (no. 20181BAB216017), the Jiangxi Science and Technology Landing Project (no. KJLD13046), and the Research Fund Program of State Key Laboratory of Rare Metals Separation and Comprehensive Utilization (no. GK-201803).

REFERENCES

Asanov, D., Filyanova, L., Zapasnyi, V., and Sukhova, N. (2016). Study of the performance indices of a dust-cleaning system at the balkhash copper smelter. *Metallurgist* 60, 331–338. doi: 10.3389/100fnins.2013.12345

Buev, E. M., Smorodina, A. A., Stepanov, M. A., Moshkin, V. S., and Sosnovskikh, V. Y. (2018). Novel synthesis of aminoacetonitriles via the selective demethylation of quaternary ammonium salts. *Tetrahedron Lett.* 59, 1638–1641. doi: 10.1016/j.tetlet.2018.03.037

Chauhan, S., and Kaur, M. (2017). Modulation of aggregation behaviour of anionic surfactant in the presence of aqueous quaternary ammonium salts. *J. Surfactants Deterg.* 20, 599–607. doi: 10.1007/s11743-017-1949-5

Christof Lanzerstorfer, C. (2016). Flowability of various dusts collected from secondary copper smelter off-gas. *Particuology* 25, 68–71. doi: 10.3389/fnins.2013.12345

Deiters, U. K. (2012). The isothermal van't Hoff equation for phase equilibria-a forgotten relation? *Fluid Phase Equilib.* 336, 22–27. doi: 10.1016/j.fluid.2012.08.028

Ermolin, M. S., Fedotov, P. S., Ivaneev, A. I., Karandashev, V. K., Burmistrov, A. A., and Tatsy, Y. G. (2019). Assessment of elemental composition and properties of copper smelter-affected dust and its nano- and micron size fractions. *Environ. Sci. Pollut. Res.* 26:5315. doi: 10.1007/s11356-018-3180-y

Guan, W.-J., and Zhang, G.-Q. (2011). Extraction of tungsten from simulated autoclave-soda leaching liquor of scheelite with quaternary ammonium salt. *Chinese J. Nonferrous Metals* 21, 1756–1762. doi: 10.1016/B978-0-444-53599-3.10005-8

Guo, X.-Y., Yi, Y., Shi, J., and Tian, Q.-H. (2016). Leaching behavior of metals from high-arsenic dust by NaOH-Na_2S alkaline leaching. *Trans. Nonferrous Metals Soc. China* 26, 575–580. doi: 10.1016/S1003-6326(16)64118-3

Hoffmann, J. E. (1993). Remediating copper smelter dusts: the arsenic problem. *J. Miner. Metals Mater. Soc.* 45, 30–31. doi: 10.1007/BF032 22401

Jarošíková A., Ettler, V., Mihaljevič, M., Drahota, P., Culka, A., and Racek, M. (2018). Characterization and ph-dependent environmental stability of arsenic trioxide-containing copper smelter flue dust. *J. Environ. Manage.* 209, 71–80. doi: 10.1016/j.jenvman.2017.12.044

Karimov, K., and Naboichenko, S. (2016). Sulfuric acid leaching of high-arsenic dust from copper smelting. *Metallurgist* 60, 456–459. doi: 10.1007/s11015-016-0313-8

Larkin, P. J. (2011). *Infrared and Raman Spectroscopy-Principles and Spectral Interpretation*. Stamford, CT: Elsevier.

Liu, W.-F., Fu, X.-X., Yang, T.-Z., Zhang, D.-C., and Chen, L. (2018). Oxidation leaching of copper smelting dust by controlling potential. *Trans. Nonferrous Metals Soc. China* 28, 1854–1861. doi: 10.1016/S1003-6326(18)64830-7

Liu, Z.-H., Zhang, P., Li, Y.-H., Liu, Z.-Y., and Li, L. (2009). Study on leaching dearsenication from waltz zinc oxide containing high as by Na_2S-NaOH mixed alkali. *Hydrometall. China* 28, 229–232. doi: 10.13355/j.cnki.sfyj.2009.04.011

Ma,. R.-J. (2009). *Extractive Metallurgy*. Beijing: Metallurgical Industry Press.

Montenegro, V., Sano, H., and Fujisawa, T. (2013). Recirculation of high arsenic content copper smelting dust to smelting and converting processes. *Miner. Eng.* 49, 184–189. doi: 10.1016/j.jenvman.1272017.12.044

Morales, A., Cruells, M., Roca, A., and Bergó, R. (2010). Treatment of copper flash smelter flue dusts for copper and zinc extraction and arsenic stabilization. *Hydrometallurgy* 105, 148–154. doi: 10.1016/j. hydromet.2010.09.001

Rappas, A., Falls, C., and Waterman, B. T. (1990). *Processes for the Treatment of Smelter Flue Dust*. U.S. Patent No 4,891,067. Wilmington, DE: US Patent.

Reynolds, J. E. (1981). *Process for Recovery Arsenic Compouds by Sodium Hydroxide Leaching*. U.S. Patent No 4,244,927. Denver, CO: US Patent.

Richards, O. W. (1926). A nomogram for the van't hoff-arrhenius temperature equation. *J. Phys. Chem.* 30, 1219–1221.

Ruiz, F., Marcilla, A., and Gomis, V. (1986). Method for equilibrium-stage calculations in liquid extraction. application to countercurrent cascade design for a quaternary system. *Indus. Eng. Chem. Process Design Dev.* 25, 631–634.

Sahu, N. K., Dash, B., Sahu, S., Bhattacharya, I. N., and Subbaiah, T. (2012). Extraction of copper by leaching of electrostatic precipitator dust and two step removal of arsenic from the leach liquor. *Korean J. Chem. Eng.* 29, 1638–1642. doi: 10.1007/s11814-012-0081-5

Sanchez de la Campa, A., de la Rosa, J., Sánchez-Rodas, D., Oliveira, V., Alastuey, A., Querol, X., et al. (2008). Arsenic speciation study of pm2.5 in an urban area near a copper smelter. *Atmos. Environ.* 42, 6487–6495. doi: 10.1016/j.atmosenv.2008.04.016

Suflet, D., Popescu, I., Pelin, I., Nicolescu, A., and Hitruc, G. (2015). Cationic curdlan: synthesis, characterization and application of quaternary ammonium salts of curdlan. *Carbohydr. Polym.* 123, 396–405. doi: 10.1016/j.carbpol.2015.01.050

Szitkai, Z., Lelkes, Z., Rev, E., and Fonyo, Z. (2002). Handling of removable discontinuities in minlp models for process synthesis problems, formulations of the kremser equation. *Comp. Chem. Eng.* 26, 1501–1516. doi: 10.1016/S0098-1354(02)00037-6

Ushenoy, U. V., and Fraser, D. M. (2003). A new formulation of the kremser equation for sizing mass exchangers. *Chem. Eng. Sci.* 58, 5121–5124. doi: 10.1016/j.ces.2003.08.007

Uslu, H. (2008). Extracion of citric acid in 2-octanol and 2-propanol solutions containing tomac: an equilibria and a LSER model. *Braz. J. Chem. Eng.* 25, 553–561. doi: 10.1590/S0104-66322008000300013

Weisshaar, D. E., Earl, G. W., Amolins, M. W., Mickalowski, K. L., Norberg, J. G., and Rekken, B. D. (2012). Investigation of the stability of quaternary ammonium methyl carbonates. *J. Surfactants Deterg.* 15, 199–205. doi: 10.1007/s11743-011-1292-1

Wu, Q., Liu, C.-L., Yang, J.-C., Guan, A.-Y., and Ma, H.-J. (2017). Design, synthesis, and herbicidal activity of novel quaternary ammonium salt derivatives. *Pest. Biochem. Physiol.* 143, 246–251. doi: 10.1016/j.pestbp.2017.05.006

Xu, Z.-F., Zhang, X.-K., and Zhao, H.-X. (2016). Thermodynamics of sulfidation of arsenite in alkaline solutions. *Nonferrous Metals* 7, 5–8. doi: 10.3969/j.issn.1007-7545.2016.07.002

Xu, Z.-H., Li, Q., and Nie, H.-P. (2010). Pressure leaching technique of smelter dust with high-copper and high-arsenic. *Trans. Nonferrous Metals Soc. China* 20, 176–181. doi: 10.1016/S1003-6326(10)60035-0

Yang, T., Fu, X., Liu, W., Chen, L., and Zhang, D. (2017). Hydrometallurgical treatment of copper smelting dust by oxidation leaching and fractional precipitation technology. *JOM* 69, 1982–1986. doi: 10.1007/s11837-017-2492-6

Zheng, Y.-J., Liu, W.-Y., Bai, M., B., and Zhang, C.-F. (2008). Preparation of arsenic trioxide from arsenic sulfide slag. *J. Central South Univ.* 9, 1157–1163.

Zhu,. T. (2005). *Extraction and Ion Exchange*. Beijing: Metallurgical Industry Press.

Conflict of Interest: The authors declare that the research was conducted in the absence of any commercial or financial relationships that could be construed as a potential conflict of interest.

frontiers in Chemistry

ORIGINAL RESEARCH
published: 19 March 2021
doi: 10.3389/fchem.2021.598228

Comparative Study on Electrochemical Treatment of Cyanide Wastewater

Siming Lei[1,2] *and Yonghui Song*[1,2*]

[1] School of Metalhurgical Engineering, Xi'an University of Architecture and Technology, Xi'an, China, [2] Key Laboratory of Gold and Resource of Shaanxi Province, Xi'an, China

The electrochemical treatment of wastewater is widely used for cleaning due to its efficiency. In this paper, two-dimensional (2D) and three-dimensional (3D) electrochemical systems were used to treat cyanide wastewater. The effect of the applied voltage and the material of the main electrode on the removal of various ions and the characteristics of chemical reactions were mainly studied. The results show that the applied voltage was the key effect of the electrochemical treatment process. The removal of ions from the wastewater at 2 V is mainly due to the effect of electro adsorption and enrichment precipitation, while at 4 V, it is mainly due to anodization and cathodic deposition. The treatment effect of the 3D electrode system was significantly better than the 2D system. The 3D electrode system by used granular activated carbon as the particle electrode, with the carbon filled stainless mesh (CM) and coal based electrode (CB) as the main electrode, the treatment effect were better than main electrode of stainless steel mesh (M). The 3D system with CB as the main electrode had an applied voltage of 4 V, a treatment time of 5 h, plate spacing of 10 mm, and the dosage of activated carbon particles was 2 g. The removal rates of CN_T, Cu, Zn, CN^-, and SCN^- were 94.14, 94.53, 98.14, 98.55, and 93.13%, respectively. The main reaction in anode was the electroly oxidation of CN^- and SCN^-, while the electrolytic deposition of Cu, Zn, and other metal ions in the cathode surface. There were not only adsorption and electric adsorption of various ions, but also an electrolytic deposition reaction of Cu, Zn, and other metal ions on the surface of the activated carbon particle electrode. During the electrochemical reaction, the concentration of hydrogen ions near the anode increases locally, which produces the precipitation of CuSCN, $Cu_2Fe(CN)_6$, and $Zn_2Fe(CN)_6$, etc. in the solution, which are helpful for the removal of cyanide and heavy metal ions in cyanide wastewater.

Keywords: voltage, electrode material, three dimensional electrode, cyanide wastewater, coal based electrode

OPEN ACCESS

Edited by:
Feng Rao,
Michoacana University of San Nicolás de Hidalgo, Mexico

Reviewed by:
Mohammad Boshir Ahmed,
Gwangju Institute of Science and Technology, South Korea
Taner Yonar,
Uludag University, Turkey

***Correspondence:**
Yonghui Song
syh1231@126.com

Specialty section:
This article was submitted to Green and Sustainable Chemistry, a section of the journal Frontiers in Chemistry

Received: *24 August 2020*
Accepted: *25 February 2021*
Published: *19 March 2021*

Citation:
Lei S and Song Y (2021) Comparative Study on Electrochemical Treatment of Cyanide Wastewater. Front. Chem. 9:598228. doi: 10.3389/fchem.2021.598228

INTRODUCTION

Cyanide wastewater treatment has been the subject of research due to the difficulty of treating its complex composition, which contains a large number of free cyanide and copper, zinc, iron metal cyanide complex ions. Three-dimensional (3D) electrode electrochemical system treatment techniques are used to remove organic material and heavy metal ions from industrial wastewater of chemical, metallurgical, and material industries (Vedula et al., 2013). Due to the advantages of short mass transfer distance, high current efficiency, short treatment time, and low energy

consumption, this method has gradually attracted the attention of researchers (Jia et al., 2013; Shilei et al., 2013). The 3D electrode system introduces a third electrode (particle electrodes) based on a two-dimensional (2D) electrode system. Under the action of the electric field, the particle electrodes and anode and cathode conduct electrochemical reactions together, resulting in higher removal efficiency (Jinzhi et al., 2015).

The 3D electrode system achieved results in terms of process and basic theory (Lei et al., 2013; Ting et al., 2018). At present, it is used for the electrochemical oxidation-reduction treatment of inorganic heavy metal ions including lead, zinc, copper, nickel, and chromium, and organic industrial wastewater from dyeing, papermaking, coking, and other industries. Xi et al. (2015) treated simulated acidic copper and nickel wastewater in the laboratory by electrodeposition, under optimal process conditions. The ion deposition rates of copper and nickel can reach 99.88 and 85.21%, which indicates the feasibility of using electrodeposition technology to treat polymetallic wastewater. Han and Zhenshan (2013) used activated carbon as particle electrodes in a 3D electrode system to treat wastewater that contained zinc. The results showed that with the voltage of 6 V, the removal rate of zinc ions was increased by 48%, the average current efficiency was increased by 40%, and energy saving was 70% compared with the 2D electrode system. Hui (2016) used a self-made coal based electrode material as an anode and cathode to treat cyanide wastewater. It was found that when the voltage was 2 V and the time was 5 h, the removal rates of CN_T, Cu, Zn, and SCN^- in the solution were 75.17, 88.48, 29.51, and 47.57%, respectively. To examine the effect of voltage on the treatment of cyanide wastewater with a 3D electrode, Yao et al. (2017) used self-made coal based electrode material as an anode and cathode, and commercial activated carbon as particle electrodes to treat cyanide gold extraction wastewater. It was found that the voltage has an obvious influence on wastewater treatment. Electrolytic deposition played an important role in the 3D electrode system when the voltage was 4 V, time 5 h, and the electrode distance was 10 mm. The removal rates of CN_T, Cu, Zn, SCN^-, and CN^- in wastewater were 93.94, 95.2, 97.23, 99.38, and 94.93%, respectively.

The above studies show that the electrochemical treatment of cyanide wastewater with 2D/3D systems has a good treatment effect, and the electrode is an important determinant worthy of further study.

In the present study used a stainless steel mesh filled with activated carbon electrode (CM) coal-based electrode (CB) and stainless steel mesh (M) electrode. Commercial activated carbon particles were used as the particle electrode. The electrochemical treatment of cyanide wastewater by 2D and 3D systems and the effects of electrode materials and applied voltage on the removal law of various ions in cyanide wastewater and its mechanism was studied.

EXPERIMENTAL

Materials

The 304 stainless steel mesh (M) used in the experiment was from a steel product factory in Jiangsu Province. The filler and the particle electrode were commercial coconut-shell activated carbon. The low rank pulverized coal and liquefaction residue was from a coal chemical factory in Yulin, Shaanxi Province. The cyanide wastewater was from a gold smelter in Henan Province, and its main composition is shown in **Table 1**, which belongs to high concentration cyanide containing wastewater (Acheampong et al., 2010). Analytical grade reagents and deionized water were used.

Experimental Procedures

Fifty milliliter cyanide wastewater was accurately measured taken into the electrolytic cell. The electrode plates were, respectively, connected with the positive and negative electrodes of the DC power supply. The plates were connected with wires plugged into the solution in parallel with 10 mm intervals. The experiment under different applied voltages, for a treatment time of 5 h, and the dosage of particle activated carbon in the 3D system was 2 g. At the end of the experiment, the solution was treated by liquid-solid separation, and several ions concentrations were regularly analyzed. The precipitates and plates were repeatedly washed with distilled water until pH 7 was reached, and then dried for analysis and characterization. The connection diagram of the experimental device was shown in Yao et al. (2017). In the experiment, the stainless steel mesh (M) used the 304 stainless steel (pore diameter $\leq$30 mesh), the activated carbon filled stainless steel mesh electrode (CM) used the stainless steel mesh as a framework (30 $\times$ 30 $\times$ 2 mm), and 2 g commercial activated carbon (had secondary activation by nitric acid) as filler. The preparation of the self-made coal based electrode (CB) followed a method previously described (Yonghui et al., 2016).

Analytical Procedures

The surface morphology of the electrode material and the composition of the loading material were analyzed by JMS-6390Lv Scanning Electron Microscope (with energy-dispersive IE300X). The composition of the precipitations was analyzed by X-ray Diffractometer (D8 ADVANCE A25). The concentration of CN_T and CN^- in wastewater were analyzed by chemical titration, the concentration of Cu and Zn were analyzed by AA-1800H

TABLE 1 | Main components of cyanide wastewater[a] used in the experiment/mg·L^{-1}.

Components	CN_T	CN^-	Cu^{2+}	Zn^{2+}	SCN^-
Content	1872.6	383.4	593.2	468.8	262.15

[a]*pH = 7.30.*

Atomic Absorption Spectrometry, and the thiocyanate ion was determined by 723PC Spectrophotometer.

RESULTS AND DISCUSSION

Removal Rate of Various Ions at 2D System

Treatment cyanide wastewater used the main electrodes of M, CM, and CB, respectively, under 2 and 4 V conditions by the 2D system. The removal rates of several main ions were shown in **Figure 1**. It can be seen from the results that the removal rates of ions for the three kinds of main electrodes were relatively low at 2 V, basically no more than 60%. While the removal rates of CN_T, Cu, Zn, CN^-, SCN^- at 4 V were all about 20% higher than those under 2 V. In addition, the treatment effect of the CM electrode was better than the CB electrode and M electrode, but the overall treatment effect was not good. When the main electrode was M, the removal rate of ions in 2 V was generally low and the highest removal rate was only 28.14% (CN^-). The removal rate of all ions was greatly improved at 4 V, but only maintained levels at about 35%. This may be due to the small contact area between the electrode and wastewater. When CM and CB were used as the main electrodes, the removal rates of each ion in the 2D system reached more than 62% under 4 V conditions, and the removal rates were significantly improved. When the main electrode was CM, the removal rates of CN_T, Cu, Zn, CN^-, and SCN^- were 69.11, 62.17, 65.45, 74.43, and 64.14%, respectively.

Removal Rate of Various Ions at 3D System

Treatment cyanide wastewater in the 3D system used various main electrodes under the conditions of 2 and 4 V. The removal rate of several main ions is shown in **Figure 2**, which shows that the removal rates of ions in the three main electrodes were not high under 2 V conditions, especially the M electrode. The removal rates of each ions were only about 30% but were significantly improved under 4 V conditions. When CM and CB as the main electrodes, the removal rates of each ions in the 3D system under 4 V conditions were all above 90%. When the main electrode was CB, the removal rates of CN_T, Cu, Zn, CN^-, and SCN^- were 94.14, 94.53, 98.14, 98.55, and 93.13%, respectively.

Compared with the 3D system, the 2D system had a low treatment efficiency and was similar to the reaction process of the main plate with the 3D system. Therefore, the SEM-EDS analysis of the main plates and particle electrodes in this paper focused on the 3D system.

SEM-EDS Spectrum Analysis of Anode

Figure 3 shows the SEM-EDS spectra of CM and CB anodes under the applied voltage of 2 V. It can be seen from the figure that the electrodes corroded after use. This was likely caused by the consumption of carbon in the reaction process and the erosion of the electrode sheet during the stirring process. Simultaneously, there were white attachments on the surface of the two kinds of anodes. The energy spectrum analysis results show that these substances were complex ions of Cu, Zn, Fe, and other anions. Besides the electrode plate's adsorption effect, the anions that were removed from the solution depend on the directional migration and adsorption on the anode surface under the electric field. The energy spectrum shows that there was a certain amount of Fe in the CM anode, which may be caused by the strong adsorption properties of activated carbon. The cyanide from wastewater and the iron in the stainless steel mesh produces ferricyanide preferential adsorption on the activated carbon.

When the voltage was 2 V, gas was produced at the anode. Oxygen evolution reaction occurs at the anode due to the

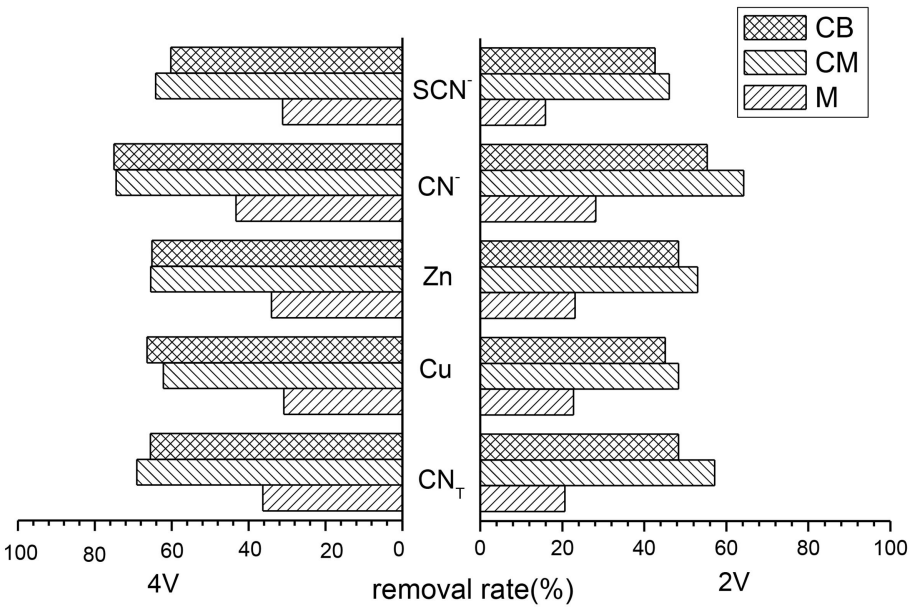

FIGURE 1 | Removal rate of various ions with different main electrodes at 2D system (pH = 9, time = 5 h, voltage = 2 V or 4 V).

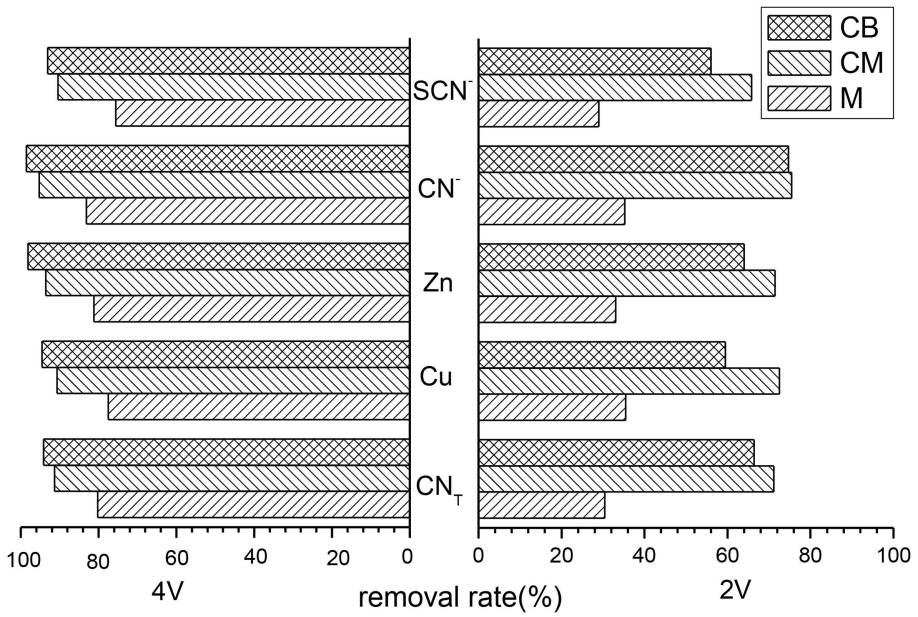

FIGURE 2 | Removal rate of various ions with different main electrodes at 3D system (pH = 9, time = 5 h, dosage of activated carbon = 2 g, voltage = 2 V or 4 V).

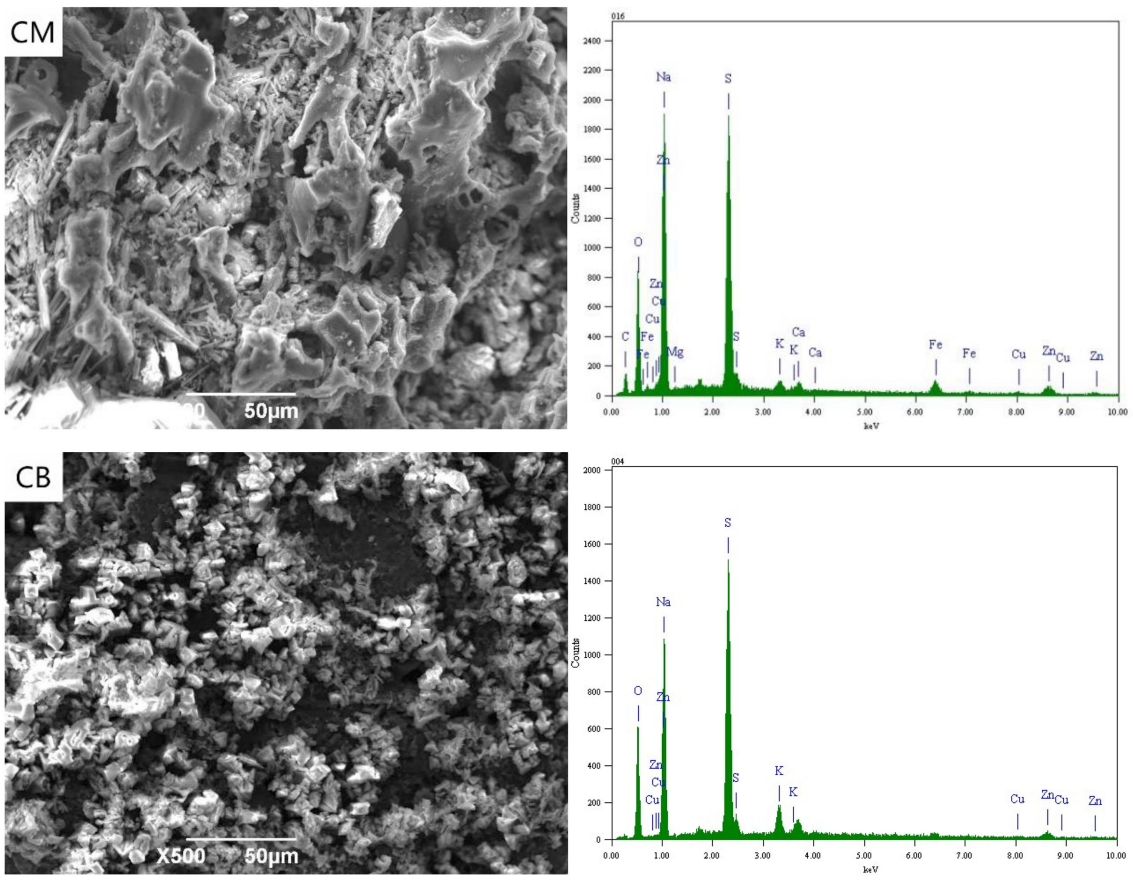

FIGURE 3 | SEM-EDS spectrum of anode under 2 V at 3D system.

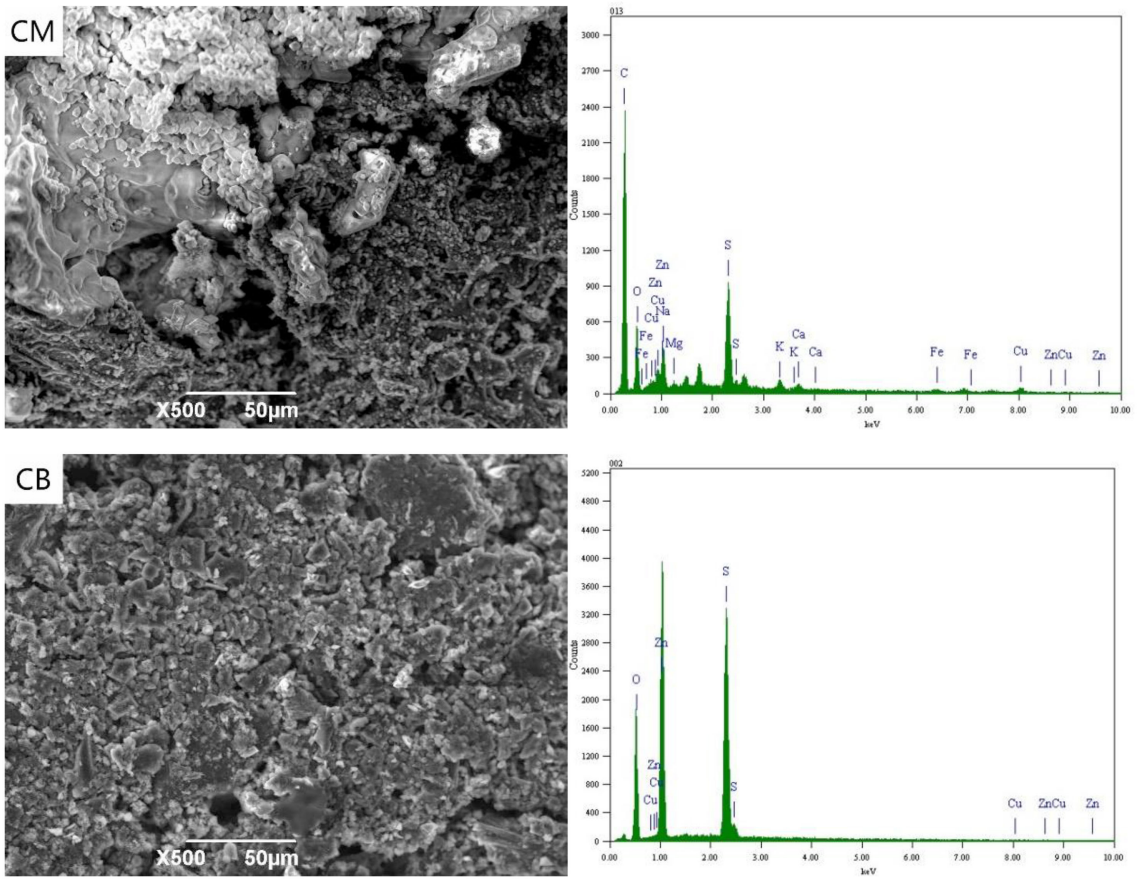

FIGURE 4 | SEM-EDS spectrum of anode under 4 V at 3D system.

electrode terminal voltage reaching the decomposition voltage of water. White precipitate appears near the anode, which was due to the high concentration of H^+ and resulted in the hydrolysis of OH^- near the anode. This was caused by the precipitate reaction of H^+ with complex ions and SCN^- in the solution, mainly including CuSCN, CuCN, $Zn(CN)_2$, $Cu_2Fe(CN)_6$, $Zn_2Fe(CN)_6$, $Cu_3Fe(CN)_6{\cdot}4H_2O$, $Zn(OH)_2$, and $Cu(OH)_2$. The removal of ions in wastewater at 2 V was thus caused by the interaction of electric adsorption and anodic precipitation.

Figure 4 shows the SEM-EDS spectrum of the CM and CB anodes in the 3D system under the applied voltage of 4 V. It can be seen from the SEM images that a small amount of white precipitates were attached to the electrode surface under 4 V conditions. These were mainly salts that adhere to the electrode surface by electrostatic adsorption. Compared with the CB electrode, a small amount of Cu, Fe, and Zn appeared in the CM anode, which was mainly due to the strong adsorption property of activated carbon in CM. With the voltage of 4 V, the actual voltage exceeds the decomposition voltage of ions in the solution. The oxidation decomposition of $CN^- \rightarrow CNO^- \rightarrow CO_2 + N_2$, and SCN^- mainly occurred and there was a small amount of hydrolysis side effects.

SEM-EDS Spectrum Analysis of Cathode

Figure 5 shows the SEM-EDS of CM and CB cathode with a voltage of 2 V. At 2 V, the applied voltage in the solution exceeds the decomposition voltage of water, and a large number of bubbles were generated in the cathode, and a hydrogen evolution reaction occurs. It can be seen from the SEM images that there were a lot of K, Mg, and other metals salts on the surface of CM and CB, which were caused by the cations' directional migration toward the cathode under the electric field. In the energy spectrum of CM, the cathode appears Fe. Due to the Fe in the stainless steel mesh, the complexing reaction with CN^- at 2 V takes place, which then adsorbs on the cathode.

Figure 6 shown the SEM-EDS spectrum of CM and CB electrodes. When the voltage is 4 V, the content of Cu, Zn, and other complex ions in the solution were greatly reduced. According to the energy spectrum, the metal content on the cathode surface was greatly increased, mainly because of the reduction deposition of Cu, Fe, and Zn on the cathode. The results show that the content of Fe in CM system was higher than that in CB, that may the stainless steel mesh dissolves in solution, by CN^- and Fe ion generated complex which was deposited on the cathode at 4 V. However, in the spectrum of the CB electrode, the higher Cu content was mainly based on

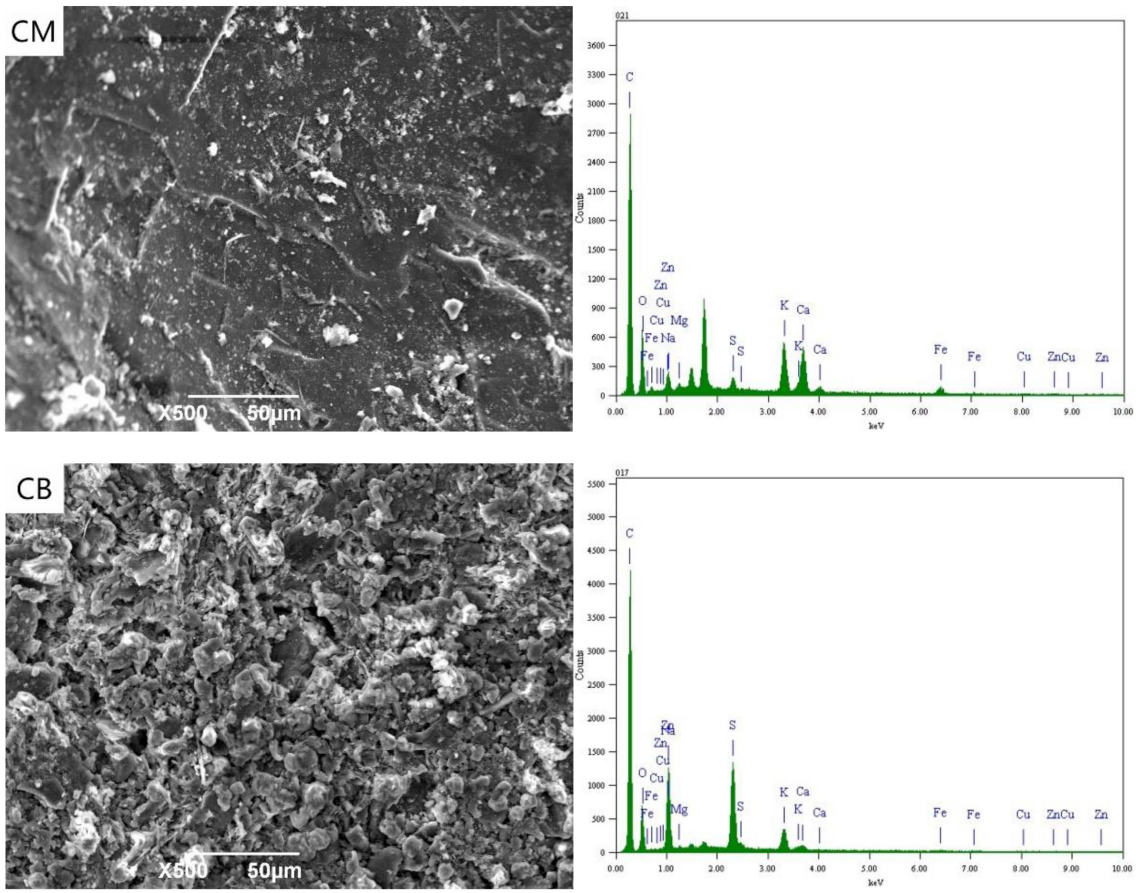

FIGURE 5 | SEM-EDS spectrum of cathode under 2 V at 3D system.

electrodeposition, while the Cu content in CM was relatively low. On the one hand, only a small part of activated carbon in the cathode was used for detection and analysis, on the other hand, this depends on the resistance and the conduction efficiency of CM.

SEM-EDS Spectrum Analysis of Particle Electrode

Figure 7 shows the SEM-EDS spectra of CM and CB at 2 V. The analysis samples were a small part of the experimental particle activated carbon. With the applied voltage of 2 V, the energy spectrum indicates that there were a lot of metal ions on the surface of the particle electrode under the action of electric adsorption. The metal complex adsorption on activated carbon in the ordered $Fe(CN)_6^{4-}$, $Zn(CN)_4^{2-}$, and $Cu(CN)_3^{2-}$ (Yonghui et al., 2017b). The ferricyanide produced by the complexation with stainless steel mesh and from wastewater will be adsorbed on the activated carbon at first, so the particle electrode surface of CM as the main electrode has a higher content of Fe ion. At 2 V, the action mechanism of the particle electrodes was electric adsorption and adsorption. Magnetic stirring would lead to the bipolar of the particle electrode, which would enhance the efficiency of electric adsorption and the removal rate of ions.

Figure 8 shows the SEM-EDS spectra of the particle electrodes at 4 V. As an important part of the 3D system, particle electrodes play the important roles of electron transfer and mass-transfer, acting as the site of an electrochemical reaction. At 4 V, the particle electrodes were considered as micro electrolysis cells. The energy spectrum indicates that there were a certain amount of metal elements present, such as Fe, Cu, and Zn on the surface of the electrode, while the contents of Cu and Zn in the particle electrodes of CB were higher than that of CM. This is mainly because the resistance and conduction efficiency of CM reduces the voltage between the particle electrodes and hinders the electrodeposition reaction of partial Cu and Zn.

XRD Analysis of the Precipitate

To study the reaction mechanism furtherly, the precipitates in the solution under different electrode systems and voltages were analyzed by XRD. The XRD analysis results of the precipitates at 2 V are shown in **Figure 9**. At 2 V, the main components of the precipitates between the activated carbon filled stainless steel mesh (CM) and coal based electrode (CB) were similar,

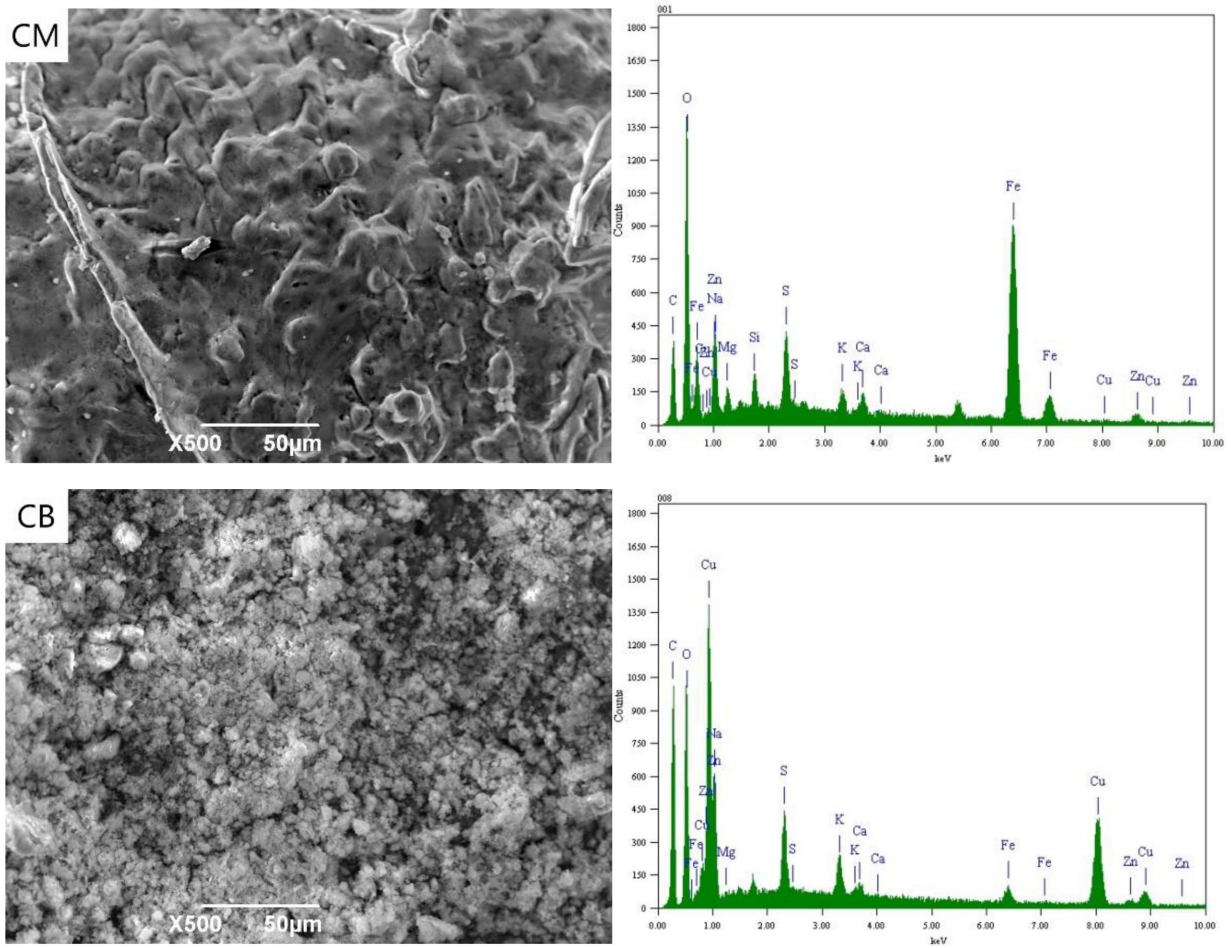

FIGURE 6 | SEM-EDS spectrum of cathode under 4 V at 3D system.

and the main precipitates were CuSCN, $Zn_2Fe(CN)_6$, $Zn(OH)_2$, and CuCN. The difference is that the precipitate contains a large amount of $Zn_2Fe(CN)_6$ when the electrode was CM. This is because the iron in the stainless steel mesh would be dissolved in the solution and combine with the cyanide ion to form a large number of iron cyanide complexes, and precipitate with zinc in the solution to generate a large amount of $Zn_2Fe(CN)_6$.

The XRD of the precipitates at 4 V is shown in **Figure 10**, which indicates that the content of $Zn_2Fe(CN)_6$ in the precipitates of the CM system was high. This is mainly caused by the Fe dissolved in the solution. The precipitation of the CM system was much larger than that of the CB electrode, which proves that under the condition of 4 V, due to the influence of the CM material's resistance and conduction efficiency, the actual voltage in the solution system may not reach the deposition voltage of Cu and Zn. It could also be because only a small amount of metal separates, so the precipitation reaction of Cu and Zn mainly occurs in the solution. However, the electrodeposition reaction of metal mainly occurs in the CB electrode system, the quantity of precipitate was smaller.

The Mechanism Analysis of 3D System

According to the research results above, which used CM and CB as an anode and cathode, and granular activated carbon (GAC) as particle electrode, when cyanide wastewater was treated by the 3D system under different voltage conditions, the ions in the solution interacted by adsorption, directional migration, enrichment precipitation, and electrolytic deposition. Under the action of different voltages, the reactions in the solution were different. The main mechanism is shown in **Figure 11**.

At a voltage of 2 V, the actual voltage in the system exceeds the decomposition voltage of water, which produced O_2 in the anode, and caused a large amount of H^+ to gather near the anode, and complex precipitation reaction (Yonghui et al., 2017b) occurred, mainly forming CuSCN, $Cu_2Fe(CN)_6$, $Zn_2Fe(CN)_6$, and so on. The iron in the CM electrode dissolution also leads to the formation of $Zn_2Fe(CN)_6$ with the iron cyanide complex and zinc

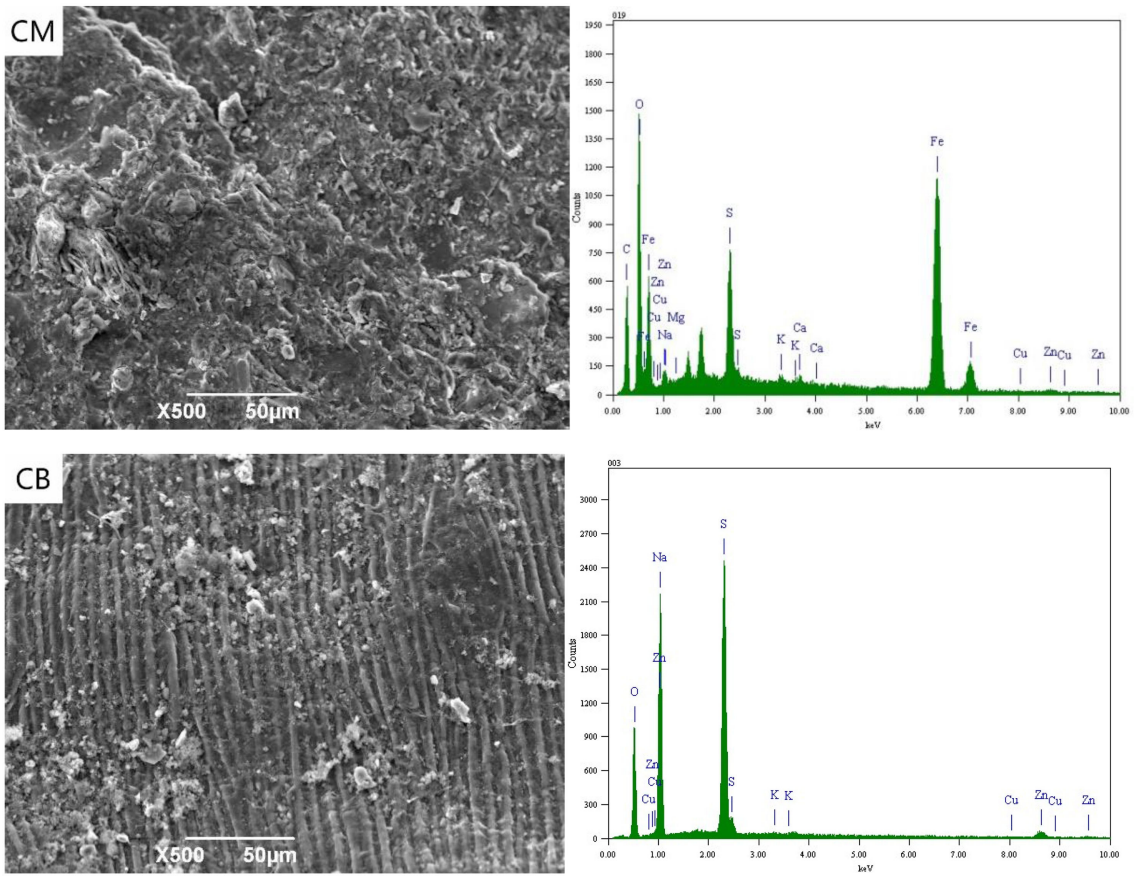

FIGURE 7 | SEM-EDS spectrum of particle electrode under 2 V at 3D system.

ion in the solution. The reaction equations were as follows:

$$4OH^- \rightarrow O_2 + 2H_2O + 4e \quad (1)$$

$$2H^+ + 2e^- \rightarrow H_2 \quad (2)$$

$$Cu(CN)_3^{2-} + 2H^+ = CuCN \downarrow + 2HCN \quad (3)$$

$$Zn(CN)_4^{2-} + 2H^+ = Zn(CN)_2 \downarrow + 2HCN \quad (4)$$

$$CuCN + SCN^- + H^+ = HCN \uparrow + CuSCN \downarrow \quad (5)$$

$$2Cu^{2+} + Fe(CN)_6^{4-} = Cu_2Fe(CN)_6 \quad (6)$$

$$2Zn^{2+} + Fe(CN)_6^{4-} = Zn_2Fe(CN)_6 \quad (7)$$

$$3Cu^+ + [Fe(CN)_6]^{3-} + 4H_2O = Cu_3Fe(CN)_6 \cdot 4H_2O \quad (8)$$

$$Zn^{2+} + 2OH^- = Zn(OH)_2 \quad (9)$$

$$Cu^{2+} + 2OH^- = Cu(OH)_2 \quad (10)$$

In the 3D system, the actual voltage at both ends of the electrode was higher than the precipitation voltage of Cu, Zn, and Fe at 4 V (Yonghui et al., 2017a), and electrodeposition occurs on the cathode, i.e., Cu, Zn, and Fe were formed, as shown in formulas (14–17). While on the anode, CN^- and SCN^- were converted into CNO^- firstly, and then CO_2 and N_2 were mainly generated. At the same time, water decomposition reaction also exists in the anode and cathode [formulas (1, 2)]. The reaction of the particle electrode is shown in the figure, under the action of the electric field the oxidation-reduction reaction occurs at both ends of the particle electrode (Yonghui et al., 2019). Thus, the 3D system is more efficient for wastewater treatment, and can reach more than 90%.

$$CN^- + 2OH^- \rightarrow CNO^- + H_2O + 2e \quad (11)$$

$$2CNO^- + 4OH^- \rightarrow 2CO_2 + N_2 + 2H_2O + 6e \quad (12)$$

$$SCN^- + 8OH^- = SO_4^{2-} + CN^- + 4H_2O + 6e \quad (13)$$

$$Cu(CN)_4^{3-} + e \rightarrow Cu + 4CN^- \varphi = -1.292 \quad (14)$$

$$Zn(CN)_4^{2-} + 2e \rightarrow Zn + 4CN^- \varphi = -1.385 \quad (15)$$

$$Fe(CN)_6^{3-} + 3e \rightarrow Fe + 6CN^- \varphi = -1.042 \quad (16)$$

$$Fe(CN)_6^{4-} + 2e \rightarrow Fe + 6CN^- \varphi = -1.742 \quad (17)$$

CONCLUSION

(1) The results of the present study show that the 3D electrode system with activated carbon filled stainless steel mesh (CM) and coal-based electrode (CB) are better than stainless steel mesh (M) as the main electrode. The CB electrode is especially

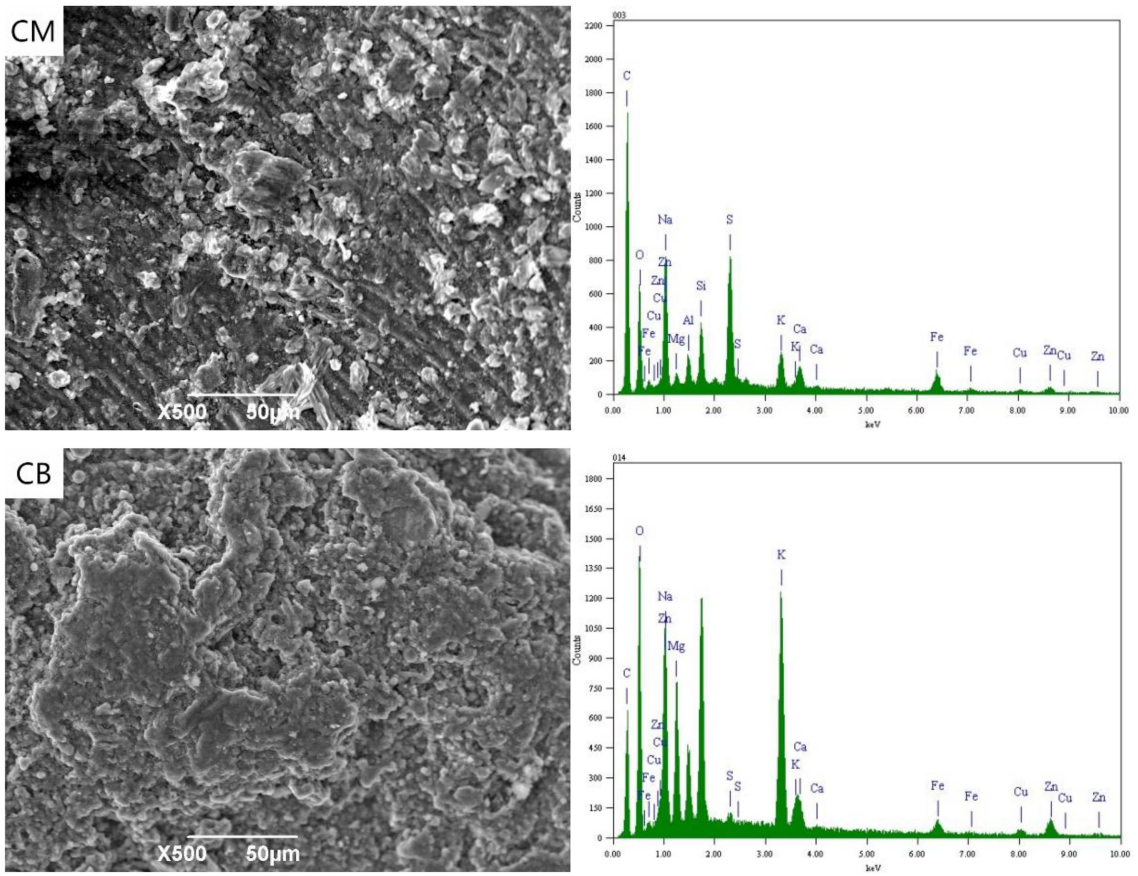

FIGURE 8 | SEM-EDS spectrum of particle electrode under 4 V at 3D system.

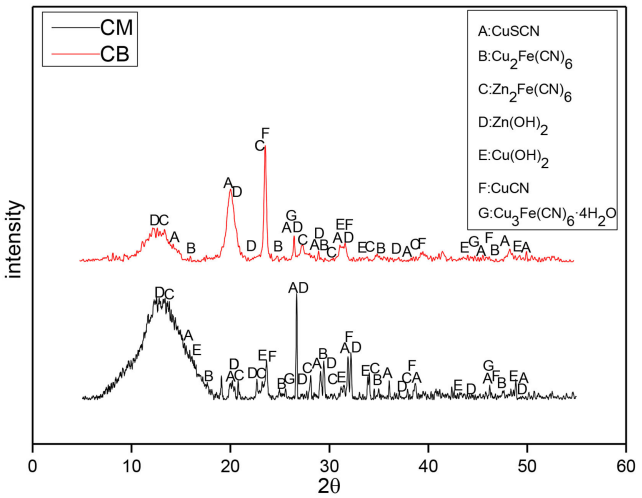

FIGURE 9 | XRD of precipitates of the different electrodes under 2 V at 3D system.

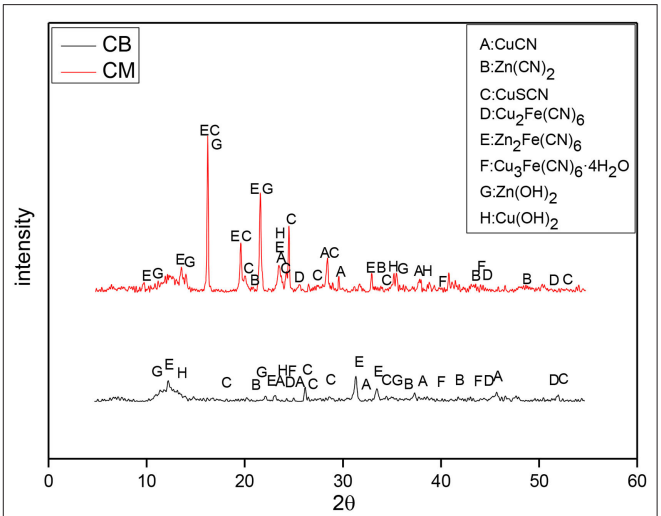

FIGURE 10 | XRD of precipitates of the different electrodes under 4 V at 3D system.

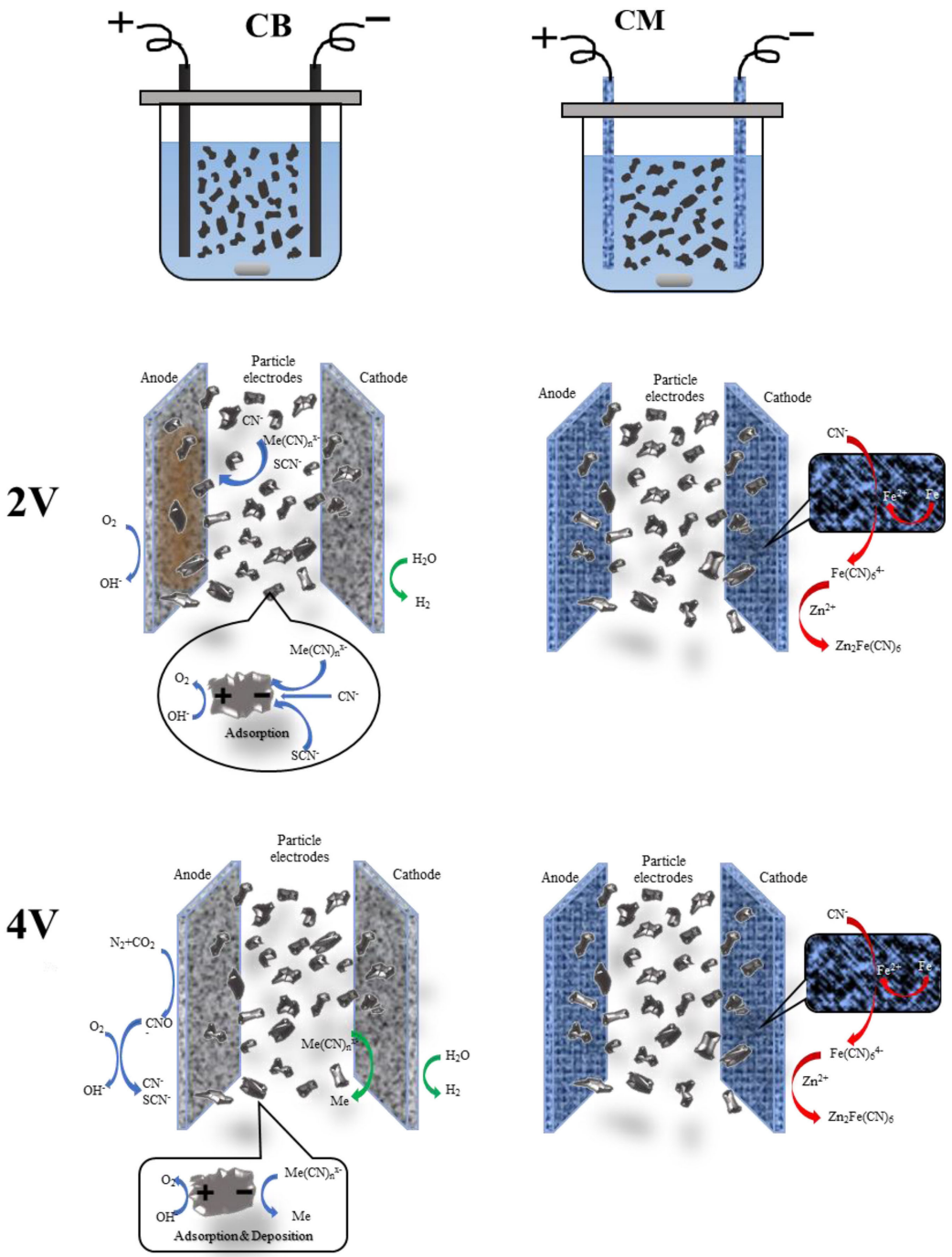

FIGURE 11 | Schematic diagram of the mechanism under different voltages. (1) Me-Cu, Zn, Fe. (2) The reaction of CM were as same as CB, except for special marked.

suitable for cyanide wastewater treatment. The main mechanism of the system of 2 V is electro adsorption and enrichment precipitation. At 4 V, the system mainly uses electrodeposition to remove all ions in wastewater, and the treatment efficiency of electrodeposition was higher than that of electro adsorption.

(2) The treatment efficiency of the 3D system is higher than that of the 2D system because of the addition of the particle electrode the reaction efficiency and removal rate of ions in wastewater improve greatly. When the applied voltage of the 3D system is 4 V, with a treatment time of 5 h, an electrode

spacing of 10 mm, and the dosage of activated carbon particles is 2 g, the removal rates of Cu, Zn, CN_T, CN^-, and SCN^- in wastewater were 94.53, 98.14, 94.14, 98.55, and 93.13%, respectively. The surface of the CB anode has an oxygen evolution reaction and electrochemical oxidation reaction of CN^-, SCN^-, and there is electrolytic deposition of Cu, Zn, and other metal ions on the cathode surface. There was adsorption and electro adsorption of various ions on the surface of the activated carbon particle electrode, and the electrolytic deposition reaction of Cu, Zn, and other metal ions at the same time.

(3) In the process of cyanide wastewater treatment by 3D electrode based on CB electrode, due to the concentration of hydrogen ion increase in the local area near the anode caused by oxygen evolution reaction, the precipitation reaction between CN^-, SCN^- and metal cyanide complex ions will occur under the action of the electric field, generating precipitation of CuSCN, $Cu_2Fe(CN)_6$, $Zn_2Fe(CN)_6$, which is the main reason for the removal of cyanide and heavy metals ions from cyanide wastewater.

DATA AVAILABILITY STATEMENT

The original contributions presented in the study are included in the article/supplementary materials, further inquiries can be directed to the corresponding author.

AUTHOR CONTRIBUTIONS

YS: conceptualization, methodology, writing—reviewing, and editing. SL: data curation, writing—original draft, software, and formal analysis. Both authors: contributed to the article and approved the submitted version.

FUNDING

This project was financially supported by the National Natural Science Foundation of China (no. 51774227), the Natural Science Basic Research Plan in Shaanxi Province of China (no. 2018JZ5011), and Joint Program of Shaanxi Natural Science Foundation (no. 2019JLM-44).

REFERENCES

Acheampong, M. A., Meulepas, R. J. W., and Lens, P. N. L. (2010). Removal of heavy metals and cyanide from gold mine wastewater. *J. Chem. Technol. Biot.* 85, 590–613. doi: 10.1002/jctb.2358

Han, L., and Zhenshan, L. (2013). Experimental research on energy consumption in zinc containing wastewater treatment by three-dimensional activated carbon electrode. *Indus. Safety Environ. Protect*. 4–7. doi: 10.3969/j.issn.1001-425X.2013.05.002

Hui, T. (2016). *Research of cyanide leaching gold tail solution treatment by electric adsorption* (Master Dissertation). Xi'an University of Architecture and Technology. Available online at: https://kns.cnki.net/KCMS/detail/detail.aspx?dbname=CMFD201701&filename=1016741012.nh

Jia, Y. N., Jiang, W. F., Hao, S. J., Zhang, Y. Z., and Zhang, L. (2013). Feasibility study on coking waste water treatment by three-dimensional electrode. *Adv. Mat. Res*. 750–752, 1437–1440. doi: 10.4028/www.scientific.net/AMR.750-752.1437

Jinzhi, W., Shaoping, Z., Qin, H., and Fangni, C. (2015). Efficiency and mechanism of three-dimensional particle electrode for treating dyes wastewater. *Chin. J. Environ. Eng*. 1715–1720.

Lei, Z., Lina, W., Benquan, F.,Pu, L., Nan, Z., and Gaoming, W. (2013). Advanced treatment of coking wastewater using three-dimensional electrode reactor. *Chin. J. Environ. Eng*. 3397–3402.

Shilei, Z., Xujia, J., Guoliang, H., and Meiping, T. (2013). Application of electrocoagulation technology to water treatment. *Indus. Water Treat*. 10–19. doi: 10.3969/j.issn.1005-829X.2013.01.003

Ting, S., Yonghui, S., Xinzhe, L., Wenwen, G., and Jun, Z. (2018). Adsorption optimization of coal-based electrode materials for cyanide wastewater treatment. *Chem. Eng.* 5–9. doi: 10.3969/j.issn.1005-9954.2018.12.002

Vedula, R. K., Dalal, S., and Majumder, C. B. (2013). Bioremoval of cyanide and phenol from industrial wastewater: an update. *Bioremediat. J.* 17, 278–293. doi: 10.1080/10889868.2013.827615

Xi, C., Xinyang, X., Bing, Z., and Haibo, L. (2015). Treatment of copper-nickel mixed wastewater by spouted bed electro-deposition method. *CIESC J*. 5060–5066. doi: 10.11949/j.issn.0438-1157.20151074

Yao, D., Song, Y., Zhang, S., Tian, Y., and Lan, X. (2017). Effect of voltage on the treatment of cyanide wastewater by three-dimensional electrode. *J. New Mat. Electr. Sys*. 20, 151–159. doi: 10.14447/jnmes.v20i4.318

Yonghui, S., Chunchen, W., Hui, T., Siming, L., and Xinzhe, L. (2016). Treatment of high-cyanide-containing wastewater using electric adsorption. *Chin. J. Rare Metals*. 492–498. doi: 10.13373/j.cnki.cjrm.2016.05.014

Yonghui, S., Di, Y., Shan, Z., Yuhong, T., and Xinzhe, L. (2017a). Study on the treatment of cyanide wastewater by three-dimensional electrode. *Gold Sci. Technol*. 116–121. doi: 10.11872/j.issn.1005-2518.2017.05.116

Yonghui, S., Hui, T., Siming, L., and Xinzhe, L. (2017b). Treatment of cyanide wastewater by electric adsorption with applied voltage. *Chin. J. Rare Metals* 904–911. doi: 10.13373/j.cnki.cjrm.XY15121002

Yonghui, S., Siming, L., Ning, Y., and Wenjin, H. (2019). Treatment cyanide wastewater dynamic cycle test by three-dimensional electrode system and the reaction process analysis. *Environ. Technol*. doi: 10.1080/09593330.2019.1677783. [Epub ahead of print].

Conflict of Interest: The authors declare that the research was conducted in the absence of any commercial or financial relationships that could be construed as a potential conflict of interest.

frontiers in Chemistry

ORIGINAL RESEARCH
published: 25 March 2021
doi: 10.3389/fchem.2021.593888

Selective Pre-leaching of Tellurium From Telluride-Type Gold Concentrate

Wei Yang[1,2]*, *Xuechen Lan*[1,2]*, *Qian Wang*[1,2], *Ping Dong*[1,2] and *Gang Wang*[1,2]

[1]School of Resource Engineering, Xi'an University of Architecture and Technology, Xi'an, China, [2]Key Laboratory of Gold and Resources in Shaanxi Province, Xi'an, China

With a telluride-type gold ore flotation concentrate as the research object, the Na_2S + NaOH collaborative leaching process was applied to selectively separate tellurium before the cyanide leaching of gold and silver. The effects of process parameters including the type of leaching agent, the amount of leaching agent, liquid-solid ratio, leaching temperature, and leaching time on the leaching rate of tellurium were investigated. The results showed that the tellurium leaching rate could reach 78.14% under the optimum conditions of −0.038 mm (95%) grinding fineness, 80 g/L Na_2S concentration, 30 g/L NaOH concentration, 4:1 liquid-solid ratio, 80°C leaching temperature and 3 h′s leaching time. The kinetic analysis showed that the leaching process of tellurium from telluride-type gold concentrate was a mixed type of chemical reaction control and diffusion control. The grain parameter in the leaching process was 0.26263 and the apparent activation energy E = 17.12 kJ/mol. Tellurium could be pre-leached from the telluride-type gold flotation concentrate through the Na_2S + NaOH alkaline leaching process to achieve the effective separation of tellurium from noble metals, which, when eliminating the adverse effects of telluride on the leaching of gold and silver, provides new ideas for the extraction of rare element tellurium.

Keywords: telluride-type gold concentrate, cooperative leaching, pre-separation, tellurium, leaching rate

OPEN ACCESS

Edited by:
Shenxu Bao,
Wuhan University of Technology, China

Reviewed by:
Hadi Abdollahi,
University of Tehran, Iran
Bo Feng,
Jiangxi University of Science and Technology, China

***Correspondence:**
Wei Yang
yangweixauat@126.com,
Xuechen Lan
lxc9802@163.com

Specialty section:
This article was submitted to Green and Sustainable Chemistry, a section of the journal Frontiers in Chemistry

Received: *11 August 2020*
Accepted: *08 February 2021*
Published: *25 March 2021*

Citation:
Yang W, Lan X, Wang Q, Dong P and Wang G (2021) Selective Pre-leaching of Tellurium From Telluride-Type Gold Concentrate. Front. Chem. 9:593888. doi: 10.3389/fchem.2021.593888

INTRODUCTION

Tellurium, a rare element, is widely used in metallurgy, chemical industry, electronics, aerospace, medical and other fields (Wang, 2011). As an additive in metallurgy, tellurium can improve the cutting properties of steel and copper, and enhance the hardness and wear resistance of "baffle alloys" (Wang, 2011); CdTe thin-film solar cells are a kind of solar cells with low price and their highest photoelectric conversion efficiency could reach 21%, holding the greatest promise for the future of thin film (Lee and Ebong, 2017; Geisthardt et al., 2015); Tellurium compounds such as ammonium trichloro(dioxo ethylene-*O*, *O*′)tellurate (AS101) have attracted much attention in cancer treatment (Sredni, 2012); besides, tellurium and its compounds have gradually become research hotspots in thermoelectric conversion, biology, and electronics (Lin et al., 2016; Ba et al., 2010; Chivers and Laitinen, 2015).

Although tellurium is widely used, its abundance in the Earth's crust is only 1 ppb, which is lower than that of the so-called "rare earth" elements, and often coexists with chalcogen elements such as gold, copper, and lead (Missen et al., 2020). Currently, tellurium comes mainly from copper-refined anode sludge from smelters, which accounts for more than 90% of its global supply (Wang, 2011; Fan et al., 2013). With the increasing demand and price of tellurium, the recovery of tellurium from tellurium-containing ores or electronic wastes has attracted researchers' attention (Rocchetti and Beolchini, 2015; Candelise et al., 2012). The Dashuigou Bismuth Tellurium Deposit in Shimian

TABLE 1 | Chemical analysis results of major elements in telluride-type gold concentrate.

Elemental	Te	Au	Ag	Pb[a]
Grade (g/t)	243.72	89.30	93.16	6.80

[a]*Means that the unit is %.*

County, Sichuan Province, China is the only independent primary tellurium deposit discovered in the world so far, so there are many studies on the recovery of tellurium from bismuth tellurium deposits (Zhang et al., 2019). The H_2SO_4 + $FeCl_3$ oxidative leaching process was applied to leach bismuth telluride ore and the leaching rate of tellurium and bismuth could reach 95.61 and 95.77% (Shao et al., 2020). A large number of flotation experiments were carried out on bismuth tellurium deposits and the tellurium grade and recovery rate of obtained concentrate products are 9.94 and 94.81%, respectively (Yu et al., 2019). This process effectively recovered bismuth, gold, and silver, which provided a reference for processing this type of minerals. Although there are some studies on the recovery of tellurium from tellurium-bearing ores, there are few studies on the recovery of tellurium from telluride-type gold ore.

The relationship between tellurium and gold is very close. Telluride-type gold ores are the most common gold-bearing minerals and also one of the refractory gold ores (Ibers, 2009). Many studies have shown that telluride-type gold ore is difficult to dissolve in the cyanide solution, resulting in a decrease in the leaching rates of gold and silver. The currently accepted explanation is that the insoluble compound—TeO_2 (or hydrated H_2TeO_3 phase) was produced during the cyanidation process, and the insoluble compound could lead to a passivation layer formed on the mineral surface, as shown in **Eqs 1,2** (Jayasekera et al., 1996; Henley et al., 2001; Dyer et al., 2017).

$$AuTe_2\,(s) + CN^- + 8OH^- \rightarrow Au\,(CN)^{2-} + 2H_2TeO_3\,(s) + 2H_2O + 7e^- \quad (1)$$

$$H_2TeO_3\,(s) + 2OH^- \rightarrow TeO_3^{2-} + 2H_2 \quad (2)$$

Therefore, such pretreatment methods as ultra-fine grinding (UFG), roasting, and biological leaching are often applied in dealing with telluride-type gold ores to increase gold recovery rate (Dyer, et al., 2017; Richmond, 2010). However, UFG increases the consumption of chemicals in subsequent processes; roasting produces SO_2 which is not friendly to the environment and the composition of the minerals after roasting is complex; the biological leaching process is slow and time-consuming, and the degree of tellurium oxidation is difficult to control (Dyer, et al., 2017; Richmond, 2010). In addition to the above methods, telluride-type gold ore can also be treated by flotation process. The telluride leaching method of The Republic of Fiji is a classic combined processing and metallurgical treatment of telluride-type gold ore. This process first concentrates telluride-type gold ore, then follows by oxidative roasting, cyanide leaching, polysulfide leaching, sodium sulfite reduction, and other processes to recover tellurium and gold (Zhou and Chen, 2008). This method has a complicated process and high investment cost, and is difficult to apply to other processing plants. Previously, the author's research team obtained tellurium-gold-silver mixed concentrates from tellurium-type gold ores typical of the Xiaoqinling area by flotation, and obtained tellurium, gold, and silver with average grades of 241.61, 90.30, and 92.74 g/t with superior recoveries of 95.42, 97.28, and 94.65%, respectively, but did not achieve the separation of tellurium from the precious metals (Yang et al., 2019). The purpose of the above methods is to remove tellurium or to recover tellurium, gold and silver at the same time. At present, there are few types of research to improve the leaching rates of gold and silver by pre-leaching tellurium.

A simple process was proposed to separate tellurium from telluride-type gold concentrate and the optimal conditions were explored for selective pre-leaching of tellurium from telluride-type gold concentrate. The effects of leaching agent type, leaching agent dosage, liquid-solid ratio, leaching temperature and leaching time on the tellurium leaching rate are investigated, so as to provide the theoretical and technological basis for the separation and recovery of valuable metals in telluride-type gold concentrate.

EXPERIMENTAL

Materials

The sample for this experiment was taken from the telluride-type gold concentrate from the Yangping mining area in Xiaoqinling, Henan Province, China. The sample was dried, ground, and thoroughly mixed by the quarter method after it was retrieved. A small amount of the mineral sample was used for XRD analysis, and the rest was stored in a dry vessel for subsequent experiments. The chemical analysis results of the telluride-type gold concentrate have been shown in **Table 1**. As shown in **Table 1**, tellurium, gold and silver grades of 243.72, 89.30, and 93.16 g/t, respectively, and lead content 6.80%. The XRD analysis

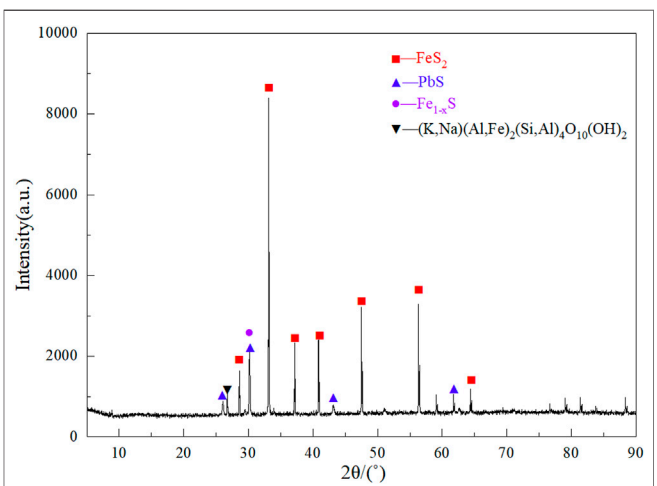

FIGURE 1 | XRD diffractograms of telluride-type gold concentrate.

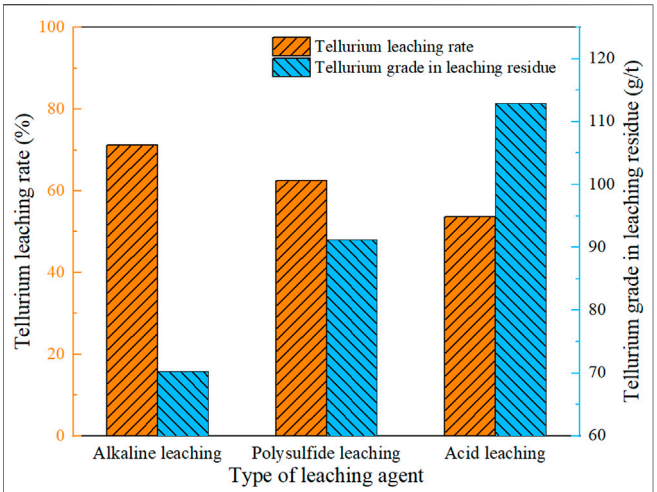

FIGURE 2 | Effect of leaching agent type on tellurium leaching rate.

results are shown in **Figure 1**. The main components of the ore sample are pyrite, galena, pyrrhotite, and muscovite.

Experimental Methods

Fifty grams telluride-type gold concentrate was weighed at a time and ground to the specified fineness in a ball mill (XMQ series ball mill) with a pulp density of 60 wt%. AR grade chemicals and deionized water were used throughout the experiment. The leaching experiment was carried out in a 250 mL beaker using a numerically controlled mechanical stirrer. In batch experiments, 50 g grinding sample was mixed with leaching agent mixture and a fixed amount of water. The pulp was leached at a stirring speed of 500 r/min and at a set temperature. The time spent in the leaching process was recorded, and the amount of water was regularly added to control the liquid-solid ratio. Finally, the leaching residue was washed five times by hot water immediately, and then dried at room temperature, weighed, sampled, and tested, and the remaining samples were kept for subsequent leaching of gold and silver. The content of tellurium in the solution was measured by ICP-MS (Agilent 7800). The leaching rate is calculated according to **Eq. 3** based on the grade of the leaching residue.

$$\varepsilon = \frac{R_0 - R}{R_0} \times 100\% \quad (3)$$

Where ε is the metal leaching rate (%); R_0 and R respectively represent the grades of the element in the original ore and leach residue (g/t).

Experimental Principle

Tellurium is mainly present in minerals or anode mud in the form of tellurium dioxide, tellurite, and tellurate, and depending on the choice of leaching agent, tellurium of different valences will undergo different reactions, and the following chemical reactions may occur during the leaching process (Zhou and Chen, 2008; Liu et al., 2020; Guo et al., 2017; Sun and Zheng, 2011; Hoffmann and Zhong, 1990).

$$TeO_2 + 2NaOH = Na_2TeO_3 + H_2O \quad (4)$$

$$Na_2TeO_3 + 3Na_2S + 3H_2O = Na_2TeS_3 + 6NaOH \quad (5)$$

$$Na_2TeO_4 + 4Na_2S + 4H_2O = Na_2TeS_4 + 8NaOH \quad (6)$$

$$Na_2TeO_4 + H_2SO_4 = H_2TeO_4 + Na_2SO_4 \quad (7)$$

$$TeO_2 + 4HCl = TeCl_4 + 2H_2O \quad (8)$$

$$Te + 3Na_2S_2 \rightarrow Na_2TeS_4 + 2Na_2S \quad (9)$$

Sodium sulfide can convert insoluble tellurite into soluble thio-tellurite (**Eqs 5**,**6**). HCl can dissolve tetravalent tellurium (**Eq. 8**), and dilute sulfuric acid converts insoluble sodium tellurate to soluble telluric acid (**Eq. 7**), which, through hydrochloric acid and sulfur dioxide reduction process, or sodium sulfite reduction, alkali solution, electrolysis, and other treatments to obtain metal tellurium (Hoffmann and Zhong, 1990). The polysulfide leaching tellurium has a better leaching effect on elemental tellurium (**Eq. 9**), while leaching tellurium, it has an inhibitory effect on lead, copper, arsenic, etc. (Yang, 1997)

RESULTS AND DISCUSSION

Effect of Leaching Agent Type

Figure 2 shows the effect of leaching agent type on the leaching effect of telluride-type gold concentrate. Based on experience and existing researches, the experiment was carried out as the grinding fineness was set at −0.038 mm (92%), leaching temperature at 80°C, liquid-solid ratio at 2:1, leaching time at 4 h and leaching agent dosage at 60 g/L (Na_2S: NaOH = 2:1).

Figure 2 shows that alkaline leaching is the most effective with the tellurium leaching rate up to 71.19%. When HCl was used as the leaching agent, the leaching was the worst, with a leaching rate of 53.68%, while HCl converted the silver to insoluble silver chloride, which made it difficult for tellurium to be subsequently separated from the precious metal, and

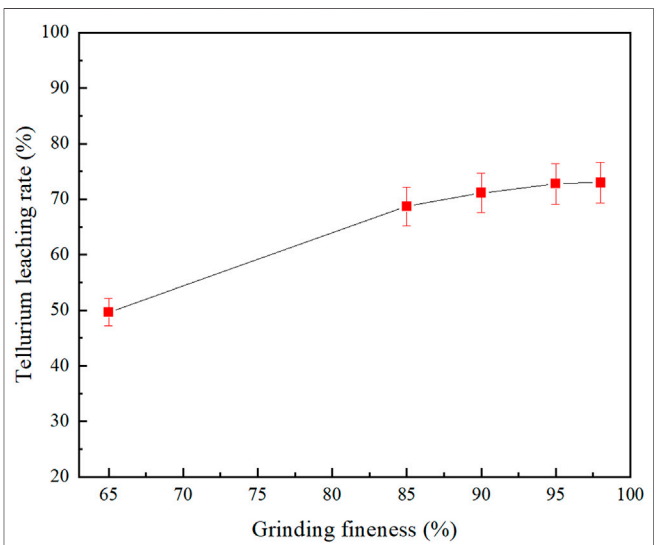

FIGURE 3 | Effect of grinding fineness on tellurium leaching.

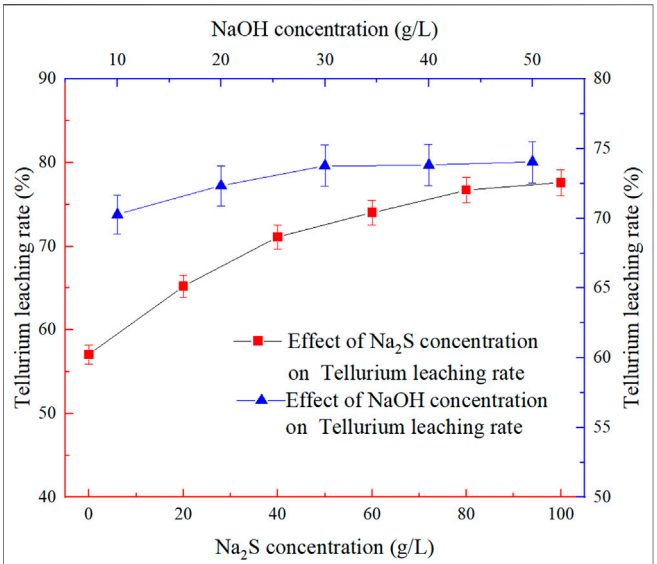

FIGURE 4 | Effect of leaching agent dosage on tellurium leaching rate.

hexavalent tellurium could oxidize HCl and produce chlorine gas which can dissolve gold (Chen and Li, 2008). Compared with acid leaching and polysulfide leaching, this type of telluride-type gold concentrate has the best alkaline leaching effect, and the subsequent gold-silver leaching process is also in an alkaline environment. In summary, the Na_2S + NaOH cooperative leaching process is adopted in the pretreatment of telluride-type gold concentrate.

Effect of Grinding Fineness

The leaching process undergoes a multiphase reaction at the solid-liquid phase boundary of the ore grains, and the phase boundary area and viscosity of the leached pulp are closely related to the grinding fineness. Therefore, in order to investigate the effect of grinding fineness on tellurium leaching rate, a grinding fineness experiment was carried out at 80°C leaching temperature, 2:1 liquid-solid ratio, 4 h's leaching time and 60 g/L leaching agent dosage (Na_2S: NaOH = 2:1). It can be seen from **Figure 3** that the leaching rate of tellurium gradually increases with the increase in grinding fineness and then stabilizes. The experimental results are shown in **Figure 3**.

When grinding fineness was −0.038 mm (95%), the tellurium leaching rate reached 72.77%, while the tellurium leaching rate was almost unchanged when the grinding fineness continued to increase. This may be due to the fact that within a certain range, as the specific surface area increases with decreasing particle size (Zheng and Chen, 2014), the contact area increases between the mineral and the leaching agent, leading to the mass transfer enhanced and the leaching rate increases accordingly. However, if the grinding is too fine, it will increase the viscosity of the pulp and the diffusion resistance, and even form a mud film on the surface of the leached minerals, resulting in the slow rise or fall of the leaching rate. And the grinding time is too long, it will increase energy consumption and cost. Therefore, the grinding fineness is determined at −0.038 mm (95%).

Effect of Leaching Agent Dosage

Na_2S is the main leaching agent for tellurium leaching, and its concentration is an important factor affecting the tellurium leaching rate. When the appropriate amount of Na_2S is used, tellurium can be selectively leached, and lead leaching can be inhibited without affecting the subsequent recovery of precious metals. The effect of Na_2S concentration on the tellurium leaching rate was shown in **Figure 4**. The fixed conditions were −0.038 mm (95%) grinding fineness, 20 g/L NaOH concentration, 80°C leaching temperature, 2:1 liquid-solid ratio and 4h′s leaching time.

From **Figure 4** it can be seen that the Na_2S concentration has a greater effect on the tellurium leaching rate than the NaOH concentration, and the tellurium leaching rate increases with the increase of Na_2S concentration and then reaches to a stable state. When the Na_2S concentration increases from 80 to 100 g/L, the tellurium leaching rate only increases by 0.9%, so the Na_2S concentration is finally determined to be 80 g/L considering the economic cost.

The NaOH concentration experiment was carried out as the grinding fineness was set at −0.038 mm (95%), Na_2S concentration at 80 g/L, leaching temperature at 80°C, liquid-solid ratio at 2:1 and leaching time at 4 h, so as to investigate the effect of NaOH concentration on the tellurium leaching rate. The results are shown in **Figure 4**.

From **Figure 4** it can also be seen that the tellurium leaching rate was 57.06% when the Na_2S concentration was 0 g/L. It can be seen that some of the tellurium-bearing minerals were leached out by milling and NaOH addition. After the Na_2S concentration was 80 g/L and the NaOH concentration was increased from 10 to 30 g/L, the leaching rate of tellurium hardly changes with the increase of NaOH concentration, and most of the tellurium was leached. Considering the pharmaceutical cost, a NaOH concentration of 30 g/L was determined at which the tellurium leaching rate could reach 73.78%.

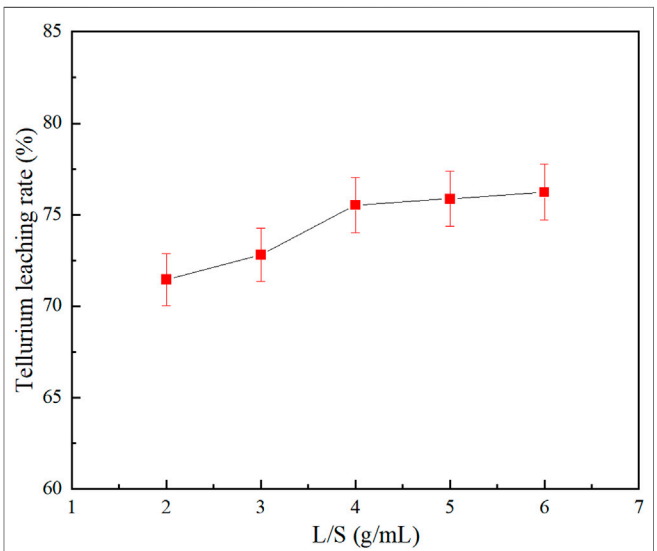

FIGURE 5 | Effect of liquid-solid ratio on tellurium leaching rate.

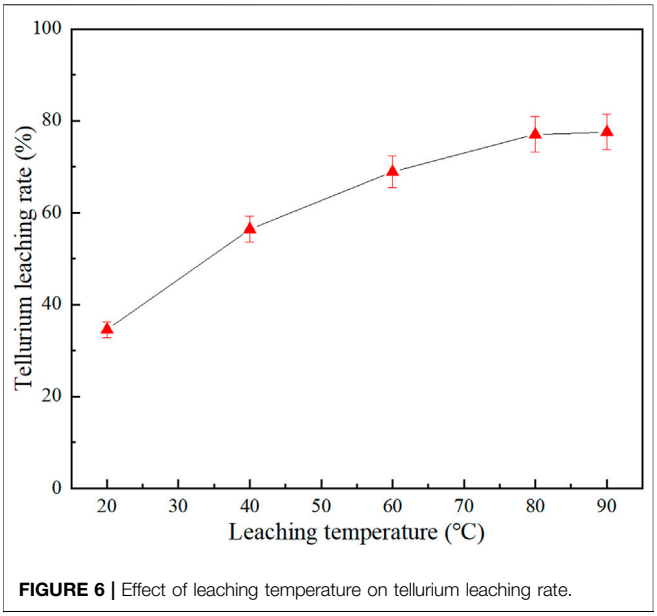

FIGURE 6 | Effect of leaching temperature on tellurium leaching rate.

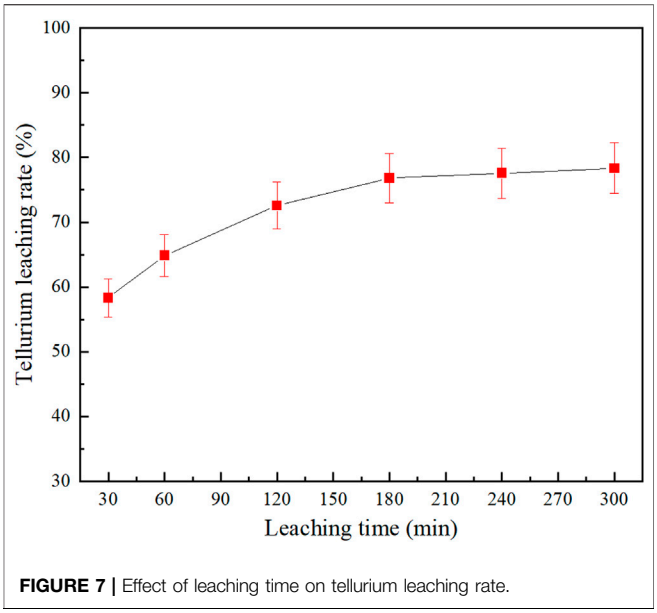

FIGURE 7 | Effect of leaching time on tellurium leaching rate.

Effect of Liquid-Solid Ratio

Figure 5 shows the effect of liquid-solid ratio on the tellurium leaching rate. The experiment was carried out as the grinding fineness was set at −0.038 mm (95%), Na_2S concentration at 80 g/L, NaOH concentration at 30 g/L, leaching temperature at 80°C and leaching time at 4 h.

As shown in **Figure 5** tellurium leaching rate increased to 75.53% with increasing liquid-solid ratio and then remained almost unchanged. In the leaching process, the size of the liquid–solid ratio directly affected the liquid-solid mass transfer in the system (Aydogan et al., 2005): if the liquid–solid ratio was too small, the pulp viscosity would be high and the leaching effect would be reduced; while if the liquid–solid ratio was too large, the processing capacity of the equipment would be affected. Thus, the liquid–solid ratio was set at 4:1.

Effect of Leaching Temperature

Figure 6 shows the effect of leaching temperature on the Na_2S + NaOH cooperative leaching process. The experiment was conducted under the conditions of −0.038 mm (95%) grinding fineness, 80 g/L Na_2S concentration, 30 g/L NaOH concentration, 4:1 liquid–solid ratio and 4 h′s leaching time.

As shown in **Figure 6**, the tellurium leaching rate increased significantly with leaching temperature increasing from 20 to 80°C, and the leaching rate of tellurium increased from 34.48 to 77.03%. However, when the temperature continued to increase beyond 80°C, the tellurium leaching rate remained almost unchanged. When the temperature is low, the reaction is controlled by diffusion; when the temperature reaches a set value, the diffusion rate is faster, and the leaching process is converted to chemical control. At this time, the increase in temperature has little effect on the leaching rate, which is consistent with the experiment results. So the reaction temperature was determined at 80°C.

Effect of Leaching Time

Figure 7 shows the effect of leaching time on the Na_2S + NaOH cooperative leaching process. The experiment was carried out as the grinding fineness was set at −0.038 mm (95%), Na_2S concentration at 80 g/L, NaOH concentration at 30 g/L, leaching temperature at 80°C and liquid-solid ratio at 4:1.

From **Figure 7**, it can be seen that the tellurium leaching rate increases with increasing the reaction time and it would come to a stable state. The leaching rate could reach 58.31% at 0.5 h; but when the time was lengthened from 2 to 3 h, the tellurium leaching rate would only increase by 4.26%; then, when the leaching time was beyond 3 h, the tellurium leaching rate would remain almost unchanged. A longer leaching time would facilitate a more thorough leaching process, but it would increase the cost and be detrimental to production, so it was determined that the leaching time was 3 h, at which the tellurium leaching rate was 76.83%.

Reaction Mechanism Analysis

Tellurium is converted to soluble thio-tellurite (TeS_3^{2-}, TeS_4^{2-}) when tellurium-bearing minerals are dissolved in Na_2S + NaOH solution (Zhou and Chen, 2008; Liu et al., 2020; Guo et al., 2017). The reaction is shown in **Eqs 4–6** and the mechanism diagram is shown in **Figure 8**. In addition to adjusting the pH value, the addition of NaOH can also effectively prevent the hydrolysis of Na_2S (**Eqs 10,11**).

$$Na_2S + H_2O = NaHS + NaOH \quad (10)$$

$$NaHS + H_2O = H_2S + NaOH \quad (11)$$

Pb in the telluride-type gold concentrate mainly exists in the form of galena (PbS), and PbS can be leached by NaOH to form soluble lead salt (**Eq. 12**). (Huang, 2012) The reaction (**Eq. 12**) caused the consumption of NaOH, thus affecting the leaching of tellurium. The addition of Na_2S inhibited the reaction (Guo, et al., 2016; Lewis, 2010), and then achieved the selective leaching of

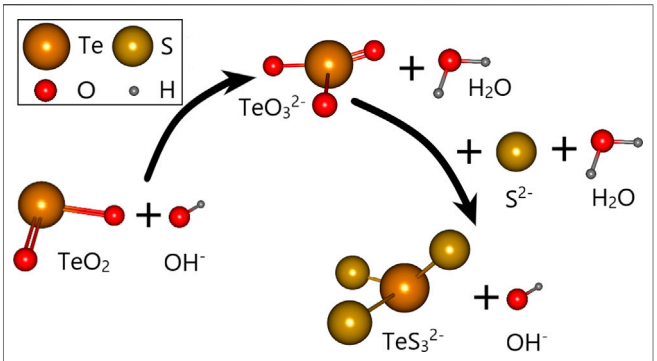

FIGURE 8 | Na_2S + NaOH cooperative leaching mechanism.

TABLE 2 | Results of an optimum experiment.

Elemental	Te	Au	Ag	Pb
Leaching residue grade/(g/t)	53.27	86.75	90.14	6.21[a]
Leaching rate/%	78.14	2.86	3.24	8.68

[a]*Means that the unit is %.*

tellurium by Na_2S + NaOH cooperative leaching process. The above mechanism may be further verified through optimum and verification experiments.

$$Na_2PbO_2 + Na_2S + 2H_2O = PbS + 4NaOH \quad (12)$$

Optimum Experiment

Through the above experiments, optimum conditions could be obtained for the Na_2S + NaOH cooperative leaching of tellurium from telluride-type gold concentrate: −0.038 mm (95%) grinding fineness, 80 g/L Na_2S concentration, 30 g/L NaOH concentration, 80°C leaching temperature, 4:1 liquid-solid ratio, 3 h′s leaching time. The leaching rate of tellurium under these conditions was 78.14% as listed in **Table 2**. XRD analysis results of the leached slag were performed as shown in **Figure 9**.

From **Figure 9**, it can be seen that the main phase of the leach residue is still pyrite and that tellurium is not shown in the XRD diffractograms due to its low content. As shown in **Table 2**, the Pb grade decreased from 6.80 to 6.21%, showing that it was almost unchanged in selective pre-leaching of tellurium from telluride-type gold concentrate. It can be concluded that the leaching of Pb is effectively inhibited by Na_2S in parallel with tellurium leaching. At the same time, the gold and silver grades are also basically unchanged. It is concluded that the Na_2S + NaOH cooperative leaching process can selectively leach tellurium from telluride-type gold concentrate, and the possibility of recovering tellurium, gold and silver from telluride-type gold concentrate will be investigated in future experiments.

Validation Experiment

Ores with conventional cyanide leaching gold leach rates of less than 80% are referred to as refractory gold ores (Fraser et al., 1991; Yannopoulos and Springerlink, 1991). The direct leaching gold leaching rate of telluride-type gold concentrate in this experiment was only 32.00%, which is refractory gold ore. To determine the effect of Na_2S + NaOH cooperative leaching on the recovery of precious metals from telluride-type gold concentrate, a validation experiment was conducted with reference to the flowchart shown in **Figure 10**, and the experiment results are listed in **Table 3**.

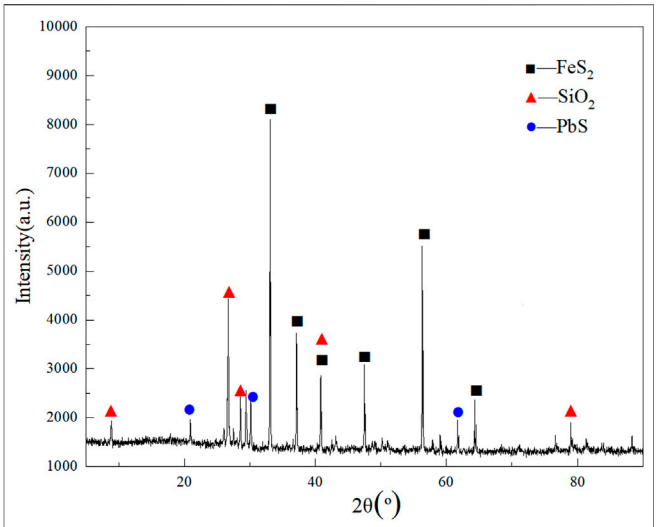

FIGURE 9 | XRD diffractograms of optimum experiment leaching residue.

The pre-leaching experiment of tellurium was carried out as the grinding fineness was set at −0.038 mm (95%), Na_2S concentration at 80 g/L, NaOH concentration at 30 g/L, leaching temperature at 80°C, liquid-solid ratio at 4:1, and leaching time at 3 h. The leaching of gold and silver was carried out under the following conditions: the grinding fineness was set at −0.038 mm (95%), pH = 12, NaCN dosage at 0.80%, liquid-solid ratio at 2:1, and leaching time at 48 h.

It can be seen from **Table 3** that the experiment results of procedure 2 are significantly better than that of procedure 1. When the telluride-type gold concentrate is directly cyanide leached to leaching gold and silver, the gold leaching rate is only 32.00%. After the telluride-type gold concentrate is selectively pre-leached with tellurium, the leaching rate of gold is significantly increased to 75.39%, and the leaching rate of silver also rises to 58.83%, indicating that the hydration film formed by tellurium can interfere with gold and silver leaching, especially gold leaching during the cyanidation process of telluride-type gold mines (Jayasekera et al., 1996; Henley et al., 2001; Dyer et al., 2017). The selective pre-leaching of tellurium before the cyanide leaching of telluride-type gold concentrate can separate and enrich tellurium and effectively improve the leaching rate of conventional cyanidation of precious metals of this type of ore. However, the leaching rates of tellurium, gold and silver are still low. In future research, it hopes to obtain better indicators by optimizing conditions and strengthening leaching, so as to realize

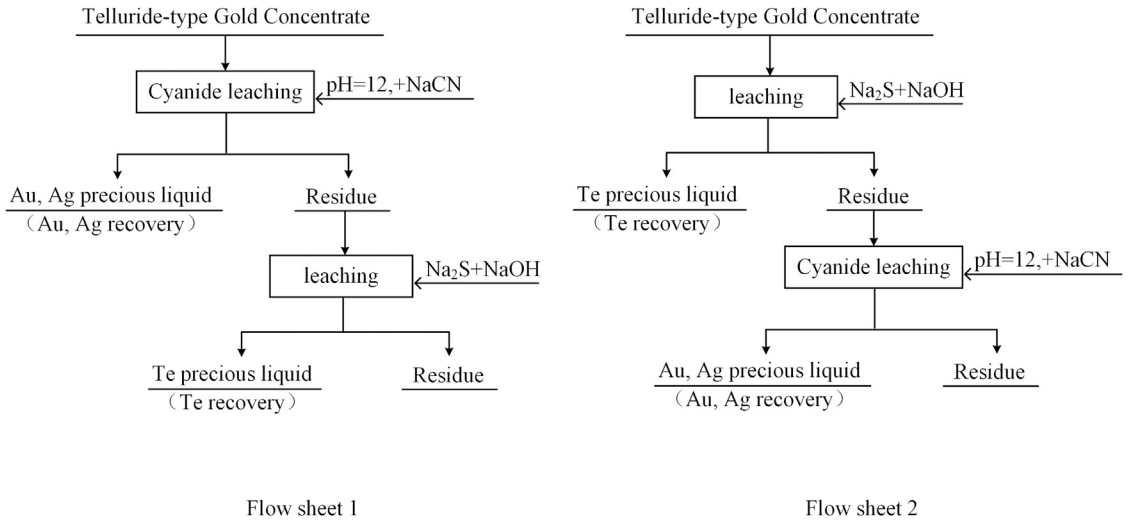

FIGURE 10 | Telluride-type gold concentrate integrated recovery of tellurium, gold, and silver experiment flow chart.

TABLE 3 | Results of Validation experiment.

Experimental procedure	Leaching rate/%	
	Au	Ag
1	32.00	50.30
2	75.39	58.83

the comprehensive recovery of tellurium, gold, and silver in telluride-type gold concentrate.

Leaching Kinetic Analysis

According to the experimental data at different temperatures, the applicability of diffusion control, interfacial chemical reaction control and mixing control are discussed based on the kinetic equations of equations (**Eqs 13**, **14**). There are many reaction models used in leaching kinetics, including the diffusion-controlled model (**Eq. 13**) and the chemical reaction-controlled model (**Eq. 14**) (Demirkıran and Künkül, 2007):

$$-\ln(1-\varepsilon) = K_1 t \tag{13}$$

$$\frac{1}{1-\varepsilon} - 1 = K_2 t \tag{14}$$

In the equations, ε is leaching rate, t leaching time, and K_1, K_2 apparent reaction constants. The plots of linear fitting are shown in **Figure 11** and the parameters are listed in **Table 4**.

From the fitting curve and related parameters, the diffusion-controlled model could not describe the leaching process of Te at different temperatures. On the other hand, the chemical reaction-controlled model fitted the tellurium leaching process well. In order to obtain a better fitting effect, the Avrami model was applied (**Eq. 15**). The results of linear fitting are shown in **Figure 11** and **Table 4**.

$$-\ln(1-\varepsilon) = Kt^n \tag{15}$$

When $0.5 \le n < 1$, the leaching process of Te is a mixed type of chemical reaction control and diffusion control (Gu et al., 2019). In **Table 4**, the average of n values is 0.26263, and it shows the reaction rate is controlled by diffusion at the beginning of the experiment, which is consistent with the experimental data.

The leaching rate can be calculated by the Arrhenius formula:

$$K = Ae^{-\frac{E}{RT}} \tag{16}$$

$$\ln k = -\frac{\mathrm{E}}{\mathrm{RT}} + \ln \mathrm{A} \tag{17}$$

K is the reaction rate constant, E (kJ/mol) the reaction activation energy, R (J/mol·k) the ideal gas constant, T (Kelvins) the absolute temperature, and A the frequency factor. lnA is a constant. **Figure 12** is drawn based on the above results. Therefore, the values of E and A are calculated to be 17.12 kJ/mol and A = 119.90.

CONCLUSION

The optimum process conditions for the tellurium leaching from Na_2S + NaOH were determined by investigating the effect of various factors on the tellurium leaching rate in the process of Na_2S + NaOH cooperative leaching of tellurium from tellurium telluride-type gold concentrate: −0.038 mm (95%) grinding fineness, 80 g/L Na_2S concentration, 30 g/L NaOH concentration, 80°C leaching temperature, 4:1 liquid-solid ratio. Under these conditions, the leaching rate of tellurium is 78.14%; the leaching rates of gold and silver are both less than 3.5%; the lead content before and after leaching is only reduced by 0.59%. The dates have shown the realization of the selective leaching of tellurium.

The effect of selective pre-leaching of tellurium by Na_2S + NaOH on the recovery of precious metals from telluride-type gold concentrate was determined by validation experiments. The

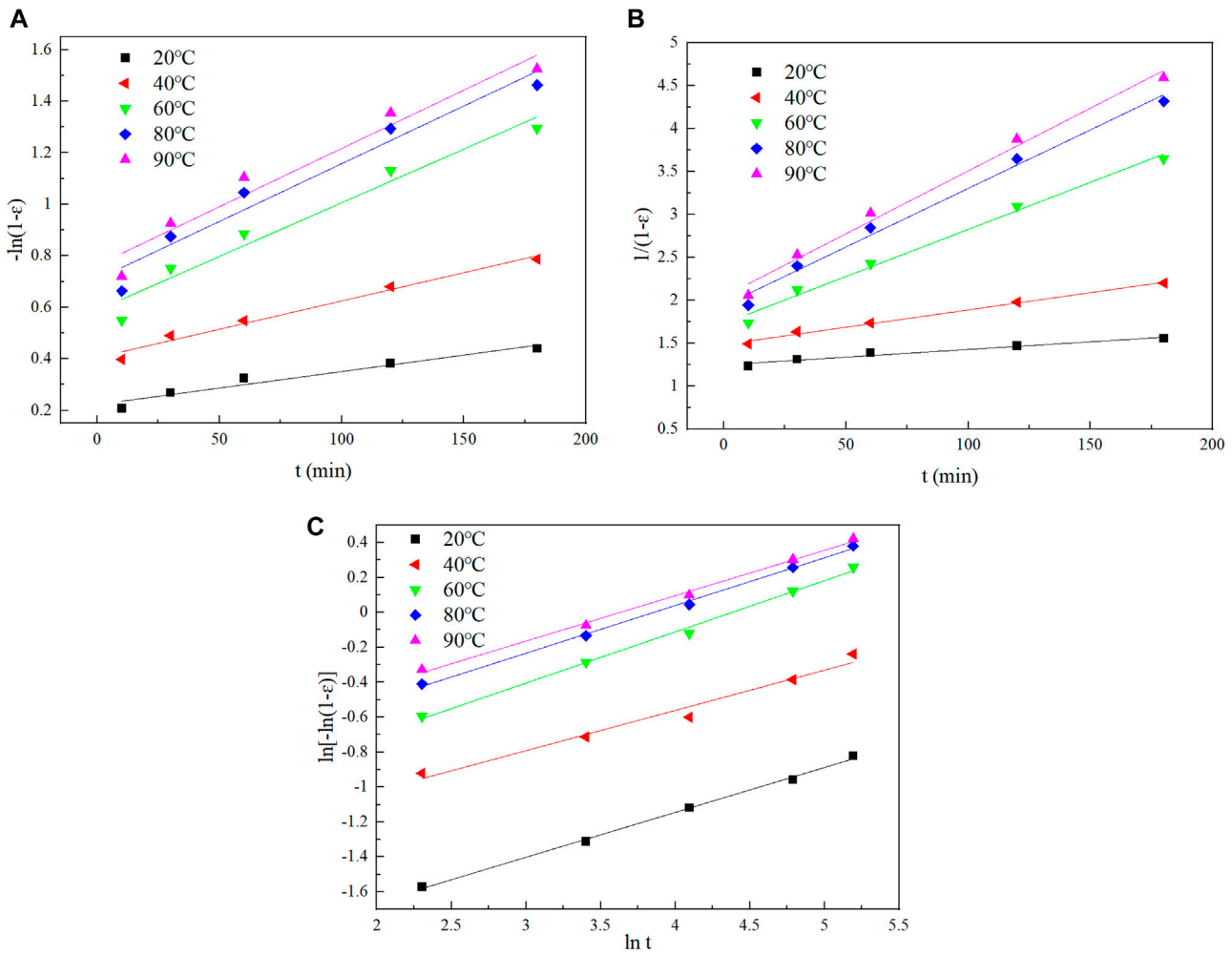

FIGURE 11 | The fitting curves using different models: **(A)** the plot of [–ln (1–ε)] vs. t, **(B)** the plot of 1/(1–ε) vs. t, **(C)** the plot of ln [–ln (1–ε)] vs. ln*t*.

TABLE 4 | Fitting results of the two models.

T/°C	Kinetic expression	Regression equation	Correlation coefficient R^2
20	$-ln(1-\varepsilon) = K_1 t$	$-ln(1-\varepsilon) = 0.22323 + 0.00128t$	0.94655
	$\frac{1}{1-\varepsilon} - 1 = K_2 t$	$\frac{1}{1-\varepsilon} - 1 = 1.24656 + 0.00179K_2 t$	0.96069
	$-\ln(1-\varepsilon) = Kt^n$	$\ln[-\ln(1-\varepsilon)] = -2.17242 + 0.25693 \ln t$	0.99777
40	$-ln(1-\varepsilon) = K_1 t$	$-ln(1-\varepsilon) = 0.40573 + 0.00219t$	0.98249
	$\frac{1}{1-\varepsilon} - 1 = K_2 t$	$\frac{1}{1-\varepsilon} - 1 = 1.48301 + 0.00403t$	0.99299
	$-\ln(1-\varepsilon) = Kt^n$	$\ln[-\ln(1-\varepsilon)] = -1.48257 + 0.23039 \ln t$	0.97555
60	$-ln(1-\varepsilon) = K_1 t$	$-ln(1-\varepsilon) = 0.58977 + 0.00416t$	0.96086
	$\frac{1}{1-\varepsilon} - 1 = K_2 t$	$\frac{1}{1-\varepsilon} - 1 = 1.72839 + 0.01096t$	0.99075
	$-\ln(1-\varepsilon) = Kt^n$	$\ln[-\ln(1-\varepsilon)] = -1.28314 + 0.29295 \ln t$	0.99578
80	$-ln(1-\varepsilon) = K_1 t$	$-ln(1-\varepsilon) = 0.70968 + 0.00448t$	0.95396
	$\frac{1}{1-\varepsilon} - 1 = K_2 t$	$\frac{1}{1-\varepsilon} - 1 = 1.9378 + 0.01364t$	0.98927
	$-\ln(1-\varepsilon) = Kt^n$	$\ln[-\ln(1-\varepsilon)] = -1.05302 + 0.27317 \ln t$	0.99764
90	$-ln(1-\varepsilon) = K_1 t$	$-ln(1-\varepsilon) = 0.76434 + 0.00452t$	0.95537
	$\frac{1}{1-\varepsilon} - 1 = K_2 t$	$\frac{1}{1-\varepsilon} - 1 = 2.04364 + 0.01462t$	0.98998
	$-\ln(1-\varepsilon) = Kt^n$	$\ln[-\ln(1-\varepsilon)] = -0.94319 + 0.25972 \ln t$	0.99651

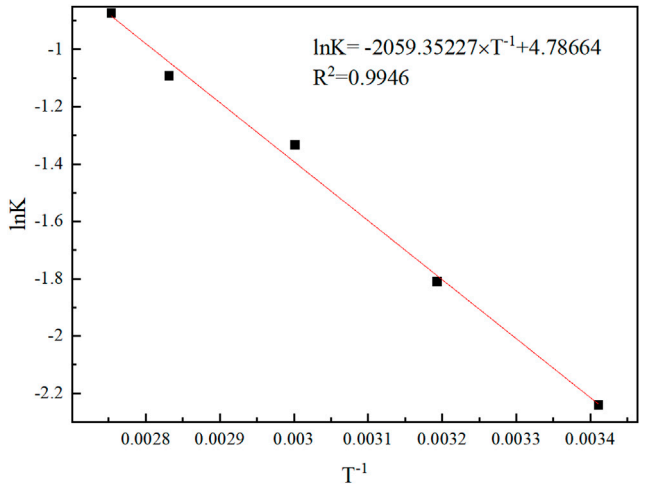

FIGURE 12 | The relation between lnK and 1/T.

tellurium leaching conditions remained unchanged, while the gold and silver leaching conditions were as follows: −0.038 mm (95%) grinding fineness, pH = 12, NaCN dosage 0.80%, liquid-solid ratio 2:1, leaching time 48 h. Under these conditions, the leaching rates of Au and Ag in the experiment results of procedure 2 (pre-leaching tellurium) are 75.39 and 58.83%, respectively, which are 43.38 and 8.53% higher than those of procedure 1 (direct cyanide leaching of gold and silver). It effectively eliminates the adverse effects of tellurium on the recovery of precious metals in telluride-type gold concentrate.

The selective leaching of tellurium from telluride-type gold concentrate by the Na_2S + NaOH cooperative leaching process has provided new ideas for the separation and extraction of tellurium, a rare element, from telluride-type gold concentrate. And pre-leaching tellurium before cyanide leaching can improve the leaching rates of gold and silver, which provides a theoretical and technological basis for the comprehensive recovery of tellurium, gold, and silver from telluride-type gold concentrate.

The kinetic analysis showed that the Na_2S + NaOH leaching process was in accordance with the diffusion-controlled type in the Avrami model, and the leaching of tellurium was clarified to mixed control type. The grain parameter in the leaching process was 0.26263 and the apparent activation energy E = 17.12 kJ/mol.

DATA AVAILABILITY STATEMENT

The raw data supporting the conclusion of this article will be made available by the authors, without undue reservation.

AUTHOR CONTRIBUTIONS

WY and XL wrote the manuscript, participated in the design of the experiments, data analysis, and data interpretation. QW, PD, and GW provided professional suggestions performed some of the experiments reported in this work and participated in discussion about the experimental results. WY supervised the work, contributed to the scope of the work and the revision of the manuscript. All authors contributed to the article and approved the submitted version.

FUNDING

Financial supports from the National Natural Science Foundation of China (No. 51474169), the Industrial Science and Technology Research Program of Shaanxi Province, China (No. 2016GY-154), and the Key Research and Development Program of Shaanxi Province, China (No. 2020SF-362) are all gratefully acknowledged.

REFERENCES

Aydogan, S., Aras, A., and Canbazoglu, M. (2005). Dissolution kinetics of sphalerite in acidic ferric chloride leaching. *Chem. Eng. J.* 114, 67–72. doi:10.1016/j.cej.2005.09.005

Ba, L. A., Döring, M., Jamier, V., and Jacob, C. (2010). Tellurium: an element with great biological potency and potential. *Org. Biomol. Chem.* 8, 4203–4216. doi:10.1039/c0ob00086h

Candelise, C., Winskel, M., and Gross, R. (2012). Implications for CdTe and CIGS technologies production costs of indium and tellurium scarcity. *Prog. Photovolt. Res. Appl.* 20, 816–831. doi:10.1002/pip.2216

Cheng, L., and Li, A. (2008). Research progress in the separation and purification of tellurium. *Chin. J. Rare Met.* 32, 115–120. doi:10.3390/met10101376

Chivers, T., and Laitinen, R. S. (2015). Tellurium: a maverick among the chalcogens. *Chem. Soc. Rev.* 44, 1725–1739. doi:10.1039/c4cs00434e

Demirkıran, N., and Künkül, A. (2007). Dissolution kinetics of ulexite in perchloric acid solutions. *Int. J. Miner. Process* 83, 76–80. doi:10.1016/j.minpro.2007.04.007

Dyer, L. G., Sauber, M., Dixon, D. G., and Asselin, E. (2017). On the refractory nature of precious metal tellurides. *Hydrometallurgy* 169, 488–495. doi:10.1016/j.hydromet.2017.03.009

Fan, Y., Yang, Y., Xiao, Y., Zhao, Z., and Lei, Y. (2013). Recovery of tellurium from high tellurium-bearing materials by alkaline pressure leaching process: thermodynamic evaluation and experimental study. *Hydrometallurgy* 139, 95–99. doi:10.1016/j.hydromet.2013.07.005

Fraser, K. S., Walton, R. H., and Wells, J. A. (1991). Processing of refractory gold ores. *Miner. Eng.* 4, 1029–1041. doi:10.1016/0892-6875(91)90081-6

Geisthardt, R. M., Topic, M., and Sites, J. R. (2015). Status and potential of CdTe solar-cell efficiency. *IEEE J. Photovolt.* 5, 1217–1221. doi:10.1109/jphotov.2015.2434594

Gu, K., Li, W., Han, J., Liu, W., Qin, W., and Cai, L. (2019). Arsenic removal from lead-zinc smelter ash by NaOH-H_2O_2 leaching. *Separat. Purif. Technol.* 209, 128–135. doi:10.1016/j.seppur.2018.07.023

Guo, X. Y., Yi, Y., Shi, J., and Tian, Q. H. (2016). Leaching behavior of metals from high-arsenic dust by NaOH–Na_2S alkaline leaching. *Trans. Nonferr. Met. Soc. China* 26, 575–580. doi:10.1016/s1003-6326(16)64118-3

Guo, X., Xu, Z., Li, D., Tian, Q., Xu, R., and Zhang, Z. (2017). Recovery of tellurium from high tellurium-bearing materials by alkaline sulfide leaching followed by sodium sulfite precipitation. *Hydrometallurgy* 171, 355–361. doi:10.1016/j.hydromet.2017.06.010

Henley, K. J., Clarke, N. C., and Sauter, P. (2001). Evaluation of a diagnostic leaching technique for gold in native gold and gold ± silver tellurides. *Miner. Eng.* 14, 1–12. doi:10.1016/s0892-6875(00)00156-4

Hoffmann, J. E., and Zhong, D. (1990). Recovery of selenium and tellurium from copper refinery anode slime. *China Nonferr. Metall.* 41, 29–34. doi:10.1016/S1003-6326(15)63729-3

Huang, L. (2012). "Atmospheric alkaline leaching," in *Chemical beneficiation*. Editor Y. Xu (Bei Jing, FL: Metallurgical Industry Press), p. 62.

Ibers, J. (2009). Tellurium in a twist. *Nat. Chem.* 1, 508. doi:10.1038/nchem.350

Jayasekera, S., Avraamides, J., and Ritchie, I. M. (1996). The electrochemical oxidation of gold telluride (AuTe2) in perchloric acid solutions. *Electrochim. Acta* 41, 879–885. doi:10.1016/0013-4686(95)00378-9

Lee, T. D., and Ebong, A. U. (2017). A review of thin film solar cell technologies and challenges. *Renew. Sustain. Energ. Rev.* 70, 1286–1297. doi:10.1016/j.rser.2016.12.028

Lewis, A. E. (2010). Review of metal sulphide precipitation. *Hydrometallurgy* 104, 222–234. doi:10.1016/j.hydromet.2010.06.010

Lin, S., Li, W., Chen, Z., Shen, J., Ge, B., and Pei, Y. (2016). Tellurium as a high-performance elemental thermoelectric. *Nat. Commun.* 7, 10287. doi:10.1038/ncomms10287

Liu, W., Jia, R., Sun, B., Zhang, D., Chen, L., Yang, T., et al. (2020). A novel process for extracting tellurium from the calcine of copper anode slime via continuous enrichment. *J. Clean. Prod.* 264, 121637. doi:10.1016/j.jclepro.2020.121637

Missen, O. P., Ram, R., Mills, S. J., Etschmann, B., Reith, F., Shuster, J., et al. (2020). Love is in the Earth: a review of tellurium (bio)geochemistry in surface environments. *Earth-Sci. Rev.* 204, 103150. doi:10.1016/j.earscirev.2020.103150

Richmond, W. (2010). Processing technologies for gold-telluride ores. *Int. J. Miner. Metall. Mater.* 17, 1–10. doi:10.1007/s12613-010-0101-6

Rocchetti, L., and Beolchini, F. (2015). Recovery of valuable materials from end-of-life thin-film photovoltaic panels: environmental impact assessment of different management options. *J. Clean. Prod.* 89, 59–64. doi:10.1016/j.jclepro.2014.11.009

Shao, L., Diao, J., Ji, C., and Li, G. (2020). A novel and clean process for extracting tellurium and bismuth from dashuigou tellurium ore by oxidizing leaching. *Hydrometallurgy* 191, 105205. doi:10.1016/j.hydromet.2019.105205

Sredni, B. (2012). Immunomodulating tellurium compounds as anti-cancer agents. *Semin. Cancer Biol.* 22, 60–69. doi:10.1016/j.semcancer.2011.12.003

Sun, Z.-M., and Zheng, Y.-J. (2011). Preparation of high pure tellurium from raw tellurium containing Cu and Se by chemical method. *Trans. Nonferr. Met. Soc. China* 21, 665–672. doi:10.1016/s1003-6326(11)60763-2

Wang, S. (2011). Tellurium, its resourcefulness and recovery. *J. Manag.* 63, 90–93. doi:10.1007/s11837-011-0146-7

Yang, W., Wang, G., Wang, Q., Dong, P., Cao, H., and Zhang, K. (2019). Comprehensive recovery technology for Te, Au, and Ag from a telluride-type refractory gold mine. *Minerals* 9, 597. doi:10.3390/min9100597

Yang, X. (1997). Wet recovery of tellurium-containing materials with different valences. *Non-ferrous Smelt.* 97, 11–20.

Yannopoulos, J. C., and SpringerLink, O. S. (1991). *Extractive metallurgy of gold*. Boston, MA: Springer.

Yu, X., Yu, F., Yang, X., and Wen, W. (2019). Experimental study on mineral processing of tellurium bismuth ore containing gold in Sichuan. *Nonferr. Met. (Mineral Process. Part)*, 81–84.

Zhang, Q., Liu, Y., Bai, J., Xu, W., and He, M. (2019). Characteristics of paragenetic elements of tellurium in stream sediments in the Dashuigou tellurobismuthite deposit and its surroundings and their prospecting significances. *Acta Min. Sin.* 39, 192–200. doi:10.1007/s12583-018-0788-2

Zheng, Y.-J., and Chen, K.-K. (2014). Leaching kinetics of selenium from selenium-tellurium-rich materials in sodium sulfite solutions. *Trans. Nonferr. Met. Soc. China* 24, 536–543. doi:10.1016/s1003-6326(14)63093-4

Zhou, L., and Chen, S. (2008). *Scattered metal extraction metallurgy*. Beijing, China: Metallurgical Industry Press. doi:10.1007/2F978-3-030-05955-2 CrossRef Full Text

Conflict of Interest: The authors declare that the research was conducted in the absence of any commercial or financial relationships that could be construed as a potential conflict of interest.

frontiers in Chemistry

ORIGINAL RESEARCH
published: 16 June 2021
doi: 10.3389/fchem.2021.592407

Selective Complex Precipitation for Ferro-Chrome Separation From Electroplating Sludge Leaching Solution

Li Jinhui, Wang Ying, Wang Yudong, Gao Yang, Yang Yang and Wang Ruixiang**

School of Metallurgy and Chemical Engineering, Jiangxi University of Science and Technology, Ganzhou, China

In this paper, aiming at the problem of chrome-iron separation in electroplating sludge, the separation of ferrochrome by complexation and precipitation with benzoic acid as complexing agent is achieved. The optimal conditions consisted of a 1: 3 molar ratio of Fe^{3+}: C_6H_5COOH, a reaction temperature of 30°C, a final pH of 2.5 and a reaction time of 2 min. The separation rate of the iron was 97.38% and the rate of loss of chromium was only 3.59%. The ferrochromium separation products were analyzed by XRD, fluorescence spectroscopy, infrared spectroscopy and H NMR Spectroscopy in order to study the mechanism of precipitation. The results showed that benzoic acid preferentially forms a complex with iron and iron benzoate precipitates with an increase pH. The iron benzoate crystals have a fine particle size, settle rapidly and are easy to filter. The separation of Cr^{3+}/Fe^{3+} was successful using our methodology.

Keywords: electroplating sludge, the separation of ferrochromium, complex precipitation, selective, transformation

OPEN ACCESS

Edited by:
Hong Peng,
The University of Queensland, Australia

Reviewed by:
Jotheeswari Kothandaraman, Pacific Northwest National Laboratory (DOE), United States
Luigi Campanella, Sapienza University of Rome, Italy

****Correspondence:***
Li Jinhui
jinhuili@jxust.edu.cn
Wang Ruixiang
82422239@qq.com

Specialty section:
This article was submitted to Green and Sustainable Chemistry, a section of the journal Frontiers in Chemistry

Received: *07 August 2020*
Accepted: *26 May 2021*
Published: *16 June 2021*

Citation:
Jinhui L, Ying W, Yudong W, Yang G, Yang Y and Ruixiang W (2021) Selective Complex Precipitation for Ferro-Chrome Separation From Electroplating Sludge Leaching Solution. Front. Chem. 9:592407. doi: 10.3389/fchem.2021.592407

INTRODUCTION

The electroplating industry in China produces approximately 10 million tons of electroplating sludge every year, which is classified as hazardous waste due to containing harmful substances, for example, chromium (Wei-hua and Xue-fu, 2006; Qiu-yue, 2014). On the other hand, the chromium present in the electroplating sludge is an important resource in the stainless steel and electroplating industry. Moreover, China is short of chromium resources and needs to import a large amount of chromium every year. Therefore, the recycling of valuable metals from electroplating sludge can not only help resolve the issue of environmental pollution but also promote the reutilization of waste resources (Chen et al., 2005; Zhang et al., 2005; Li et al., 2013; Liqing et al., 2019). At present, common methods for the utilization of chromium-containing electroplating sludge mainly includes acid leaching, ammonia leaching, electrodeposition, microbial metallurgy, and material utilization among others (Jin-ping et al., 1996; Yi et al., 1999; Fu de, 2002; Silva J. E. et al., 2005; Silva J. et al., 2005; Chen Ke, 2007; Cheng et al., 2010; Guo et al., 2010; Xian, 2012; Zheng et al., 2014). The most popular method used in industry is acid leaching, step precipitation and solvent extraction. In the hydrometallurgy process, the separation of chrome-iron is a relatively important step because of the similarity between Fe^{3+} and Cr^{3+}. When the Fe^{3+} ion is separated via neutralization, the Cr^{3+} ion is usually wrapped around or precipitated as hydroxide with iron hydroxide, which results in the loss of chromium and secondary pollution (Cheng-yan et al., 2008; Yuan et al., 2013). Majone (1986), Hu et al. (2006), Jian-Hui et al. (2011), respectively, used the goethite method, the Mohr salt

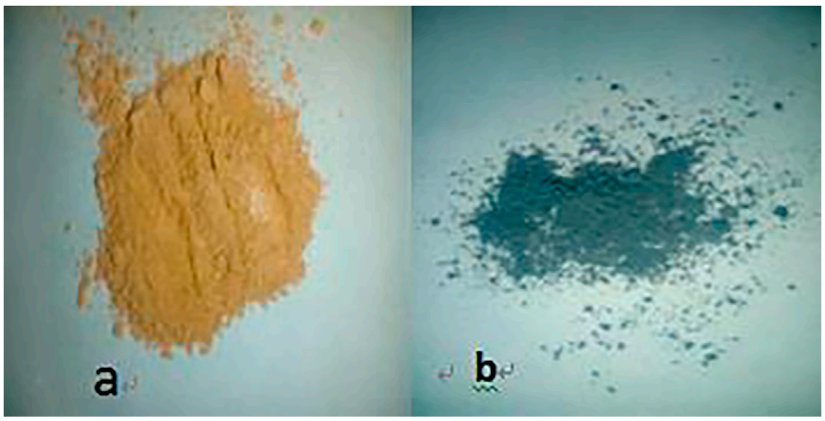

FIGURE 1 | (A) Coordination products of benzoic acid and iron ions; **(B)** Coordination products of benzoic acid and chromium ions.

crystallization method and cupferron as a precipitating agent to separate chromium and iron successfully, but the processes are relatively complicated and the problem of secondary pollution cannot be completely resolved. This prevents these methods from been widely used in industry. Silva et al. (2006) oxidized Cr^{3+} to Cr^{6+} and used the solubility difference between $Cr^{6+}$and Fe^{3+}in an alkaline system to achieve separation, however, $Cr^{6+}$is highly toxic. Zheng et al. (2020) used crystal modification to recover Cr from electroplating nano sludge. The process control is complex and the crystallinity control is not easy. kolthoff et al. (2002) used ammonium benzoate to separate chromium and iron can not solve the problem of wastewater discharge of amine, so this method can not be applied. Bewtra et al. (1995) used the adsorption of metal ions by bacteria to treat electroplated sludge, but poor biological selectivity to metal ions of this method limits its application.

In order to realize the recovery of chromium from electroplating sludge, an efficient procedure for the separation of chrome-iron must be developed. In this study, a new method for the separation of ferrochromium by a selective complexation precipitation is achieved using benzoic acid as complexing agent which can form a insoluble complex with iron in aqueous solution. The results of our study provide a new method for the comprehensive recovery of chromium from mixed electroplating sludge.

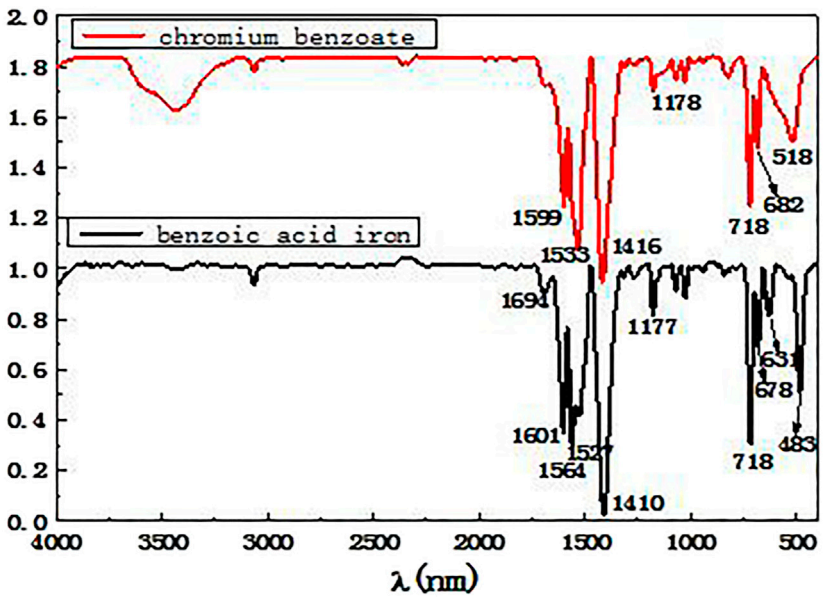

FIGURE 2 | Infrared spectra of chromium benzoate and benzoic acid iron products.

EXPERIMENTAL

Reaction Principle

Benzoic acid was found to be the best ligand. Under certain conditions, benzoic acid can coordinate with Fe^{3+} and Cr^{3+} to form stable complexes, which will crystallize and precipitate after saturation. The coordination of Fe^{3+} and Cr^{3+} with benzoic acid in aqueous solution is shown in **Eqs. 1, 2**.

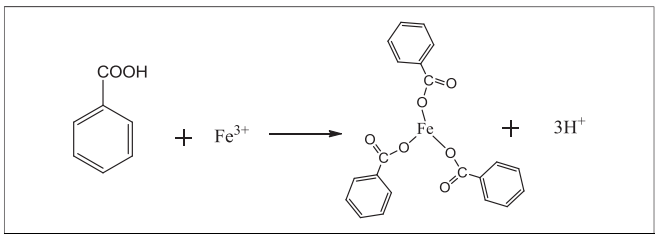

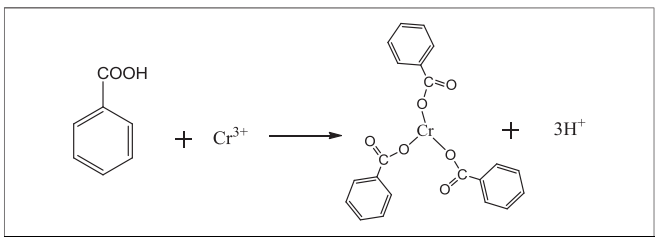

In the experiment, pure Fe^{3+} and Cr^{3+} sulfate solutions with the same concentrations were prepared, and the benzoic acid ethanol solution was slowly added under the action of magnetic stirring in a constant temperature water bath. The products obtained by filtration, separation and drying are shown in **Figure 1**.

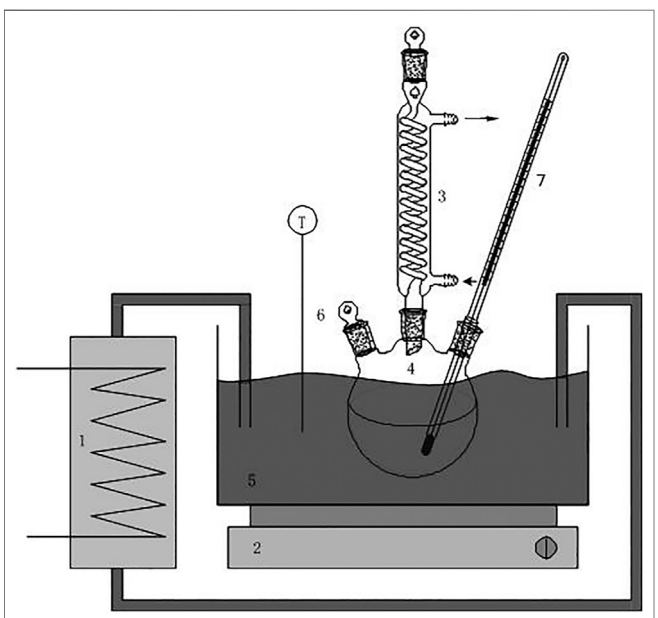

FIGURE 3 | Equipment sketch: 1: temperature-controlled bath with external flow; 2: magnetic stirrer; 3: tap water-cooled condenser; 4: round-bottom flask with three holes; 5: water bath; 6: outlets for batch addition and solution sampling; 7: thermometer.

The reaction products of benzoic acid with both iron and chromium were analyzed by infrared spectroscopy, and the resulting infrared spectra are shown in **Figure 2**.

From the analysis of the spectra 2, it can be seen that the absorption peaks around 1,601 and 1314 cm^{-1} correspond to the stretching vibration absorption bands of the benzene ring carbon-carbon bonds. The peaks at 3,058, 1,601, and 718 cm^{-1} can be ascribed to the three characteristic absorption peaks of the benzene ring. The strong absorption peaks appearing around 1,527 and 1,410 cm^{-1} correspond to the asymmetrical and symmetrical stretching vibration peaks of the carboxylate groups in the benzoate. The above results show that the coordination reaction of benzoic acid with chromium and iron ions produced the corresponding products. The spectrum of the product formed from the reaction of benzoic acid and iron shows significant peaks at 631 and 483 cm^{-1}, whereas the spectrum of the benzoic acid and chromium reaction products show broad absorption peaks at 518 cm^{-1} and no peaks at 631 cm^{-1}. However, the coordination ability of benzoic acid with different metal ions varies, and conditions such as reaction temperature, solution acidity and basicity must be adjusted in order for the benzoic acid to form stable complexes with Fe^{3+} and Cr^{3+} ions. Thus, benzoic acid was added to a mixed solution of ferrochrome, and an appropriate reaction temperature and reaction time were selected. Subsequently, by adjusting the pH of the solution, the reaction was promoted and benzoic acid was selectively precipitated and separated from the ferrochrome.

Experiment Concerning the Separation of Ferrochromium by Selective Benzoic Acid Complexation and Precipitation

In the electroplating sludge leaching solution mixed with chromium and iron, the benzoic acid coordination agent which was used was that

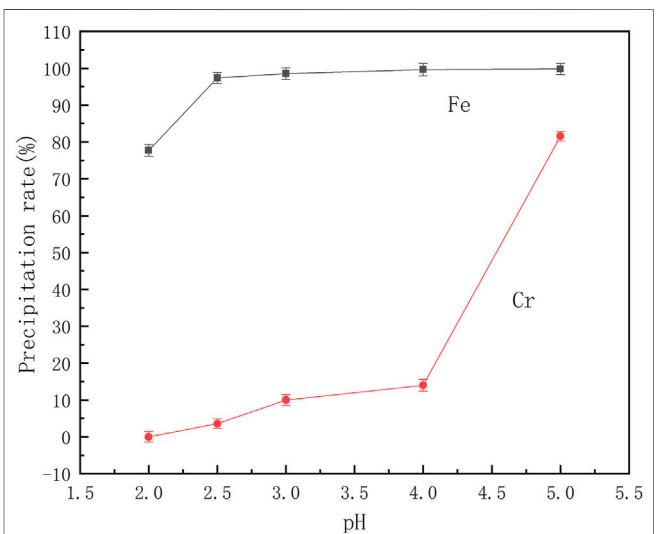

FIGURE 4 | Effect of reaction pH on the precipitation rate of ferrochrome.

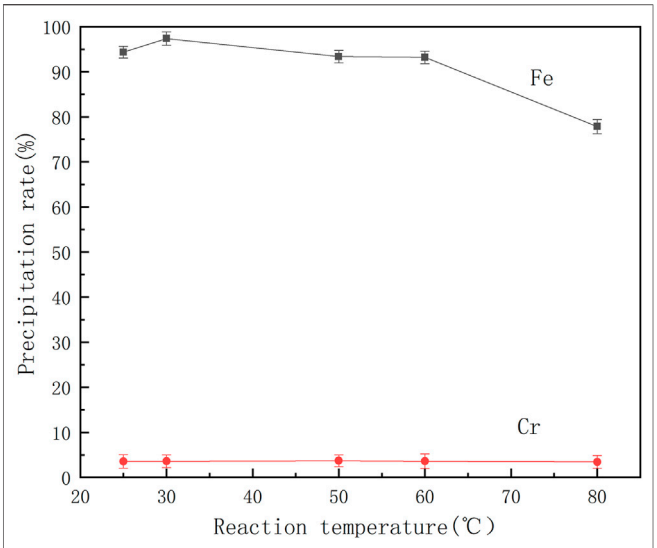

FIGURE 5 | Effect of reaction temperature on precipitation rate of ferrochrome.

of an ethanol solution of benzoic acid. The experiment was carried out by stirring at a constant temperature in a water bath. The benzoic acid ethanol solution was slowly added dropwise to the mixed chromium-iron solution, and then the pH was adjusted with ammonia water to achieve selective complexation and precipitation of the iron ions. The effects of reaction time, reaction temperature and benzoic acid dosage on the separation of ferrochromium by the selective benzoic acid complexation and precipitation method were investigated. The experimental setup is shown in **Figure 3**.

Analysis Method

In this experiment, o-phenanthroline spectrophotometry was used to determine the Fe^{3+} content in the filtrate after the reaction, and WFX-1380 atomic absorption spectrophotometer was used to determine the Cr^{3+} content in the filtrate after the reaction.

The formula for the calculation of the precipitation rate of the ferrochrome ions in this paper is as follows:

$$\text{Precipitation rate} = \frac{C_1 \times V_1 - C_2 \times V_2}{C_1 \times V_1} \times 100\%$$

In the formula, C_1 is the initial solution concentration (g/L), V_1 is the initial solution volume (L); C_2 is the concentration of metal ions (g/L) in the filtrate at constant volume, and V_2 is the volume of the solution at constant volume of the filtrate (L).

RESULTS AND DISCUSSION

Separation of Ferrochromium by Precipitation of a Benzoic Acid Complex

Effect of Solution pH on Ferrochrome Separation

From the reaction **Eqs. 1, 2** it can be shown that the coordination between benzoic acid and iron and chromium ions is affected by the pH of the solution. Therefore, a series of mixed ferrochromium solutions were prepared. After adding benzoic acid, the pH of the solution was adjusted to different values, and the effect of pH on the separation of ferrochromium was investigated. The results are shown in **Figure 4**.

It can be seen from **Figure 4** that the precipitation rate of ferrochromium increases with an increase in pH. At a pH of 2.5, the rate of precipitation of Fe is 93.37%, and that of Cr only 3.61%. Following an increase in the pH value, the rate of precipitation of the iron did not change significantly. However, due to the hydrolysis of chromium ions, the rate of loss of Cr ions increased. Thus at a reaction pH of 2.5, chromium and iron ions can be effectively separated in the acid leaching solution of

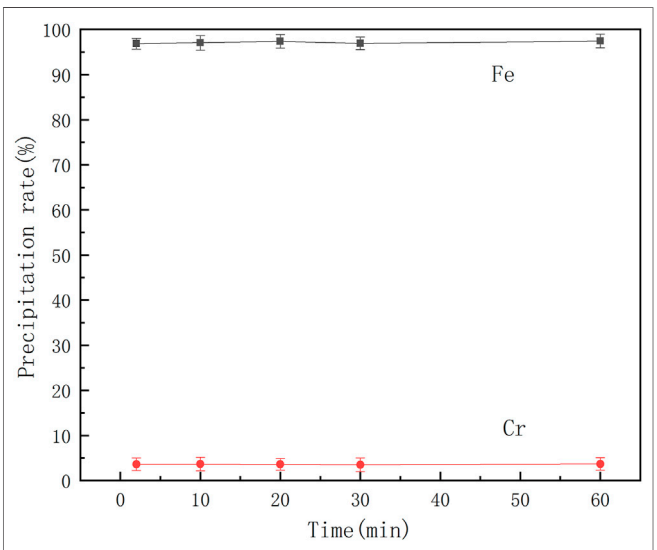

FIGURE 6 | Effect of reaction time on separation of ferrochromium.

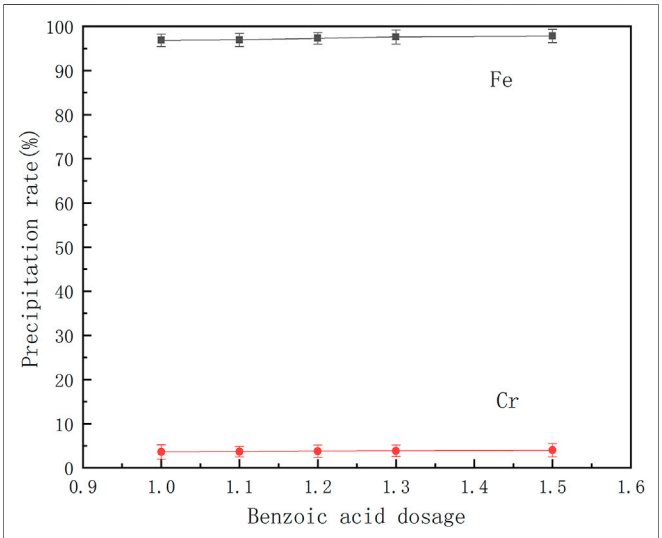

FIGURE 7 | Effect of benzoic acid dosage on the separation of ferrochromium.

the electroplating sludge. At this point, the iron precipitation rate is 97.38% and the rate of loss of chromium is 3.59%.

Effect of Reaction Temperature on Ferrochrome Separation

The coordination reaction between organic ligands and metal ions is easily affected by the temperature of the solution. Therefore, a series of mixed ferrochrome solutions were prepared, benzoic acid was added at different temperatures and the pH of the solution was adjusted to 2.5 for the reactions. The effect of temperature on the separation of ferrochrome is shown in **Figure 5**.

It can be seen from **Figure 5** that the precipitation rate of chromium is extremely low and does not significantly change with increasing temperature. When the temperature exceeds 60°C, the precipitation rate of iron begins to decrease significantly, indicating that the high temperature is not conducive to the coordination of benzoic acid and iron ions. When the reaction temperature is controlled at 30°C, the chromium-iron ions can be effectively separated from the acid leaching solution of the electroplating sludge. At this temperature, the iron precipitation rate is 97.38% and the rate of loss of chromium is 3.59%.

Effect of Reaction Time on the Separation of Ferrochrome

A series of mixed ferrochrome solutions were prepared, and reactions performed by adding benzoic acid and adjusting the solution pH to 2.5 at 30°C. The effect of the reaction time on the separation of ferrochrome was studied, and the results are shown in **Figure 6**.

It can be seen from **Figure 6** that the precipitation rates of chromium and iron change little with time. The iron precipitation rate remains at almost 97%, while the chromium loss rate remains at 3.6%. Therefore, when the reaction time is controlled to approximately 2 min, chromium-iron ions can be effectively separated from the acid leaching solution of the electroplating sludge. At this time, the iron precipitation rate is 96.85% and the chromium loss rate is 3.62%.

TABLE 1 | Orthogonal experiments and horizontal design.

Horizontal design	Factors			
	A Temperature (°C)	B Time (min)	C pH	D Benzoic acid dosage
1	30	2	2	1
2	50	20	2.5	1.2
3	70	60	3	1.5

TABLE 2 | Results of the orthogonal test and range analysis L_9 (3^4).

Order number	A Temperature (°C)	B Time (min)	C pH	D Benzoic acid dosage	Iron precipitation rate (%)
1	1(30)	1(2)	1(2)	1(1)	67.28
2	1(30)	2(20)	2(2.5)	2(1.2)	96.86
3	1(30)	3(60)	3(3)	3(1.5)	99.35
4	2(50)	1(2)	2(2.5)	3(1.5)	97.93
5	2(50)	2(20)	3(3)	1(1)	98.56
6	2(50)	3(60)	1(2)	2(1.2)	86.32
7	3(70)	1(2)	3(3)	2(1.2)	97.66
8	3(70)	2(20)	1(2)	3(1.5)	83.58
9	3(70)	3(60)	2(2.5)	1(1)	83.60
K1	87.830	87.623	79.060	83.147	
K2	94.270	93.000	92.797	93.613	
K3	88.280	89.757	98.523	93.620	
R	6.440	5.377	19.463	10.473	

TABLE 3 | Variance results of orthogonal experiment.

Factors	The sum of variances	Degree of freedom	F Values	F critical-values
Temperature	77.556	2	0.330	4.460
Time	43.979	2	0.187	4.460
pH	600.312	2	2.552	4.460
Benzoic acid dosage	219.242	2	0.932	4.460
Error	941.09	8		

FIGURE 8 | A) Separation of ferrochrome products by complexing precipitation at 30°C; **(B)** Separation of ferrochrome products by complexing precipitation at 50°C; **(C)** Separation of ferrochrome product by complexing precipitation at 80°C.

Effect of Benzoic Acid Dosage on Separation of Ferrochrome

From **Eqs. 1, 2**, it can be seen that the coordination reaction between benzoic acid and iron and chromium ions is affected by the concentration of the reaction materials. Therefore, a series of mixed ferrochrome solutions were prepared. Different amounts of benzoic acid, for complete reaction with iron ions, were added at 30°C, and then the pH of the solution was adjusted to 2.5 to study the effects of the amount of benzoic acid on the separation of ferrochrome. The results are shown in **Figure 7**.

It can be seen from **Figure 7** that the precipitation rates of chromium and iron both increase with an increase in benzoic acid dosage, but the increase is very small. An increased amount of benzoic acid does not achieve better separation of the ferrochromium. In conclusion, the ratio of benzoic acid to iron ions in the solution was adjusted to 3:1, so as to effectively separate chromium and iron ions in the acid leaching solution of the sludge.

Orthogonal Experiment

Based on the four parameters of reaction temperature, time, and solution pH, and according to the benzoic acid consumption and the precipitation rate of iron ions, three levels were designed using orthogonal experimental methods. The results are shown in **Tables 1**, **2**, and **3**.

TABLE 4 | The elements in the separated products of the ferrochromium at different temperatures.

	Element content/%				
	O	Fe	Cr	S	Other
Separated product at 30°C	9.535	36.132	0.017	0.147	54.169
Separated product at 50°C	9.838	41.078	0.211	0.148	48.725
Separated product at 80°C	12.037	41.809	0.325	2.784	43.045

It can be seen from **Tables 2**, **3** that according to the selected factors and horizontal analysis, the order of the influence of each factor on the separating effect of ferrochrome is: C > D > A > B, that is, solution pH > benzoic acid dosage > reaction temperature > reaction time. The pH of the solution had the greatest effect on the separation of ferrochrome, and the reaction time had the least effect on the separation of ferrochrome. Therefore, the effect of solution pH on the rate of the precipitation of iron ions should be considered to be the major factor for the separation of benzoic acid complexed chromium iron.

In summary, benzoic acid was used as a complexing precipitant to separate Cr^{3+} and Fe^{3+} in the solution. The benzoic acid was added in a 1:3 molar ratio of benzoic acid: $Fe^{3+}$and the temperature maintained at 30°C. The pH of the solution was adjusted to 2.5 with ammonia water and stirred for 2 min. During this period of time, the rate of precipitation of the iron reaches 96.85%, and the rate of loss of chromium is only 3.62%.

Study on the Separation Mechanism of the Complexation Precipitation

Apparent Morphology Analysis

The benzoic acid complex precipitation products and separation of ferrochrome at different temperatures was conducted using different experiments. The actual products are shown in **Figure 8**.

It can be seen from **Figure 8** that as the temperature increases, the appearance of the benzoic acid and ferrochrome complex changes, and its apparent color changes from cinnamon to dark-red, and gradually deepens. As the conditions of each experiment were the same except for temperature, it was speculated that the complexation mechanism of benzoic acid and ferrochrome is different at different temperatures. The mechanism cannot be determined from a change in apparent shape. Therefore, further analysis on the characteristics of the material structure of the separated products of the ferrochrome was conducted.

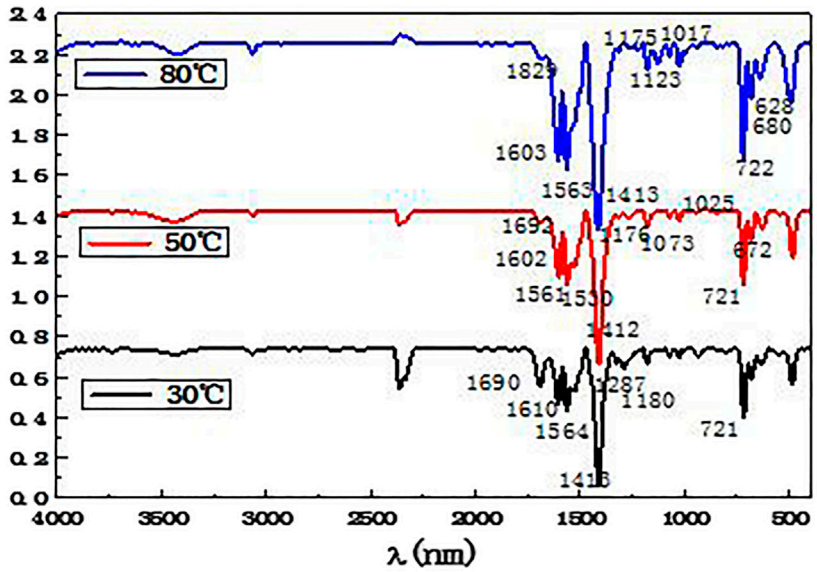

FIGURE 9 | Infrared spectrogram of the product of the benzoic acid and ferrochrome mixed reaction.

X-Ray Fluorescence Analysis

X-ray fluorescence analysis was used to detect the elements in the separated products of ferrochromium at different temperatures, as shown in **Figure 8** and the test results are shown in **Table 4**.

From the data in **Table 4**, it can be seen that from 30 to 50°C, the iron content increases while the chromium content remains almost unchanged. It can be concluded that within this temperature range, the rate of precipitation of iron increases, and the loss of chromium remains mostly unchanged. When the temperature rises from 50 to

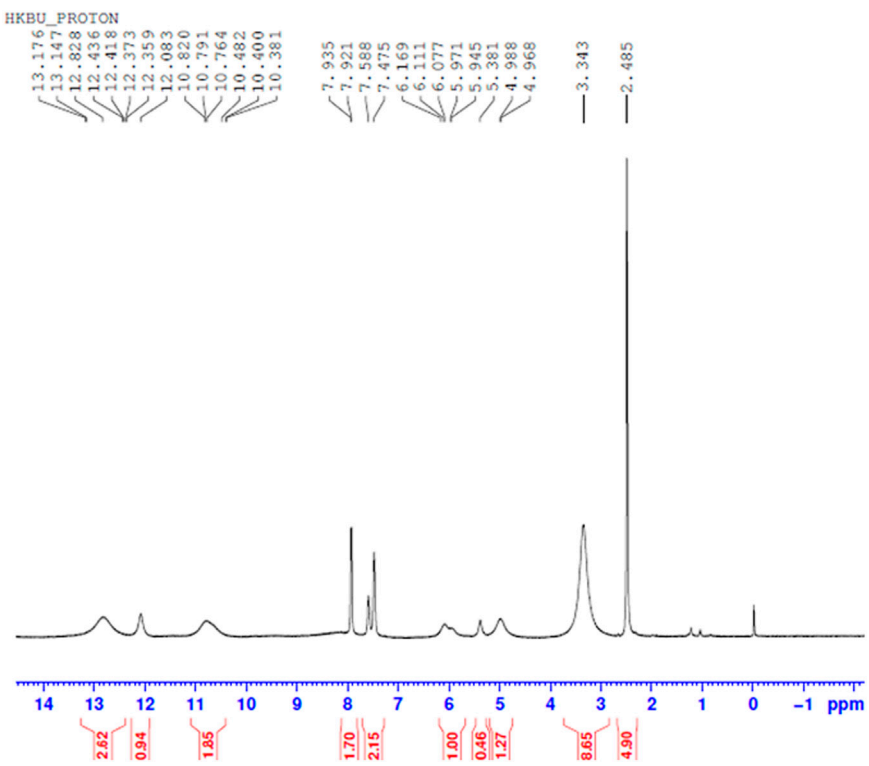

FIGURE 10 | ^{1}H NMR spectrum resulting from the addition of benzoic acid to ferric sulfate solution at 30°C to obtain precipitated product.

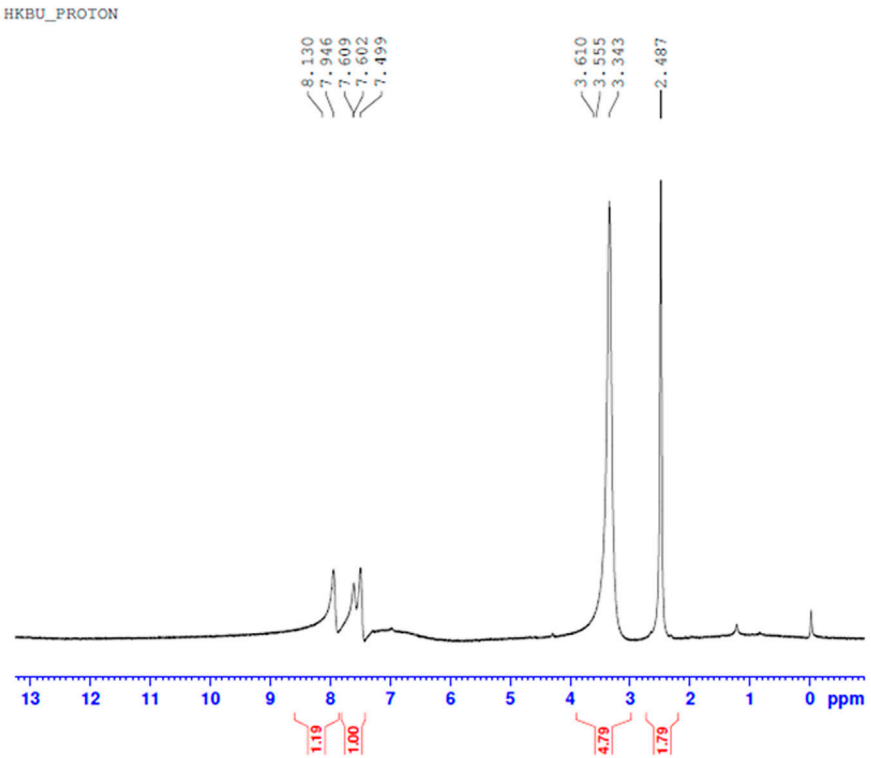

FIGURE 11 | ^{1}H NMR spectrum resulting from the addition of benzoic acid to chromium sulfate solution at 30°C to obtain precipitated product.

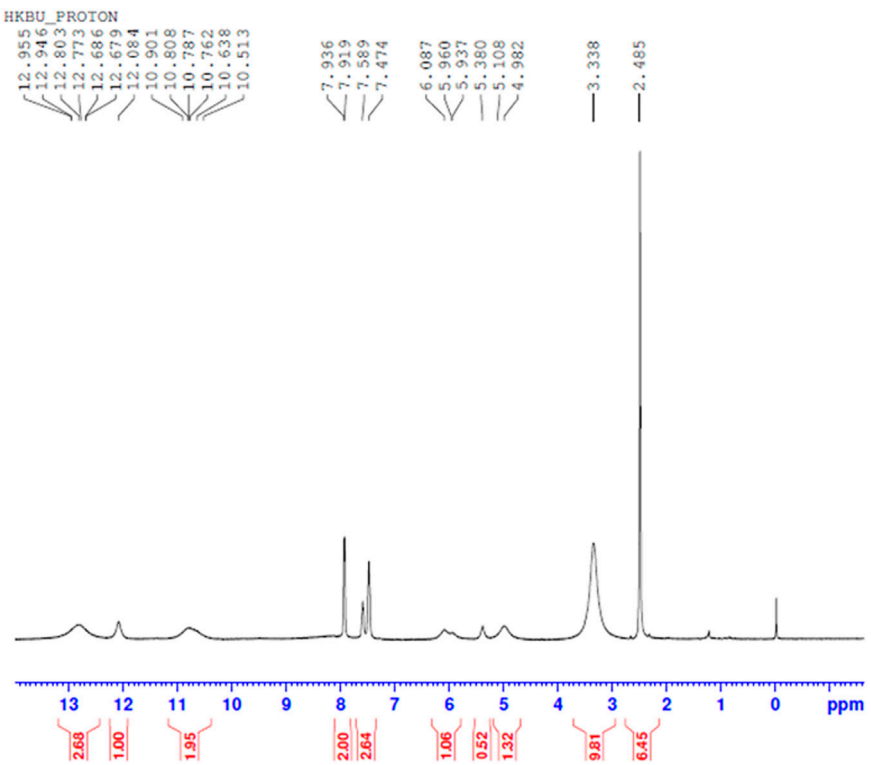

FIGURE 12 | ^{1}H NMR spectrum resulting from the addition of benzoic acid to ferric sulfate and chromium sulfate mixed solution at 30°C.

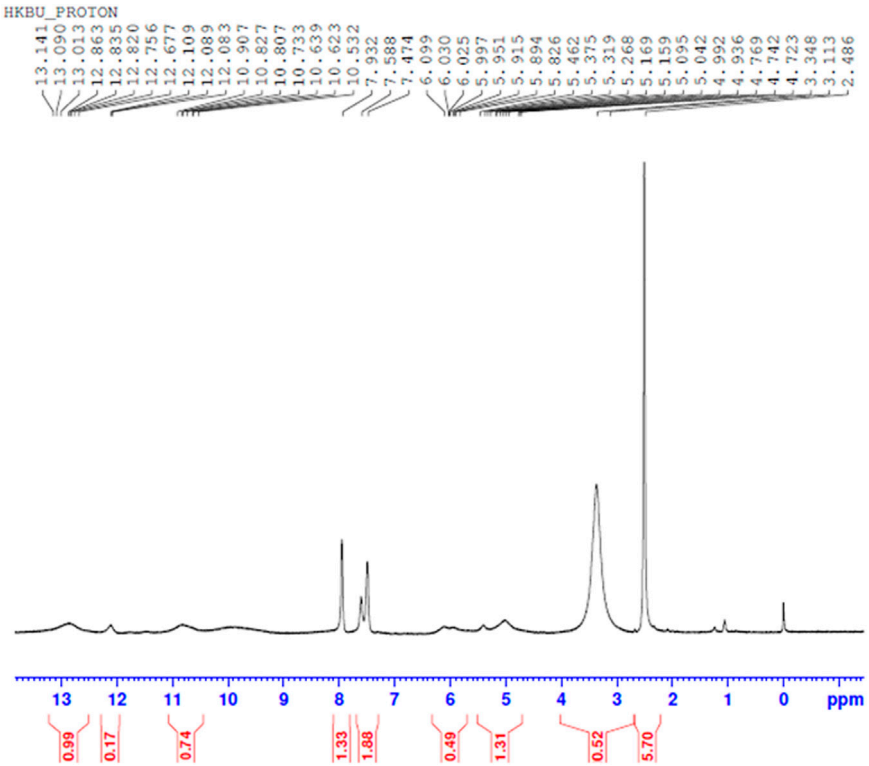

FIGURE 13 | ^{1}H NMR spectrum resulting from the addition of benzoic acid to iron sulfate and chromium sulfate mixed solution at 80°C to obtain precipitated product.

80°C, the ferrochromium content remains almost unchanged. Therefore, in this temperature range, the rate of chromium precipitation increases, while the rate loss of iron is mostly unchanged.

Infrared Spectroscopic Analysis

Combined with **Table 4**, the elements present in the separated ferrochrome products at different temperatures were analyzed by infrared spectroscopy. The results are shown in **Figure 9**.

From the analysis in **Figure 9**, it can be seen that the absorption peaks appearing at approximately 1,601 and 1315cm $^{-1}$ in the three infrared spectra obtained at 30, 50, and 80°C correspond to the stretching vibration absorption bands of the benzene ring carbon bonds. The three characteristic absorption peaks of the benzene ring can be seen at 3,061, 1,601, and 721 cm^{-1}. The strong absorption peaks at 1,564 and 1413 cm^{-1} can be ascribed to the asymmetrical and symmetrical stretching vibrations of the carboxylate ion in the benzoate. In all the spectra, strong absorption peaks can be observed at 636 and 492 cm^{-1}, corresponding to iron benzoate. This proves that there are benzoic acid molecules in the products resulting from the precipitation and coordination reaction between benzoic acid and the iron ions. Combined with the results of the X-ray fluorescence analysis, it can be seen that the precipitated and separated product contains a significant number of iron and oxygen elements, which shows that the complexation of iron with benzoic acid is significant, whereas the amount of complexation with the chromium is small. Thus, selective complexation and separation of ferrochromium in the acid leaching solution of the electroplating sludge has been successfully achieved.

H NMR Spectral Analysis

Comparing **Figures 10–13** H NMR spectrum, it can be seen that in the H NMR spectra of the reaction products obtained from the mixing of ferric sulfate and chromium sulfate with benzoic acid, the signals are in agreement with those of the reaction products of ferric sulfate and benzoic acid. The ability of ferric sulfate to react with benzoic acid is stronger than the ability of chromium sulfate to react with benzoic acid. This characteristic of benzoic acid can be used to achieve separation of chromium and iron from a mixed system (Note: DMSO was used as the solvent to dissolve the samples for testing).

CONCLUSION

(1) An operationally simple procedure for the separation and precipitation of Cr^{3+} and Fe^{3+} using benzoic acid as a complexing agent and adjustment of the reaction solution pH with ammonia, has been developed. By adding benzoic acid in a 1:3 molar ratio of Fe^{3+}: C_6H_5COOH, controlling the temperature at 30°C, adjusting the pH of the solution to 2.5 with ammonia, and stirring for 2 min, iron could be precipitated at a rate of 96.85% with only a 3.62% rate loss of chromium. The chromium and iron concentrations in the precipitated solution are 0.063 and 1.790 g/L, respectively.

(2) After using benzoic acid as a complexing agent, the crystal form of the precipitate changes. The precipitated iron benzoate particles are finer, the settlement rate is rapid, and the product is easy to filter. The problem associated with the filtration of colloidal ferric hydroxide produced by precipitation and neutralization of chromium and iron ions is avoided. The separation of Cr^{3+}/Fe^{3+} from the acid leaching solution of electroplating sludge has been successfully achieved and the developed procedure will help promote further research in this area.

DATA AVAILABILITY STATEMENT

The original contributions presented in the study are included in the article/Supplementary Material, further inquiries can be directed to the corresponding authors.

AUTHOR CONTRIBUTIONS

JL: Proposed the topic and instructed the writing and revision process. WY: Helped to draft and revise the manuscript. GLiHelped to anlyze and review the cases. WY: Collected the references for case study author. GY: Instructed the writing and revsion process. YY: Helped to calculate and draft. WR: Instructed the experiments.

ACKNOWLEDGMENTS

The project was sponsored by National Natural Science Foundation (51974140), (51564021), and (5176040277), Department of Education of Jiangxi Province (GJJ160593), and Jiangxi Province Postdoctoral Science Fund (2017KY17).

REFERENCES

Bewtra, J. K., Biswas, N., Henderson, W. D., and Nicell, J. A. (1995). Recent Advances in Treatment of Selected Hazardous Wastes. *Water Qual. Res. J. Can.* 30 (1), 115–126. doi:10.2166/wqrj.1995.016

Chen, C., Cao, S., and Wang, J. (2005). Rational Utilization of Mineral Resources and Development of Recycling Economy. *Eng. Sci.* 7 (Suppl. l), 143–146.

Chen Ke, S. T.-h., Wang, Z.-C., and Su, M. (2007). Research Progress of Recovery and Reclamation of Chromium from Electroplating Sludge. *Electroplating & Finishing* 26 (5), 43–46. doi:10.1016/S1872-5791(08)60002-0

Cheng, J. H., Chen, X., Feng, K., and Zhou, Q. F. (2010). Recovery of Copper and Nickel from Electroplating Sludge by Ammonia Leaching and Hydrogen Reduction under High Pressure. *Environ. Sci. Tech.* 33 (6), 135–137. doi:10.3969/j.issn.1003-6504.2010.6E.037

Cheng-yan, W., Ding-fan, Q., and Sheng-ming, X. (2008). Significance,status and Important Issues for Recycling Utilization of Metal Secondary Resource in China. *Chin. J. Nonferrous Met.* 18 (Suppl. 1), 359–366. doi:10.1016/s1003-6326(09)60017-0

Fu de, L. I. (2002). A New Technology of Electroplating Waste Water Treatment by Microbes. *Plating & Finishing* 3 (4), 35–37.

Guo, X. Y., Shi, W. T., Dong, L. I., and Tian, Q. H. (2010). Recovery of Copper and Nickel from Electroplating Sludge by Cyclone Electrowinning. *Chin. J. Nonferrous Met.* 20 (12), 2425–2430. doi:10.1016/S1001-0742(09)60222-9

Hu, G. R., Guo, L. I., Deng, X. R., Peng, Z. D., and Cao, Y. B. (2006). Removal of Iron from Sulfuric Acid Leaching Solution of Ferrochromium Alloy by Goethite. *Hydrometallurgy of China* 25 (4), 195–200. doi:10.13355/j.cnki.sfyj.2006.04.009

Jian-Hui, W. U., Yang, L. Z., Zhan, J., and Zhang, C. F. (2011). Research on Separation of Chromium and Iron in Waste Ferrochromium Alloy. *Hydrometallurgy of China* 30 (1), 51–56. doi:10.13355/j.cnki.sfyj.2011.01.016

Jin-ping, J., Yi, H., Zhao-juan, C., and Yong, C. (1996). Synthesizing of Magnetic Powder from Electroplating Sludge. *Shanghai Environ. Sci.* 15 (4), 31–33.

Kolthoff, I. M., Stenger, V. A., and Moskovitz, B. (2002). The Benzoate Method, A New Procedure for the Separation of Iron, Aluminum and Chromium from the Other Ions of the Third Group and the Alkaline Earth Ions. *J. Am. Chem. Soc.* 56 (4), 812–815. doi:10.1021/ja01319a012

Li, L., Tang, W., Zhu, Y. B., Gu, W. X., Wang, H. J., and Zou, L. Y. (2013). Study on Ferrite Process of Electroplating Sludge. *Xiandai Huagong/modern Chem. Industry* 33 (10), 62–65. doi:10.16606/j.cnki.issn0253-4320.2013.10.029

Liqing, L., Jinghua, Z., Yiran, S., Fei, Y., and Jie, M. (2019). Ionically Cross-Linked Sodium Alginate/κ-Carrageenan Double-Network Gel Beads with Low-Swelling, Enhanced Mechanical Properties, and Excellent Adsorption Performance. *Chem. Eng. Journal* 372, 1091–1103. doi:10.1016/j.cej.2019.05.007

Majone, M. (1986). Aluminium and Iron Separation from Chromium Solutions by Precipitation with Cupferron. *Environ. Tech. Lett.* 7 (1–12), 531–538. doi:10.1080/09593338609384442

Qiu-yue, J. (2014). New Technological Study on Green Recovery of Germanium and Indium from Zinc Slag with High Lead and Silicon Contents. *Nonferrous Metals (Extractive Metallurgy)* 4, 51–53. doi:10.3969/j.issn.1007-7545.2014.04.015

Silva, J. E., Paiva, A. P., Soares, D., Labrincha, A., and Castro, F. (2005a). Solvent Extraction Applied to the Recovery of Heavy Metals from Galvanic Sludge. *J. Hazard. Mater.* 120 (1/3), 113–118. doi:10.1016/j.jhazmat.2004.12.008

Silva, J., Soares, D., Paiva, A., Labrincha, J., and Castro, F. (2005b). Leaching Behaviour of a Galvanic Sludge in Sulphuric Acid and Ammoniacal media. *J. Hazard. Mater.* 121 (1–3), 195–202. doi:10.1016/j.jhazmat.2005.02.008

Silva, P. T. D. S. E., Mello, N. T. D., Duarte, M. M. M., Montenegro, M. C. O. B. S. M., Araújo, A. N., Neto, B. D. B., et al. (2006). Extraction and Recovery of Chromium from Electroplating Sludge. *J. Hazard. Mater.* 128 (1), 39–43. doi:10.1016/j.jhazmat.2005.07.026

Wei-hua, C., and Xue-fu, Z. (2006). On Comprehensive Recovery of Leaching Slag in Wet Smelting of Zinc. *Metal Mine* (1), 98–100. doi:10.3321/j.issn:1001-1250.2006.01.026

Xian, C. (2012). Recovery of Copper from Galvanic Sludge by Pyrometallurgical and Hydrometallurgical Process. *Environ. Eng.* 30 (2), 68–71. doi:10.13205/j.hjgc.2012.02.005

Yi, Z., Zhi-kuan, W., Xia, X., Yong-qi, C., and Tao, Q. (1999). Recovery of Heavy Metals from Electroplating Sludge and Stainless Steel Pickle Waste Liquid by Ammonia Leaching Method. *J. Environ. Sci.* 11 (3), 381–384. doi:10.3321/j.issn:1001-0742.1999.03.023

Yuan, W. H., Wang, C. Y., Zhi-Feng, X. U., and Chen, J. F. (2013). Research Progress on Resource Utilization of Chromium-Containing Electroplating Sludge. *Hydrometallurgy of China* 32 (5), 284–287. doi:10.13355/j.cnki.sfyj.2013.05.008

Zhang, Y., Li, Z.-H., Qi, T., Zheng, S.-L., Li, H.-Q., and Xu, H.-B. (2005). Green Manufacturing Process of Chromium Compounds. *Environ. Prog.* 24 (1), 44–50. doi:10.1002/ep.10033

Zheng, J., Lv, J., Liu, W., Dai, Z., Liao, H., Deng, H., et al. (2020). Selective Recovery of Cr from Electroplating Nanosludge via crystal Modification and Dilute Acid Leaching. *Environ. Sci. Nano* 7. doi:10.1039/d0en00196a

Zheng, S., Jin-Hui, L. I., Yang-Yang, L. I., Xiong, D. L., and Yang, J. X. (2014). Process of Chloridizing Roasting-Weak Acid Leaching for Electroplating Sludge. *Mining Metallurgical Eng.* 34 (6), 105–109. doi:10.3969/j.issn.0253-6099.2014.06.026

Conflict of Interest: The authors declare that the research was conducted in the absence of any commercial or financial relationships that could be construed as a potential conflict of interest.

frontiers in Chemistry

ORIGINAL RESEARCH
published: 13 August 2021
doi: 10.3389/fchem.2021.592760

Synthesis of Tert-Octylsalicylaldoxime and Its Application in Extraction of Cu(II)

Liqing Li[1], Luo Feng[1], Chunfa Liao[1], Fangxu Li[2]* and Liqin Yang[1]*

[1]*Faculty of Materials Metallurgy and Chemistry, Jiangxi University of Science and Technology, Ganzhou, China,* [2]*Institute of Resources Comprehensive Utilization, Guangdong Academy of Science, Guangzhou, China*

The alkyl salicylaldoxime has attracted more and more attention recently due to the complex branched alkyl groups. In this study, a novel alkyl salicylaldoxime, tert-octylsalicylaldoxime, was successfully synthesized by the one-pot method. The yield and purity by the elemental analysis were 96.17 and 94.13%, respectively. The structure was confirmed by elemental analysis, FT-IR, ^{1}H NMR (Nuclear Magnetic Resonance), ^{13}C NMR spectroscopy, and MS. Results showed that tert-octylsalicylaldoxime with a new structure exhibited excellent extraction ability and selectivity for Cu(II) and can be successfully used to recover Cu from copper-nickel alloy electroplating wastewater. Thus, this product has the potential to be used as a powerful copper extractant in the future.

Keywords: tert-octylsalicylaldoxime, synthesis, characteristic, extraction performances, plating wastewater

OPEN ACCESS

Edited by:
Shenxu Bao,
Wuhan University of Technology, China

Reviewed by:
Wuping Liao,
Changchun Institute of Applied Chemistry (CAS), China
Zhenyue Zhang,
Wuhan Institute of Technology, China

****Correspondence:***
Liqing Li
liliqing79@126.com
Fangxu Li
lifangxu28@163.com

Specialty section:
This article was submitted to Green and Sustainable Chemistry, a section of the journal Frontiers in Chemistry

Received: *08 August 2020*
Accepted: *13 July 2021*
Published: *13 August 2021*

Citation:
Li L, Feng L, Liao C, Li F and Yang L (2021) Synthesis of Tert-Octylsalicylaldoxime and Its Application in Extraction of Cu(II). Front. Chem. 9:592760. doi: 10.3389/fchem.2021.592760

INTRODUCTION

Because copper is one of the most important base metals, the big economic development year by year will cause a serious copper supply and demand contradiction (Yu et al., 2020). Although there are many ways to extract and recover copper ions, solvent extraction is still the most effective and key technique (Farrell et al., 2010; Watling et al., 2014; Edebali and Pehlivan, 2016; Wang et al., 2018; Elizalde et al., 2019; Wang et al., 2020). Therefore, it is urgent to improve the solvent extraction technology and develop novel extractants to overcome this contradiction (Li et al., 2011). In nearly one hundred years of hydrometallurgy history, the importance of chemical factors in achieving the targeted performance of extraction has been widely recognized. Alkyl salicylaldoxime series (AS), the N-O type chelating organic agents, is widely used as extractants to extract copper, nickel, zirconium, and molybdenum (Moradi Ali, 2012; Jain et al., 2016). Jiang et al. have investigated the performance of DZ988N (a mixture of equal volumes of 5-nonylsalicylaldoxime and 2-hydroxy-5-nonyl-acetophenone oxime) in separating copper from sulfate solution containing Cu^{2+}, Fe^{3+}, and Zn^{2+} (Jiang et al., 2018). Lasheen et al. have investigated the recovery of Mo(VI) from sulfate leach liquor containing Mo(VI) and U(VI) using 5-nonylsalicylaldoxime in a kerosene system (Lasheen et al., 2014). Sastre and Alguacil have used Lix 622 as an extractant to co-extract and selectively strip copper(II) (Sastre and Alguacil, 2001). Gameiro et al. have used Lix 84-I as an extractant to extract copper from the ammoniacal medium (Gameiro et al., 2010). 5-Nonylsalicylaldoxime (NSO) (Zhang et al., 2010), a kind of AS extractant, has been most widely used to extract Cu(II) as the main effective component in the common commercial extractants (see **Table 1**). In addition, minor changes to the chemical structure of the extracting molecule can have a very significant effect on the extracting agent's performance in the extraction process.

TABLE 1 | Alkyl salicylaldoxime investigated by some previous references.

Commercial name	Compounds	References
LIX622	2-Hydroxy-5-dodecyl salicylaldoxime, tridecyl alcohol	Alguacil and Cobo (1998)
LIX84	2-Hydroxy-5-mercaptoacetophenone oxime	Parija and Bhaskara Sarma (2000)
LIX984	2-Hydroxy-5-dodecyl salicylaldoxime, 2-hydroxy-5-mercaptoacetophenone oxime(1:1)	Aminian and Bazin (2000)
LIX984N	5-Nonylsalicylaldoxime, 2-hydroxy-5-mercaptoacetophenone oxime(1:1)	Zhang et al. (2010)
P50/M5640	5-Nonylsalicylaldoxime, nonylphenol	Yang et al. (2016)

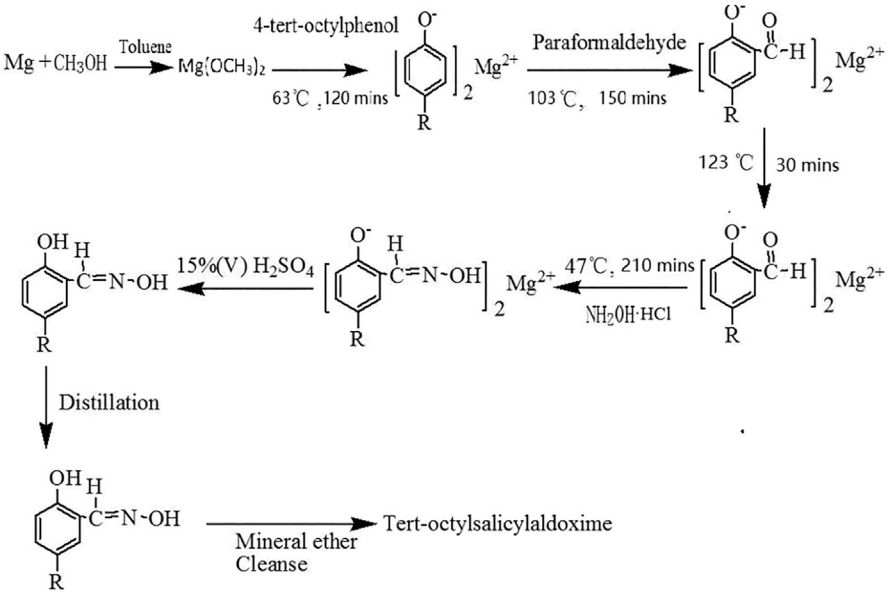

SCHEME 1 | Synthesis of tert-octylsalicylaldoxime [R = $-C(CH_3)_2CH_2C(CH_3)_3$].

The focus of this study was to create novel salicylaldoximes with new structures for Cu(II) extraction. Tert-octylsalicylaldoxime (TOSO) was successfully synthesized by the one-pot method in the laboratory (Li et al., 2017). Moreover, its properties and extraction ability for Cu(II) were investigated using the extraction test. This study may provide a promising extractant for the recovery and separation of Cu(II).

The NSO was chosen as a reference extractant. Because the structures of NSO and TOSO are very similar and belong to salicylic oxime, and NSO is the most successful copper commercial extractant.

EXPERIMENTAL

Materials and Reagents

All chemicals used in this work were of analytical grade, and all solutions at specified concentrations were prepared or diluted by deionized water. The stock solutions (0.1 mol/L) of Cu(II), Co(II), Fe(III), and Ni(II) were prepared from the sulfate salts in 1% H_2SO_4. The working solutions of metals were obtained by diluting these stock solutions before use. Salicylaldoxime (SA) solution was prepared by dissolving SA in kerosene. The pH values were adjusted by 20% (v/v) sodium hydroxide solution or sulfuric acid solution. The reagent was prepared daily.

The copper-nickel alloy electroplating wastewater was kindly supplied by Chengdu Quanrui Technology Co., Ltd. (Sichuan, China), which is produced by electroplating a copper-nickel alloy in a sulfate system. The wastewater mainly contains copper ions, nickel ions, and a small amount of electroplating additives. The copper content was 3.21 g/L, the nickel content was 1.52 g/L, and the pH was 1–2.

Synthesis and Characterization of Tert-Octylsalicylaldoxime

Synthesis

The synthetic routes to TOSO are outlined in **Scheme 1**. Tert-octylsalicylaldoxime is mainly synthesized by magnesium, 4-tert-octylphenol, paraformaldehyde, and hydroxylamine hydrochloride. The optimized mole ratio of the four reactants is Mg:4-tert-octylphenol:paraformaldehyde:hydroxylamine hydrochloride = 0.55:1:2.40:1.50.

Formylation

Magnesium ribbons (0.022 mol) were added to the solution consisting of anhydrous methanol (50 ml) and toluene (30 ml), and then the mixture was heated to 63°C for reaction with stirring until all the magnesium was dissolved and H_2 generation stopped. Then, 4-tert-octylphenol (8.25 g, 0.04 mol) was added to the mixture and refluxed for 120 min. Finally, the paraformaldehyde (0.096 mol) was added and then heated to 103°C for reaction with stirring for 150 min and subsequently heated to 123°C for reaction with stirring for 30 min.

Oximation

Firstly, the mixture was cooled to 47°C. Secondly, the hydroxylamine hydrochloride (0.06 mol) dissolved in deionized water was added to the above mixture and reacted for 210 min. Finally, tert-octylsalicylaldoxime (9.58 g, purity of 94.13%), appearing as white needle solid, was obtained after additional processes, including acidification, reduced pressure distillation, and petroleum ether cleaning.

Analytical Methods

The concentrations of C, H, and N of the final product were measured by Elementar-Vario elemental analyzer (Elementar Co., Germany). The purity and yield can be calculated by **Eq 1** and **Eq 2**, respectively. Fourier Transform Infrared Spectrum (FT-IR) of the synthesized tert-octylsalicylaldoxime was surveyed from 400 to 4000 cm^{-1} by AVATR-360 FT-IR infrared spectrophotometer (Nicolet Co., United States) using KBr pellet technique. The ^1H NMR (Nuclear Magnetic Resonance) and ^{13}C NMR spectroscopy of the final product were obtained by ADVANCE III 500 NMR spectrometer (Bruker Co., Germany) using deuterium chloroform as solvent. The mass spectrometry was recorded by a GCMS-QP2010 analyzer (Japan) (Li et al., 2019; Wang et al., 2019).

$$\text{Purity}\,(\%) = \frac{\text{The measured concentration of N}}{\text{The theoretical concentration of N}} \times 100\%. \quad (1)$$

$$\text{Yield}\,(\%) = \frac{\text{The real product weight}}{\text{The theoretical product weight}} \times 100\%. \quad (2)$$

Solvent Extraction Experiments

All the extraction and stripping experiments were conducted in a programmable air bath shaker with the organic phase (volume ratio W/O = 1). The stirring speed was maintained at 300 rpm with a stirring time ranging from 1 to 5 min to obtain extraction equilibrium. Initial pH was adjusted in the range of 1.0–3.5 with sulfuric acid or sodium hydroxide. The organic phase (extract) was stripped with sulfuric acid at a volume ratio W/O = 1. Unless otherwise stated, all other experiments were carried out at room temperature. A small amount of the raffinate (1 ml) was drawn out and diluted to the appropriate concentration for analysis.

Effects of extraction time, equilibrium pH, volume content, and A:O were investigated. The extraction efficiencies (E) of Cu(II) can be calculated from the differences between the concentrations of Cu(II) in the aqueous phase before and after extraction, as expressed by **Eq. 3**. The separation factor of the extractants for copper(II) to one metal ($\beta_{Cu/metal}$) is evaluated by **Eq. 4**.

$$E = \frac{C_1V_1 - C_2V_2}{C_1V_1} \times 100\%; \quad (3)$$

$$\beta_{Cu/metal} = \frac{C_{Cu(O)} \bullet C_{metal(A)}}{C_{Cu(A)} \bullet C_{metal(O)}}, \quad (4)$$

where E is the metal extraction efficiency, C_1 and C_2 are the metal concentrations in the aqueous phase before and after extraction, V_1 and V_2 are the volumes of the aqueous phase before and after the extraction; $C_{Cu(O)}$ and $C_{Cu(A)}$ indicate the concentration of copper(II) in the organic phase and aqueous phase (g/L), respectively, and $C_{metal(O)}$ and $C_{metal(A)}$ indicate the concentration of organic phase and aqueous phase (g/L), respectively. The concentration of metals in an aqueous solution is analyzed by Inductively Coupled Plasma-Atomic Emission Spectrometry (ICP-AES).

RESULTS AND DISCUSSION

Characterization of Tert-Octylsalicylaldoxime

Chemical spectral data of TOSO were demonstrated as follows.

Element analysis results (%): (1) calculated, C 61.14, H 9.55, N8.92; (2) found, C 61.02, H 9.48, N 8.72. IR (KBr, cm^{-1}): 3400 (OH), 2960 (CH_3, CH_2), 2800 (CH_3, CH_2), 1630(C=N), 1600 (aromatic CH), 1500 (aromatic CH), 1580 (aromatic CH), 1350 (NO).^1H NMR ($CDCl_3$, ppm): = 0.719 (t, 3H, J = 6.0 Hz, CH_3), 1.343 (t,3H, J = 6.0 Hz, CH_3), 1.701 (s, 1H, CH_2), 7.13 (s, 1H, CH), 6.90 (d, 1H, CH),7.28 (d, 1H, J = 6.4 Hz, CH), 7.50 (t, 1H, J = 6.0 Hz, CH), 9.646–9.668 (s, 1H, OH), 8.233 (s, 1H, J = 6.4 Hz, OH).^{13}C NMR ($CDCl_3$, ppm): = 31.56, 31.79, 32.33, 56.89, 37.88,115.46, 129.47, 128.15, 141.47, 116.05, 154.88 and 153.62. MS for $C_{15}H_{23}NO_2$ (M^+): 249.35. Found: 249.

Extraction and Stripping of Cu(II) Ion

Effects of extraction time, equilibrium pH, volume content, and A:O on extraction efficiency are shown in **Figure 1**. Those experiments were carried out in H_2SO_4 media with an initial Cu(II) concentration of 1.92 g L^{-1}, 15% (V/V) of extractants, and the phase ratio (aqueous phase to organic phase) of 1 and were single-stage.

As can be seen in **Figure 1A**, extraction efficiency increased with pH under the experimental pH 1.0–3.5. At pH 3.0, TOSO and NSO extracted out 90.3 and 91.3% of Cu(II) from the aqueous phase, respectively. **Figure 1B** indicates that with the increase of phase ratio, TOSO and NSO exhibited more satisfactory extraction efficiency for Cu(II). When the phase ratios (O:A) were 0.5, 1, and 2, the copper extraction efficiencies of TOSO were 86.53, 91.20, and 94.32%, respectively, and those NSO were 88.71, 91.80, and 96.82%, respectively. It indicated that the extraction efficiency increased when the phase ratio (O:A) increased from 1 to 2. However, the operation with a higher O:A ratio has a potential risk of phase separation. Therefore, it is reasonable to use a phase ratio of 1 in the experiment. **Figure 1C** shows that TOSO and NSO have a similar tendency of extraction efficiency within a fixed time; more than 90% Cu(II) was recovered in 60 s. In

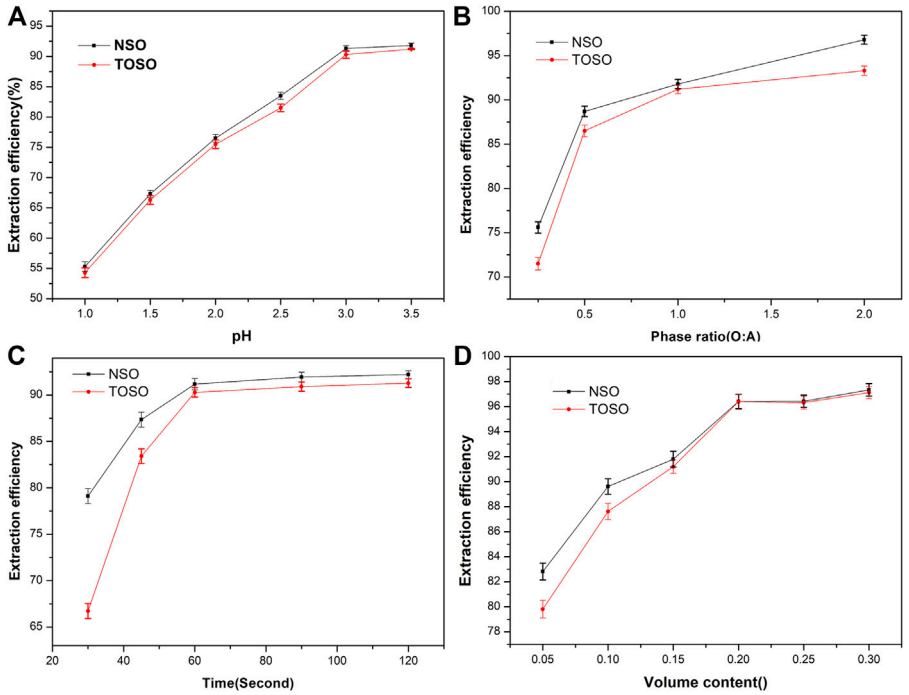

FIGURE 1 | Effects of equilibrium pH **(A)**, phase ratio A:O **(B)**, extraction time **(C)**, and volume content **(D)** on the recovery of Cu(II) with TOSO and NSO.

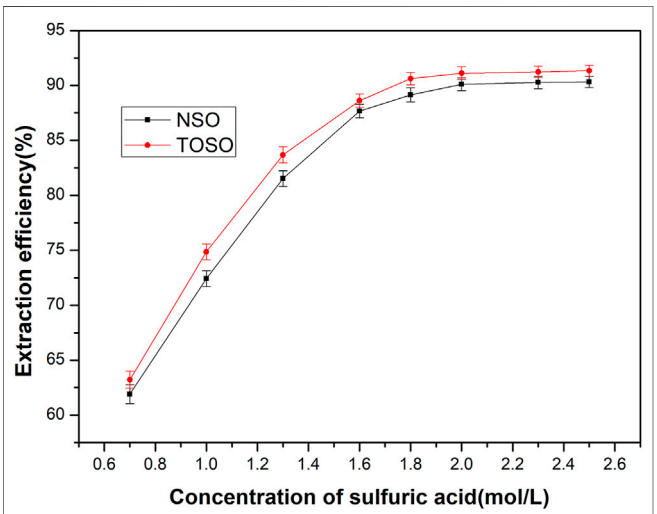

FIGURE 2 | Influence of H_2SO_4 on Cu^{2+} stripping efficiency.

addition, TOSO and NSO revealed similar extraction efficiency in high extractant concentrations, as shown in **Figure 1D**.

The copper-loaded organic was stripped at a 1:1 phase ratio with H_2SO_4 in a single stage. Results of these tests are listed in **Figure 2**. It is clear that the stripping efficiency of TOSO and NSO increased rapidly with the concentration of sulfuric acid and reached around 90% at the concentration of 1.8 mol/L. Further increase of sulfuric acid concentration did not have a significant effect on the stripping efficiency. Meanwhile, TOSO delivered better results than NSO in terms of stripping efficiency.

Copper(II) Selectivity

In industrial applications, there are many different types of metal ions present in a single hydrometallurgical process, which can significantly interfere with the extraction of Cu(II). Therefore, it is necessary to investigate the selectivity of extractants for metals.

The extraction experiments were conducted in H_2SO_4 media with a phase ratio (O:A) of 1. A single-stage extraction was applied with an extraction time of 3 min at room temperature. The pH of the solution was adjusted by 20% (v/v) sodium hydroxide solution or sulfuric acid solution. The concentration of Cu^{2+} was 0.03 mol/L, while the concentrations of Fe^{3+}, Zn^{2+}, Ni^{2+}, and Co^{2+} were set as 0.02 mol/L.

The experimental results are shown in **Figure 3**. As shown in **Figure 3A**, the synthesized tert-octylsalicylaldoxime presents a good extraction selectivity of Cu from other metals in the H_2SO_4 medium. The selectivity increased with the increase of pH from 1 to 3. The separation factor can be ranked in the following order: $\beta_{Cu/Co} > \beta_{Cu/Ni} > \beta_{Cu/Zn} \approx \beta_{Cu/Fe}$ within the pH studied, indicating that TOSO can selectively extract Cu from the complex solution. The strong selectivity for Cu may be caused by the particular umbrella-like structure of TOSO, which can provide a stronger steric effect than that of other AS series extractants with straight-chain R groups.

As can been seen in **Figure 3B**, when pH was 3.0, the $\beta_{Cu/Fe}$, $\beta_{Cu/Zn}$, $\beta_{Cu/Ni}$, and $\beta_{Cu/Co}$ values of TOSO in sulfuric acid are 1128, 1368, 15,375, and 16,787, respectively; the $\beta_{Cu/Fe}$, $\beta_{Cu/Zn}$, $\beta_{Cu/Ni}$, and $\beta_{Cu/Co}$ values of NSO are 1009, 1251, 14,875, and

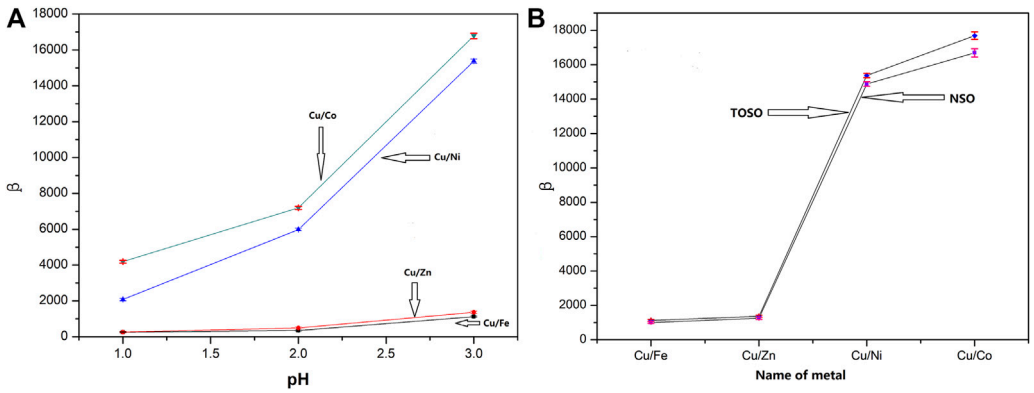

FIGURE 3 | Selectivity of TOSO and NSO for Cu^{2+}/metal ion in H_2SO_4 medium. **(A)** Selectivity of TOSO; **(B)** selectivity of TOSO and NSO at pH 3.

TABLE 2 | The experimental results of plating wastewater with Cu and Ni.

Name	Max extraction efficiency (%)	Max stripping efficiency (%)	Extraction separation time (s)	Stripping separation time (s)	$\beta_{Cu/Ni}$
TOSO	88.42	85.61	42	45	131
NSO	89.21	84.83	35	39	101

15,867, respectively. Compared with NSO, TOSO showed better selectivity for Cu/metal separation.

Tert-Octylsalicylaldoxime Application in Recovery of Cu(II) From Plating Wastewater

Considering the excellent separation performance of TOSO in Cu/Ni system, TOSO was selected for recovering Cu(II) from copper-nickel alloy electroplating wastewater. The experimental results, including extraction and stripping efficiency, extraction and stripping time, and $\beta_{Cu/Ni}$ for all the copper extraction experiments, are summarized in **Table 2**.

The maximum extraction, maximum stripping efficiency, extraction separation time, stripping separation time, and separation factor of TOSO were 88.42%, 85.61%, 42 s, 45 s, and 131, respectively. Moreover, those of NSO were 89.21%, 84.83%, 35 s, 39 s, and 101, respectively. It indicated that NSO exhibited better performance in extraction efficiency and extraction and stripping phase separation time. However, TOSO showed advantages in separation factor and stripping efficiency.

Based on the above results, NSO has higher extraction ability and shorter phase separation time for Cu(II) than TOSO, while TOSO is superior to NSO in terms of the separation ability for metals (Ni, Co, Cu, Zn) and stripping efficiency. The alkyl side chains link of TOSO (C_8) is shorter than that of NSO (C_9), and the molecular sizes and Log P (Represents the hydrophobicity value) of TOSO are also smaller than those of NSO. This means that TOSO has a lower probability of capturing Cu(II) ions and weaker hydrophobicity, which results in a longer phase separation time. Compared with NSO, the better extraction selectivity of TOSO might be due to the particular umbrella-like structure of the tert-octyl group and shorter carbon chain (Mowafy and Mohamed, 2014).

CONCLUSION

In this article, the extraction behavior of tert-octylsalicylaldoxime (TOSO) for Cu has been investigated by extraction and stripping tests. Based on the experimental results, the following conclusions could be drawn:

1) TOSO, a novel AS series extractant for Cu(II), was successfully synthesized by a one-pot reaction with a yield of 96.17% and purity of 94.13%. The structure of the synthesized TOSO was verified by elemental analysis, FT-IR, ^{1}H NMR, and ^{13}C NMR spectroscopy.
2) The results showed that TOSO exhibited powerful extraction and stripping performance. Compared with 5-nonylsalicylaldoxime (NSO), tert-octylsalicylaldoxime (TOSO) presents a stronger affinity to Cu(II) than to Co, Ni, Zn, and Fe in H_2SO_4 media, indicating it is suitable to extract Cu from these complex solutions selectively. Moreover, TOSO has been proved effective as a special extractant in the copper-nickel alloy electroplating wastewater. Therefore, TOSO can be considered a powerful extractant candidate for copper extraction in the hydrometallurgical process, which is of great significance to the development and utilization of copper resources.

DATA AVAILABILITY STATEMENT

The original contributions presented in the study are included in the article/supplementary material; further inquiries can be directed to the corresponding authors.

AUTHOR CONTRIBUTIONS

LL performed the experiments, analyzed all the data, drafted all the figures, and prepared the manuscript. FL and LY performed the experiments. CL and LL conceived and designed the experiments. FL revised the manuscript.

FUNDING

This research was supported by the National Natural Science Foundation of China (Nos. 21406097 and U1607108), the National Science Foundation for Postdoctoral Scientists of China (No. 2016M592118), the Jiangxi Province Postdoctoral Sustentation Fund of China (Nos. 2015KY11 and 2015RC17), the Jiangxi Province Funds for Distinguished Young Scientists (Nos. 20192BCB23016), and GDAS' Project of Science and Technology Development (2020GDASYL-20200302004).

ACKNOWLEDGMENTS

The authors thank Hong Zhong from Central South University in China for this research.

REFERENCES

Alguacil, F. J., and Cobo, A. (1998). Extraction of Nickel from Ammoniacal/ammonium Carbonate Solutions Using Acorga M5640 in Iberfluid. *Hydrometallurgy* 50 (2), 143–151. doi:10.1016/s0304-386x(98)00047-4

Aminian, H., and Bazin, C. (2000). Solvent Extraction Equilibria in Copper (II)-Iron (III)-LIX984 System. *Minerals Eng.* 13 (6), 667–672. doi:10.1016/s0892-6875(00)00049-2

Edebali, S., and Pehlivan, E. (2016). Evaluation of Chelate and Cation Exchange Resins to Remove Copper Ions. *Powder Technol.* 301, 520–525. doi:10.1016/j.powtec.2016.06.011

Elizalde, M. P., Rúa, M. S., Menoyo, B., and Ocio, A. (2019). Solvent Extraction of Copper from Acidic Chloride Solutions with LIX 84. *Hydrometallurgy* 183, 213–220. doi:10.1016/j.hydromet.2018.12.013

Farrell, M., Perkins, W. T., Hobbs, P. J., Griffith, G. W., and Jones, D. L. (2010). Migration of Heavy Metals in Soil as Influenced by Compost Amendments. *Environ. Pollut.* 158, 55–64. doi:10.1016/j.envpol.2009.08.027

Gameiro, M. L. F., Machado, R. M., Ismael, M. R. C., Reis, M. T. A., and Carvalho, J. M. R. (2010). Copper Extraction from Ammoniacal Medium in a Pulsed Sieve-Plate Column with LIX 84-I. *J. Hazard. Mater.* 183, 165–175. doi:10.1016/j.jhazmat.2010.07.006

Jain, V., Pradip, and Rai, B. (2016). Density Functional Theory Computations for Design of Salicylaldoxime Derivatives as Selective Reagents in Solvent Extraction of Copper. *Trans. Indian Inst. Met.* 69 (1), 135–141. doi:10.1007/s12666-015-0722-6

Jiang, F., Yin, S., Zhang, L., Peng, J., Ju, S., Miller, J. D., et al. (2018). Solvent Extraction of Cu(II) from Sulfate Solutions Containing Zn(II) and Fe(III) Using an Interdigital Micromixer. *Hydrometallurgy* 177, 116–122. doi:10.1016/j.hydromet.2018.03.004

Lasheen, T. A., Ibrahim, M. E., Hassib, H. B., and Helal, A. S. (2014). Recovery of Molybdenum from Uranium Bearing Solution by Solvent Extraction with 5-Nonylsalicylaldoxime. *Hydrometallurgy* 146, 175–182. doi:10.1016/j.hydromet.2014.03.011

Li, L., Wang, Y., An, W., and Bao, S. (2017). Effect of the Structure of Alkyl Salicylaldoxime on Extraction of Copper(II). *Minerals* 7 (4), 61–66. doi:10.3390/min7040061

Li, L., Zhao, J., Sun, Y., Yu, F., and Ma, J. (2019). Ionically Cross-Linked Sodium Alginate/κ-Carrageenan Double-Network Gel Beads with Low-Swelling, Enhanced Mechanical Properties, and Excellent Adsorption Performance. *Chem. Eng. J.* 372, 1091–1103. doi:10.1016/j.cej.2019.05.007

Li, L., Zhong, H., Cao, Z., and Yuan, L. (2011). Recovery of Copper(II) and Nickel(II) from Plating Wastewater by Solvent Extraction. *Chin. J. Chem. Eng.* 19 (6), 926–930. doi:10.1016/s1004-9541(11)60073-6

Moradi Ali, P. (2012). Characterization of 5-nonylsalicylaldoxime Production and the Effects of Modifiers on its Extracting/stripping Properties. *Res. Chem. Intermed.* 38, 2401–2409. doi:10.1007/s11164-012-0556-3

Mowafy, E. A., and Mohamed, D. (2014). Extraction Behavior of Trivalent Lanthanides from Nitric Acid Medium by Selected Structurally Related Diglycolamides as Novel Extractants. *Separat. Purif. Technol.* 128, 18–24. doi:10.1016/j.seppur.2014.03.005

Parija, C., and Bhaskara Sarma, P. (2000). Separation of Nickel and Copper from Ammoniacal Solutions through Co-extraction and Selective Stripping Using LIX84 as the Extractant. *Hydrometallurgy* 54 (2-3), 195–204. doi:10.1016/s0304-386x(99)00069-9

Sastre, A. M., and Alguacil, F. J. (2001). Co-extraction and Selective Stripping of Copper (II) and Molybdenum (VI) Using LIX 622. *Chem. Eng. J.* 81, 109–112. doi:10.1016/s1385-8947(00)00237-0

Wang, Y.-C., Wang, R.-X., Qiu, G., Zhou, H., Xie, W., and Liu, J.-B. (2019). ortho-Amide-directed 2,4-dibromohydration of Conjugated Enynes. *Org. Chem. Front.* 6, 2471–2479. doi:10.1039/c9qo00540d

Wang, Y., Chen, X., and Zhou, H. (2018). Disentangling Effects of Temperature on Microbial Community and Copper Extraction in Column Bioleaching of Low Grade Copper Sulfide. *Bioresour. Technol.* 268, 480–487. doi:10.1016/j.biortech.2018.08.031

Wang, Y., Li, J., Gao, Y., Yang, Y., Gao, Y., and Xu, Z. (2020). Removal of Aluminum from Rare-Earth Leaching Solutions via a Complexation-Precipitation Process. *Hydrometallurgy* 191, 105220. doi:10.1016/j.hydromet.2019.105220

Watling, H. R., Collinson, D. M., Li, J., Mutch, L. A., Perrot, F. A., Rea, S. M., et al. (2014). Bioleaching of a Low-Grade Copper Ore, Linking Leach Chemistry and Microbiology. *Minerals Eng.* 56, 35–44. doi:10.1016/j.mineng.2013.10.023

Yang, R., Wang, S., Duan, H., Yuan, X., Huang, Z., Guo, H., et al. (2016). Efficient Separation of Copper and Nickel from Ammonium Chloride Solutions through the Antagonistic Effect of TRPO on Acorga M5640. *Hydrometallurgy* 163, 18–23. doi:10.1016/j.hydromet.2016.03.006

Yu, B., Kou, J., Xing, Y., and Sun, C. (2020). Enhanced Extraction of Copper from Cupriferous Biotite by Organic Intercalation. *Hydrometallurgy* 192, 105286. doi:10.1016/j.hydromet.2020.105286

Zhang, W., Cui, C., Ren, Z., Dai, Y., and Meng, H. (2010). Simultaneous Removal and Recovery of Copper(II) from Acidic Wastewater by Hollow Fiber Renewal Liquid Membrane with LIX984N as Carrier. *Chem. Eng. J.* 157, 230–237. doi:10.1016/j.cej.2009.12.032

Conflict of Interest: The authors declare that the research was conducted in the absence of any commercial or financial relationships that could be construed as a potential conflict of interest.

Publisher's Note: All claims expressed in this article are solely those of the authors and do not necessarily represent those of their affiliated organizations, or those of the publisher, the editors and the reviewers. Any product that may be evaluated in this article, or claim that may be made by its manufacturer, is not guaranteed or endorsed by the publisher.

Advantages of publishing in Frontiers

OPEN ACCESS
Articles are free to read for greatest visibility and readership

FAST PUBLICATION
Around 90 days from submission to decision

HIGH QUALITY PEER-REVIEW
Rigorous, collaborative, and constructive peer-review

TRANSPARENT PEER-REVIEW
Editors and reviewers acknowledged by name on published articles

Frontiers
Avenue du Tribunal-Fédéral 34
1005 Lausanne | Switzerland

Visit us: www.frontiersin.org
Contact us: frontiersin.org/about/contact

REPRODUCIBILITY OF RESEARCH
Support open data and methods to enhance research reproducibility

DIGITAL PUBLISHING
Articles designed for optimal readership across devices

FOLLOW US
@frontiersin

IMPACT METRICS
Advanced article metrics track visibility across digital media

EXTENSIVE PROMOTION
Marketing and promotion of impactful research

LOOP RESEARCH NETWORK
Our network increases your article's readership